SOLUTIONS TO THE N-BODY PROBLEM

T. A. Bauer

Solutions to the N-Body Problem

Solutions to the N-Body Problem

By

T. A. Bauer

Cambridge Scholars Publishing

Solutions to the N-Body Problem

By T. A. Bauer

This book first published 2022

Cambridge Scholars Publishing

Lady Stephenson Library, Newcastle upon Tyne, NE6 2PA, UK

British Library Cataloguing in Publication Data
A catalogue record for this book is available from the British Library

ISBN (10): 1-5275-8261-2
ISBN (13): 978-1-5275-8261-3

CONTENTS

PREFACE

The n-body problem of 6n-12 degrees of freedom with the twelve inherent constraints creates a difficult situation in working the equations of motion for three or more masses. This befalls the mathematical physicist to remedy the situation by determining proper constraints to get past this dilemma by requiring a specialized set of conditions to define a unique problem. Procedurally, this results in working n-body problems in a case by case environment. On the assumption that deterministic solutions are of interest, then the population of problems solved under these conditions appear to be limited. The question arises, if a general approach to solving certain classes of n-body problems exists and how they could be formulated to meet the deterministic constraint. Existing in this work is a large body of n-body problems that can be formulated and solved using methods whereby the given initial conditions defining these structured mass configurations allows deterministic solutions. In the following chapters specialized n-body configurations will be structured systematically and analyzed revealing characteristics of their behavior.

The n-body problem is usually approached in a deductive manner as implied above, that is, searching for a general solution of the equations of motion over a finite or infinite interval. This method can be quite daunting due to the lack of constraints. However, approaching the n-body problem in an inductive manner, such as the inverse problem of dynamics, can reduce the degrees of freedom as a result of the forces being determined by the given properties of their motion. Using the infinitesimal interval method for tiered n-body systems with type one geometry and the sidereal synodic relations at time zero relative to the barycenter in the configuration plane of motion is a compromise that exploits both deductive and inductive approaches. Combined deductive and inductive processes simplify the formulation complexity of the tiered n-body problem resulting in a more intuitive understanding of particle interactions in terms of configuration subsystems. Binary, trinary, quadruple etc. subsystem finite stability within the n-body configuration is one such example. Subsystem perturbations, particle velocities, state vectors, period ratios and sphere of influence are other examples. The first two chapters address the tiered structure of the n-body problem using the methodology just described. These configuration

solutions are a specialized subset of all possible solutions contained in Newton's equations of motion.

Concentric regular n-gons are covered in the third chapter using methods for n-body deterministic solutions similar to that of the collinear n-body infinitesimal interval problem. Systematically, starting with solving the single polygon structure and then proceeding by evolving to more complex systems results in analysis that allows solving the multiple and infinite concentric polygon problem. Central to the concentric n-gon formulation are determinations of structured particle distributions necessary to find unique solutions of regular multi-polygon configurations. Required distributions necessary to solve this problem involve determining intra/inter perturbations, multi-polygon separation distance and mass scaling. These distributions are not unique therefore requiring further analysis using numerical optimization to find the minimum (extrema) potential energy solution. Depending on how multi-polygons are structured can force the intra/inter perturbations to have singularities. Resolving this situation leads to greater structural complexity requiring non-regular as well as regular n-gons to make the concentric polygon structure singularity free.

The Orthogonal collinear configuration presented in chapter four is a variation of the collinear infinitesimal interval problem worked in chapters one and two. This class of structured configurations use collinear masses along the inertial x and y axes possessing symmetry where the geometric center and the barycenter coincide. Masses on the x-axis as well as on the y-axis are balanced relative to the barycenter in a restricted problem to maintain this symmetry. Several of these configurations are solved beginning with the most fundamental restricted double binary, which is composed of one mass on either side of the x axis relative to the barycenter and one mass on either side of the y-axis relative to the barycenter and then proceeding to a quadruple binary with two binaries on each axis symmetric to the barycenter. Stability analysis for the double binary configuration has been worked in the sense of Lagrange using the first order approximation from the eigen value problem to compare to numerically integrated state vectors trajectories with the purpose to show that although a trajectory is not stable for all time, it can easily be stable for a finite time.

Placing collinear configurations at the L4 and L5 equilibrium locations with the purpose of verifying that finite stable orbital systems can exist there is studied in the appendix. Two such configurations are investigated. Approximate state vectors have been derived for binary and double binary configurations orbiting the equilibrium locations at the Lagrange L4 and L5

points assuming that a pseudo mass resides there. Numerically integrating these state vectors has verified that they can be finite stable. It is suspected this analysis could be extended to show that large numbered collinear mass systems can be finite stable at the L4 and L5 locations for extended periods of time.

In presenting a specialized work on the collinear infinitesimal interval and other related n-body problems, it has been assumed that a back ground in the basic mathematical and physical concepts forming the foundations of celestial mechanics are already known. There exists a plethora of work on celestial and classical dynamics, non-linear differential equations, figures of equilibrium and stability of motion published over the last several centuries that substantially embody this field. To this end a collection of these publications have been listed pertaining to celestial mechanics, classical mechanics, stability theory and linear/nonlinear differential equations. These references can be found posted in the reference section at the end of this book.

CHAPTER ONE

COLLINEAR N-BODY PROBLEM

Within its elegant mathematical formulation, the n-body equations of motion comprise every possible classical trajectory per any given set of masses (dense set). Infinite problems of great complexity reside within these coupled sets of non-linear differential equations. It would be of interest to formulate complex systems by structuring the n-body configurations in such a manner where they could be solved under the proper constraints resulting in systematic deterministic solutions consistent with the given conservation laws of physics. Therefore, it would be within capability to reduce the 'every possible' particle trajectories to just the possible structured subset that is properly constrained to get a deterministic solution. Although these configurations are a subset of the 'every possible' n-body solutions and do not encompass the whole classical 'real universe' of solutions, they are still viable and provide the mathematical physicist with insight into the nature of particle motion.

No general agreed on, or accepted finite/infinite time interval deterministic solution to the n-body equations of motion exists, including any particular general solution of three, four or more bodies. Trying to solve the n-body problem starting directly from the equations of motion for a particular n-body configuration can be a difficult way to proceed, whereas, determining the forces from the given properties of motion as in the inverse problem of dynamics (Besant, 1914, pp 140-144, Ramsey, 1929, pp 253-254, Galiullin, 1984, pp 25-28, Santilli, 1978, pp 219-223) may be more instructive. Constraints on particle position reduce 'every possible position' to just one possible collinear particle distribution, thereby reducing the degrees of freedom. Constraints on particle velocity and acceleration will reduce 'every possible velocity and acceleration' to just one possible velocity and acceleration distribution thus further reducing the degrees of freedom. Finally, using sidereal synodic relations, type one geometry and constraining time to the infinitesimal interval will reduce the degrees of freedom to zero. Properly constraining the structured n-body position,

velocity and acceleration at time zero, results in a solution domain only existing at one point, that is, a state vector solution domain.

Formulating the n-body problem into a tiered structured collinear system of particles constrained by type one geometry, sidereal synodic relations that are rotating within an infinitesimal interval at time zero, will allow deterministic state vector solutions. Infinite families comprise the tiered n-body configurations where every family is populated by infinite members and those infinite members have infinite variations. Deterministic solutions can be found for every one of these collinear configurations using Jacoby coordinates within the infinitesimal interval relative to the barycenter. Particles at time zero are in instantaneous circular orbits verified by showing the collinear solution is consistent with conservation of energy where twice the kinetic energy is equal to the potential energy. Numerical integration of the instantaneous solution state vectors will result in trajectories that are the most circular or least elliptical of all orbits for that particular configuration. This orbital characteristic is due to the type one geometry constraint where all particle velocity vectors are perpendicular to all particle position vectors within the infinitesimal interval relative to the barycenter at time zero in the given plane of motion.

1.1 Collinear N-Body Structure

The structured collinear n-body configurations are defined to exist over an infinitesimal interval at time zero (t = 0). Newtonian equations of motion are infinitesimally rotated in the complex plane within the infinitesimal interval relative to the barycenter and constrained by type one geometry and the sidereal synodic relations. The Newtonian system is defined as a dynamical, discrete, classical non-relativistic Euclidean space and consistent with the laws of conservation (all masses are non-zero).

Collinear n-body configurations are conservative dynamical systems centered at the barycenter (0,0,0) fixed in three-dimensional Euclidean space with an inertial right-handed coordinate system x, y, z. The n-body equations of motion are formulated in the complex plane over the infinitesimal interval (Lass, 1957, pp 314-319, Pollard, 1966, p-49) as specified below

$$\ddot{z}_k + 2wi\dot{z}_k - w^2 z_k = G\sum_{\substack{j=1 \\ j\neq k}}^{N} \frac{m_j}{r_{jk}^3} z_{jk} \quad k = 1, 2, 3, \ldots, N \qquad \text{Equation 1.1.1}$$

where $i = \sqrt{-1}$, $z_k = x'_k + iy'_k$ and $r_{jk} = |z_j - z_k|$

The sidereal synodic relations (Kurth, 1959, pp 1-8, Bauer, 2001, pp 1-2) that specify the general geometric conditions under which the collinear n-body configurations rotate

$$n_N P_N = (n_N + n_{N-1})P_{N-1} = \cdots = (n_N + n_{N-1} + \cdots + n_1)P_1$$

Equation 1.1.2

where P_i is the period of the given motion at time zero and n_i the corresponding coefficients.

Collinear configurations in the n-body complex formulation are transformed into Jacoby coordinates reducing the number of equations per configuration to n – 1 coupled equations of motion. By systematically coupling these n – 1 Jacoby configurations, tiered structures can be created and solved by using equations 1.1.1 and 1.1.2 with type one geometry. Any tiered collinear configuration can be illustrated in terms of its basic component subsystems as defined by their Jacoby coordinates. For example, the three-body collinear family is composed of one member (symbolically written as 123) with five additional variations. These six total configurations represent an ordered set where mass three is systematically placed in all possible gravitational subsystems relative to mass one and mass two. The six total configurations can be written out in the following manner

312 312 132 132 123 123 Equation 1.1.3

where underscoring represents Jacoby coordinate coupling. A mirror image solution exists for each of the configurations however, they are considered redundant. General form of a collinear three-body solution can be written as a quintic polynomial which results in the above six configurations expressed as six quintic equations. The first two quintic equations (configurations) in equation 1.1.3 intersect, with that intersection resulting in an additional quintic equation. This is also true of the third and fourth configurations and of the fifth and sixth configurations. There now exists three intersection quintics resulting from the paired six configurations, and it can be shown that the three intersection quintic equations are the same quintic equations derived by Euler (Roy, 1988, p 119, Pollard, 1966, p 51, Wintner, 1964, p 430, Szebehely, 1967, p 297) for his solution of the collinear three-body problem.

Adding another mass, the collinear four-body problem can be described in a similar manner as the collinear three-body problem where the four-body family is composed of two members written as 1234 and 12 34. The second configuration is a double binary system with masses one and two representing the first binary subsystem and masses three and four representing the second binary subsystem with each subsystem in orbit about the other at time zero. Two collinear four body family members plus the member variations consist of approximately fifty unique configurations. Complexities arising from four body ordering account for the large increase in configuration number. Two four body ordered subset systems analogous to the three-body ordered system can be written as follows

3(124) (312)4 (312)4 (132)4 (132)4 (123)4 (123)4 1234 1243 (124)3

3(214) (321)4 (321)4 (231)4 (231)4 (213)4 (213)4 2134 2143 (214)3

Equation 1.1.4

where ordering is defined by systematically arranging particle configurations in such a manner that the resultant systems are unique configurations.

Interchanging mass one with mass two differentiates the second mass ordered system from the first. The first ordered set is by convention the reference set. Three-body ordered configurations in equation 1.1.3 can be seen sequentially embedded in the second through seventh four-body configurations of the first four-body ordered set. Parenthesis are used to delineate the three-body subsets. By systematically interchanging the masses one and three, two and three, one and four, two and four and three and four in the reference set, the remaining combinations can be generated. Approximately thirty unique combinations out of these remaining configurations will be left after removing redundant mirror and duplicate configurations. It will be noted that all mass interchanging has been done relative to the first ordered reference set.

This collinear n-body process can be continued by the method described ad infinitum. With each additional mass added there results a significant increase in configurations due to complexity in generating all possible unique combinations. Every collinear n-body configuration is solvable producing a state vector at time zero which can be numerically integrated to determine trajectory behavior for stability analysis (Lehnigh, 1966, pp 25-71, Merkin, 1996, pp 103-111). The n-body collinear configuration hierarchy sequence can be represented as a mathematical logical system.

Found below is a listing of the first six-tiered n-body family configurations not including the family variations.

1 Equation 1.1.5

12

12 3

12 34 12 34

12 345 12 34 5 12 3 45

12 3456 12 34 56 12 3 45 6 12 34 56 12 34 56 12 3, 45 6

12 34567...

This mathematical logical system can be generated by either sequencing mass from the left or right of the unary mass. The above listing is generated from mass addition to the right and is a mirror image of a left mass generated mathematical logical system. With each additional mass the listing becomes more intricate as the mass number approaches infinity. For example, the last entry for the six-body configuration is a double trinary system represented as two three body configurations separated by a comma. For clarification, as masses are added, trinary subsystems may require a set of parentheses about each trinary to distinguish them systematically from every other subsystem when generating higher order configurations. In general, a system of underscoring, parentheses commas etc. will be needed to illustrate the n-body tiered configurations accurately. There are many possible ways in which this structuring can be symbolically formatted. However, whichever systematic representation employed, the proper perspective is needed to maintain the correct collinear rotating subsystems that compose the n-body configurations.

Each column in the mathematical logical system of equation 1.1.5 is a family of configurations that can be solved as one set of deterministic solutions using equations 1.1.1 and 1.1.2. Analysis of these fundamental configuration structures requires formulating the collinear n-body problem in terms of Jacoby coordinates. Jacoby coordinates can be classified into three distinct categories. They are, mass to mass distance, mass to sub-configuration center of gravity distance and sub-configuration center of gravity to sub-configuration center of gravity distance. Using the

infinitesimally rotating Jacoby coordinates with type one geometry, sidereal synodic relations in the infinitesimal interval at time zero results in a deterministic solution set. This solution set includes inertial velocities, state vectors, period ratios, perturbation coefficients and sphere of influence. The solution for the first column of the mathematical logical system is presented in the next subsection.

1.2 First Infinite Family Configurations

Although theoretically, the n-body mathematical logical system symbolically represented by equation 1.1.5 could be solved as one formulation of infinite configurations, only two subsets will be considered in this chapter due to the complexity of the general problem. The first infinite family is column one, as listed in equation 1.1.5 and defined in equation 1.1.1, have sidereal synodic relations under which the individual masses within the n-body configurations rotate consistent with equation 1.1.2. First family Jacoby coordinates in the infinitesimal interval at time zero are $\vec{r}_{21}, \vec{\rho}_1, \vec{\rho}_2, \vec{\rho}_3, \ldots, \vec{\rho}_{N-2}$ where $\vec{r}_{21}$ represents the Jacoby coordinate for the mass one mass two binary subsystem, $\vec{\rho}_1$ represents the Jacoby coordinate from the center of gravity of the binary subsystem to mass three, $\vec{\rho}_2$ represents the Jacoby coordinate from the center of gravity of the trinary subsystem to mass four etc.

First infinite family collinear equations of motion in the complex plane using equation 1.1.1 describing infinitesimal rotations in the infinite interval at time zero, are as follows

$$\ddot{z}_{21} + 2wi\acute{z}_{21} - w^2 z_{21} = -\frac{G\mu_{r1}}{r_{21}^3} z_{21} + \frac{Gm_3}{r_{32}^3} z_{32} - \frac{Gm_3}{r_{31}^3} z_{31} + \cdots + \frac{Gm_N}{r_{N2}^3} z_{N2} - \frac{Gm_N}{r_{N1}^3} z_{N1}$$

$$\ddot{z}_3 + 2wi\acute{z}_3 - w^2 z_3 = \frac{Gm_1}{r_{13}^3} z_{13} + \frac{Gm_2}{r_{23}^3} z_{23} + \frac{Gm_4}{r_{43}^3} z_{43} + \cdots + \frac{Gm_N}{r_{N3}^3} z_{N3}$$

$$\ddot{z}_4 + 2wi\acute{z}_4 - w^2 z_4 = \frac{Gm_1}{r_{14}^3} z_{14} + \frac{Gm_2}{r_{24}^3} z_{24} + \frac{Gm_3}{r_{34}^3} z_{34} + \cdots + \frac{Gm_N}{r_{N4}^3} z_{N4}$$

$$-w^2 z_N = \frac{Gm_1}{r_{1N}^3} z_{1N} + \frac{Gm_2}{r_{2N}^3} z_{2N} + \frac{Gm_3}{r_{3N}^3} z_{3N} + \cdots + \frac{Gm_N}{r_{(N-1),N}^3} z_{(N-1),N}$$

First equation is a result of coupling $\ddot{z}_1$ and $\ddot{z}_2$ where $\mu_{r1} = m_1 + m_2$, and N is mass number. The last relation is the equation of motion from the

barycenter to mass N. This vector is along the x' axis rotating relative to the x axis at inertial angular velocity w in the infinitesimal interval (with $\ddot{z}_N = \acute{z}_N = 0$), the x' and x axis are coincident at time zero. Modifying sidereal syndic relations equation 1.1.2 for the first family gives

$$n_N P_N = (n_N + n_{N-1})P_{N-1} = \cdots = (n_N + n_{N-1} + \cdots + n_{21})P_{21}$$

Starting from the three-body problem through to higher tiered first family collinear n-body configurations, solutions can be found by use of vector and scalar geometry. Using the sidereal synodic relations in conjunction with the vector and scalar geometry allows determination of the infinitesimal rotation of the Jacoby coordinates in the infinitesimal interval relative to the x' axis. For example, rotating Jacoby coordinate z_{21} can be formulated

$$z_{21} = r_{21} e^{i\frac{n_{N-1}+\cdots+n_3+n_{21}}{n_N}wt}$$

Substituting the second derivative of the above equation into the $\ddot{z}_{21}$ equation and using the vector configuration geometry will give after some analysis

$$\frac{G\mu_{r1}}{w^2 r_{21}^3} - \frac{P_N^2}{P_{21}^2} = \frac{G}{w^2 r_{21}^3}\left(\left(\frac{r_{21}^2}{r_{32}^2} - \frac{r_{21}^2}{r_{31}^2}\right)m_3 + \left(\frac{r_{21}^2}{r_{42}^2} - \frac{r_{21}^2}{r_{41}^2}\right)m_4 + \right.$$
$$\left. \ldots + \left(\frac{r_{21}^2}{r_{N2}^2} - \frac{r_{21}^2}{r_{N1}^2}\right)m_N\right) = \frac{G}{w^2 r_{21}^3}\phi_1 \qquad \text{Equation 1.2.1}$$

where $\phi_1 = \left(\frac{r_{21}^2}{r_{32}^2} - \frac{r_{21}^2}{r_{31}^2}\right)m_3 + \left(\frac{r_{21}^2}{r_{42}^2} - \frac{r_{21}^2}{r_{41}^2}\right)m_4 + \cdots + \left(\frac{r_{21}^2}{r_{N2}^2} - \frac{r_{21}^2}{r_{N1}^2}\right)m_N$

Continuing this derivation with the acceleration vectors $\ddot{z}_3, \ddot{z}_4, \ldots z_N$ will yield the complete set of $\phi_i's$ needed to find the Jacoby velocities for the first family state vectors

$$\phi_2 = \frac{r_{21}^2}{r_{31}^2}m_1 + \frac{r_{21}^2}{r_{32}^2}m_2 - \frac{r_{21}^2}{r_{34}^2}m_4 - \cdots - \frac{r_{21}^2}{r_{3N}^2}m_N$$

$$\phi_3 = \frac{r_{21}^2}{r_{41}^2}m_1 + \frac{r_{21}^2}{r_{42}^2}m_2 + \frac{r_{21}^2}{r_{43}^2}m_3 - \cdots - \frac{r_{21}^2}{r_{4N}^2}m_N$$

$$\phi_{N-1} = \frac{r_{21}^2}{r_{N1}^2}m_1 + \frac{r_{21}^2}{r_{N2}^2}m_2 + \frac{r_{21}^2}{r_{N3}^2}m_3 + \cdots + \frac{r_{21}^2}{r_{N,(N-1)}^2}m_{N-1}$$

where $\phi_1, \phi_2, \phi_3, \ldots, \phi_{N-1}$ are the perturbation coefficients associated with the respective $\vec{r}_{21}, \vec{\rho}_1, \vec{\rho}_2, \ldots, \vec{\rho}_{n-2}$ Jacoby coordinates.

Period ratios are another aspect of the first family collinear n-body solution and result as a function of using the sidereal synodic relations in solving the infinitesimal interval problem, with the number of ratio combinations determined by $\frac{(N-1)!}{2(N-3)!}$ for mass number N greater than or equal to three. The period ratio structure for the first family configurations are

$$\frac{P_3}{P_{21}} \quad \frac{P_4}{P_{21}} \quad \frac{P_5}{P_{21}} \cdots\cdots \frac{P_N}{P_{21}} \qquad \text{Equation 1.2.2}$$

$$\frac{P_4}{P_3} \quad \frac{P_5}{P_3} \cdots\cdots \frac{P_N}{P_3}$$

$$\frac{P_5}{P_4} \cdots\cdots \frac{P_N}{P_4}$$

$$\cdot \quad \cdot \quad \cdot$$

$$\frac{P_N}{P_{N-1}}$$

Collinear n-body period ratio solutions as structured in equation 1.2.2 and determined from the equations of motion as found described in equation1.2.1 are

$$\frac{P_A^2}{P_{21}^2} = \frac{\mu - \phi_1}{\phi_{A-1} + \frac{1}{\sum_{i=1}^{A} m_i} \sum_{i=1}^{n-A} m_{A+i} \phi_{A+i-1}} \frac{\sum_{i=1}^{A-1} m_i}{\sum_{i=1}^{A} m_i} l_{A-2} \qquad \text{Equation 1.2.3}$$

where $A \geq 3 \qquad A = 3, 4, 5, \ldots, N$

Additional period ratios are calculated from $\frac{P_A^2}{P_{21}^2}$ by systematically inverting and multiplying the ratios of each configuration set. For example, the five body first family configuration period ratios determined from equation 1.2.3 are $(\frac{P_3}{P_{21}}, \frac{P_4}{P_{21}}, \frac{P_5}{P_{21}})$ and after inverting and multiplying results $(\frac{P_4}{P_3}, \frac{P_5}{P_3}, \frac{P_5}{P_4})$ consistent with $\frac{(N-1)!}{2(N-3)!}$.

Perturbation coefficients ϕ_i in equation 1.2.3 as determined from first family collinear n-body solutions found in equation 1.2.1 are used to construct the instantaneous state vectors. Summary of first family perturbation coefficients from equation 1.2.1 in matrix format are listed below

$$\begin{pmatrix}\phi_1\\ \phi_2\\ \phi_3\\ \phi_4\\ .\\ \phi_\alpha\end{pmatrix} = r_{21}^2 \begin{pmatrix} ..0.. & ..0.. & e13 & e14 & e15 & ..... & e1n \\ e21 & e22 & ..0.. & e24 & e25 & ..... & e2n \\ e31 & e32 & e33 & ..0.. & e35 & ..... & e3n \\ e41 & e42 & e43 & e44 & ..0.. & ..... & e4n \\ ..... & ..... & ..... & ..... & ..... & ..... & ..... \\ e\alpha1 & e\alpha2 & e\alpha3 & e\alpha4 & e\alpha5 & ..... & ..0.. \end{pmatrix} \begin{pmatrix} m_1\\ m_2\\ m_3\\ m_4\\ m_5\\ .\\ m_n \end{pmatrix}$$

Equation 1.2.4

where $e21 = \frac{1}{r_{31}^2}$ $e22 = \frac{1}{r_{32}^2}$

$e31 = \frac{1}{r_{41}^2}$ $e32 = \frac{1}{r_{42}^2}$ $e33 = \frac{1}{r_{43}^2}$

$e41 = \frac{1}{r_{51}^2}$ $e42 = \frac{1}{r_{52}^2}$ $e43 = \frac{1}{r_{53}^2}$ $e44 = \frac{1}{r_{54}^2}$

$e\alpha1 = \frac{1}{r_{n1}^2}$ $e\alpha2 = \frac{1}{r_{n2}^2}$ $e\alpha3 = \frac{1}{r_{n3}^2}$ $e\alpha4 = \frac{1}{r_{n4}^2}$ $e\alpha5 = \frac{1}{r_{n5}^2}$

$e24 = -e33$ $e25 = -e43$ $e2n = -e\alpha3$

$e35 = -e44$ $e3n = -e\alpha4$

$e4n = -e\alpha5$

$e13 = e22 - e21$ $e14 = e32 - e31$ $e15 = e42 - e41$ $e1n = e\alpha2 - e\alpha1$

$$\alpha = n - 1$$

First row double zeros in the equation 1.2.4 perturbation matrix denote a physical Jacoby binary coupling between mass one and mass two. In general, double zeros in the perturbation matrix denote mass coupling in hierarchical families.

Scalar position differences r_{jk} from equation 1.2.4 determined from the n-body configuration geometry can be expressed

$$\frac{r_{21}}{r_{31}} = \frac{1}{x_1+1}, \ldots\ldots\ldots\ldots, \frac{r_{21}}{r_{n1}} = \frac{1}{x_{n-2}+1} \qquad \text{Equation 1.2.5}$$

$$\frac{r_{21}}{r_{32}} = \frac{1}{x_1}, \ldots\ldots\ldots\ldots, \frac{r_{21}}{r_{n2}} = \frac{1}{x_{n-2}}$$

$$\frac{r_{21}}{r_{43}} = \frac{1}{x_2 - x_1}, \ldots\ldots\ldots\ldots, \frac{r_{21}}{r_{n3}} = \frac{1}{x_{n-2} - x_1}$$

$$\frac{r_{21}}{r_{54}} = \frac{1}{x_3 - x_1}, \ldots\ldots\ldots\ldots, \frac{r_{21}}{r_{n4}} = \frac{1}{x_{n-2} - x_2}$$

$$\frac{r_{21}}{r_{n,n-1}} = \frac{1}{x_{n-2} - x_{n-3}}$$

Distance between masses m_2m_3, m_2m_4, m_2m_5,…,m_2m_n is defined to be $x_1, x_2, x_3, \ldots, x_{n-2}$ respectively.

Scaling parameters $l_1, \ldots, l_{n-2}$ in equation 1.2.3 determined from the scalar configuration geometry are defined as follows

$$\rho_1 = l_1 r_{21}, \rho_2 = l_2 r_{21}, \ldots, \rho_{n-2} = l_{n-2} r_{21} \qquad \text{Equation 1.2.6}$$

where

$$l_1 = x_1 + \frac{m_1}{\mu_1}$$

$$l_2 = x_2 - \frac{m_3}{\mu_2} x_1 + \frac{m_1}{\mu_2}$$

$$l_3 = x_3 - \frac{m_4}{\mu_3} x_2 - \frac{m_3}{\mu_3} x_1 + \frac{m_1}{\mu_3}$$

.

$$l_{n-2} = x_{n-2} + \frac{1}{\sum_{i=1}^{n-1} m_i} \left(m_1 - \sum_{i=1}^{n-3} m_{i+2}\, x_i\right)$$

$$\mu_i = \sum_{i=1}^{n-1} m_i \qquad n \geq 3$$

The three-dimensional first family collinear state vector solution defined in the infinitesimal interval at time zero is presented below and is a line of nodes solution defined in the barycentric inertial coordinate system. Required inputs are configuration masses, perturbation coefficients, inertial velocities, Jacoby coordinates and inclination angles.

$$x_1 = -\frac{m_2}{\mu_1} r_{21} - \frac{m_3}{\mu_2} \rho_1 - X \qquad \dot{x}_1 = 0 \qquad 1.2.7$$

$$y_1 = 0 \qquad \dot{y}_1 = -\frac{m_2}{\mu_1} V_{r_{21}} cosi_{r_{21}} - \frac{m_3}{\mu_2} V_{\rho_1} cosi_{\rho_1} - \dot{Y}$$

$$z_1 = 0 \qquad \dot{z}_1 = -\frac{m_2}{\mu_1} V_{r_{21}} sini_{r_{21}} - \frac{m_3}{\mu_2} V_{\rho_1} sini_{\rho_1} - \dot{Z}$$

$$x_2 = \frac{m_1}{\mu_1} r_{21} - \frac{m_3}{\mu_2} \rho_1 - X \qquad \dot{x}_2 = 0$$

$$y_2 = 0 \qquad \dot{y}_2 = \frac{m_1}{\mu_1} V_{r_{21}} cosi_{r_{21}} - \frac{m_3}{\mu_2} V_{\rho_1} cosi_{\rho_1} - \dot{Y}$$

$$z_2 = 0 \qquad \dot{z}_2 = \frac{m_1}{\mu_1} V_{r_{21}} sini_{r_{21}} - \frac{m_3}{\mu_2} V_{\rho_1} sini_{\rho_1} - \dot{Z}$$

$$x_3 = \frac{\mu_1}{\mu_2} \rho_1 - X \qquad \dot{x}_3 = 0$$

$$y_3 = 0 \qquad \dot{y}_3 = \frac{\mu_1}{\mu_2} V_{\rho_1} cosi_{\rho_1} - \dot{Y}$$

$$z_3 = 0 \qquad \dot{z}_3 = \frac{\mu_1}{\mu_2} V_{\rho_1} sini_{\rho_1} - \dot{Z}$$

$$x_{n-\lambda} = Q\rho_{n-\lambda-2} - R\rho_{n-i+1} \qquad \dot{x}_{n-\lambda} = 0$$

$$y_{n-\lambda} = 0 \qquad \dot{y}_{n-\lambda} = QV_{\rho_{n-\lambda-2}} cosi_{n-\lambda-2} - RV_{n-i-1} cosi_{n-i+1}$$

$$z_{n-\lambda} = 0 \qquad \dot{z}_{n-\lambda} = QV_{\rho_{n-\lambda-2}} sini_{n-\lambda-2} - RV_{n-i-1} sini_{n-i+1}$$

where $X = \sum_{i=1}^{n-3} \frac{m_{i+3}}{\sum_{j=1}^{i+3} m_j} \rho_{i+1}$ $\dot{Y} = \sum_{i=1}^{n-3} \frac{m_{i+3}}{\sum_{j=1}^{i+3} m_j} V_{\rho_{i+1}} cosi_{\rho_{i+1}}$

$$\dot{Z} = \sum_{i=1}^{n-3} \frac{m_{i+3}}{\sum_{j=1}^{i+3} m_j} V_{\rho_{i+1}} sini_{\rho_{i+1}}$$

$$Q = \frac{\sum_{i=1}^{n-\lambda-1} m_i}{\sum_{i=1}^{n-\lambda} m_i} \qquad R = \sum_{i=1}^{\lambda} \frac{m_{n-i+1}}{\sum_{j=1}^{n-i+1} m_j}$$

and $\lambda = 0, 1, 2, \ldots, n-4 \quad n \geq 4$

Collinear state vector instantaneous inclination angles $i_{r_{21}}, i_{\rho_1}, \ldots, i_{\rho_{n-2}}$ in equation 1.2.7 are relative to the velocities $V_{r_{21}}, V_{\rho_1}, \ldots, V_{\rho_{n-2}}$ in Jacoby r and

ρ coordinates. First family state vector velocities are calculated from the following equations

$$V_{r_{21}}^2 = \frac{G}{r_{21}}(\mu_{r_{21}} - \phi_1) \quad V_{\rho_j}^2 = \frac{G l_j^2}{\rho_j \sum_{i=1}^{j+1} m_i}(\phi_{j+1} \sum_{i=1}^{j+2} m_i + \sum_{k=j+3}^{n} m_k \phi_{k-1})$$

for $j = 1, 2, 3, \ldots, n-2$ Equation 1.2.8

The first family collinear state vector equations 1.2.7 are formulated relative to the three-body configuration. Any configurations greater than three-bodies will need to use the $n - \boldsymbol{\lambda}$ position and velocity coordinate equations. These state vector equations are only valid for the first family and not for the first family variations. Due to constraint conditions placed on this problem, the resultant state vectors when numerically integrated produce trajectories that are the most circular/least elliptical for that mass, position and velocity combination.

Kinetic and potential energy equations formulated for the first family are as follows

$$2T = \frac{m_1 m_2}{\mu} V_{r_{21}}^2 + \sum_{i=1}^{n-2} \frac{m_{i+2} \sum_{j=1}^{i+1} m_j}{\sum_{j=1}^{i+2} m_j} V_{\rho_i}^2 \qquad \text{Equation 1.2.9}$$

$$U = G \sum_{1 \le j < k \le n}^{n} \frac{m_j m_k}{r_{jk}}$$

All collinear configurations are consistent with conservation of energy where twice the kinetic energy is equal to the potential energy within the infinitesimal interval at time zero. This is realized for the first infinite family configurations when the velocity equations 1.2.8 are substituted into the energy equations 1.2.9 to show consistency with the conservation laws. Conservation of energy for the first family can also be verified by use of the Lagrange-Jacoby identity $\ddot{I} = 2T - U$. Where I is the moment of inertia and defined to be

$$I = \frac{1}{2} \sum_k m_k r_k^2$$

Since distance within the infinitesimal interval for the n-body configurations at time zero is constant, the second derivative of the moment of inertia is zero and therefore twice the kinetic energy will be equal to the potential energy, thus, giving the expected result.

1.3 Infinite Binary Configurations

Any family of configurations in the mathematical logical system should be solvable in the manner presented in subsection 1.2 using Jacoby coordinates with the sidereal synodic relations and type one geometry in the infinitesimal interval at time zero. Hierarchical solutions can also be constructed between families by grouping binary, trinary, quadruple etc. configurations in the proper order under the same constraints. In this section the collinear infinite binary solution will be presented, that is, formatting the collinear n-body equations of motion in terms of double binary, triple binary, quadruple binary etc. configurations. Jacoby coordinates will be designated by $r1, r2, \ldots rN$ for each binary subsystem with the Jacoby coordinates $\rho 1, \rho 2, \ldots \rho(N-1)$ designate the distance between the binary centers of gravity. The vector between the binary center of gravity is also a binary subsystem.

Infinite binary collinear equations of motion in the complex plane describing infinitesimal rotations in the infinite interval at time zero, are listed below. These coupled binary equations of motion will be used to determine the perturbation coefficients, inertial velocities, period ratios and state vectors for the infinite binaries.

$$\ddot{z}_{21} + 2wi\acute{z}_{21} - w^2 z_{21} = -\frac{G\mu_{r1}}{r_{21}^3} z_{21} + \frac{Gm_3}{r_{32}^3} z_{32} - \frac{Gm_3}{r_{31}^3} z_{31} + \cdots + \frac{Gm_n}{r_{n,2}^3} z_{n,2} - \frac{Gm_n}{r_{n,1}^3} z_{n,1}$$

$$\ddot{z}_{43} + 2wi\acute{z}_{43} - w^2 z_{43} = -\frac{G\mu_{r2}}{r_{43}^3} z_{43} + \frac{Gm_1}{r_{14}^3} z_{14} - \frac{Gm_1}{r_{13}^3} z_{13} + \cdots + \frac{Gm_n}{r_{n,4}^3} z_{n,4} - \frac{Gm_n}{r_{n,3}^3} z_{n,3}$$

$$\ddot{z}_{65} + 2wi\acute{z}_{65} - w^2 z_{65} = -\frac{G\mu_{r3}}{r_{65}^3} z_{65} + \frac{Gm_1}{r_{16}^3} z_{16} - \frac{Gm_1}{r_{15}^3} z_{15} + \cdots + \frac{Gm_n}{r_{n,6}^3} z_{n,6} - \frac{Gm_n}{r_{n,5}^3} z_{n,5}$$

$$\ddot{z}_{n,(n-1)} + 2wi\acute{z}_{n,(n-1)} - w^2 z_{n,(n-1)} = -\frac{G\mu_{rN}}{r_{n,(n-1)}^3} z_{n,(n-1)} + \frac{Gm_1}{r_{1,n}^3} z_{1,n} - \frac{Gm_1}{r_{1,(n-1)}^3} z_{1,(n-1)} + \cdots + \frac{Gm_{n-2}}{r_{(n-2),n}^3} z_{(n-2),n} - \frac{Gm_{n-2}}{r_{(n-2),(n-1)}^3} z_{(n-2),(n-1)}$$

The initial equations of motion using equation 1.1.1 have been reduced by a factor of two by converting to Jacoby coordinates where $\ddot{z}_{21}, \ddot{z}_{43}, \ldots, \ddot{z}_{n(n-1)}$ represents this coupling. Total mass number is represented by n (even) and total binary number by N ($n = 2N$) with mass sums $\mu_{rN} = m_{2N-1} + m_{2N}$. The $r_{21}, r_{43}, \quad r_{n,n-1}$ Jacoby coordinates will be referenced as $r1, r2, \ldots rN$ in future equations.

Sidereal synodic relations in equation 1.1.2 have been reformatted to apply to the infinite binary configurations. They are more complex than first family n-body configurations due to the intricate nature of the binary geometry. Differentiation is made between r binaries and ρ binaries when writing out the sidereal synodic relations, where P_{ri} represents the period of the ri binary subsystem and $P_{\rho i}$ represents the period of the vector between the ri binary centers of gravity. Infinite binary sidereal synodic relations can be written as designated below where N indicates the number of binaries in a given configuration.

$$n_{\rho(N-1)}P_{\rho(N-1)} = (n_{\rho(N-1)} + n_{rN})P_{rN} \qquad \text{Equation 1.3.1}$$

$$n_{\rho(N-1)}P_{\rho(N-1)} = (n_{\rho(N-1)} + n_{\rho(N-2)})P_{\rho(N-2)}$$

$$n_{\rho(N-1)}P_{\rho(N-1)} = (n_{\rho(N-1)} + n_{\rho(N-2)} + n_{r(N-1)})P_{r(N-1)}$$

$$n_{\rho(N-1)}P_{\rho(N-1)} = (n_{\rho(N-1)} + n_{\rho(N-2)} + n_{\rho(N-3)})P_{\rho(N-3)}$$

$$n_{\rho(N-1)}P_{\rho(N-1)} = (n_{\rho(N-1)} + n_{\rho(N-2)} + \cdots + n_{\rho 1} + n_{r(N-2)})P_{r(N-2)}$$

$$n_{\rho(N-1)}P_{\rho(N-1)} = (n_{\rho(N-1)} + n_{\rho(N-2)} + \cdots + n_{\rho 1})P_{\rho 1)}$$

.

$$.n_{\rho(N-1)}P_{\rho(N-1)} = (n_{\rho(N-1)} + n_{\rho(N-2)} + \cdots + n_{\rho 1} + n_{r2})P_{r2}$$

$$n_{\rho(N-1)}P_{\rho(N-1)} = (n_{\rho(N-1)} + n_{\rho(N-2)} + \cdots + n_{\rho 1} + n_{r1})P_{r1}$$

The double binary subsystem has two r and one ρ Jacoby coordinates, triple binary subsystem has three r and two ρ Jacoby coordinates, quadruple binary subsystem has four r and three ρ Jacoby coordinates etc., where this geometry is incorporated in equation 1.3.1. Terms used in the sidereal synodic period relations and their coefficients are defined

P_{r1} period of first binary subsystem (mass one mass two)

P_{r2} period of second binary subsystem (mass three mass four)

P_{rN} period of N^{th} binary subsystem

$P_{\rho 1}$ period of double binary subsystem (m_1m_2 *and* m_3m_4 center of gravity distance)

$P_{\rho 2}$ period of triple binary subsystem (m_1m_2 *and* m_3m_4 center of gravity distance to m_5m_6)

$P_{\rho(N-1)}$ period of $\rho(N-1)^{th}$ binary subsystem

It is necessary to diagram the vector binary geometry structure to identify rotating vectors in the complex plane. Formulating these rotating vectors as exponentials to substitute into the coupled equations of motion with the sidereal synodic relations (equation 1.3.1) and type one geometry will result in a collinear solution. To start this process for example, the rotating Jacoby coordinate z_{21} relative to the x' axis can be formulated

$$z_{21} = r1e^{i\frac{n_{\rho(N-2)}+\cdots+n_{\rho 1}+n_{r1}}{n_{\rho(N-1)}}wt} \qquad \text{Equation 1.3.2}$$

Substituting the first and second derivatives of equation 1.3.2 with respect to time into the $\ddot{z}_{21}$ equation of motion and using the vector configuration geometry will give after analysis

$$\frac{G\mu_{r1}}{w^2r_{21}^3} - \frac{P_{N-1}^2}{P_{21}^2} = \frac{G}{w^2r_{21}^3}\left(\left(\frac{r_{21}^2}{r_{32}^2} - \frac{r_{21}^2}{r_{31}^2}\right)m_3 + \left(\frac{r_{21}^2}{r_{42}^2} - \frac{r_{21}^2}{r_{41}^2}\right)m_4 + \cdots + \left(\frac{r_{21}^2}{r_{n2}^2} - \frac{r_{21}^2}{r_{n1}^2}\right)m_n\right) = \frac{G}{w^2r_{21}^3}\phi_{r1} \qquad \text{Equation 1.3.3}$$

where $\phi_{r1} = \left(\frac{r_{21}^2}{r_{32}^2} - \frac{r_{21}^2}{r_{31}^2}\right)m_3 + \left(\frac{r_{21}^2}{r_{42}^2} - \frac{r_{21}^2}{r_{41}^2}\right)m_4 + \cdots + \left(\frac{r_{21}^2}{r_{n2}^2} - \frac{r_{21}^2}{r_{n1}^2}\right)m_n$

(no $r1$ binary terms)

Continuing this derivation with the acceleration vectors $\ddot{z}_{43}$, $\ddot{z}_{65}$,… $\ddot{z}_{n(n-1)}$ will yield the complete set of $\phi_{ri}{}'s$ using the z_{43}, z_{65}, , $z_{n,n-1}$ rotating Jacoby coordinates with the sidereal synodic relations (equation 1.3.1) to find the velocities for the infinite binary state vectors.

$$\phi_{r2} = \left(\frac{r_{21}^2}{r_{41}^2} - \frac{r_{21}^2}{r_{31}^2}\right) m_1 + \left(\frac{r_{21}^2}{r_{42}^2} - \frac{r_{21}^2}{r_{32}^2}\right) m_2 + \cdots + \left(\frac{r_{21}^2}{r_{n3}^2} - \frac{r_{21}^2}{r_{n4}^2}\right) m_n.$$

$$\phi_{r3} = \left(\frac{r_{21}^2}{r_{61}^2} - \frac{r_{21}^2}{r_{51}^2}\right) m_1 + \left(\frac{r_{21}^2}{r_{62}^2} - \frac{r_{21}^2}{r_{52}^2}\right) m_2 + \cdots + \left(\frac{r_{21}^2}{r_{n5}^2} - \frac{r_{21}^2}{r_{n6}^2}\right) m_n$$

$$\phi_{rN} = \left(\frac{r_{21}^2}{r_{61}^2} - \frac{r_{21}^2}{r_{51}^2}\right) m_1 \left(\frac{r_{21}^2}{r_{62}^2} - \frac{r_{21}^2}{r_{52}^2}\right) m_2 + \ldots + \left(\frac{r_{21}^2}{r_{n,(n-2)}^2} - \frac{r_{21}^2}{r_{(n-1),(n-2)}^2}\right) m_{n-2}$$

. Equation 1.3.4

where ϕ_{r1}, ϕ_{r2}, ϕ_{r3},…, ϕ_{rN} are the perturbation coefficients associated with the respective $r1, r2, r3, \ldots, rN$ Jacoby coordinates. Perturbation coefficient ϕ_{r2} has no $,r2$ binary terms, ϕ_{r3} has no $r3$ binary terms and ϕ_{rN} has no rN binary terms.

To find the perturbation coefficients of the infinite binary subsystems $\rho 1, \rho 2, \ldots \rho(N-1)$ that are between the binary centers of gravity, the equations of motion will be in terms of the vector from the barycenter to the given binary subsystem center. The equation of motion for the Jacoby coordinate $\rho 1$ between the first binary $r1$ and the second binary $r2$ can be derived by using $z_{43c} = \frac{m_3 z_3 + m_4 z_4}{\mu_{r2}}$, which is the vector from the barycenter to the center of gravity of the mass three and mass four binary subsystem. This $\rho 1$ equation of motion can also be obtained by following a different vector path, that is, by using $z_{21c} = \frac{m_1 z_1 + m_2 z_2}{\mu_{r1}}$, which is the vector from the barycenter to the center of gravity of the mass one and mass two binary subsystem. Either vector pathway calculation will give the correct answer for the perturbation coefficient. There is no Gm_3 or Gm_4 multiplier in the following equation

$$\ddot{z}_{43c} + 2wi\acute{z}_{43c} - w^2 z_{43c} = \frac{Gm_1}{\mu_{r2}}\left(\frac{m_3}{r_{13}^3} z_{13} + \frac{m_4}{r_{14}^3} z_{14}\right) + \frac{Gm_2}{\mu_{r2}}\left(\frac{m_3}{r_{23}^3} z_{23} + \frac{m_4}{r_{24}^3} z_{24}\right) + \cdots + \frac{Gm_n}{\mu_{r2}}\left(\frac{m_3}{r_{n3}^3} z_{n3} + \frac{m_4}{r_{n4}^3} z_{n4}\right)$$

Equation 1.3.5

The equation of motion for Jacoby coordinate $\rho 2$, the vector between the center of gravity of the double binary subsystem $r1$, $r2$ and the center of gravity of $r3$ can be derived by using $z_{65c} = \frac{m_5 z_5 + m_6 z_6}{\mu_{r3}}$ which is the vector from the barycenter to the center of gravity of the mass five and mass six

binary subsystem. There is no Gm_5 or Gm_6 multiplier in the following equation

$$\ddot{z}_{65c} + 2wi\acute{z}_{65c} - w^2 z_{65c} = \frac{Gm_1}{\mu_{r3}}\left(\frac{m_5}{r_{15}^3}z_{15} + \frac{m_6}{r_{16}^3}z_{16}\right) + \frac{Gm_2}{\mu_{r3}}\left(\frac{m_5}{r_{25}^3}z_{25} + \frac{m_6}{r_{26}^3}z_{26}\right) + \cdots + \frac{Gm_n}{\mu_{r3}}\left(\frac{m_5}{r_{n5}^3}z_{n5} + \frac{m_6}{r_{n6}^3}z_{n6}\right)$$

Equation 1.3.6

Equation of motion for Jacoby coordinate $\rho(N-1)$, the vector between center of gravity of the $N-1$ binary sub-configuration and the center of gravity of the rN binary can be derived by using equation $z_{n,(n-1)c} = \frac{m_{n-1}z_{n-1}+m_n z_n}{\mu_{rN}}$ which is the vector from the barycenter to the center of gravity of the rN binary subsystem. There is no Gm_{n-1} or Gm_n multiplier in the following equation

$$\ddot{z}_{n,(n-1)c} + 2wi\acute{z}_{n,(n-1)c} - w^2 z_{n,(n-1)c} = \qquad \text{Equation 1.3.7}$$

$$\frac{Gm_1}{\mu_{rN}}\left(\frac{m_{n-1}}{r_{1,(n-1)}^3}z_{1,(n-1)} + \frac{m_n}{r_{1,n}^3}z_{1,n}\right) + \frac{Gm_2}{\mu_{rN}}\left(\frac{m_{n-1}}{r_{2,(n-1)}^3}z_{2,(n-1)} + \frac{m_n}{r_{2,n}^3}z_{2,n}\right) + \cdots + \frac{Gm_{n-2}}{\mu_{rN}}\left(\frac{m_{n-1}}{r_{(n-2),(n-1)}^3}z_{(n-2),(n-1)} + \frac{m_n}{r_{(n-2),n}^3}z_{(n-2),n}\right)$$

Infinitesimal rotating vectors z_{43c}, z_{65c}, , $z_{n(n-1)c}$ derived from the binary geometry (equation 1.3.2) when substituted into the acceleration vectors $\ddot{z}_{43c}$, $\ddot{z}_{65c}$,…, $\ddot{z}_{n(n-1)c}$ will give the $\phi_{\rho i}{}'s$ necessary to find the Jacoby velocities for the infinite binary state vectors. Summarizing the perturbation coefficient results from equations 1.3.5, 1.3.6 and 1.3.7 yields

$$\phi_{\rho 1} = \frac{r_{21}^2}{\mu_{r2}}\sum_{i=1}^{2}\left(\frac{m_4}{r_{4i}^2} + \frac{m_3}{r_{3i}^2}\right)m_i - \frac{r_{21}^2}{\mu_{r2}}\sum_{i=5}^{n}\left(\frac{m_4}{r_{4i}^2} + \frac{m_3}{r_{3i}^2}\right)m_i \qquad \text{Equation 1.3.8}$$

$$\phi_{\rho 2} = \frac{r_{21}^2}{\mu_{r3}}\sum_{i=1}^{4}\left(\frac{m_6}{r_{6i}^2} + \frac{m_5}{r_{5i}^2}\right)m_i - \frac{r_{21}^2}{\mu_{r3}}\sum_{i=7}^{n}\left(\frac{m_6}{r_{6i}^2} + \frac{m_5}{r_{5i}^2}\right)m_i$$

$$\phi_{\rho 3} = \frac{r_{21}^2}{\mu_{r4}}\sum_{i=1}^{6}\left(\frac{m_8}{r_{8i}^2} + \frac{m_7}{r_{7i}^2}\right)m_i - \frac{r_{21}^2}{\mu_{r4}}\sum_{i=9}^{n}\left(\frac{m_8}{r_{8i}^2} + \frac{m_7}{r_{7i}^2}\right)m_i$$

$$\phi_{\rho(N-1)} = \frac{r_{21}^2}{\mu_{r4}}\sum_{i=1}^{n-2}\left(\frac{m_n}{r_{ni}^2} + \frac{m_{n-1}}{r_{(n-1)i}^2}\right)m_i$$

where $\phi_{\rho 1}, \phi_{\rho 2}, \phi_{\rho 3}, \ldots, \phi_{\rho(N-1)}$ are the perturbation coefficients associated with the respective $\vec{\rho}_1, \vec{\rho}_2, \vec{\rho}_2, \ldots, \vec{\rho}_{n-1}$ Jacoby coordinates. Parameter n is the total number of masses and N is the total number of binaries with $N = \frac{n}{2}$ for $n \geq 4$ and N even. Binary masses are summed $\mu_{r1} = m_1 + m_2$, $\mu_{r2} = m_3 + m_{4,}, \ldots, \mu_{rN} = m_{2N-1} + m_{2N,}$. The x' axis is defined to be from the configuration barycenter to the center of gravity of the N^{th} binary rotating relative to the x axis at inertial velocity w in the infinitesimal interval.

Equation 1.3.1 sidereal synodic relations in conjunction with knowledge of equations 1.3.3, 1.3.4 and 1.3.8 perturbation coefficients result in determination of the binary period ratios. These period ratios numbering $\frac{(n-1)!}{2(n-3)!}$ where n is the number of masses, can be structured in the following manner as presented below

$$\frac{P_{r2}}{P_{r1}} \quad \frac{P_{\rho 1}}{P_{r1}} \quad \frac{P_{\rho 2}}{P_{r1}} \ldots\ldots\ldots\ldots\ldots \frac{P_{rN}}{P_{r1}} \qquad \text{Equation 1.3.9}$$

$$\frac{P_{\rho 1}}{P_{r2}} \quad \frac{P_{\rho 2}}{P_{r2}} \ldots\ldots\ldots\ldots \frac{P_{rN}}{P_{r2}}$$

$$\frac{P_{\rho 2}}{P_{\rho 1}} \ldots\ldots\ldots\ldots \frac{P_{rN}}{P_{\rho 1}}$$

$$\cdot \quad \cdot \quad \cdot$$

$$\frac{P_{rN}}{P_{\rho(N-1)}}$$

The individual binary periods for the $r1, r2, \ldots rN$ Jacoby coordinates as a function of the perturbation coefficients from equation 1.3.4 are

$$P_{r1}^2 = 4\pi^2 \left(\frac{r_{r1}^3}{G(\mu_{r1} - \phi_{r1})}\right) \qquad \text{Equation 1.3.10}$$

$$P_{r2}^2 = 4\pi^2 \left(\frac{r_{r2}^3}{G(\mu_{r2} - \Phi_{r2})}\right)$$

$$P_{rN}^2 = 4\pi^2 \left(\frac{r_{rN}^3}{G(\mu_{rN} - \Phi_{rN})}\right) \qquad \Phi_{rN} = x_{N-1}^2 \phi_{rN}$$

$$N \geq 2 \qquad N \text{ is even}$$

$$x_1 = \frac{r2}{r1} \qquad x_2 = \frac{r3}{r1} \qquad x_3 = \frac{r4}{r1} \qquad x_n = \frac{r(n+1)}{r1}$$

where $\mu_{r1} = m_1 + m_2, \quad \mu_{r2} = m_3 + m_{4,}, \ldots \mu_{rN} = m_{2N-1} + m_{2N}$. Parameter ϕ is the perturbation coefficient and scaling factor x is the $r1, r2, \ldots rN$ binary separation distance ratioed to $r1$.

The corresponding periods for the $\rho 1, \rho 2, \ldots \rho(N-1)$ Jacoby coordinates as a function of the perturbation coefficients from equation 1.3.8 are

$$P_{\rho 1}^2 = 4\pi^2\left(\frac{\rho_1^3}{G\frac{l_1^2}{\mu_{r1}}(\mu_{\rho 1}\phi_{\rho 1} + \mu_{r3}\phi_{\rho 2} + \cdots + \mu_{rN}\phi_{\rho(N-1)})}\right)$$

$$P_{\rho 2}^2 = 4\pi^2\left(\frac{\rho_2^3}{G\frac{l_2^2}{\mu_{\rho 1}}(\mu_{\rho 2}\phi_{\rho 2} + \cdots + \mu_{rN}\phi_{\rho(N-1)})}\right)$$

$$P_{\rho(N-1)}^2 = 4\pi^2\left(\frac{\rho_{N-1}^3}{G\frac{\mu_{\rho(N-1)}}{\mu_{\rho(N-2)}}l_{N-1}^2\phi_{\rho(N-1)}}\right) \qquad \text{Equation 1.3.11}$$

where $\mu_{\rho 1} = \mu_{r1} + \mu_{r2}$, $\mu_{\rho 2} = \mu_{r1} + \mu_{r2} + \mu_{r3}$, and $\mu_{\rho N} = \sum_{i=1}^{N+1} \mu_{ri}$

Summarizing $r1, r2, \ldots rN$ Jacoby perturbation coefficients from equations 1.3.3 and 1.3.4 in matrix format gives a visual interpretation of the binary structure. Double zeros in each row of the matrix demonstrate the location of every binary in this infinite N binary configuration.

$$\begin{pmatrix} \phi_{r1} \\ \phi_{r2} \\ \phi_{r3} \\ \phi_{r4} \\ . \\ \phi_{rN} \end{pmatrix} = r_{21}^2 B \begin{pmatrix} m_1 \\ m_2 \\ m_3 \\ m_4 \\ m_5 \\ m_6 \\ m_7 \\ m_8 \\ . \\ m_n \end{pmatrix}$$

$$B = \begin{pmatrix} ..0.. & ..0.. & e13 & e14 & e15 & e16 & e17 & e18 & & e1n \\ e21 & e22 & ..0.. & ..0.. & e25 & e26 & e27 & e28 & & e2n \\ e31 & e32 & e33 & e34 & ..0.. & ..0.. & e37 & e38 & & e3n \\ e41 & e42 & e43 & e44 & e45 & e46 & ..0.. & ..0.. & & e4n \\ & . & & & & & . & & & \\ eN1 & eN2 & eN3 & eN4 & e65 & e66 & e67 & e68 & ..0.. & ..0.. \end{pmatrix}$$

where

$$\phi_{r1} = r_{21}^2 \sum_{i=3}^{n} \left(\frac{1}{r_{2i}^2} - \frac{1}{r_{1i}^2}\right) m_i$$

$$\phi_{r2} = -r_{21}^2 \sum_{i=1}^{2} \left(\frac{1}{r_{4i}^2} - \frac{1}{r_{3i}^2}\right) m_i + r_{21}^2 \sum_{i=5}^{n} \left(\frac{1}{r_{4i}^2} - \frac{1}{r_{3i}^2}\right) m_i$$

$$\phi_{r3} = -r_{21}^2 \sum_{i=1}^{4} \left(\frac{1}{r_{6i}^2} - \frac{1}{r_{5i}^2}\right) m_i + r_{21}^2 \sum_{i=7}^{n} \left(\frac{1}{r_{6i}^2} - \frac{1}{r_{5i}^2}\right) m_i$$

$$\phi_{rN} = -r_{21}^2 \sum_{i=1}^{n-2} \left(\frac{1}{r_{ni}^2} - \frac{1}{r_{(n-1)i}^2}\right) m_i$$

Each term in the above ϕ_{rN} series corresponds to an element in the rN row. Summarized perturbation coefficients from equation 1.3.8 for the $\rho 1, \rho 2, \ldots \rho(N-1)$ Jacoby N binaries are presented below in matrix format. Double zeros show binary coupling existing in this matrix structure as well.

$$\begin{pmatrix} \phi_{\rho 1} \\ \phi_{\rho 2} \\ \phi_{\rho 3} \\ . \\ \phi_{\rho \beta} \end{pmatrix} = r_{21}^2 C \begin{pmatrix} m_1 \\ m_2 \\ m_3 \\ m_4 \\ m_5 \\ m_6 \\ m_7 \\ m_8 \\ . \\ m_n \end{pmatrix}$$

$$C = \begin{pmatrix} e11 & e12 & ..0.. & ..0.. & e15 & e16 & e17 & e18 & & e1n \\ e21 & e22 & e23 & e24 & ..0.. & ..0.. & e27 & e28 & & e2n \\ e31 & e32 & e33 & e34 & e35 & e36 & ..0.. & ..0.. & & e3n \\ & . & & & & & . & & & \\ e\beta 1 & e\beta 2 & e\beta 3 & e\beta 4 & e\beta 5 & e\beta 6 & e\beta 7 & e\beta 8 & ..0.. & ..0.. \end{pmatrix}$$

where

$$\phi_{\rho 1} = \frac{r_{21}^2}{\mu_{r2}} \sum_{i=1}^{2} \left(\frac{m_4}{r_{4i}^2} + \frac{m_3}{r_{3i}^2}\right) m_i - \frac{r_{21}^2}{\mu_{r2}} \sum_{i=5}^{n} \left(\frac{m_4}{r_{4i}^2} + \frac{m_3}{r_{3i}^2}\right) m_i$$

$$\phi_{\rho 2} = \frac{r_{21}^2}{\mu_{r3}} \sum_{i=1}^{4} \left(\frac{m_6}{r_{6i}^2} + \frac{m_5}{r_{5i}^2}\right) m_i - \frac{r_{21}^2}{\mu_{r3}} \sum_{i=7}^{n} \left(\frac{m_6}{r_{6i}^2} + \frac{m_5}{r_{5i}^2}\right) m_i$$

$$\phi_{\rho 3} = \frac{r_{21}^2}{\mu_{r4}} \sum_{i=1}^{6} \left(\frac{m_8}{r_{8i}^2} + \frac{m_7}{r_{7i}^2}\right) m_i - \frac{r_{21}^2}{\mu_{r4}} \sum_{i=9}^{n} \left(\frac{m_8}{r_{8i}^2} + \frac{m_7}{r_{7i}^2}\right) m_i$$

$$\phi_{\rho\beta} = \frac{r_{21}^2}{\mu_{rN}} \sum_{i=1}^{n-2} \left(\frac{m_n}{r_{ni}^2} + \frac{m_{n-1}}{r_{(n-1)i}^2}\right) m_i \qquad \beta = N-1$$

Each term in the above $\phi_{\rho(N-1)}$ series corresponds to an element in the $\rho(N-1)$ row.

The r_i and ρ_i Jacoby velocities compose part of the infinite binary solution sequenced in equations 1.3.2 through equation 1.3.8. These $r1, r2, \ldots rN$ Jacoby coordinate velocities $V_{r1}, V_{r2}, \ldots, V_{rN}$ are a function of the perturbation coefficients $\phi_{r1}, \phi_{r2} \ldots, \phi_{rN}$ that are input into the infinite binary state vectors

$$V_{r1}^2 = \frac{G}{r1}(\mu_{r1} - \phi_{r1}) \qquad \text{Equation 1.3.12}$$

$$V_{r2}^2 = \frac{G}{r2}(\mu_{r2} - \Phi_{r2})$$

.

$$V_{rN}^2 = \frac{G}{rN}(\mu_{rN} - \Phi_{rN}) \qquad \Phi_{rN} = x_{N-1}^2 \phi_{rN}$$

The $\rho 1, \rho 2, \ldots \rho(N-1)$ Jacoby coordinate velocities $V_{\rho 1}, V_{\rho 2}, \ldots, V_{\rho(N-1)}$ are a function of the perturbation coefficients $\phi_{\rho 1}, \phi_{\rho 2}, \ldots, \Phi_{\rho(N-1)}$ that complete the infinite binary velocity set.

$$V_{\rho 1}^2 = \frac{G}{\rho 1}\frac{l_1^2}{\mu_{r1}}(\mu_{\rho 1}\phi_{\rho 1} + \mu_{r3}\phi_{\rho 2} + \cdots + \mu_{rN}\phi_{\rho(N-1)})$$

$$V_{\rho 2}^2 = \frac{G}{\rho 2}\frac{l_2^2}{\mu_{\rho 1}}(\mu_{\rho 2}\phi_{\rho 2} + \cdots + \mu_{rN}\phi_{\rho(N-1)})$$

$$V_{\rho(N-1)}^2 = \frac{G}{\rho(N-1)}\frac{l_{N-1}^2}{\mu_{\rho(N-2)}}\mu_{\rho(N-1)}\phi_{\rho(N-1)} \qquad \text{Equation 1.3.13}$$

Scaling parameters for the infinite binary periods needed for input to equation1.3.11 and velocity $\rho 1, \rho 2, \ldots \rho(N-1)$ Jacoby coordinates needed for input to equation 1.3.13 are determined from the infinite collinear binary scalar geometry. Scalar geometry is diagrammed as a collinear plot that allows computation of the scaled distance ratios for every mass subsystem relative to every other mass subsystem at time zero. Mass scaling simplifies the relations in modelling collinear n-body solutions. The scaling parameters for the infinite binary are summarized below

$$\rho_1 = l_1 r_1 \quad \rho_2 = l_2 r_1 \quad \rho_3 = l_3 r_1 \quad \rho_{N-1} = l_{N-1} r_1 \qquad \text{Equation 1.3.14}$$

$$l_1 = x_N + \frac{m_1}{\mu_{r1}}$$

$$l_2 = x_{N+1} - \frac{\mu_{r2}}{\mu_{\rho 1}} x_N + \frac{m_1}{\mu_{\rho 1}}$$

$$l_3 = x_{N+2} - \frac{\mu_{r3}}{\mu_{\rho 2}} x_{N+1} - \frac{\mu_{r2}}{\mu_{\rho 2}} x_N + \frac{m_1}{\mu_{\rho 2}}$$

$$l_{N-1} = x_{2N-2} - \frac{\mu_{r(N-1)}}{\mu_{\rho(N-2)}} x_{2N-3} \ldots - \frac{\mu_{r2}}{\mu_{\rho(N-2)}} x_N + \frac{m_1}{\mu_{\rho(N-2)}}$$

The terms x_N, x_{N+1} etc. and l_1, l_2 etc. in equation 1.3.14 are $\rho 1, \rho 2, \ldots \rho(N-1)$ Jacoby coordinate scaling factors. They are evaluated from the infinite binary scalar geometry which is composed of Jacoby coordinates given as input by the analyst.

Infinite binary position differences used in the perturbation coefficients determined from the binary scalar geometry are evaluated in terms of Jacoby coordinates, mass fractions and scaling parameters from equation 1.3.14.

Equation 1.3.15

$$\frac{r_{31}}{r_{21}} = x_4 - B_1 + 1 \qquad \frac{r_{41}}{r_{21}} = x_4 + A_1 + 1$$

$$\frac{r_{32}}{r_{21}} = x_4 - B_1 \qquad \frac{r_{42}}{r_{21}} = x_4 + A_1$$

$$\frac{r_{51}}{r_{21}} = x_5 + 1 - B_2 \qquad \frac{r_{61}}{r_{21}} = x_5 + 1 + A_2$$

$$\frac{r_{52}}{r_{21}} = x_5 - B_2 \qquad \frac{r_{62}}{r_{21}} = x_5 + A_2$$

$$\frac{r_{53}}{r_{21}} = (x_5 - B_2) - (x_4 - B_1) \qquad \frac{r_{63}}{r_{21}} = (x_5 + A_2) - (x_4 - B_1)$$

$$\frac{r_{54}}{r_{21}} = (x_5 - B_2) - (x_4 + A_1) \qquad \frac{r_{64}}{r_{21}} = (x_5 + A_2) - (x_4 + A_1)$$

$$\frac{r_{71}}{r_{21}} = x_6 - B_3 + 1 \qquad \frac{r_{81}}{r_{21}} = x_6 + A_3 + 1$$

$$\frac{r_{72}}{r_{21}} = x_6 - B_3 \qquad \frac{r_{82}}{r_{21}} = x_6 + A_3$$

$$\frac{r_{73}}{r_{21}} = (x_6 - B_3) - (x_4 - B_1) \qquad \frac{r_{83}}{r_{21}} = (x_6 + A_3) - (x_4 - B_1)$$

$$\frac{r_{74}}{r_{21}} = (x_6 - B_3) - (x_4 + A_1) \qquad \frac{r_{84}}{r_{21}} = (x_6 + A_3) - (x_4 + A_1)$$

$$\frac{r_{75}}{r_{21}} = (x_6 - B_3) - (x_5 - B_2) \qquad \frac{r_{85}}{r_{21}} = (x_6 + A_3) - (x_5 - B_2)$$

$$\frac{r_{76}}{r_{21}} = (x_6 - B_3) - (x_5 + A_2) \qquad \frac{r_{86}}{r_{21}} = (x_6 + A_3) - (x_5 + A_2)$$

where $A_i = \frac{m_{2i+1}}{\mu_{r(1+i)}} x_i \qquad B_i = \frac{m_{2i+2}}{\mu_{r(1+i)}} x_i$

Scaling parameters $x_1 = \frac{r2}{r1}$, $x_2 = \frac{r3}{r1}$, $x_3 = \frac{r4}{r1}, \ldots, x_n = \frac{r(n+1)}{r1}$ are Jacoby $r1, r2, r3, \ldots, rN$ coordinates representing the binary separation distance relative to $r1$. The x_i scalar binary sequence for Jacoby $r1, r2, r3, \ldots, rN$ coordinates is $x_1, \ldots, x_{N-1}$ and for the Jacoby $\rho 1, \rho 2, \ldots \rho(N-1)$ coordinates is $x_N, \ldots, x_{2N-2}$.

The three-dimensional infinite binary collinear state vector solution defined in the infinitesimal interval at time zero is presented below and is a line of nodes solution defined in the barycentric inertial coordinate system. Required inputs are configuration masses, Jacoby coordinate distances, perturbation coefficients, scaling parameters, inertial velocities and inclination angles. Perturbation coefficients, scaling parameters and inertial velocities are determined from equations 1.3.2 through 1.3.8 and equations 1.3.12 through 1.3.15 respectively. Configuration masses, Jacoby coordinate distances and inclination angles are input by the analyst.

First Binary

$$x_1 = -\frac{m_2}{\mu_{r1}} r1 - \frac{\mu_{r2}}{\mu_{\rho 1}} \rho 1 - X \qquad \dot{x}_1 = 0 \qquad \text{Equation 1.3.16}$$

$$y_1 = 0 \qquad \dot{y}_1 = -\frac{m_2}{\mu_{r1}} V_{r1} cosi_{r1} - \frac{\mu_{r2}}{\mu_{\rho 1}} V_{\rho 1} cosi_{\rho 1} - \dot{Y}$$

$$z_1 = 0 \qquad \dot{z}_1 = -\frac{m_2}{\mu_{r1}} V_{r1} sini_{r1} - \frac{\mu_{r2}}{\mu_{\rho 1}} V_{\rho 1} sini_{\rho 1} - \dot{Z}$$

$$x_2 = \frac{m_1}{\mu_{r1}} r1 - \frac{\mu_{r2}}{\mu_{\rho 1}} \rho 1 - X \qquad \dot{x}_2 = 0$$

$$y_2 = 0 \qquad \dot{y}_2 = \frac{m_1}{\mu_{r1}} V_{r1} cosi_{r1} - \frac{\mu_{r2}}{\mu_{\rho 1}} V_{\rho 1} cosi_{\rho 1} - \dot{Y}$$

$$z_2 = 0 \qquad \dot{z}_2 = \frac{m_1}{\mu_{r1}} V_{r1} sini_{r1} - \frac{\mu_{r2}}{\mu_{\rho 1}} V_{\rho 1} sini_{\rho 1} - \dot{Z}$$

Second Binary

$$x_3 = -\frac{m_4}{\mu_{r2}} r2 + \frac{\mu_{r1}}{\mu_{\rho 1}} \rho 1 - X \quad \dot{x}_3 = 0$$

$$y_3 = 0 \qquad \dot{y}_3 = -\frac{m_4}{\mu_{r2}} V_{r2} cosi_{r2} + \frac{\mu_{r1}}{\mu_{\rho 1}} V_{\rho 1} cosi_{\rho 1} - \dot{Y}$$

$$z_3 = 0 \qquad \dot{z}_3 = -\frac{m_4}{\mu_{r2}} V_{r2} sini_{r2} + \frac{\mu_{r1}}{\mu_{\rho 1}} V_{\rho 1} sini_{\rho 1} - \dot{Z}$$

$$x_4 = \frac{m_3}{\mu_{r2}} r2 + \frac{\mu_{r1}}{\mu_{\rho 1}} \rho 1 - X \qquad \dot{x}_4 = 0$$

$$y_4 = 0 \qquad \dot{y}_4 = \frac{m_3}{\mu_{r2}} V_{r2} cosi_{r2} + \frac{\mu_{r1}}{\mu_{\rho 1}} V_{\rho 1} cosi_{\rho 1} - \dot{Y}$$

$$z_4 = 0 \qquad \dot{z}_4 = \frac{m_3}{\mu_{r2}} V_{r2} sini_{r2} + \frac{\mu_{r1}}{\mu_{\rho 1}} V_{\rho 1} sini_{\rho 1} - \dot{Z}$$

N^{th} Binary

$$x_{2N-1} = -\frac{m_{2N}}{\mu_{rN}} rN + \frac{\mu\rho(N-2)}{\mu\rho(N-1)} \rho(N-1) \qquad \dot{x}_{2N-1} = 0$$

$$y_{2N-1} = 0 \qquad \dot{y}_{2N-1} = -\frac{m_{2N}}{\mu_{rN}} V_{rN} cosi_{rN} + \frac{\mu\rho(N-2)}{\mu\rho(N-1)} V_{\rho(N-1)} cosi_{\rho(N-1)}$$

$$z_{2N-1} = 0 \qquad \dot{z}_{2N-1} = -\frac{m_{2N}}{\mu_{rN}} V_{rN} sini_{rN} + \frac{\mu\rho(N-2)}{\mu\rho(N-1)} V_{\rho(N-1)} sini_{\rho(N-1)}$$

$$x_{2N} = \frac{m_{2N-1}}{\mu_{rN}} rN + \frac{\mu\rho(N-2)}{\mu\rho(N-1)} \rho(N-1) \qquad \dot{x}_{2N} = 0$$

$$y_{2N} = 0 \qquad \dot{y}_{2N} = \frac{m_{2N-1}}{\mu_{rN}} V_{rN} cosi_{rN} + \frac{\mu\rho(N-2)}{\mu\rho(N-1)} V_{\rho(N-1)} cosi_{\rho(N-1)}$$

$$z_{2N} = 0 \qquad \dot{z}_{2N} = \frac{m_{2N-1}}{\mu_{rN}} V_{rN} sini_{rN} + \frac{\mu\rho(N-2)}{\mu\rho(N-1)} V_{\rho(N-1)} sini_{\rho(N-1)}$$

where

$$X = \sum_{i=1}^{N-2} \frac{\mu r(i+2)}{\mu \rho(i+1)} \rho(i+1) \qquad \dot{Y} = \sum_{i=1}^{N-2} \frac{\mu r(i+2)}{\mu \rho(i+1)} V_{\rho(i+1)} cosi_{\rho(i+1)}$$
$$\dot{Z} = \sum_{i=1}^{N-2} \frac{\mu r(i+2)}{\mu \rho(i+1)} V_{\rho(i+1)} sini_{\rho(i+1)}$$

The infinite binary collinear state vector equations 1.3.16 are formulated relative to the double binary configuration. Any binary configurations greater than double binary will need to use the x_{2N-1}, $\dot{x}_{2N-1}$, x_{2N}, $\dot{x}_{2N}$ etc. position and velocity binary coordinate equations. For example, when $N = 3$ the x_{2N-1}, $\dot{x}_{2N-1}$, x_{2N}, $\dot{x}_{2N}$ binary equations generate the position and velocity components for the mass five and mass six triple binary subsystem. The double binary components will then be updated using the X, $\dot{Y}$ and $\dot{Z}$ equations for $N = 3$. When $N = 4$, the x_{2N-1}, $\dot{x}_{2N-1}$, x_{2N}, $\dot{x}_{2N}$ equations generate the position and velocity components for the mass seven and mass eight quadruple binary subsystem. The triple binary components will be generated from the X, $\dot{Y}$ and $\dot{Z}$ equations for $N = 4$. This same process continues for higher tiered binary structures. Due to the constraint conditions placed on this problem, the resultant state vectors when numerically integrated produce trajectories that are the most circular/least elliptical for that mass, position and velocity distribution.

Infinite binary collinear configuration kinetic and potential energy equations are as follows

$$2T = \frac{m_1 m_2}{\mu_{r1}} V_{r_1}^2 + \frac{m_3 m_4}{\mu_{r2}} V_{r_2}^2 + \cdots + \frac{m_{2N-1} m_N}{\mu_{rN}} V_{r_N}^2 + \frac{\mu_{r1} \mu_{r2}}{\mu_{\rho 1}} V_{\rho 1}^2 + \frac{\mu_{r3} \mu_{\rho 1}}{\mu_{\rho 2}} V_{\rho 2}^2 + \ldots + \frac{\mu_{rN} \mu_{\rho(N-2)}}{\mu_{\rho(N-1)}} V_{\rho(N-1)}^2$$

$$U = G \sum_{1 \le j < k \le n}^{n} \frac{m_j m_k}{r_{jk}}$$

Infinite binary collinear configurations are consistent with conservation of energy meeting the condition twice the kinetic energy is equal to the potential energy within the infinitesimal interval at time zero for type one geometry.

1.4 Problems

Section 1.1

1. Show symbolically that the three-body configuration 123 has five variations as listed in equation 1.1.3. Also show symbolically, using the same method of equation 1.1.3 the existence of the six three-body mirror configurations.
2. By systematically interchanging the masses to the first ordered reference set in equation 1.1.4 as described in the text, complete the listing of the four body configurations to find all unique configurations.
3. Starting from the first set of four-body contiguous configurations in equation 1.1.4, form five-body contiguous configurations by adding a fifth mass to the right of the four-body contiguous configurations. This mass structured system will be populated by the three five-body configurations (and their variations) shown in equation 1.1.5.
4. Set up the seventh tier of masses using the same logic as in equation 1.1.5. Be careful to delineate the binary and trinary subsystems etc.

Section 1.2

1. Set up a vector diagram defining the geometry for a collinear 1234 four-body problem and verify equation 1.2.1. Find the three perturbation coefficients (ϕ_1, ϕ_2, ϕ_3) for this geometry.
2. For a given mass verify that the structure shown in equation 1.2.2. is consistent with the number of ratio combinations determined by $\frac{(N-1)!}{2(N-3)!}$ for $N \geq 3$.
3. Using equation 1.2.3 compute the period ratio equations for a 12345 five-body first family configuration. Find all the period ratios by systematically inverting and multiplying the ratios determined from equation 1.2.3. Verify the total number is consistent with $\frac{(N-1)!}{2(N-3)!}$ for $N \geq 3$.
4. Using a scalar diagram analogous to the vector diagram in problem one in this set compute the scalar position differences r_{jk} for the 12345 five-body first family configuration. Check results against equation 1.2.5 for consistency.
5. Using the same scalar diagram as in the previous problem find the scaling parameters l_1, l_2 and l_3 for the 12345 five-body first family configuration. These scaling parameters are derived and listed in equation 1.2.6.

6. Derive the kinetic energy formula in equation 1.2.9. Then write out the kinetic energy for the 12345 five-body first family configuration using the velocities derived in equations 1.2.8. Show for the 12345 configuration that twice the kinetic energy is equal to the potential energy.

Section 1.3

1. Verify the format of the infinite binary sidereal synodic relation structure in equation 1.3.1 by writing out the sidereal synodic relations for a triple binary and a quadruple binary configuration ($N = 3,4$).
2. Using the sidereal synodic relations of equation 1.3.1 formulate the Jacoby coordinates z_{43}, z_{65} and $z_{n,(n-1)}$ in the manner of equation 1.3.2. Take the first and second derivates of these vectors and substitute into the left side of the acceleration equations $\ddot{z}_{43}$, $\ddot{z}_{65}$,…, $\ddot{z}_{n(n-1)}$. The result should be in the form of the left side of equation 1.3.3.
3. Compute the binary perturbation coefficient ϕ_{r1} shown in equation 1.3.3 using the rotating z_{21} Jacoby coordinate exponential formulation. Will also need to use period ratios, scaling parameters, and binary position difference equations to solve this problem.
4. The $\phi_{\rho i}$'s are more difficult to determine resulting from their binary to binary center of gravity geometry. Using the vector from the barycenter to the center of gravity of the mass three and mass four binary system $z_{43c} = \frac{m_3 z_3 + m_4 z_4}{\mu_{r2}}$ verify equation1.3.5.
5. Vector from the infinite binary barycenter to the center of gravity of the rN binary subsystem is $z_{n,(n-1)c} = \frac{m_{n-1} z_{n-1} + m_n z_n}{\mu_{rN}}$. Verify equation 1.3.7 with $z_{n,(n-1)c}$ and show that the perturbation coefficient is $\phi_{\rho(N-1)}$ as determined in equation 1.3.8.
6. For a triple binary configuration derive the individual binary periods for the $r1, r2$ and $r3$ Jacoby coordinates (equation 1.3.10). Also derive the triple binary configuration velocities V_{r1}, V_{r2} and V_{r3} (equation 1.3.12).
7. Write out the three-dimensional triple binary state vector with the perturbation coefficients, scaling parameters and inertial velocities etc. Use equation 1.3.16 as a guide for this problem. Make a three-dimensional illustration of the triple binary state vector geometry.

1.5 References

Bauer, T. A., 2001, *Resonance Induced Coupled Planar N-Body Collinear Point Solutions*, AAS 01-201, Santa Barbara, CA, AAS/AIAA Space Flight Mechanics Meeting.

Besant, W. H., Ramsey, A. S., 1914, *A Treatise on Dynamics*, London, Bell and Sons.

Galiullin, A. S., 1984, *Inverse Problem of Dynamics*, Moscow, MIR Publishers.

Kurth, R., 1959, *Introduction to the Mechanics of the Solar System*, Oxford, Pergamon Press.

Lass, H., 1957, *Elements of Pure and Applied Mathematics*, New York, McGraw-Hill.

Lehnigh, S. H., 1966, *Stability Theorems for Linear Motions with an Introductions to Liapunov's Direct Method*, Englewood Cliffs, NJ, Prentice Hall.

Merkin, D. R., 1996, *Introduction to the Theory of Stability*, New York, Springer Verlag.

Pollard, H., 1966, *Mathematical Introduction to Celestial Mechanics*, Englewood Cliffs, NJ, Prentice Hall.

Ramsey, A. S., 1929, *Dynamics*, London, Cambridge at the University Press.

Roy, A. E., 1988, *Orbital Motion*, Bristol, Institute of Physics Publishing.

Santilli, R. M., 1978, *Foundations of Theoretical Mechanics I-The inverse Problem in Newtonian Mechanics*, New York, Springer-Verlag.

Szebehely, V. G., 1967, *Theory of Orbits*, New York, Academic Press.

Wintner, A., 1964, *The Analytical Foundations of Celestial Mechanics*, Princeton NJ, Princeton University Press.

CHAPTER TWO

COLLINEAR N-BODY PROBLEM—APPLICATIONS

Chapter one dealt with presenting the collinear n-body mathematical logical system and its three-dimension solution of the equations of motion resulting in period ratios, perturbation coefficients, inertial velocities and state vectors within an infinitesimal interval. Theoretically all configurations in the mathematical logical system can be solved using the infinitesimal interval with type one geometry and sidereal synodic relations at time zero. Determining solutions of these tiered configurations was restricted to infinite first family and the infinite binary systems for they are representative to a good extent of the collinear n-body configurations in general. Chapter two is an extension of chapter one where selected configurations are taken from the infinite first family and the infinite binary configuration solutions to study their particle structure. Although collinear n-body solutions exist over an infinitesimal interval, they reveal crucial information regarding aspects of particle motion and trajectory evolution.

Specifically, on close examination of the period ratio structure of individual configurations, regions exist, such as possible spheres of influence, that appear to bound particle motion. Other period ratio analysis when using contiguous configurations reveals Euler points as well as resonance structure as a function of the individual masses. Configuration plots using period ratio information allow identification of the important regions to investigate. Points taken from these interesting regions (configuration space into phase space) determine state vectors, which when numerical integrated, do show relatively stable, relatively unstable, very unstable and escape orbit trajectories. Period ratios also give a measure of finite stability for subset configurations. For example, rather than compute stability for all time in the sense of Lagrange or Lyapunov considering the entire configuration, it is constructive to look at the binary or trinary sub-components in the configuration of interest. Stability in the sense of Lagrange or Lyapunov analysis will more than likely give an instability for all time result. Since a configuration deemed unstable can be stable for finite

periods, it would be of interest to know approximately when that configuration/sub-configuration ceases to maintain its structure. Lagrange or Lyapunov stability will not be of help to determine how long a multiple particle system can be finite stable. The infinitesimal interval method cannot determine periods of finite stability, however, it can show configuration structure that is in finite stable regions. Numerical integration of state vectors in these finite stable regions will confirm this.

2.1 Three Body Configurations

Infinite first collinear family was solved in chapter one. The first member of this family and the most fundamental is the three-body problem 123. There are five additional variations where all six three-body configurations possess one r and one ρ Jacoby coordinate. General structure of these three-body variations is represented symbolically in equation 1.1.3 where each of the six configurations when mathematically analyzed results in a quintic polynomial. The 123 solution from the previous chapter will be analyzed in more detail in this chapter in addition to solving the three-body variations for the purpose of showing configuration continuity. Solving these configurations in the infinitesimal interval at time zero with type one geometry will initially require the sidereal synodic relations of equation 1.1.2. Starting with the 123 three-body configuration

$$n_{\rho 1}P_{\rho 1} = (n_{\rho 1} + n_{r1})P_{r1} \qquad \text{Equation 2.1.1}$$

First binary notation will vary where r_{21}, $r1$ and r_{r_1} represent the same quantity. The collinear coupled equations of motion in the complex plane are

$$\ddot{z}_{r1} + 2wi\dot{z}_{r1} - w^2 z_{r1} = -\frac{G\mu_{r1}}{r_{r1}^3}z_{r1} + \frac{Gm_3}{r_{32}^3}z_{32} - \frac{Gm_3}{r_{31}^3}z_{31} \qquad \text{Equation 2.1.2}$$

$$w^2 z_3 = \frac{Gm_1}{r_{13}^3}z_{13} + \frac{Gm_2}{r_{23}^3}z_{23}$$

The vector z_3 is on the x' axis rotating at angular velocity w with respect to the inertial x axis and this therefore results in $\ddot{z}_3$ and $\dot{z}_3$ equaling zero.

Formulating the rotating Jacoby coordinate z_{r1} in the infinitesimal interval using the sidereal synodic relations gives

$$z_{r1} = r1e^{i\frac{n_{r1}}{n_{\rho 1}}wt} \qquad \text{Equation 2.1.3}$$

where z_{r1} is rotating relative to the x' axis by $\frac{n_{r1}}{n_{\rho 1}}w$. Taking the second time derivative of equation 2.1.3 and substituting into equation 2,1,2 gives for the $\ddot{z}_{r1}$ equation of motion

$$\left(\frac{G}{w^2 r_{r1}^3}\mu_{r1} - \frac{P_{\rho 1}^2}{P_{r1}^2}\right) z_{r1} = \frac{G}{w^2 r_{32}^3} m_3 z_{32} - \frac{G}{w^2 r_{31}^3} m_3 z_{31} \qquad \text{Equation 2.1.4}$$

Rewriting the z_3 equation

$$-\frac{\mu_{r1}}{\mu_{\rho 1}} z_{\rho 1} = \frac{G m_1}{w^2 r_{13}^3} z_{13} + \frac{G m_2}{w^2 r_{23}^3} z_{23}$$

where $z_3 = \frac{\mu_{r1}}{\mu_{\rho 1}} z_{\rho 1}$ and parameter l_1 determined by configuration geometry is $z_{\rho 1} = l_1 z_{r1}$ with the position differences derived to be

$$\frac{r_{31}}{r1} = l_1 + \frac{m_2}{\mu_{r1}} \qquad \frac{r_{32}}{r1} = l_1 - \frac{m_1}{\mu_{r1}}$$

there results after mathematical reduction of equation 2.1.4 to scalar terms

$$\frac{G}{w^2 r_{r1}^3}\mu_{r1} - \frac{P_{\rho 1}^2}{P_{r1}^2} = \frac{G}{w^2 r_{r1}^3}\left(\frac{r_{r1}^2}{r_{32}^2} - \frac{r_{r1}^2}{r_{31}^2}\right) m_3 = \frac{G}{w^2 r_{r1}^3}\phi_1 \qquad \text{Equation 2.1.5}$$

$$\frac{\mu_{r1}}{\mu_{\rho 1}} l_1 = \frac{G}{w^2 r_{r1}^3}\left(\frac{r_{r1}^2}{r_{32}^2} m_2 + \frac{r_{r1}^2}{r_{31}^2} m_1\right) = \frac{G}{w^2 r_{r1}^3}\phi_2$$

and $$\phi_1 = \left(\frac{r_{r1}^2}{r_{32}^2} - \frac{r_{r1}^2}{r_{31}^2}\right) m_3 \qquad \phi_2 = \frac{r_{r1}^2}{r_{32}^2} m_2 + \frac{r_{r1}^2}{r_{31}^2} m_1$$

The collinear three-body period ratio for the 123 configuration can be determined by solving for $\frac{P_{\rho 1}^2}{P_{r1}^2}$ from equation 2.1.5

$$\frac{P_{\rho 1}^2}{P_{r1}^2} = \frac{\mu_{r1} - \phi_1}{\phi_2}\frac{\mu_{r1}}{\mu_{\rho 1}} l_1 \qquad \text{Equation 2.1.6}$$

Individual r and ρ periods are

$$P_{r1}^2 = 4\pi^2 \frac{r_{r1}^3}{G(\mu_{r1} - \phi_1)} \qquad P_{\rho 1}^2 = 4\pi^2 \frac{\mu_{r1}}{\mu_{\rho 1}} \frac{\rho_1^3}{G l_1^2 \phi_2}$$

Scalar geometry illustrated in figure 2.1 defines scaling parameters x and l_1 which can be calculated from

$$\rho 1 = l_1 r1 = xr1 + \frac{m_1}{\mu_{r1}} r1$$

where $l_1 = x + \frac{m_1}{\mu_{r1}}$ $r_{32} = xr1$ $r_{31} = (x+1)r1$

Equation 2.1.6 can be rewritten in terms of scaling parameter x

$$\frac{P_{\rho 1}^2}{P_{r1}^2} = \frac{Bx^2(1+x)^2 - (2x+1)S}{x^2 + Q(x+1)^2}\left(\frac{Bx+1}{B+S}\right) \qquad \text{Equation 2.1.7}$$

where $S = \frac{m_3}{m_1}$ $Q = \frac{m_2}{m_1}$ $B = 1 + Q$

The period ratio equation 2.1.7 can further be expressed as a fifth order polynomial when expanded

$$\left(ym_2 + \frac{m_1 + ym_2}{\mu_{r1}} m_3\right) + \left(2ym_2 + \left(2\frac{m_1 + ym_2}{\mu_{r1}} + 1\right)m_3\right)x + \qquad \text{Equation 2.1.8}$$

$$\begin{aligned}&\big((y-1)m_1 + ym_2 + (2+y)m_3\big)x^2 - (3m_1 + m_2)x^3 \\ &-(3m_1 + 2m_2)x^4 - (m_1 + m_2)x^5 = 0\end{aligned}$$

where $y = \frac{P_{\rho 1}^2}{P_{r1}^2}$

For the special case when the instantaneous $r1$ binary period is equal to the $\rho 1$ period gives $y = 1$ then equation 2.1.8 simplifies to

$$(m_2 + m_3) + (2m_2 + 3m_3)x + (m_2 + 3m_3)x^2 \qquad \text{Equation 2.1.9}$$

$$-(3m_1 + m_2)x^3 - (3m_1 + 2m_2)x^4 - (m_1 + m_2)x^5 = 0$$

This result is the Euler quintic equation that has been derived by using sidereal synodic relations with type one geometry over an infinitesimal interval relative to the barycenter within the configuration plane of motion at time zero (Pollard, 1966, 51, Wintner, 1964, 430, Szebehely, 1967, 297). In general, equation 2.1.8 when plotted can be used as a configuration map to determine trajectories of interest.

Points off this map can be transformed into state vectors to numerically integrate for study of mass three in orbit of the binary.

Jacoby r and ρ velocities for the 12̲3 configuration can be found from equation 2.1.5

$$V_{r1}^2 = \frac{G}{r1}(\mu_{r1} - \phi_1) \quad V_{\rho 1}^2 = \frac{Gl_1^2}{\rho 1}\frac{\mu_{\rho 1}}{\mu_{r1}}\phi_2 \qquad \text{Equation 2.1.10}$$

Equation 2.1.10 is consistent with the infinite first family velocity solution in equation 1.2.8. The three-body three-dimensional state vector for the 123 configuration using Jacoby velocities from equation 2.1.10 and perturbation coefficients from equation 2.1.5 can be determined as shown below

$$x_1 = -\frac{m_2}{\mu_{r1}}r1 - \frac{m_3}{\mu_{\rho 1}}\rho 1 \qquad \dot{x}_1 = 0 \qquad \text{Equation 2.1.11}$$

$$y_1 = 0 \qquad \dot{y}_1 = -\frac{m_2}{\mu_{r1}}V_{r1}cosi_{r1} - \frac{m_3}{\mu_{\rho 1}}V_{\rho 1}cosi_{\rho 1}$$

$$z_1 = 0 \qquad \dot{z}_1 = -\frac{m_2}{\mu_{r1}}V_{r1}sini_{r1} - \frac{m_3}{\mu_{\rho 1}}V_{\rho 1}sini_{\rho 1}$$

$$x_2 = \frac{m_1}{\mu_{r1}}r1 - \frac{m_3}{\mu_{\rho 1}}\rho 1 \qquad \dot{x}_2 = 0$$

$$y_2 = 0 \qquad \dot{y}_2 = \frac{m_1}{\mu_{r1}}V_{r1}cosi_{r1} - \frac{m_3}{\mu_{\rho 1}}V_{\rho 1}cosi_{\rho 1}$$

$$z_2 = 0 \qquad \dot{z}_2 = \frac{m_1}{\mu_{r1}}V_{r1}sini_{r1} - \frac{m_3}{\mu_{\rho 1}}V_{\rho 1}sini_{\rho 1}$$

$$x_3 = \frac{\mu_{r1}}{\mu_{\rho 1}}\rho 1 \qquad \dot{x}_3 = 0$$

$$y_3 = 0 \qquad \dot{y}_3 = \frac{\mu_{r1}}{\mu_{\rho 1}}V_{\rho 1}cosi_{\rho 1}$$

$$z_3 = 0 \qquad \dot{z}_3 = \frac{\mu_{r1}}{\mu_{\rho 1}}V_{\rho 1}sini_{\rho 1}$$

Equation 2.1.11 is consistent with the three-dimensional first family state vector solution presented in equation 1.2.7 and is a line of nodes solution in the barycentric inertial coordinate system. An illustration of the three-dimensional geometry for the 123 configuration can be viewed in figure 2.2.

Verifying conservation of energy requires showing that twice the kinetic energy is equal to the potential energy in the infinitesimal interval at time zero. This can be accomplished by substituting the velocities calculated in equation 2.1.10 into the conservation of energy equation (see equation 1.2.8)

$$2T = \frac{m_1 m_2}{\mu_{r1}} V_{r1}^2 + \frac{m_3 \mu_{r1}}{\mu_{\rho 1}} V_{\rho 1}^2 \qquad \text{Equation 2.1.12}$$

Reformulating the V_{r1}^2 and $V_{\rho 1}^2$ equations as a function of scaling parameter x will simplify this calculation

$$V_{r1}^2 = \frac{G}{r1}(\mu_{r1} - \phi_1) = \frac{Gm_1}{r1}\left(B - \left(\frac{1}{x^2} - \frac{1}{(x+1)^2}\right) S\right)$$

$$V_{\rho 1}^2 = \frac{Gl_1^2}{\rho 1}\frac{\mu_{\rho 1}}{\mu_{r1}}\phi_2 = \frac{Gm_1}{r1}\left(\frac{B+S}{B}\right)\left(x + \frac{1}{B}\right)\left(\frac{1}{(x+1)^2} + \frac{Q}{x^2}\right)$$

$$\phi_1 = \left(\frac{1}{x^2} - \frac{1}{(x+1)^2}\right) m_3 \qquad \phi_2 = \frac{m_1}{(x+1)^2} + \frac{m_2}{x^2}$$

the result after velocity substitution for the conservation of energy verification will be

$$2T = G\frac{m_1 m_2}{r1} + G\frac{m_1 m_3}{(1+x)r1} + G\frac{m_2 m_3}{xr1} = U \qquad \text{Equation 2.1.13}$$

This completes the solution for the 123 three-body configuration. The five remaining variations can be solved in the same manner by interchanging the three mass sequence of equations 2.1.1 through 2.1.13. A summary of these variations in terms of period ratios, velocities, perturbation coefficients and scaling factors will be given below. Care must be taken in observing the Jacoby coupling geometry.

123 three-body configuration

$$P_{23}^2 = 4\pi^2 \frac{r_{r1}^3}{G(\mu_{23} - \phi_1)} \qquad P_1^2 = 4\pi^2 \frac{\mu_{23}}{\mu_{\rho 1}} \frac{\rho_1^3}{Gl_1^2 \phi_2} \qquad \text{Equation 2.1.14}$$

$$\frac{P_{23}^2}{P_1^2} = \frac{x^3(S + (x+1)^2 Q)}{(Q+S)(x+1)^2 - x^3(2+x)}\left(\frac{B+S}{S(x+1)+Q}\right)$$

$$V_{23}^2 = \frac{G}{r_{23}}(\mu_{23} - \phi_1) = \frac{Gm_1}{xr1}\left(Q + S - \left(1 - \frac{1}{(x+1)^2}\right) x^2\right)$$

$$V_{\rho_1}^2 = \frac{Gl_1^2}{\rho_1}\frac{\mu_{\rho 1}}{\mu_{23}}\phi_2 = \frac{Gm_1}{r1}\left(\frac{B+S}{Q+S}\right)\left(1 + \frac{S}{Q+S}x\right)\left(\frac{S}{(x+1)^2} + Q\right)$$

$$\phi_1 = \left(1 - \frac{1}{(x+1)^2}\right) x^2 m_1 \qquad \phi_2 = \left(m_2 + \frac{m_3}{(x+1)^2}\right) x^2$$

$$l_1 = \frac{1}{x} + \frac{m_3}{\mu_{23}} \qquad r_{32} = xr1 \qquad r_{31} = (1+x)r1$$

132 three-body configuration

$$P_{32}^2 = 4\pi^2 \frac{r_{23}^3}{G(\mu_{23}-\phi_1)} \qquad P_1^2 = 4\pi^2 \frac{\mu_{23}}{\mu_{\rho 1}} \frac{\rho_1^3}{Gl_1^2\phi_2} \qquad \text{Equation 2.1.15}$$

$$\frac{P_{32}^2}{P_1^2} = \frac{x^3(S+(1-x)^2Q)}{(Q+S)(1-x)^2 - x^3(2-x)} \left(\frac{B+S}{S(1-x)+Q}\right)$$

$$V_{32}^2 = \frac{G}{r_{23}}(\mu_{23}-\phi_1) = \frac{Gm_1}{r_{23}}\left(Q+S-\left(\frac{1}{(1-x)^2}-1\right)x^2\right)$$

$$V_{\rho_1}^2 = \frac{Gl_1^2}{\rho_1}\frac{\mu_{\rho 1}}{\mu_{23}}\phi_2 = \frac{Gm_1}{r1}\left(\frac{B+S}{Q+S}\right)\left(1-\frac{S}{Q+S}x\right)\left(\frac{S}{(1-x)^2}+Q\right)$$

$$\phi_1 = \left(\frac{1}{(x-1)^2}-1\right)x^2 m_1 \qquad \phi_2 = \left(m_2 + \frac{m_3}{(x-1)^2}\right)x^2$$

$$l_1 = \frac{1}{x} - \frac{m_3}{\mu_{23}} \qquad r_{32} = xr1 \qquad r_{31} = (1-x)r1$$

132 three-body configuration

$$P_{13}^2 = 4\pi^2 \frac{r_{13}^3}{G(\mu_{13}-\phi_1)} \qquad P_2^2 = 4\pi^2 \frac{\mu_{13}}{\mu_{\rho 1}} \frac{\rho_1^3}{Gl_1^2\phi_2} \qquad \text{Equation 2.1.16}$$

$$\frac{P_{13}^2}{P_2^2} = \frac{x^3(S+(1-x)^2)}{(1+S)(1-x)^2 - x^3(2-x)Q} \left(\frac{B+S}{S(1-x)+1}\right)$$

$$V_{13}^2 = \frac{G}{r_{13}}(\mu_{13}-\phi_1) = \frac{Gm_1}{r_{13}}\left(1+S-\left(\frac{1}{(1-x)^2}-1\right)x^2 Q\right)$$

$$V_{\rho_1}^2 = \frac{Gl_1^2}{\rho_1}\frac{\mu_{\rho 1}}{\mu_{13}}\phi_2 = \frac{Gm_1}{r1}\left(\frac{B+S}{1+S}\right)\left(1-\frac{S}{1+S}x\right)\left(\frac{S}{(1-x)^2}+1\right)$$

$$\phi_1 = \left(\frac{1}{(x-1)^2}-1\right)x^2 m_2 \qquad \phi_2 = \left(m_1 + \frac{m_3}{(x-1)^2}\right)x^2$$

$$l_1 = \frac{1}{x} - \frac{m_3}{\mu_{13}} \qquad r_{32} = (1-x)r1 \qquad r_{31} = xr1$$

312 three-body configuration

$$P_{31}^2 = 4\pi^2 \frac{r_{13}^3}{G(\mu_{13}-\phi_1)} \qquad P_2^2 = 4\pi^2 \frac{\mu_{13}}{\mu_{\rho 1}} \frac{\rho_1^3}{Gl_1^2\phi_2} \qquad \text{Equation 2.1.17}$$

$$\frac{P_{31}^2}{P_2^2} = \frac{x^3(S+(1+x)^2)}{(1+S)(1+x)^2 - x^3(2+S)Q}\left(\frac{B+S}{S(1+x)+1}\right)$$

$$V_{31}^2 = \frac{G}{r_{13}}(\mu_{13} - \phi_1) = \frac{Gm_1}{r_{13}}\left(1 + S - \left(1 - \frac{1}{(1+x)^2}\right)x^2 Q\right)$$

$$V_{\rho_1}^2 = \frac{Gl_1^2}{\rho_1}\frac{\mu_{\rho 1}}{\mu_{13}}\phi_2 = \frac{Gm_1}{r1}\left(\frac{B+S}{1+S}\right)\left(1 + \frac{S}{1+S}x\right)\left(\frac{S}{(1+x)^2} + 1\right)$$

$$\phi_1 = \left(1 - \frac{1}{(x+1)^2}\right)x^2 m_2 \qquad \phi_2 = \left(m_1 + \frac{m_3}{(x+1)^2}\right)x^2$$

$$l_1 = \frac{1}{x} + \frac{m_3}{\mu_{13}} \qquad r_{32} = (1+x)r1 \qquad r_{31} = xr1$$

3<u>12</u> three-body configuration

$$P_{r1}^2 = 4\pi^2\frac{r_{12}^3}{G(\mu_{r1} - \phi_1)} \qquad P_{\rho 1}^2 = 4\pi^2\frac{\mu_{r1}}{\mu_{\rho 1}}\frac{\rho_1^3}{Gl_1^2\phi_2} \quad \text{Equation 2.1.18}$$

,

$$\frac{P_{\rho 1}^2}{P_{r1}^2} = \frac{Bx^2(1+x)^2 - (2x+1)S}{(1+x)^2 + Qx^2}\left(\frac{Bx+Q}{B+S}\right)$$

$$V_{r1}^2 = \frac{G}{r1}(\mu_{r1} - \phi_1) = \frac{Gm_1}{r1}\left(B - \left(\frac{1}{x^2} - \frac{1}{(1+x)^2}\right)S\right)$$

$$V_{\rho_1}^2 = \frac{Gl_1^2}{\rho_1}\frac{\mu_{\rho 1}}{\mu_{r1}}\phi_2 = \frac{Gm_1}{r1}\left(\frac{B+S}{B}\right)\left(x + \frac{Q}{B}\right)\left(\frac{Q}{(1+x)^2} + \frac{1}{x^2}\right)$$

$$\phi_1 = \left(\frac{1}{x^2} - \frac{1}{(1+x)^2}\right)m_3 \qquad \phi_2 = \frac{m_1}{x^2} + \frac{m_2}{(x+1)^2}$$

$$l_1 = x + \frac{m_2}{\mu_{r1}} \qquad r_{32} = (1+x)r1 \qquad r_{31} = xr1$$

Masses one, two and three can hold any value in any order due to consistency with conservation of energy. That is, no mass is restricted to zero. However, for the purpose of discussion a mass ordered system will be used where mass one is dominant with mass two and mass three being sequentially smaller. Therefore, the above six three-body variations represent mass three either orbiting the mass one mass two binary or mass three in orbit about mass one and mass two individually. Configurations 3<u>12</u> and <u>12</u>3 are mass three orbiting the binary, configurations <u>31</u>2 and <u>13</u>2 are mass three orbiting mass one and configurations 1<u>32</u> and 1<u>23</u> are mass three orbiting mass two. This can be illustrated by plotting period ratios (with respect to the scaling parameter x) in mass order for each three-body

variation resulting in a map of every possible mass three orbit about mass one and mass two at time zero. An example of this mapping of contiguous three-body variations is shown in figure 2.3 where mass one is a solar mass, mass two is a Jovan mass and mass three approaches a probe mass (zero mass or cometary mass). The distance separating mass one and mass two is one unit or 5.2 AU. Intersections in figure 2.3 are the equal period points between mass three and mass one and mass three and mass two. These are the three Euler points as shown symbolically below with the corresponding period ratios. Leftmost intersection is not visible due to mass two magnitude (Jovan) being small relative to mass one (solar).

$$\underline{3}12\,,\,\underline{3}12 \qquad \underline{1}32\,,\,\underline{1}32 \qquad 1\underline{2}3\,,\,1\underline{2}3$$

$$\frac{P_3}{P_{21}}\ \frac{P_{31}}{P_2} \qquad \frac{P_{13}}{P_2}\ \frac{P_{32}}{P_1} \qquad \frac{P_{23}}{P_1}\ \frac{P_3}{P_{21}}$$

A characteristic of the Euler point is that the state vector position and velocity components at the intersection of the corresponding period ratios are equal.

Period ratios about mass two (1$\underline{3}$2 and 1$\underline{2}$3) approach infinity as x moves away from mass two. These are the r_∞ points where the sunward point is approximately 58.5 million km and the anti-sunward point is approximately 63.2 million km relative to mass two. The inner r_∞ point is deeper in the solar gravity field and therefore closer to mass two, whereas the outer r_∞ point is further from the solar mass and therefore more distant from mass two. As the distance between mass one and mass two approaches infinity the inward and outward r_∞ distances become equal. For planets near to the central mass, inner and outer r_∞ distances are close to the planet which could result in an unstable region for satellites. The r_∞ points are the greatest distances in which Jacoby couplings can exist, it is the distance between two orbiting masses that results in those masses having an infinite orbital period when embedded within the gravitational field(s) of additional mass(es). For a two-body problem the r_∞ point is at infinity. Mathematically, the region beyond the r_∞ point is imaginary.

An example of mapping contiguous three-body configurations where mass one and mass two are of a similar order of magnitude and mass three is near the magnitude of mass one and mass two can be found in figure 2.4. This plot is based on the approximate mass and distance of the 40 Eridani trinary star system components and does not model the real 40 Eridani star system. Mass three (.2 solar masses) orbits mass two (.44 solar masses) with

a binary separation distance of 34 AU, and the binary orbits mass one (.75 solar masses) with a separation distance of 400 AU relative to the center of gravity of the mass two mass three binary. Mass three location is shown marked relative to mass two in figure 2.4. It will be noticed that there are two intersection points between $\frac{P_{23}}{P_1}$, $\frac{P_3}{P_{21}}$ and $\frac{P_3}{P_{21}}$, $\frac{P_{31}}{P_2}$ where the inward intersection state vector only matches the position components and the outward intersection state vector matches both position and velocity components (Euler point). The 40 Eridani system is not the 'classic' trinary star system where mass three orbits the mass one and mass two binary component (Harrington, 1977, Szebehely, 1977). Between mass two and the 123 period ratio quintic along the scaled distance axis in figure 2.4 lies a null interval. This is a region where state vectors do not exist. Mathematically the state vectors are imaginary. The same holds true for the region between mass one and the 312 period ratio quintic.

The 40 Eridani collinear three-body state vector was integrated over a period of a million years and was well behaved in this time span. Binary period estimated from this trajectory was about 248 years consistent with the real 40 Eridani system. The binary orbiting mass one was about 7100 years which is less than the estimated 8000 years for the real trinary system. Characteristic of the infinitesimal interval solution is that it will give the most circular orbits for a given set of n-bodies.

Using the period ratio from the 123 configuration an approximate r_∞ can be calculated for the sun, where the geometry for this three-body configuration is illustrated in figure 2.1. Mass three is the total galactic mass concentrated at its center, mass one is the Sun and mass two is the probe mass used to find the r_∞ point. The 123 three-body period ratio can be written in the following form

$$\frac{P_{T1}^2}{P_{\rho 1}^2} = \frac{(1+S)x^2}{(x^2(1+x)^2 - S(1+2x))(1+x)} \qquad \text{Equation 2.1.19}$$

In order to find the r_∞ point it is necessary to have this ratio approach infinity. To do this the denominator must be set equal to zero which results in finding the solution of the quartic polynomial

$$x^4 + 2x^3 + x^2 - 2Sx - S = 0 \qquad \text{Equation 2.1.20}$$

Once x is known from equation 2.1.20 the r_∞ point can be found using the scaling parameter equation determined from the geometry in figure 2.1.

$$\rho 1 = \frac{m_1}{\mu_{r1}} r1 + xr1 \qquad m_2 \to 0$$

$$r1 \to r_\infty = \frac{\rho 1}{1+x} \qquad \text{Equation 2.1.21}$$

Since the galactic mass and the distance of the Sun from the galactic core is not that well known, a parametric table for the inward Solar r_∞ point will be given rather than a single calculation. Results of this study can be found in table I.

Table I--Solar r_∞ Point

	Solar r_∞ Distance		
	Distance ($\rho 1$) from Galactic Center in Light Years		
Galactic Mass (S)	20,000	25,000	30,000
$2x10^{11}$	2.71	3.39	4.07
$(x = 7367.563)$			
$2x10^{12}$	1.26	1.57	1.89
$(x = 15{,}873.502)$			
$2x10^{13}$	.585	.731	.877
$(x = 34{,}199.019)$			

Galactic mass S is in Solar masses. As can be seen from the table, both increased Galactic mass and decreased Galactic core distance results in reduced Solar r_∞ distance.

Solar r_∞ distance as determined by the three-body infinite interval method comes under the category of sphere of influence. Since there are multiple concepts describing particle behavior in the gravitational domain of masses in their vicinity, it is therefore necessary to compare the various sphere of influence definitions and computations in order to understand how they may relate (Belbruno, Marsden, 1997). Cheboterav, (Cheboterav, 1967, 266-274) in consideration of these concepts, defines and computes

the activity sphere, sphere of attraction and Hill's gravitation sphere for the gravitational sphere of the Sun and the planets.

Activity sphere (Roy, 1978, 160,351) was introduced into Astronomy by Laplace in the study of cometary motion in the immediate realm of the major planets, specifically in the activity sphere of Jupiter. Chebotarev defines sphere of attraction as the space within which the planetary attraction dominates over the Solar attraction and Hill's gravitational sphere is the inner Euler libration point defining the maximum radius of a space in which stable motion of satellites can occur. As stated by Cheboterav, Hill's gravitational sphere can be considered the theoretical limit of satellite existence. Applying these sphere of influence definitions to find the gravitational spheres of the Sun, Chebotarev calculated values for each of the gravitational spheres using the following Galactic mass and Galactic core radii

Galactic mass = 1.3×10^{11} (solar masses)	Galactic core radii = 26,000 (light years)
Activity Sphere	60,000 AU
Sphere of Attraction	4,500 AU
Hill's Sphere	230,000 AU

Using the three-body infinite interval method to compute the Solar r_∞ distance with the same Galactic mass and core radii yields approximately

r_∞ distance	258,500 AU

The Solar r_∞ distance is beyond the Hill's gravitational sphere as would be expected from viewing figures 2.3 and 2.4. Geometrically the r_∞ point will always be further distant than the Euler libration point. To get an idea of the magnitude of these distances the star Proxima Centauri is approximately 268,800 AU from the Sun. The Alpha Centauri star system has a combined mass of over two solar masses with a r_∞ point greater than five light years. The Sun/Alpha Centari star systems overlap relative to their r_∞ points.

It will be noticed in figures 2.3 and 2.4 that the quintic generated by the 132 three-body configuration goes to infinity within the region bounded by the quintic generated by the 132 three-body configuration. The 132 quintic goes to infinity at the inward r_∞ point relative to mass two by definition.

Determination needs to be made as to the physical nature of the 132 configuration at infinity. Their intersection is already known to be the inner Euler point of mass two which was determined from the period ratios. Period ratios can also solve this problem starting with $\frac{P_{13}^2}{P_2^2}$ from equation 2.1.16

$$\frac{P_{13}^2}{P_2^2} = \frac{x^3(S+(1-x)^2)}{(1+S)(1-x)^2-x^3(2-x)Q}\left(\frac{B+S}{S(1-x)+1}\right) \quad \text{Equation 2.1.22}$$

Letting the mass one mass three period go to infinity means letting the denominator of equation 2.1.22 go to zero in order to solve for the scaling parameter x. This results in a quartic

$$x^4 - 2x^3 + Q'x^2 - 2Q'x + Q' = 0 \quad \text{Equation 2.1.23}$$

where $m_3 \to 0$ and $Q' = \frac{1}{Q}$. Equation 2.1.23 is difficult to solve due to the number or decimal places to carry. It can be modified by multiplying through by r_{21}^4

$$r_{13}^4 - 2r_{21}r_{13}^3 + Q'r_{21}^2r_{13}^2 - 2Q'r_{21}^3r_{13} + Q'r_{21}^4 = 0 \quad \text{Equation 2.1.24}$$

where $r_{13} = xr_{21}$. The Jacoby coordinate r_{21} is a constant in equation 2.1.24 with the only variable being r_{13}. Once x is known, using $r_{23} = \frac{1-x}{x}r_{13}$ will give the distance to where mass three goes to infinity relative to mass two. This distance r_{23} will be defined as sphere of influence (SOI). Compilation summary of the various planetary sphere of influences is in table II.

Table II—Planetary Spheres of Influence

	SOA	SOI	AS	HGS	r_∞	
Mercury	.024	.024	.113	.220	.252	.253
Venus	.170	.170	.617	1.008	1.151	1.169
Earth	.262	.262	.929	1.496	1.704	1.723
Mars	.130	.130	.578	1.083	1.237	1.244
Jupiter	23.33	23.33	48.21	51.90	58.48	63.23

Saturn	23.90	23.90	54.54	64.00	72.40	76.40
Uranus	18.85	18.85	51.80	69.50	79.10	81.30
Neptune	32.06	32.06	86.85	115.06	130.9	134.8

All table distances are multiplied by 10^6 kilometers. The sphere of attraction (SOA), sphere of influence (SOI) and activity sphere (AS) are determined using mean distance from the sun. Hill's gravitational sphere is represented as HGS. Differences between SOA and SOI are non-existent when using the same planetary masses in the calculations. Double values for the r_∞ distances are for the sunward and anti-sunward r_∞ points.

Although the SOA and SOI formulations are quite different their final results produce a close match. Therefore, both formulations, using Chebotarev's definition, appear to be calculating where the planetary attraction dominates over the Solar attraction of a probe mass. The problem here is that there is only one planet where this boundary closely defines the farthest region where satellites are found to exist and that is Jupiter. Planets beyond Jupiter have moons well within this limit, and inside the orbit of Jupiter, the Earth, has the Moon, which is well outside this limit. Venus and Mercury have no moons at all. It is not clear exactly what the SOA/SOI calculations signify, however, the interesting fact is that they both agree. Could a situation exist that the formulation of a hereto unknown optimization problem, has as a solution, that the Jupiter sun mass ratio relative to their separation distance, results in what is currently observed to exist at present? Something analogous to a Titius Bode relation (Nieto,1972,)? The Chebotarev SOA equation tends to give that impression

$$\Delta_2 = rm^{\frac{1}{2}} \qquad \text{Equation 2.1.25}$$

where r is the planet to sun distance and m is the planet to sun mass ratio.

Relevant to the SOA/SOI question of significance, numerical integration was performed using 132 three-body state vectors to calculate trajectories for evaluation of the sun-probe mass-earth, sun-probe mass-Jupiter and the 40 Eridani trinary star system configurations. This is a simulation using approximate mass distance astronomical data and not a modelling of the real planetary/star systems. Probe mass for the sun earth configuration was the actual lunar mass and probe mass for the Sun Jupiter configuration was zero mass. Purpose of this study was to find regions of relative stability/ instability/escape orbits of mass three and not to determine the orbital

lifetime existence of the mass two mass three binary. Searches were conducted for trajectories showing unmistakable signs of instability, that is, looking for mass three heliocentric escape orbits. Knowing domains where escape trajectories exist can help determine relative stable/relative unstable/escape orbit boundaries. Also, the actual trajectory waveform of the plotted apsides gives an indication of the trajectory maintaining relatively stable orbits before evolving into the relatively unstable/very unstable/escape orbit regime.

A close relationship was found to exist between the semi-major axis and eccentricity of mass three (probe mass) over the domain where mass three goes from a relatively stable trajectory to a relatively unstable trajectory and finally an escape trajectory. As would be expected, the boundary between relatively stable/relative unstable/escape trajectory is gradual and not sharply defined. It was clearly apparent (with increasing semi-major axis) that prior to entering the unstable region, small changes in the semi-major axis resulted in small changes in the eccentricity. Upon entering the unstable domain small changes in the semi-major axis results in large changes to the eccentricity. This is due to the mass three trajectory periapsis approaching mass two as mass three apoapsis simultaneously approaches the Hill's gravitational sphere in such a way that the semi-major axis shows slight increase over the unstable region. Basically, both apsides are being constrained by dynamical boundaries in such a manner that all possible relatively stable trajectories cease to exist. When the mass three apoapsis approaches the vicinity of Hill's gravitational sphere the trajectory becomes very unstable. Mass three spends increasingly greater periods at apoapsis until the trajectory eventually becomes heliocentric due to the solar perturbations dominating over the planetary gravity field. However, to make things more complicated, at the exact Euler point the trajectory becomes less unstable. The period of this collinear relatively stable/relatively unstable point cannot be determined due to the mass two mass three distance being an irrational number. If this distance was a rational number perhaps a definitive period could be determined. In very close proximity either side of the Euler point the trajectory displays interesting behavior. On the planetward side of the Euler point after a period where all three masses orbit in collinear formation, mass three goes into a highly unstable elliptical orbit about mass two. On the sunward side of the Euler point after the collinear formation mass three abruptly escapes. Numerically integrating a state vector at the Jupiter sunward r_∞ point resulted in the probe mass trajectory going directly into what would be the asteroid belt. For the Jupiter anti-

sunward r_{∞} point the numerically integrated probe mass trajectory orbits between Jupiter and what would be Saturn.

Specifically, looking at the three cases, the same 132 three-body semi-major axis eccentricity behavior is observed to exist for all configurations. The difference is that each individual case resides in a different regime of the semi-major axis eccentricity curve. For example, the sun-probe mass-earth configuration shows the probe mass semi-major axis approximately over 80,000 kilometers above the SOA/SOI but still over 200,000 kilometers from being in the unstable region relative to a lunar mean semi-major axis of 384,400 kilometers. That is, the lunar probe mass is in a relatively early phase on the semi-major axis eccentricity curve. However, the outermost Jovan moons of the sun-probe mass-Jupiter configuration are at the relatively stable/relatively unstable boundary on the semi-major axis eccentricity curve, where small changes in the semi-major axis could result in those masses to escape into a heliocentric trajectory. In the unstable regions there are sub-regions of trajectories that are relatively more stable and in the relatively stable regions there are some trajectories that are relatively less stable. It was observed in one of these unstable regions, a semi-major axis at approximately 24 million kilometers, that the probe mass escaped Jupiter into a heliocentric trajectory after a short orbital period only to be recaptured by Jupiter at some period later. This suggests that there is the possibility that some masses exist in quasi-periodic trajectories whereby they orbit Jupiter for a short time span before escaping into a heliocentric orbit for some intermediate period and then back again to Jupiter etc. (Kurth, 1957, 38,58,60, Arnold, 1978, 71, Hagihara, 1975, 1150). Additional work would be needed to investigate this sun-probe mass-Jupiter-trajectory region to verify if these quasi-periodic orbits actually exist. For both the sun-probe mass-earth and sun-probe mass-Jupiter configurations there is a region at about half way between the Euler point and mass two where the trajectory apoapsis takes on a distinctly different waveform as compared to the surrounding regions. This region appears to correlate approximately with the relatively stable/relatively unstable boundary.

Analyzing the 40 Eridani trinary star system required longer integration times resulting from the greater mass separation distances. Although, the stellar masses were approximately the same order of magnitude as compared to the two previous examples where mass three was near zero, a similar semi-major axis eccentricity curve was found to exist. Location of the third component in the 40 Eridani star system on the semi-major axis eccentricity curve appears to be in a relatively stable region where the SOI is approximately 120 AU further out from the semi-major axis for this star

(mass three). The semi-major axis eccentricity curve region in which small changes in semi-major axis result in large changes in eccentricity is approximately 50 AU below the SOI. As the Euler point was successively carried to increased digital accuracy, numerical integration of the trinary state vector showed the collinear orbital formation increasing in duration. The irrationality of the mass two mass three Euler point distance makes it difficult to find the absolute period the collinear formation can be maintained. Approaching the Euler point, the mass three semi-major axis relative to mass two displays the collinear formation characteristic geometry many AU before reaching the actual Euler point. Determination of relative stability/instability when all masses are similar in magnitude becomes more complex than when mass three is of near zero magnitude. In conclusion, this study shows that using SOA/SOI to determine trajectory stability can be elusive. It is clear that the SOA/SOI does not determine the orbital stability limit of mass three relative to mass two for all cases. Using SOA/SOI in conjunction with HGS aids finding relative stability/relative instability/ escape orbit domains for the 132 configuration.

2.2 Higher Ordered Configurations

It is necessary to include the study of higher order configurations in the first family collinear n-body problem to better understand the complexities involved and how to apply structured methods to analytically decipher system motion. A good example is to analyze the six-body first family problem to see the additional information provided about particle interactions. As seen in equation 1.1.5 there are six families comprising the collinear six-body problem with an unknown number of variations. Every six-body configuration has ten period ratios associated with that configuration as opposed to the three-body configuration which has only one. These six-body configurations can be linked together like that seen for the three-body problem shown in figure 2.3, however, the complexity involved in understanding what this period ratio array signifies can be difficult. Some period ratios intersect at Euler points, some period ratios go to infinity at the r_∞ points and some period ratios indicate resonance points. Other period ratios are less obvious to their meaning as for example there appears to be multiple r_∞ points per planet/star beyond the ones already discussed, period ratios that approach zero and many period ratios with intersection points that seem to indicate a correlation with unknown particle motion. There is even a period ratio that has only one point.

The six-mass system used in this study (Bauer, 2001) will be m_1 (Solar mass), m_2 (Mars mass), m_3 (probe mass), m_4 (Jupiter mass), m_5 (Saturn mass) and m_6 (Uranus mass). This is a simulation using approximate mass distance astronomical data and not a modelling of the real solar system. The only six-mass period ratios that will be shown for these masses of interest are m_4, m_5 and m_6. There are ten period ratios for each six-mass configuration that concerns the m_4, m_5 and m_6 sequence. These configurations are

12 3456 12 34 56 12 43 56 12 4356 12 4 35 6 12 4 53 6 12 4536

12 45 36 12 45 63 12 4563

This sequence contains members and member variations of the first four six-mass configurations in equation 1.1.5. The first sequence of six-mass configurations models m_4 (12 3456 12 34 56 12 43 56 12 43 56). The second configuration sequence models m_5 (12 43 56 12 4 35 6 12 4 53 6 12 4536) and the third configuration sequence models m_6 (12 4536 12 45 36 12 45 63 12 4563). It will be noticed that these sequences overlap at 12 43 56 for m_4 and m_5 and at 12 4536 for m_5 and m_6.

Euler point period ratio intersections for each mass are listed below

Inner Euler point	Mass	Outer Euler point
12 3456 , 12 34 56	m_4	12 43 56 , 12 4356
12 43 56 , 12 4 35 6	m_5	12 4 53 6 , 12 4536
12 4536 , 12 45 36	m_6	12 45 63 , 12 4563

Writing out the six-mass period ratio structure as a function of period ratios for m_4, m_5 and m_6 can be found below

m_4

12 3456

$\frac{P_3}{P_{21}}\ \frac{P_4}{P_{21}}\ \frac{P_5}{P_{21}}\ \frac{P_6}{P_{21}}$

$\frac{P_4}{P_3}\ \frac{P_5}{P_3}\ \frac{P_6}{P_3}$

$\frac{P_5}{P_4}\ \frac{P_6}{P_4}$

$\frac{P_6}{P_5}$

12 34 56

$\frac{P_{43}}{P_{21}}\ \frac{P_Q}{P_{21}}\ \frac{P_5}{P_{21}}\ \frac{P_6}{P_{21}}$

$\frac{P_Q}{P_{43}}\ \frac{P_5}{P_{43}}\ \frac{P_6}{P_{43}}$

$\frac{P_5}{P_Q}\ \frac{P_6}{P_Q}$

$\frac{P_6}{P_5}$

12 43 56

$\frac{P_6}{P_{21}}\ \frac{P_5}{P_{21}}\ \frac{P_Q}{P_{21}}\ \frac{P_{43}}{P_{21}}$

$\frac{P_6}{P_{43}}\ \frac{P_5}{P_{43}}\ \frac{P_Q}{P_{43}}$

$\frac{P_6}{P_Q}\ \frac{P_5}{P_Q}$

$\frac{P_6}{P_5}$

12 43 56

$\frac{P_6}{P_{21}}\ \frac{P_5}{P_{21}}\ \frac{P_4}{P_{21}}\ \frac{P_3}{P_{21}}$

$\frac{P_6}{P_3}\ \frac{P_5}{P_3}\ \frac{P_4}{P_3}$

$\frac{P_6}{P_4}\ \frac{P_5}{P_4}$

$\frac{P_6}{P_5}$

m_5

12 4356

$\frac{P_3}{P_{21}}\ \frac{P_4}{P_{21}}\ \frac{P_5}{P_{21}}\ \frac{P_6}{P_{21}}$

$\frac{P_4}{P_3}\ \frac{P_5}{P_3}\ \frac{P_6}{P_3}$

$\frac{P_5}{P_4}\ \frac{P_6}{P_4}$

$\frac{P_6}{P_5}$

12 4 35 6

$\frac{P_{53}}{P_{21}}\ \frac{P_4}{P_{21}}\ \frac{P_Q}{P_{21}}\ \frac{P_6}{P_{21}}$

$\frac{P_4}{P_{53}}\ \frac{P_Q}{P_{53}}\ \frac{P_6}{P_{53}}$

$\frac{P_Q}{P_4}\ \frac{P_6}{P_4}$

$\frac{P_6}{P_Q}$

12 4 53 6

$\frac{P_6}{P_{21}}\ \frac{P_Q}{P_{21}}\ \frac{P_4}{P_{21}}\ \frac{P_{53}}{P_{21}}$

$\frac{P_6}{P_{53}}\ \frac{P_Q}{P_{53}}\ \frac{P_4}{P_{53}}$

$\frac{P_6}{P_4}\ \frac{P_Q}{P_4}$

$\frac{P_6}{P_Q}$

12 4536

$\frac{P_6}{P_{21}}\ \frac{P_5}{P_{21}}\ \frac{P_4}{P_{21}}\ \frac{P_3}{P_{21}}$

$\frac{P_6}{P_3}\ \frac{P_5}{P_3}\ \frac{P_4}{P_3}$

$\frac{P_6}{P_4}\ \frac{P_5}{P_4}$

$\frac{P_6}{P_5}$

m_6

12 4536

$\frac{P_3}{P_{21}}\ \frac{P_4}{P_{21}}\ \frac{P_5}{P_{21}}\ \frac{P_6}{P_{21}}$

$\frac{P_4}{P_3}\ \frac{P_5}{P_3}\ \frac{P_6}{P_3}$

$\frac{P_5}{P_4}\ \frac{P_6}{P_4}$

$\frac{P_6}{P_5}$

12 45 36

$\frac{P_{63}}{P_{21}}\ \frac{P_4}{P_{21}}\ \frac{P_5}{P_{21}}\ \frac{P_Q}{P_{21}}$

$\frac{P_4}{P_{63}}\ \frac{P_5}{P_{63}}\ \frac{P_Q}{P_{63}}$

$\frac{P_5}{P_4}\ \frac{P_Q}{P_4}$

$\frac{P_Q}{P_5}$

12 45 63

$\frac{P_Q}{P_{21}}\ \frac{P_5}{P_{21}}\ \frac{P_4}{P_{21}}\ \frac{P_{63}}{P_{21}}$

$\frac{P_Q}{P_{63}}\ \frac{P_5}{P_{63}}\ \frac{P_4}{P_{63}}$

$\frac{P_Q}{P_4}\ \frac{P_5}{P_4}$

$\frac{P_Q}{P_5}$

12 4563

$\frac{P_6}{P_{21}}\ \frac{P_5}{P_{21}}\ \frac{P_4}{P_{21}}\ \frac{P_3}{P_{21}}$

$\frac{P_6}{P_3}\ \frac{P_5}{P_3}\ \frac{P_4}{P_3}$

$\frac{P_6}{P_4}\ \frac{P_5}{P_4}$

$\frac{P_6}{P_5}$

Parameter P_Q can be the period of a double binary or of a binary trinary combination depending on the geometry of the probe mass, m_4, m_5 and m_6 positions in the six-mass configuration. This comes about from the structure of the sidereal synodic relations when solving the equations of motion in the infinitesimal interval problem.

Euler point period ratio evaluations for m_4, m_5 and m_6

m_4	m_5	m_6
Inner/outer	inner/outer	inner/outer
$\frac{P_3}{P_{21}} = \frac{P_4}{P_{21}} = \frac{P_{43}}{P_{21}}$	$\frac{P_3}{P_{21}} = \frac{P_5}{P_{21}} = \frac{P_{53}}{P_{21}}$	$\frac{P_3}{P_{21}} = \frac{P_6}{P_{21}} = \frac{P_{63}}{P_{21}}$
$\frac{P_4}{P_3} = 1 = \frac{P_Q}{P_{43}}$	$\frac{P_4}{P_3} = \frac{P_4}{P_{53}}$	$\frac{P_4}{P_3} = \frac{P_4}{P_{63}}$
$\frac{P_5}{P_3} = \frac{P_5}{P_{43}}$	$\frac{P_5}{P_3} = 1 = \frac{P_Q}{P_{53}}$	$\frac{P_5}{P_3} = \frac{P_5}{P_{63}}$
$\frac{P_6}{P_3} = \frac{P_6}{P_{43}}$	$\frac{P_6}{P_3} = \frac{P_6}{P_{53}}$	$\frac{P_6}{P_3} = 1 = \frac{P_Q}{P_{63}}$

Plotting the m_4, m_5 and m_6 period ratios as a function of the binary scaled distance in the same manner as figure 2.3 can be found in figures 2.5 through 2.7. First family period ratios can be found derived in chapter one by using methods described in equations 1.2.1 through 1.2.3. Period ratios for configurations such as 12 34 56 etc. can be derived by combining methods employed for the first family and the multiple binary collinear systems. The actual plots for this six-mass sequence would normally be one contiguous set of masses relative to binary scaled distance, however, due to lack of presentation space they are shown as individual illustrations.

Period ratio descriptions are complex because of the number of mass interactions/perturbations involved. With every mass in the n-body system there are a total of $\frac{(n-1)!}{2(n-3)!}$ period ratios per configuration to analyze and mass interactions to explain. For example, the period ratio curve $\frac{P_3}{P_{21}}$ (red line) which is probe mass period ratioed to the $m_1\, m_2$ binary period, runs through masses four, five and six as shown in figures 2.5 through 2.7. This $\frac{P_3}{P_{21}}$ curve is not continuous and bifurcates at each of those masses. If masses two through six were all zero then the $\frac{P_3}{P_{21}}$ curve would be continuous, that is, the

$\frac{P_3}{P_{21}}$ curve would default to a Kepler two-body period curve. The $\frac{P_3}{P_{21}}$ curve intersects all of the binary period ratios $\frac{P_{43}}{P_{21}}$, $\frac{P_{53}}{P_{21}}$ and $\frac{P_{63}}{P_{21}}$ (brown lines) which are the Euler points for m_4, m_5 and m_6. This can be seen in the illustrations, especially in figures 2.6 and 2.7. On the m_1 side of m_4 in the $\underline{12}$ 3456 region there occur intersections at approximately 2.81 AU and 3.8 AU for period ratios $\frac{P_4}{P_3}$ (black line) and $\frac{P_5}{P_3}$ (gold line) respectively with the $\frac{P_3}{P_{21}}$ curve. The 2.81 AU intersection at a 2.51 resonance corresponds to a gap (Kirkwood) at 5/2 resonance in the asteroid belt. At the 3.8 AU intersection a 3.95 resonance corresponds to the gap between the Cybele and Hilda group of asteroids. As can be seen in figure 2.5 there are a plethora of intersections relative to m_4 whereby some of these intersections tend to correspond with the grouping of m_4 moons. Not all intersections have been identified with observed probe mass motion. There are also what appear to be additional r_∞ points as well as zero period ratios for each of the planets. Observing the period ratio structure for m_5 and m_6 it will be noticed that the period ratio curves become increasingly more compressed for these outermost masses. This corresponds with the moons grouping increasing closer to the planet relative to the SOA/SOI. In general, period ratios are monotonic showing no extrema. However, points of inflection are found to exist with some period ratios, such as $\frac{P_3}{P_{21}}$ in the $\underline{123}$ configuration at approximately 249 thousand kilometers from m_4. It is not clear to what extent point of inflection affects probe mass motion. Numerical integration of m_4 sunward r_∞ point state vector results in an elliptical probe mass orbit in the asteroid belt with an approximate semi-major axis of 3.8 AU. If a probe mass could drift into this r_∞ region of m_4 then there is the possibility it may orbit in the asteroid belt between m_4 and m_2.

The theoretical collinear infinitesimal interval problem three-dimension state vector is a line of nodes solution. For all the planetary nodes to line up at the same time would not be expected to occur in the real solar system. However, if such an event were to come about it would be on the order of what may be theoretically consistent with Poincare's recurrence theorem (Arnold, 1978, 68-70, Kurth, 1957, 40-51, Hagihara, 1976, 1244,1516). This quasi-periodic event would take place at intervals of possibly billions (?) of years if a time could even be given for such an occurrence. State vector at time zero initializes the start of the sidereal period for the quasi-periodic configuration orbits. The nodes at each quasi-period recurrence would be close to the initial collinear state vector, however, the nodes would not be expected to be in an exact alignment as found in the initial state vector. The Poincare quasi-period is composed of many synodic subsystem periods. Each subsystem of masses in the configuration will have a range of synodic periods spanning from relatively short periods to increasingly long synodic periods approaching that of the n-body configuration sidereal period. Over the course of a quasi- periodic epoch, the greatest number of synodic periods will occur for the short-term synodic subsystems with a decreasing number of synodic periods for the larger mass subsystems, that is, the subsystems may tend to settle into finite stable resonant sub-configurations. With the evolution of time, depending on the configuration mass structure over the quasi-period, there is a possibility that the subsystems would stay or migrate into other finite stable configurations. This is assuming that there are no external perturbations or that the external perturbations are so small as not to affect the configuration finite stability over the quasi-period. The other possibility is that subsystem structure disintegrates and/or escapes the n-body configuration thus making the configuration unstable. This seems to be consistent with Hopf's first theorem, that a system is either recurrent or dissipative.

Question here is how to apply this collinear infinitesimal interval method to study particle behavior for multi-mass configurations. Possible applications would require analyzing configurations on a subsystem-by-subsystem basis. For example, looking at subsystem finite stability, resonance locations, determination of r_∞/Euler point oscillations etc. Oscillations of the r_∞/Euler points can be found by taking into account the synodic nature of the infinitesimal interval problem. Consider that the m_4 r_∞ and Euler points oscillate over the m_4-m_5 synodic period. Turning off the m_5 and m_6 masses ($m_5 = m_6 = 0$) and computing the r_∞/Euler points for m_4 yields the following values in millions of kilometers

sunward		anti-sunward	
r_∞	Euler point	Euler point	r_∞
58.496	51.908	54.325	63.249
with all masses turned on yields			
58.488	51.905	54.320	63.235

This oscillation in the r_∞/Euler points is mainly due to m_5 with very small effect from m_2 and minor effect from m_6. When m_4 is in line with m_5 as seen in the second set values, the r_∞/Euler points move closer to m_4. When m_4 is out of alignment with m_5 as seen in the first set of values the r_∞/Euler points will move away from m_4. One oscillation is completed over the m_4/m_5 synodic period of approximately 19.86 years. Masses m_4 and m_5 may show the most pronounced r_∞/Euler oscillation effect of large masses in the solar system. This effect may not be observable.

In general, over many synodic periods, masses may drift into resonance regions (or their vicinity) that were created by the planets/moons etc. These regions can theoretically be determined from studying the period ratios or subsets of the period ratios. Results from these analyses can then be verified against astrodynamics tables.

2.3 Multiple Binary Structure

Collinear Double Binary Configuration

Basic mathematical logic has been developed and used in section 1.3 for the infinite binary collinear configuration solutions. These binary structures when analyzed can aid in the understanding of particle motion for the purpose of determining system and sub-system relative stability. Specifically, the double binary configuration (Roy, Steves, 2000, 299-318, Szell, Steves, 2002, 45-50) is a candidate of interest for this purpose. Conventional methods of stability such as stability in the sense of Lagrange or Lyapunov are used to determine stability for all time. Stability in the sense of Lagrange analyzes the first order linear differential equations with constant coefficients and then solves the eigenvalue problem assuming exponential solutions where positive exponents tend to indicate unstable systems and negative exponents tend to indicate stable systems. In Lyapunov stability theory (first method) the linear approximation is usually not sufficient to determine stability and more advanced non-linear analysis is required. In this study, stability in the sense of Lagrange will be presented for only the first order approximation will be derived. Stability results in the sense of Lagrange will then be compared to finite stability analysis using numerically integrated state vectors from the infinitesimal interval method

Initially, after some manipulation, the four-body vector equations of motion can be transformed into scalar Jacoby coordinates structured as a collinear double binary system over an infinitesimal real interval at time zero. These equations of motion are only valid within a small neighborhood of time zero.

$$\ddot{r}_{r1} = \frac{G\mu_{r1}}{r_{r1}^2} - \left(\frac{1}{r_{32}^2} - \frac{1}{r_{31}^2}\right) Gm_3 - \left(\frac{1}{r_{42}^2} - \frac{1}{r_{41}^2}\right) Gm_4 \qquad \text{Equation 2.3.1}$$

$$\ddot{r}_{r2} = \frac{G\mu_{r2}}{r_{r2}^2} - \left(\frac{1}{r_{31}^2} - \frac{1}{r_{41}^2}\right) Gm_1 - \left(\frac{1}{r_{32}^2} - \frac{1}{r_{42}^2}\right) Gm_2$$

$$\ddot{\rho}_1 = \frac{G\mu_{\rho 1}}{\mu_{r1}\mu_{r2}} \left(\left(\frac{m_3}{r_{31}^2} + \frac{m_4}{r_{41}^2}\right) m_1 + \left(\frac{m_3}{r_{32}^2} + \frac{m_4}{r_{42}^2}\right) m_2\right)$$

Using the Taylor series linear expansion (or the Euler-Lagrange method) in three variables

$$f(r_{r1}, r_{r2}, \rho_1) = f(r_{r10}, r_{r20}, \rho_{10}) + (\frac{\partial f}{\partial r_{r1}}\epsilon_{r1} + \frac{\partial f}{\partial r_{r2}}\epsilon_{r2} + \frac{\partial f}{\partial \rho_1}\epsilon_{\rho_1}) \mid_{r_{r10}, r_{r20}, \rho_{10}}$$

equation 2.3.1 can be transformed into linearized equations of motion expanded about initial conditions r_{r10}, r_{r20} and ρ_{10} where

$$r_{r1} = r_{r10} + \epsilon_{r1} = r_{r10}(1 + {}^{\epsilon_{r1}}/_{r_{r10}}) \qquad r_{r10} > \epsilon_{r1}$$

$$r_{r2} = r_{r20} + \epsilon_{r2} = r_{r20}(1 + {}^{\epsilon_{r2}}/_{r_{r20}}) \qquad r_{r20} > \epsilon_{r2}$$

$$\rho_1 = \rho_{10} + \epsilon_{\rho 1} = \rho_{10}(1 + {}^{\epsilon_{\rho 1}}/_{\rho_{10}}) \qquad \rho_{10} > \epsilon_{\rho 1}$$

and then substituting these equations into the scalar form of equation 2.3.1 with ϵ_{r1}, ϵ_{r2} and $\epsilon_{\rho 1}$ representing small changes in the respective binary distances and the distance between the binaries within a small neighborhood of time zero. This results in a coupled set of second order linear homogeneous differential equations with constant coefficients in ϵ_{r1}, ϵ_{r2} and $\epsilon_{\rho 1}$ coordinates where only linear ϵ_{r1}, ϵ_{r2} and $\epsilon_{\rho 1}$ terms are considered in the transformation. Equation 2.3.1 has been reduced to a workable form to determine stability in the sense of Lagrange for the collinear double binary configuration

$$\ddot{\epsilon}_{r1} = (x\alpha_1 - l\beta_1)\epsilon_{r1} - \alpha_1\epsilon_{r2} + \beta_1\epsilon_{\rho 1} \qquad \text{Equation 2.3.2}$$

$$\ddot{\epsilon}_{r2} = \alpha_2\epsilon_{r1} - \left(\frac{\alpha_2}{x} + \frac{l}{x}\beta_2\right)\epsilon_{r2} + \beta_2\epsilon_{\rho 1}$$

$$\ddot{\epsilon}_{\rho 1} = -a_3\epsilon_{r1} + \beta_3\epsilon_{r2} + \left(\frac{\alpha_3}{l} - \frac{x}{l}\beta_3\right)\epsilon_{\rho 1}$$

Coefficients α_i and β_i in equation 2.3.2 from the expansion are as follows

$$\alpha_1 = 2\frac{Gm_3m_4}{\mu_{r2}}\left(\left(\frac{1}{r_{320}^3} - \frac{1}{r_{310}^3}\right) - \left(\frac{1}{r_{420}^3} - \frac{1}{r_{410}^3}\right)\right)$$

$$\beta_1 = 2G\left(\left(\frac{1}{r_{320}^3} - \frac{1}{r_{310}^3}\right)m_3 + \left(\frac{1}{r_{420}^3} - \frac{1}{r_{410}^3}\right)m_4\right)$$

$$\alpha_2 = 2\frac{Gm_1m_2}{\mu_{r1}}\left(\left(\frac{1}{r_{310}^3} - \frac{1}{r_{410}^3}\right) - \left(\frac{1}{r_{320}^3} - \frac{1}{r_{420}^3}\right)\right)$$

$$\beta_2 = 2G\left(\left(\frac{1}{r_{310}^3} - \frac{1}{r_{410}^3}\right)m_1 + \left(\frac{1}{r_{320}^3} - \frac{1}{r_{420}^3}\right)m_2\right)$$

$$\alpha_3 = 2\frac{Gm_1m_2}{\mu_{r1}^2\mu_{r2}}\mu_{\rho 1}\left(\left(\frac{m_3}{r_{310}^3}+\frac{m_4}{r_{410}^3}\right)-\left(\frac{m_3}{r_{320}^3}+\frac{m_4}{r_{420}^3}\right)\right)$$

$$\beta_3 = 2\frac{Gm_3m_4}{\mu_{r2}^2\mu_{r1}}\mu_{\rho 1}\left(\left(\frac{1}{r_{310}^3}-\frac{1}{r_{410}^3}\right)m_1+\left(\frac{1}{r_{320}^3}-\frac{1}{r_{420}^3}\right)m_2\right)$$

where $r_{r10}, r_{r20}, \rho_{10}, r_{310}$, etc. are the initial values at time zero with scaling factors defined by $r_{r20} = xr_{r10}$ and $\rho_{10} = lr_{r10}$.

Reformatting equation 2.3.2 to work the eigenvalue problem

$$\begin{pmatrix}\ddot{\epsilon}_{r1}\\ \ddot{\epsilon}_{r2}\\ \ddot{\epsilon}_{\rho 1}\end{pmatrix} = \begin{pmatrix}a_{11} & a_{12} & a_{13}\\ a_{21} & a_{22} & a_{23}\\ a_{31} & a_{32} & a_{33}\end{pmatrix}\begin{pmatrix}\epsilon_{r1}\\ \epsilon_{r2}\\ \epsilon_{\rho 1}\end{pmatrix} \qquad \text{Equation 2.3.3}$$

where

$$a_{11} = x\alpha_1 - l\beta_1 \qquad a_{12} = -\alpha_1 \qquad a_{12} = \beta_1$$

$$a_{21} = \alpha_2 \qquad a_{22} = -\left(\frac{\alpha_2}{x}+\frac{l}{x}\beta_2\right) \qquad a_{23} = \beta_2$$

$$a_{31} = -\alpha_3 \qquad a_{22} = \beta_3 \qquad a_{23} = \left(\frac{\alpha_3}{l}-\frac{x}{l}\beta_3\right)$$

Considering that a n^{th} order differential equation can be reduced to n first order differential equations, then equation 2.3.3 can be rewritten in terms of six first order differential equations

$$\begin{pmatrix}\dot{x}_1\\ \dot{x}_2\\ \dot{x}_3\\ \dot{x}_4\\ \dot{x}_5\\ \dot{x}_6\end{pmatrix} = \begin{pmatrix}0 & 0 & 0 & 1 & 0 & 0\\ 0 & 0 & 0 & 0 & 1 & 0\\ 0 & 0 & 0 & 0 & 0 & 1\\ a_{11} & a_{12} & a_{13} & 0 & 0 & 0\\ a_{21} & a_{22} & a_{23} & 0 & 0 & 0\\ a_{31} & a_{32} & a_{33} & 0 & 0 & 0\end{pmatrix}\begin{pmatrix}x_1\\ x_2\\ x_3\\ x_4\\ x_5\\ x_6\end{pmatrix} \qquad \text{Equation 2.3.4}$$

with the new variables for the double binary configuration being redefined as $x_1 = \epsilon_{r1}$, $x_2 = \epsilon_{r2}$, $x_3 = \epsilon_{\rho 1}$, $x_4 = \dot{\epsilon}_{r1}$, $x_5 = \dot{\epsilon}_{r2}$ and $x_6 = \dot{\epsilon}_{\rho 1}$. Assuming the solution for equation 2.3.4 can be represented in terms of exponentials

$x(t) = Ae^{\lambda t}$, then the eigenvalue problem can be written $(A - \lambda)X = 0$. Evaluating the determinant for the λ eigenvalue solution

$$\begin{vmatrix} \lambda' & 0 & 0 & 1 & 0 & 0 \\ 0 & \lambda' & 0 & 0 & 1 & 0 \\ 0 & 0 & \lambda' & 0 & 0 & 1 \\ a_{11} & a_{12} & a_{13} & \lambda' & 0 & 0 \\ a_{21} & a_{22} & a_{23} & 0 & \lambda' & 0 \\ a_{31} & a_{32} & a_{33} & 0 & 0 & \lambda' \end{vmatrix} = 0 \qquad \lambda' = -\lambda \qquad \text{Equation 2.3.5}$$

results in a sixth order polynomial which can be reduced to a third order polynomial of the form

$$Y^3 - \delta Y^2 + \sigma Y = 0 \qquad Y = \lambda^2 \qquad \text{Equation 2.3.6}$$

with $\delta = a_{11} + a_{22} + a_{33}$

$$\sigma = (a_{11}a_{22} - a_{12}a_{21}) + (a_{11}a_{33} - a_{13}a_{31}) + (a_{22}a_{33} - a_{23}a_{32})$$

The six solutions are

$$\lambda_{1,2} = \pm\frac{1}{2}(\delta + (\delta^2 - 4\sigma)^{1/2} \qquad \lambda_1 = -\lambda_2$$

$$\lambda_{3,4} = \pm\frac{1}{2}(\delta - (\delta^2 - 4\sigma)^{1/2} \qquad \lambda_3 = -\lambda_4$$

$$\lambda_{5,6} = 0$$

The solution to equation 2.3.6 is

$$x_1(t) = A_{11}\left(e^{\lambda_1 t} - 1\right) + A_{12}\left(e^{-\lambda_1 t} - 1\right) + A_{13}\left(e^{\lambda_3 t} - 1\right) + A_{14}\left(e^{-\lambda_3 t} - 1\right) \qquad \text{Equation 2.3.7}$$

$$x_2(t) = A_{21}\left(e^{\lambda_1 t} - 1\right) + A_{22}\left(e^{-\lambda_1 t} - 1\right) + A_{23}\left(e^{\lambda_3 t} - 1\right) + A_{24}\left(e^{-\lambda_3 t} - 1\right)$$

$$x_3(t) = A_{31}\left(e^{\lambda_1 t} - 1\right) + A_{32}\left(e^{-\lambda_1 t} - 1\right) + A_{33}\left(e^{\lambda_3 t} - 1\right) + A_{34}\left(e^{-\lambda_3 t} - 1\right)$$

Due to the double binary differential equations being homogeneous with initial conditions set at zero at time zero, the coefficients A_{ij} cannot be determined resulting in non-unique solutions. Evaluating initial conditions at time zero gives $x_1(0) = \epsilon_{r1}(0) = 0$, $x_2(0) = \epsilon_{r2}(0) = 0$ and $x_3(0) = \epsilon_{\rho 1}(0) = 0$ which is consistent with the formulation of the problem. When time approaches infinity then equation 2.3.7 approaches infinity and the double binary configuration first order approximation will be unstable in the sense of Lagrange. If this problem was analyzed using the more complex non-linear approximation methods in the sense of Lyapunov, it should also result in an unstable condition. These results reflect equation 2.3.1 which is valid only in a small neighborhood of time zero.

Stability for all time is not of paramount importance when considering configurations in the 'real' universe, because, the universe is theoretically not time infinite. Concern is for finite stability, or more relevant, how long a system can maintain its configuration structural integrity before being compromised by internal/external perturbations. The double binary configuration can be made finite stable for extended periods of time by controlling the ratio of the binary separation distance relative to the separation distance between their respective centers of gravity. Assuming that conservation of energy is not violated, that is, mass distance differences and masses cannot be equal to zero, the double binary configuration can approach stability for all time but not equal it. There will always be system perturbations and no matter how small those perturbations are, over a great period of time, small perturbations will grow to be large perturbations that will disrupt the double binary configuration.

An alternate way of analyzing finite stability relative to Lagrange and Lyapunov stability methods involves looking at the double binary period structure in the infinitesimal interval at time zero. The derived periods for each of the double binary Jacoby coordinates r_{r1}, r_{r2} and ρ_1, starting from the equations developed in section 1.3 in chapter one can be put in the following form

$$P_{r1}^2 = 4\pi^2 \frac{r1^3}{G\mu_{r1}} \left(\frac{\mu_{r1}}{\mu_{r1} - \phi_{r1}}\right) = 4\pi^2 \frac{r1^3}{G\mu_{r1}} D_{r1} \qquad \text{Equation 2.3.8}$$

$$P_{r2}^2 = 4\pi^2 \frac{r2^3}{G\mu_{r2}} \left(\frac{\mu_{r2}}{\mu_{r2} - x^2\phi_{r2}}\right) = 4\pi^2 \frac{r2^3}{G\mu_{r2}} D_{r2}$$

$$P_{\rho 1}^2 = 4\pi^2 \frac{\rho 1^3}{G\mu_{\rho 1}} \left(\frac{1}{\frac{l^2}{\mu_{r1}}\phi_{\rho 1}}\right) = 4\pi^2 \frac{\rho 1^3}{G\mu_{\rho 1}} D_{\rho 1}$$

with the scaling factors l and x defined by $\rho 1 = lr1$ and $r2 = xr1$. Each period equation P_{r1}, P_{r1} and $P_{\rho 1}$ in equation 2.3.8 is composed of a Kepler component multiplied by its respective disturbing function D_{r1}, D_{r2} and $D_{\rho 1}$. Since by definition, the Kepler period component is stable for all time, the only way that the individual Jacoby coordinate periods could be stable for all time would be if D_{r1}, D_{r1} and $D_{\rho 1}$ were all equal to one. This situation could only occur if the perturbation coefficients ϕ_{r1} and ϕ_{r2} were equal to zero and $\phi_{\rho 1}$ was equal to $\frac{\mu_{r1}}{l^2}$. Analyzing these perturbation coefficients in the disturbing functions individually shows that this cannot happen without violating conservation of energy. The perturbation coefficients below can only approach these values but not equal them.

$$\phi_{r1} = \left(\frac{r_{21}^2}{r_{32}^2} - \frac{r_{21}^2}{r_{31}^2}\right) m_3 + \left(\frac{r_{21}^2}{r_{42}^2} - \frac{r_{21}^2}{r_{41}^2}\right) m_4$$

$$\phi_{r2} = \left(\frac{r_{21}^2}{r_{41}^2} - \frac{r_{21}^2}{r_{31}^2}\right) m_1 + \left(\frac{r_{21}^2}{r_{42}^2} - \frac{r_{21}^2}{r_{32}^2}\right) m_2$$

$$\phi_{\rho 1} = \left(\frac{r_{21}^2}{r_{31}^2} m_3 + \frac{r_{21}^2}{r_{41}^2} m_4\right) \frac{m_1}{\mu_{r2}} + \left(\frac{r_{21}^2}{r_{32}^2} m_3 + \frac{r_{21}^2}{r_{42}^2} m_4\right) \frac{m_2}{\mu_{r2}}$$

For example, if $\rho 1 \to \infty$ then $r_{32} \to r_{31}$, $r_{42} \to r_{41}$, $r_{41} \to r_{31}$, $r_{42} \to r_{32}$ resulting in ϕ_{r1} and ϕ_{r2} approaching zero. As the terms $\frac{r_{21}^2}{r_{31}^2}$, $\frac{r_{21}^2}{r_{41}^2}$, $\frac{r_{21}^2}{r_{32}^2}$, and $\frac{r_{21}^2}{r_{42}^2}$ multiplied by l^2 approach one for $\rho 1 \to \infty$, then the term $\frac{l^2}{\mu_{r1}} \phi_{\rho 1}$ reduces to $\frac{m_1 + m_2}{\mu_{r1}}$ which approaches one in the limit. The double binary configuration in the infinitesimal interval at time zero can only approach stability for all time but not equal it. Determination of how long a double binary can maintain a given configuration is the subject of finite stability time analysis and this aspect of the problem has not been studied. Accurate solutions may not be possible unless a method of incorporating sphere of influence criteria into the equations of motion can be found.

Collinear Triple Binary Configuration

One of the six-body members of the mathematical logical system is the triple binary configuration which was solved in chapter one. It is the second of the hierarchical solutions constructed in the infinite binary collinear system. This multiple binary structure is representative of real

configurations and can be studied to gain insight into unstable and finite stable mass structures. Stability analysis as applied to the double binary configuration developed in the previous discussion can be extended to the triple binary using the same methodology.

Triple binary configurations can be subdivided into three general classes. They are planetary, planetary/stellar and stellar systems. Planetary triple binary configurations contain only one stellar mass with the remaining masses being of planetary size. Planetary/stellar triple binary configurations contain a combination of stellar and planetary masses. From astronomical observation, the third class is a triple binary star system, which is not common in nature, leading to the conclusion that they may have a narrow stability range evolving into binary component subsystems relatively early in their history.

The infinitesimal interval triple binary configuration can be applied in modelling various mass ordered systems such as a triple binary star configuration. By constructing a theoretical triple binary star system for the purpose of studying the behavior of its subsystem components as well as its overall stability is an example of this applied modelling. Example vector and collinear geometry for a triple binary configuration can be viewed in figures 2.8 and 2.9. Initial mass and mass separation distance values for this theoretical star system are

First Binary	Second Binary	Third Binary
$m_1 = 1.00\ SM$	$m_3 = .60\ SM$	$m_5 = .20\ SM$
$m_2 = .75\ SM$	$m_4 = .45\ SM$	$m_6 = .15\ SM$
$r1 = 1.00\ AU$	$r2 = 1.00\ AU$	$r3 = 1.00\ AU$

$\rho_1 = 50\ AU$ for the initial separation distance between $m_1 m_2$ and $m_3 m_4$

$\rho_2 = 66\ AU$ for the initial separation distance between $m_1 m_2 m_3 m_4$ and $m_5 m_6$

$SM = Solar\ Mass$

$AU = Astronomical\ Unit$

A planar triple binary state vector was computed from the above mass distance data and numerically integrated for a period of one thousand years. Results of this triple binary star system numerical integration for the first fifty years can be found illustrated in figure 2.10 where binary separation distance for each binary component has been plotted against time. The triple binaries have been structured such that they are successively less massive which is consistent with observation of known triple binary star systems. The first binary (red line) is the most massive and shows the least separation distance variation and the third binary (black line) is the least massive showing the most separation variation. This triple binary star system has been designed specifically to be very short-term stable as can be seen with the separation distance $\rho_2 = 66\ AU$. In this unstable configuration the third binary has the greatest separation distance variation due to its close proximity to the double binary subsystem. At about nine hundred and twenty-eight years, the third binary of this theoretical star system has decoupled leaving a double binary configuration as an end result. This is on the assumption that the decoupled third binary does not disrupt the double binary system in its decoupling at some future time. Third binary decoupling is illustrated in figure 2.11 where the third binary exhibits the greatest separation distance variation. Multiple numerical integrators with different time steps and global orders were used to integrate the same individual triple binary trajectories in this study to be assured of the trajectory accuracy (Varadi et al, 1996).

A finite stable theoretical triple binary star system like in the above example would expect to have a ρ_2 approximately in the order of 1000 AU. Numerically integrating a test trajectory where $\rho_2 = 1000\ AU$ for a period of fifty thousand and fifty years with results for the last fifty years can be found illustrated in figure 2.12. This theoretical triple binary star system is now finite stable with the second binary the most eccentric and the third binary showing the most circular orbit.

There exists in the real galaxy triple binary star configurations of which Alpha Geminorum (Castor) is one. Castor is obviously a finite stable star system and would be of interest to study in terms of its period structure using the infinitesimal interval method. A simulation has been made using approximate astronomical data and is not considered a modelling of the real star system. Approximate mass and mass separation distances for the Castor triple binary star system are

First Binary	Second Binary	Third Binary
$m_1 = 2.15\ SM$	$m_3 = 1.70\ SM$	$m_5 = .62\ SM$
$m_2 = .50\ SM$	$m_4 = .50\ SM$	$m_6 = .57\ SM$
$r1 = .119\ AU$	$r2 = .052\ AU$	$r3 = .018\ AU$

$\rho_1 = 101.9\ AU$ for the separation distance between $m_1 m_2$ and $m_3 m_4$

$\rho_2 \sim 1100\ AU +$ for the separation distance between $m_1 m_2 m_3 m_4$ and $m_5 m_6$

$SM = Solar\ Mass$

$$AU = Astronomical\ Unit$$

As can be seen from the astronomical data the Castor star system is composed of a low mass third binary in orbit around a more massive double binary subsystem. All three binaries are relatively close pairs showing high angular momentum indicative of the individual binaries being very stable. The Castor configuration resembles a classic trinary star system where each Castor close binary is like an individual star. The least stable components of the Castor system are the Jacoby coordinates ρ_1 and ρ_2 with $r1$, $r2$ and $r3$ being the most stable. Extending double binary period equation 2.3.8 to find the disturbing functions for triple binary configuration stability analysis yields

$$P_{r1}^2 = 4\pi^2 \frac{r1^3}{G\mu_{r1}} \left(\frac{\mu_{r1}}{\mu_{r1} - \phi_{r1}}\right) = 4\pi^2 \frac{r1^3}{G\mu_{r1}} D_{r1} \quad \text{Equation 2.3.9}$$

$$P_{r2}^2 = 4\pi^2 \frac{r2^3}{G\mu_{r2}} \left(\frac{\mu_{r2}}{\mu_{r2} - x_1^2 \phi_{r2}}\right) = 4\pi^2 \frac{r2^3}{G\mu_{r2}} D_{r2}$$

$$P_{r3}^2 = 4\pi^2 \frac{r3^3}{G\mu_{r3}} \left(\frac{\mu_{r3}}{\mu_{r3} - x_2^2 \phi_{r3}}\right) = 4\pi^2 \frac{r3^3}{G\mu_{r3}} D_{r3}$$

$$P_{\rho 1}^2 = 4\pi^2 \frac{\rho 1^3}{G\mu_{\rho 1}} \left(\frac{1}{\frac{l_1^2}{\mu_{r1}}(\phi_{\rho 1} + \frac{\mu_{r3}}{\mu_{r1}}\phi_{\rho 2})}\right) = 4\pi^2 \frac{\rho 1^3}{G\mu_{\rho 1}} D_{\rho 1}$$

$$P_{\rho 2}^2 = 4\pi^2 \frac{\rho 2^3}{G\mu_{\rho 2}} \left(\frac{1}{\frac{l_2^2}{\mu_{\rho 1}}\phi_{\rho 2}}\right) = 4\pi^2 \frac{\rho 2^3}{G\mu_{\rho 2}} D_{\rho 2}$$

with the corresponding perturbing functions

$$\phi_{r1} = \left(\frac{r_{21}^2}{r_{32}^2} - \frac{r_{21}^2}{r_{31}^2}\right) m_3 + \left(\frac{r_{21}^2}{r_{42}^2} - \frac{r_{21}^2}{r_{41}^2}\right) m_4 + \left(\frac{r_{21}^2}{r_{52}^2} - \frac{r_{21}^2}{r_{51}^2}\right) m_5 + \left(\frac{r_{21}^2}{r_{62}^2} - \frac{r_{21}^2}{r_{61}^2}\right) m_6$$

$$\phi_{r2} = \left(\frac{r_{21}^2}{r_{41}^2} - \frac{r_{21}^2}{r_{31}^2}\right) m_1 + \left(\frac{r_{21}^2}{r_{42}^2} - \frac{r_{21}^2}{r_{32}^2}\right) m_2 + \left(\frac{r_{21}^2}{r_{53}^2} - \frac{r_{21}^2}{r_{54}^2}\right) m_5 + \left(\frac{r_{21}^2}{r_{63}^2} - \frac{r_{21}^2}{r_{64}^2}\right) m_6$$

$$\phi_{r3} = \left(\frac{r_{21}^2}{r_{61}^2} - \frac{r_{21}^2}{r_{51}^2}\right) m_1 + \left(\frac{r_{21}^2}{r_{62}^2} - \frac{r_{21}^2}{r_{52}^2}\right) m_2 + \left(\frac{r_{21}^2}{r_{63}^2} - \frac{r_{21}^2}{r_{53}^2}\right) m_3 + \left(\frac{r_{21}^2}{r_{64}^2} - \frac{r_{21}^2}{r_{54}^2}\right) m_4$$

$$\phi_{\rho 1} = \left(\frac{r_{21}^2}{r_{31}^2} m_3 + \frac{r_{21}^2}{r_{41}^2} m_4\right) \frac{m_1}{\mu_{r2}} + \left(\frac{r_{21}^2}{r_{32}^2} m_3 + \frac{r_{21}^2}{r_{42}^2} m_4\right) \frac{m_2}{\mu_{r2}} - \left(\frac{r_{21}^2}{r_{53}^2} m_3 + \frac{r_{21}^2}{r_{54}^2} m_4\right) \frac{m_5}{\mu_{r2}} - \left(\frac{r_{21}^2}{r_{63}^2} m_3 + \frac{r_{21}^2}{r_{64}^2} m_4\right) \frac{m_6}{\mu_{r2}}$$

$$\phi_{\rho 2} = \left(\frac{r_{21}^2}{r_{51}^2} m_5 + \frac{r_{21}^2}{r_{61}^2} m_6\right) \frac{m_1}{\mu_{r3}} + \left(\frac{r_{21}^2}{r_{52}^2} m_5 + \frac{r_{21}^2}{r_{62}^2} m_6\right) \frac{m_2}{\mu_{r3}} + \left(\frac{r_{21}^2}{r_{53}^2} m_5 + \frac{r_{21}^2}{r_{63}^2} m_6\right) \frac{m_3}{\mu_{r3}} + \left(\frac{r_{21}^2}{r_{54}^2} m_5 + \frac{r_{21}^2}{r_{64}^2} m_6\right) \frac{m_4}{\mu_{r3}}$$

Plotting D_{r1},. D_{r2}, D_{r3}, $D_{\rho 1}$ and $D_{\rho 2}$ as a function of the respective perturbing functions ϕ_{r1}, ϕ_{r2}, ϕ_{r3}, $\phi_{\rho 1}$ and $\phi_{\rho 2}$, letting ρ_2 vary, keeping all other astronomical parameters constant, is an example of how the relative stability of the Castor system would change by placing the third binary at different distances from the double binary subsystem. Figure 2.13 shows the relative stability of the three binary subsystems D_{r1},. D_{r2} and D_{r3} with the third binary being the most stable for $\rho_2 \sim 1100 AU$. Approaching 110 AU (and closer) the third binary would become the most unstable as it neared the double binary system center of gravity. The values along the ordinate have been subtracted from one, with the zero-value indicating stability for all time. The Jacoby coordinate $\rho_2 = 1100\ AU +$ is marked on the plot to locate the Castor star system. An analogous plot for the theoretical triple binary configuration for $\rho_2 = 66\ AU$ can be found in figure 2.14 for comparison. Binaries in the Castor system are relatively more stable than binaries in the theoretical triple binary system due to their closer separation distance.

Relative stability $D_{\rho 1}$ and $D_{\rho 2}$ for the Castor Jacoby coordinates ρ_1 and ρ_2 are plotted in figure 2.15. As previously noted, ρ_1 and ρ_2 are the least stable components in the trinary star system with ρ_2 being the most unstable. In the real galaxy where external perturbations exist the third binary would eventually be perturbed out of the triple binary configuration. The relative

stability $D_{\rho 1}$ and $D_{\rho 2}$ for the theoretical triple binary can be found in plot 2.16 for comparison to the Castor system. All relative stability numbers are only valid in the infinitesimal interval at time zero and it is not known how they relate to absolute time.

The question may arise if multiple binary star systems beyond the triple binary star system could exist. In consideration that the triple binary star system exists in a narrow stability window as a function of time, then the existence of a quadruple binary star system would be very problematic. There is definitely a limit to how many binary star system components can exist in a finite stable configuration. It may very well be three. This would not be true for the planetary and stellar/planetary configurations where more complicated systems can be structured.

Higher Order Collinear Binary Configurations

In chapter one, the infinite collinear binary problem was solved under a given set of conditions. Using those solutions in conjunction with the applications for the double and triple binary systems just reviewed, allows moving on to work with more complex quadruple and other multiple binary configurations to determine additional trajectory characteristics. By convention, mass one was usually used as the dominant mass in n-body applications. However, in the more general collinear n-body case, any mass in the configuration can be assigned any value, thus, giving greater flexibility in multi-mass systems applications.

An example would be to determine external perturbations on a given multi-mass configuration demonstrating a more realistic trajectory modelling. This can be achieved by having one subset of masses (a star system) perturbed by another subset of masses (another star system or galactic core). For example, in the quadruple binary configuration mass one is a star with mass two through mass six being planets. Mass seven and mass eight (the perturbing masses) could be either a planet/star or a double star configuration. By extending ρ_3, which is the distance between the fourth binary and the triple binary center of gravity to interstellar distances, the state vector of this configuration can be numerically integrated to determine the perturbation effects on both mass subsets.

Modelling collinear n-body configurations to study trajectory perturbations is not limited to multi-binary systems. Any n-body configuration or sets of configurations such as in equation 1.1.5 and figures 2.5 through 2.7 can be arrayed to analyze complex systems.

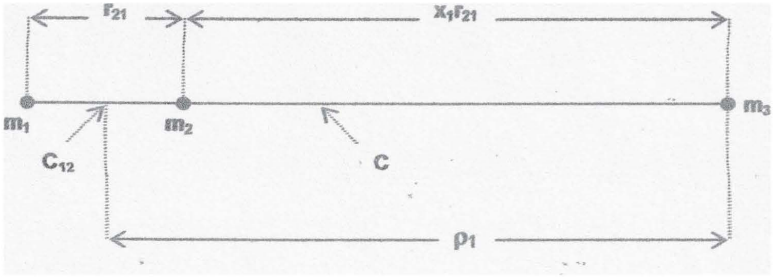

FIGURE 2.1. Collinear Three-Body Geometry

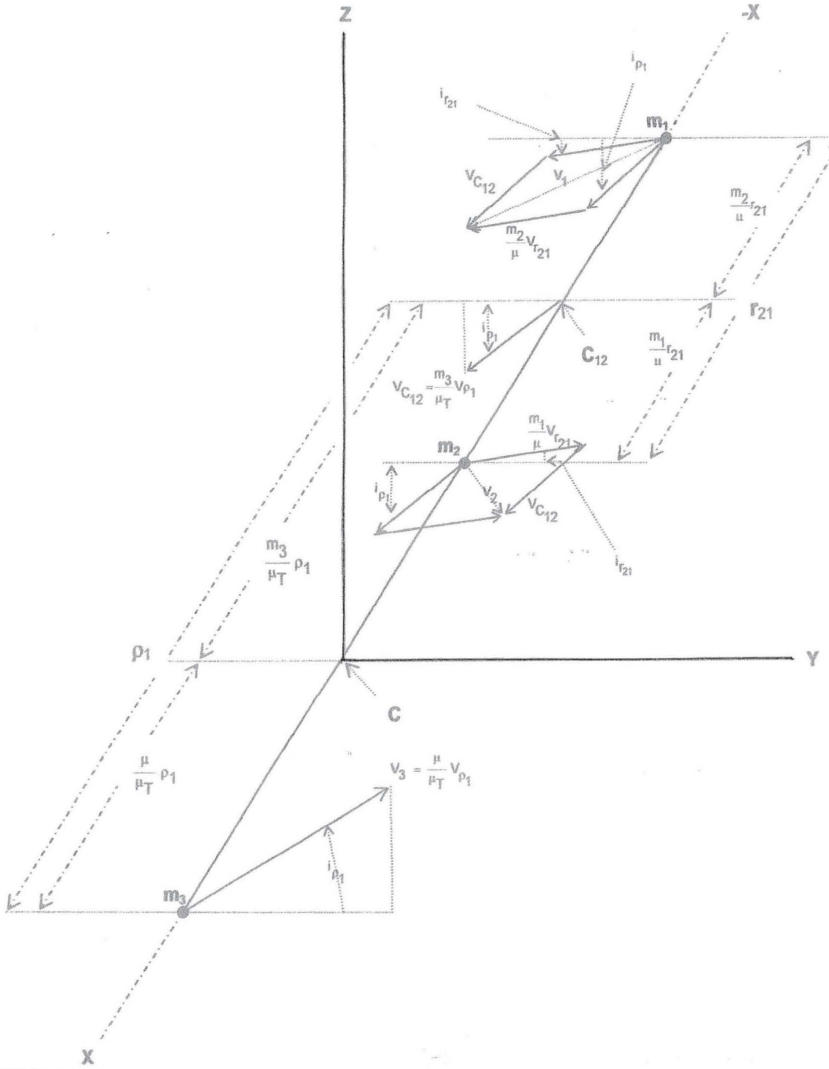

FIGURE 2.2. 123 Three-Dimensional Geometry

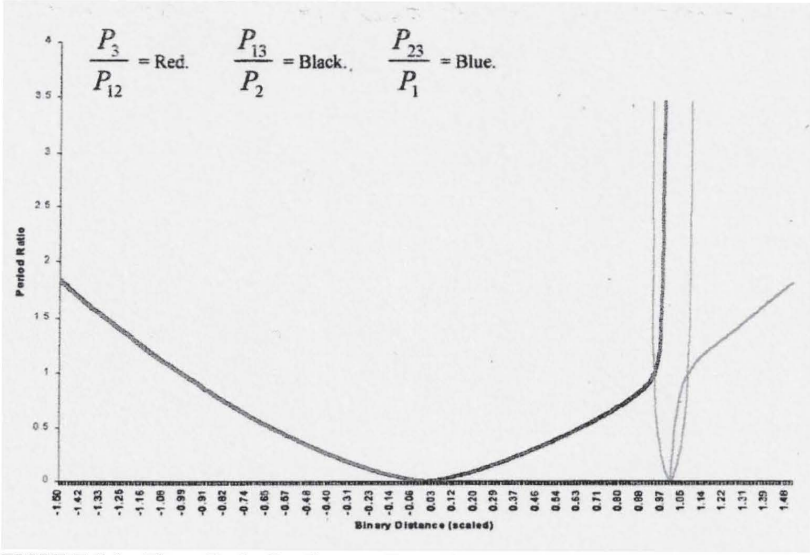

FIGURE 2.3. Three-Body Contiguous Geometry

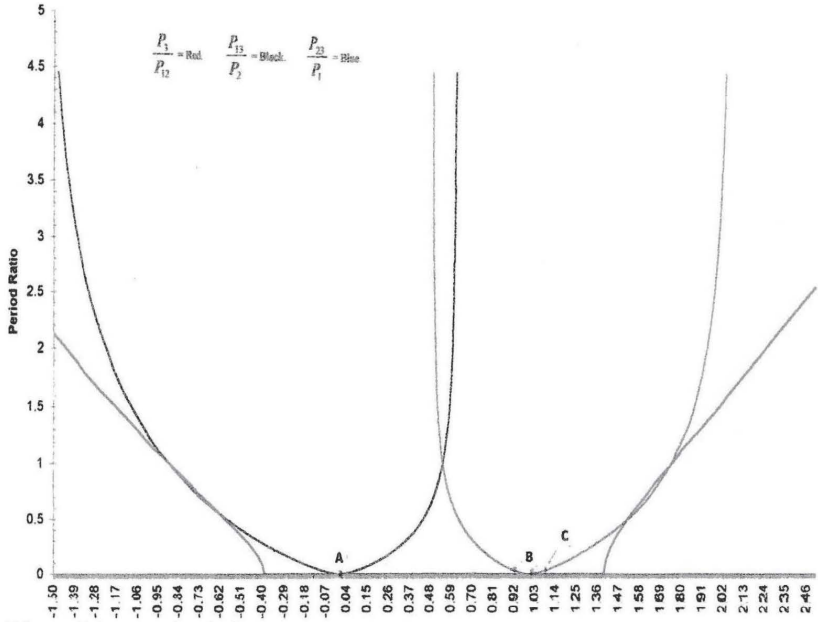

Binary Distance (scaled)

FIGURE 2.4. Collinear 40 Eridani Trinary Star Geometry

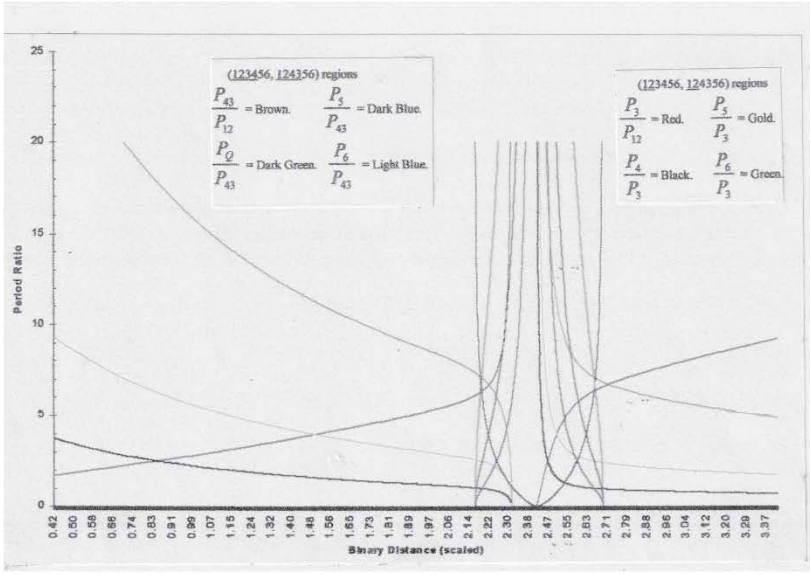

FIGURE 2.5. Six-Body Period Ratios (Jupiter)

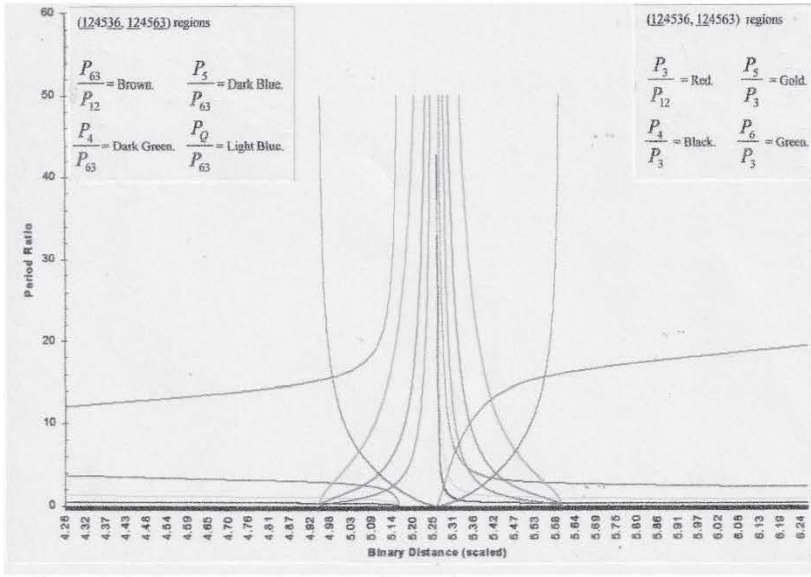

FIGURE 2.6. Six-Body Period Ratios (Saturn)

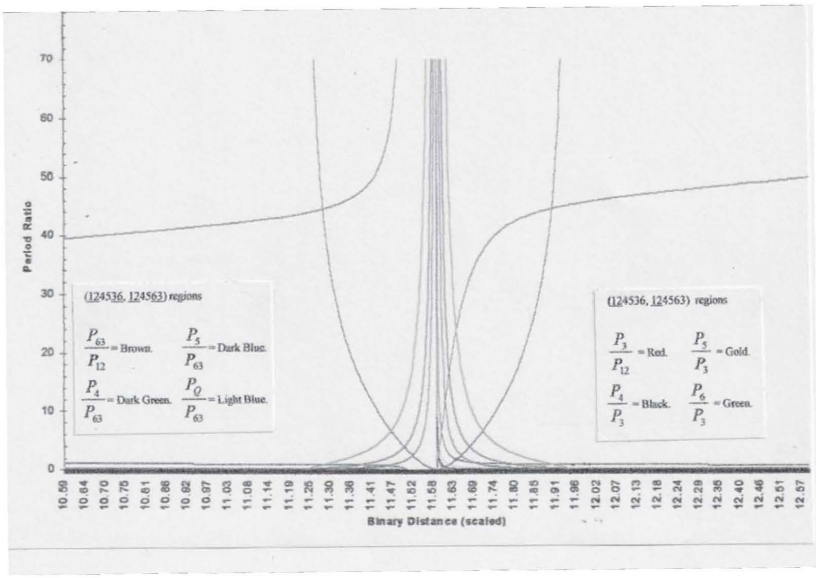

FIGURE 2.7. Six-Body Period Ratios (Uranus)

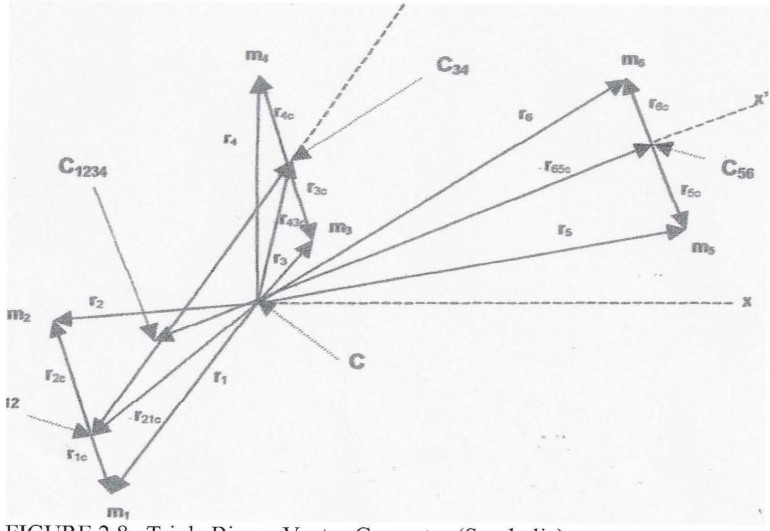

FIGURE 2.8. Triple Binary Vector Geometry (Symbolic)

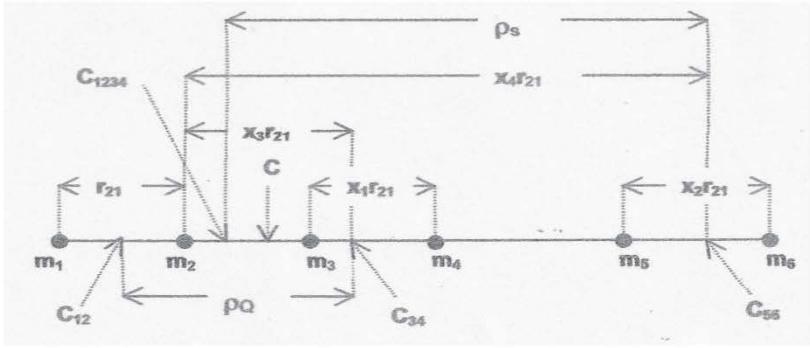

FIGURE 2.9. Triple Binary Collinear Geometry

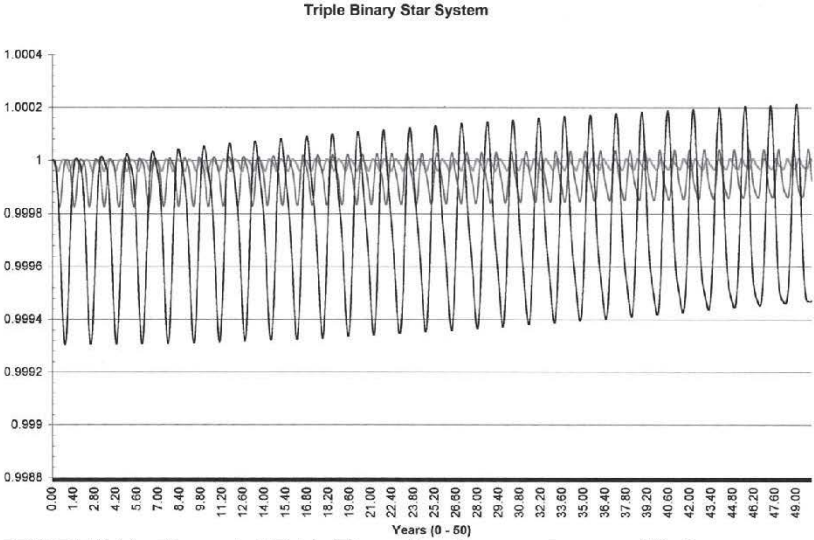

FIGURE 2.10. Theoretical Triple Binary Star System—Integrated Trajectory

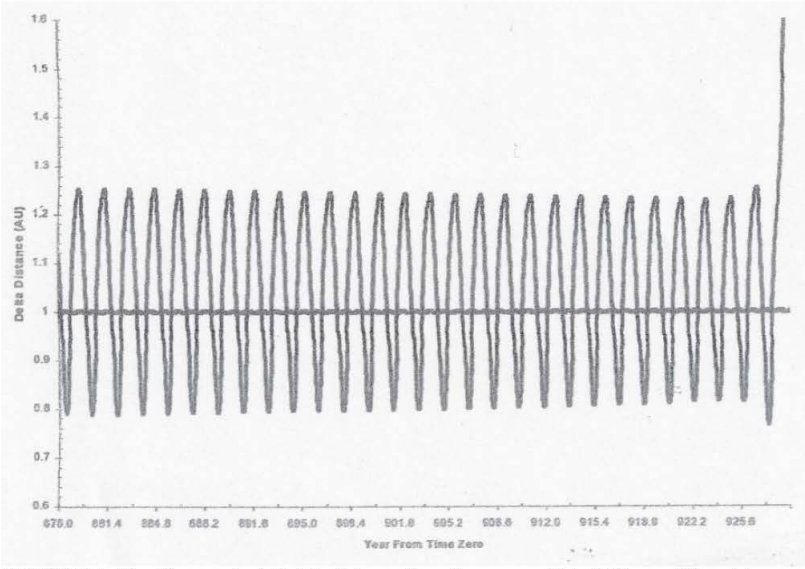

FIGURE 2.11. Theoretical Triple Binary Star System—Third Binary Unstable

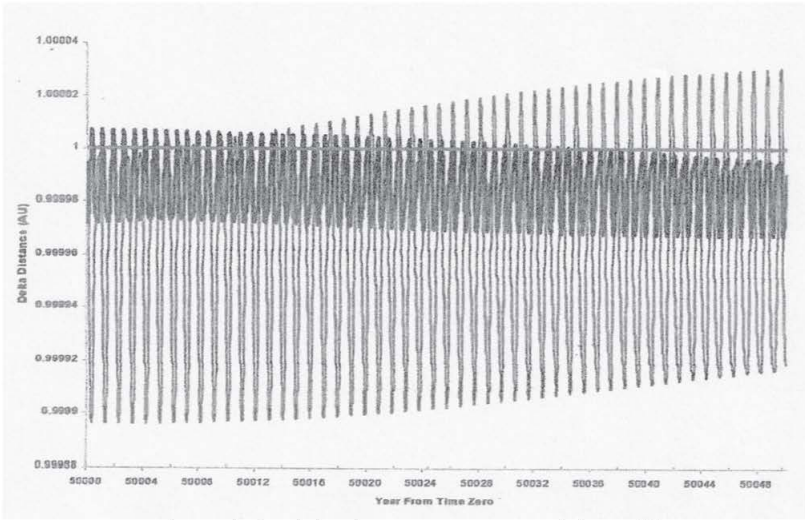

FIGURE 2.12. Theoretical Triple Binary Star System—Finite Stable

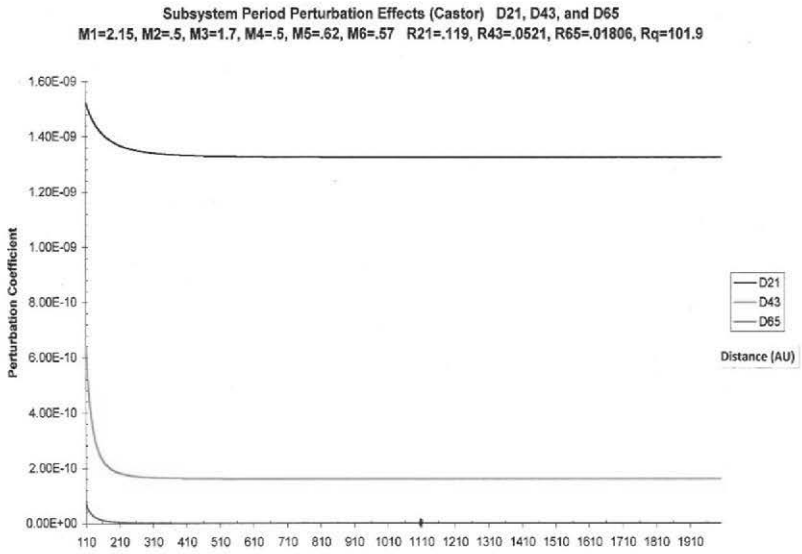

FIGURE 2.13. Castor Triple Binary Star System Binary Subsystem Finite Stability

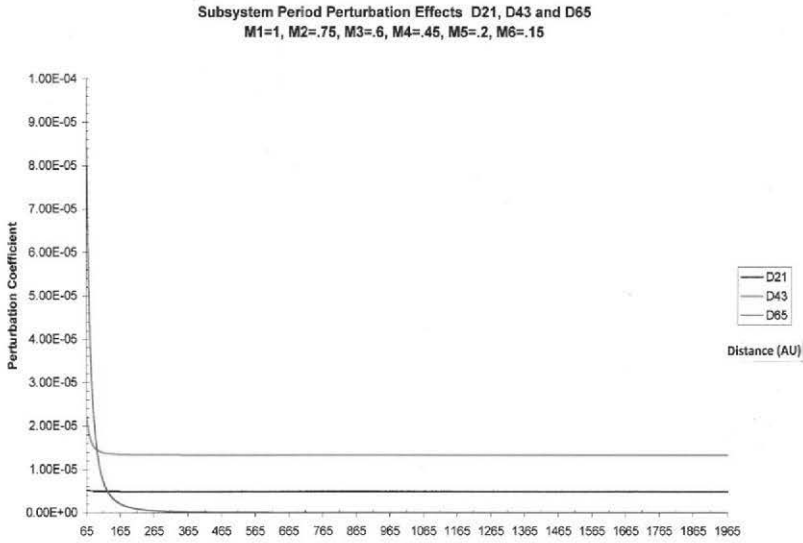

FIGURE 2.14. Theoretical Triple Binary Star System Binary Subsystem Finite Stability

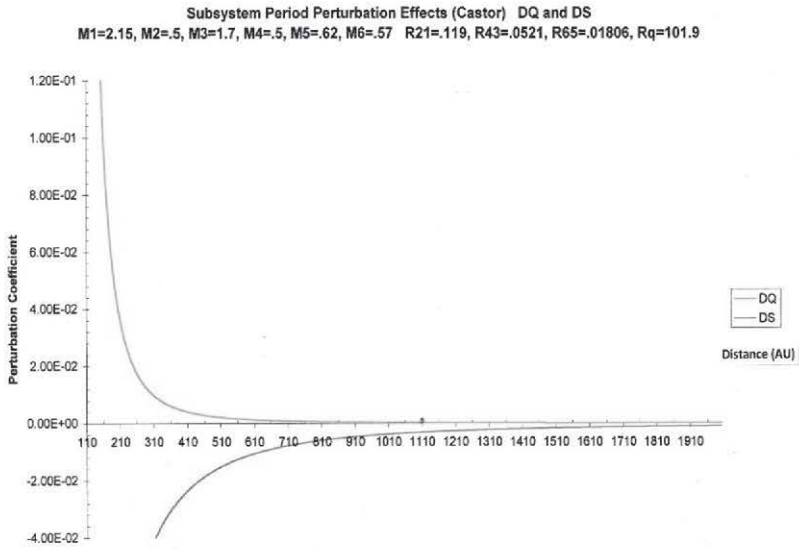

FIGURE 2.15. Castor Triple Binary Star System ρ_1 and ρ_2 Finite Stability

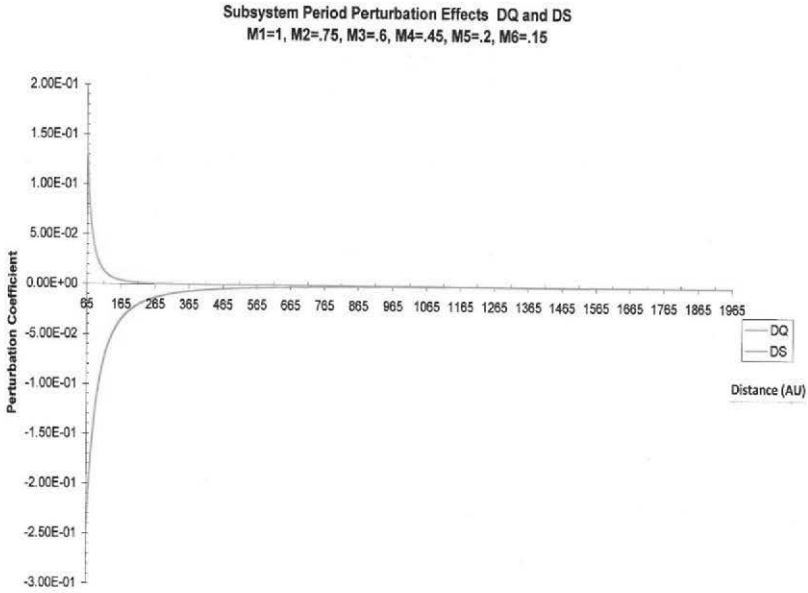

FIGURE 2.16. Theoretical Triple Binary Star System ρ_1 and ρ_2 Finite Stability

2.4 Problems

Section 2.1

1. Starting from the 123 three-body configuration equations of motion shown in equation 2.1.5 derive the period ratio and expand it as a function of x to verify that it is a fifth order polynomial that reduces to the Euler quintic equation for the special case when the period of the binary is equal to the period of mass three about the binary.
2. Calculate the Jacoby 123 r and ρ velocities from equation 2.1.5 and verify the results listed in equation 2.1.10. Show that twice the kinetic energy is equal to the potential energy thus verifying conservation of energy in the infinitesimal interval at time zero.
3. Using the solution method set forth in equations 2.1.1 through 2.1.13 calculate the period ratios, inertial velocities, perturbation coefficients, scaling factors and three-dimensional state vector for the 123 three-body configuration listed in equation 2.1.14.
4. Using a diagram in like manner to figure 2.2, show the three-dimensional geometry at time zero for the 123 three-body configuration.
5. Calculate the intersection point between the three-body period ratios for the 123 and 123 configurations and show that the result is an Euler point.
6. Compute the Jupiter r_∞ points using the three-body period ratios from the 132 and 123 configurations. The Jupiter to sun mass ratio is $9.5479\text{x}10^{-4}$ and mass three is approximately zero. Distance between mass one and mass two is 5.203 AU.
7. Determine solar r_∞ points for the case where the galactic mass (S) is $2x10^{10}$ solar masses and at distances 20,000 LY, 25,000LY and 30,000LY from the galactic center. Compare this to the results for the r_∞ points listed in table I.
8. Sphere of influence (SOI) was derived using the infinitesimal interval method and is a general equation in that mass three is not zero. Show that when mass three approaches zero SOI defaults to the Cheboterav SOA equation where $\Delta_2 = rm^{\frac{1}{2}}$.

Section 2.2

1. Using equation 1.2.1 through 1.2.3 compute the ten period ratios of the six-mass configuration 123456. By systematically inverting and multiplying the results of equation 1.2.3 can reduce the effort to determine these ratios.
2. Determine the velocities and perturbation coefficients for the six-mass configuration 123456. Write out the three-dimensional state vector for this configuration. Show that twice the kinetic energy is equal to the potential energy.
3. Plot the Jupiter period ratios as a function of the binary scaled distance like that illustrated in figures 2.5 through 2.7. The period ratios to be evaluated are 1234 and 12 34 on the sunward side of Jupiter and 12 43 and 1243 on the anti-sunward side of Jupiter, where mass one is the sun, mass two is Mars, mass three is the probe mass ($m_3 \to 0$) and mass four is Jupiter.
4. Compute all the period ratios for the six-mass configuration 12 34 56. Will need to determine the sidereal synodic relations to find the perturbation coefficients and velocities to start this problem.
5. Determine mathematically the period ratio $\frac{P_3}{P_{21}}$ point of inflection for the 123 configuration. Also, for the period ratios $\frac{P_4}{P_3}$, $\frac{P_5}{P_3}$ and $\frac{P_6}{P_3}$ determine points of inflection in the 123456 configuration.

Section 2.3

1. Derive the double binary scalar equations of motion starting with the four-body vector equations of motion. Initially, convert the vector equations into Jacoby coordinates by coupling mass one with mass two and mass three with mass four. Consider the relationship between the mass acceleration vectors and the mass position vectors when setting up the collinear equations of motion to match equation 2.3.1.
2. Using the Taylor expansion, transform equation 2.3.1 into linearized equations of motion in terms of coordinates ϵ_{r1}, ϵ_{r2} and $\epsilon_{\rho 1}$ for the initial conditions r_{r10}, r_{r20} and ρ_{10} respectively. Check this result against equation 2.3.2.
3. Show that the determinant of $\begin{vmatrix} a_{11} & a_{12} & a_{13} \\ a_{21} & a_{22} & a_{23} \\ a_{31} & a_{32} & a_{33} \end{vmatrix}$ is equal to zero. This will verify equation 2.3.6 which is the result of evaluating the six by six determinant in equation 2.3.5.

4. Derive equation 2.3.8 double binary Jacoby coordinate r_{r1}, r_{r2} and ρ_1 periods using the equations developed in section 1.3 in chapter one. Verify that the double binary cannot be stable for all time in the infinite interval at time zero.
5. Show, using equation 2.3.9 that the theoretical triple binary star configuration can approach stability for all time yet never be stable for all time as ρ_2 approaches infinity. Use the same line of reasoning that was put forth for the double binary system with equation 2.3.8.

2.5 References

Arnold, V. I., 1978, *Mathematical Methods of Classical Mechanics*,Berlin, Springer Verlag.

Bauer, T. A., 2001, *Resonance Induced Coupled Planar N-Body Collinear Point Solutions*, Santa Barbara, CA, AAS/AIAA Space Flight Mechanics Meeting.

Belbruno, E., Marsden, B. G.1997. Resonance Hopping in Comets. *Astronomical Journal, Volume 113, Number 4, April.*

Cheboterav, G. A.,1967, *Analytical and Numerical Methods of Celestial Mechanics*, New York., American Elsevier,

Hagihara, Y., 1975, *Celestial Mechanics-Periodic and Quasi-Periodic Solutions Volume IV Part 2*, Japan, Society for the Promotion of Science, .

Hagihara, Y., 1976, *Celestial Mechanics-Topology of the Three-Body Problem Volume V Part 1*, Japan, Society for the Promotion of Science.

Harrington, R. S., 1977, A Review of the Dynamics of Classical Triple Stars, *Revista Mexicana de Astronomia.*

Kurth, R.,1957, *Introduction to the Mechanics of Stellar Systems*, Oxford, Pergamon Press.

Nieto, M. M., 1972, *The Titius-Bode Law of Planetary Distances–Its History and Theory*, Oxford, Pergamon Press.

Pollard, H., 1966, *Mathematical Introduction to Celestial Mechanics*, Englewood Cliffs, NJ, Prentice Hall.

Roy, A. E., 1978, *Orbital Motion*, Bristol, Dorking, Surrey, England, Adam Hilger Ltd.

Roy, A. E., Steves B. A., 2000, The Caledonian Symmetrical Double Binary Four-Body Problem I: Surfaces of Zero-Velocity Using the Energy Integral, *Celestial Mechanics and Dynamical Astronomy.*

Szebehely, V. G., 1967, *Theory of Orbits*, New York, Academic Press.

Szebehely V., 1977, Review of the Dynamical Aspects of Triple Systems, *Revista Mexicana de Astronomia.*

Szell, A., Steves, B. A., Roy A. E. 2002, Numerical investigation of the Phase Space of the Caledonian Symmetric Double Binary Problem, *PADEU* 12.

Varadi, F., Ghil, M., Newman, W. I., Kaula, W. M., Grazier, K., Goldstein, D. and Lessnick M., 1996, *NBI-A Set of Numerical Integrators for the Gravitational N-Body Problem*, Los Angeles, CA, UCLA.

Wintner, A., 1964, *The Analytical Foundations of Celestial Mechanics*, Princeton, NJ, Princeton University Press.

CHAPTER THREE

CONCENTRIC N-GONS

Particles reside in mass distributions in instantaneous circular planar orbit about a central body. This chapter analyzes structured distributions of these particles starting with the development of the single regular n-gon and evolving to concentric regular multi-polygon configurations. The regular n-gon configuration is a Newtonian system of particles defined as discrete, nonrelativistic and rotating in classical two-dimensional Euclidean space. This is a physical system consistent with the laws of conservation (non-zero mass).

The single regular n-gon or (n-1)-gon configuration (Chenciner, 2003, 286, Hagihara, 1970, 255, Kurth, 1959, 137, Roy, 1998, 1475, Wintner, 1964, 279,306) is composed of particles placed at the vertices of an equal sided polygon. Concentric regular multi-polygon structure is more complex and involves analyzing and solving two basic problems. First is the knowledge of n-gon interaction to determine particle perturbations, where there exist sidereal synodic relations under specified geometrical conditions that mathematically describe these particle perturbations. Sidereal synodic relations with type one geometry within the infinitesimal interval at time zero provide the necessary constraints to solve the planar n-body equations of motion allowing a formulation of n-gon radii, mass and angular velocity distributions. However, non-unique mass and angular velocity distributions result thus requiring further analysis to find the minimum potential energy solution (second problem).

Unique regular concentric n-gon configurations are found by searching for the absolute minimum potential energy solutions. Due to the regular n-gon symmetry these unique solutions possess inter n-gon singularities. Inter n-gon singularities can be removed by differentially rotating the n-gon assemblies such that when collapsed these n-gons form one regular n-gon. The differentially rotated regular n-gon configurations that are inter singularity free are geometrically incompatible with the solution methodology employed in this chapter. Therefore, differentially rotated regular n-gon configurations can not be made inter singularity free.

However, there are inter singularity free n-gon configurations that can be solved by the methods in this chapter but they are composed of a combination of regular and non-regular n-gons. This type of problem is of greater complexity and not dealt with here.

3.1 Single N-Gon Configurations

Before continuing with the concentric n-gon configuration analysis it is necessary to define the coordinate system and basic geometry in which these n-gon problems will be worked. This is in addition to the basic fundamental properties such as the constraints and initial conditions that allow formulation and solution of the structured n-body equations of motion.

Consider a conservative dynamical system described as follows. Define at origin m_1 fixed in two dimensional Euclidean space an inertial right handed coordinate system x,y,z where z = 0 is the concentric n-gon plane of motion. Let x and y be the inertial planar coordinate system, with m_1 located at the barycenter (also the geometrical center). The inertial y-axis is perpendicular to and counterclockwise from the x-axis. Let x' and y' define a coincident coordinate system in the same plane as x and y rotating at angular velocity w with respect to x and y and origin at barycenter m_1, where the vector from m_1 to some designated point on the outermost n-gon orients the x'-axis. Outermost n-gon radius R is at rest with respect to the rotating barycentric coordinate system. The y'-axis is perpendicular to and counterclockwise from the x'-axis, with inertial and rotating coordinate system x and x'-axes coincident at t = 0 (time zero).

For the n-body formulation, it is necessary to perform an infinitesimal orthogonal transformation about the z-axis of the n-body equations of motion in the $x'y'$ coordinate system rotating at angular velocity w relative to the inertial xy coordinate system. Reformulating into the complex plane (Lass, 1957, 314-319, Pollard, 1966, 49) results in

$$\ddot{z}_k + 2wi\dot{z}_k - w^2 z_k = G\sum_{\substack{j=1 \\ j\neq k}}^{N} \frac{m_j}{r_{jk}^3} z_{jk} \qquad k = 1,2,3,\ldots N \qquad \text{Equation 3.1}$$

where $i = \sqrt{-1}$, $z_k = x'_k + iy'_k$ and $r_{jk} = |z_j - z_k|$

Planar n-body equations of motion exist over time interval Δt with sidereal synodic relations defining interaction between successive n-gons. To properly utilize equations of motion and synodic relations requires Δt to be

sufficiently small, such that, Δt approaches zero as a limit. Consequently: Δt is an infinitesimal. This is a necessary condition that allows the infinitesimal orthogonal transformation and corresponding infinitesimal rotation of the equations of motion to be consistent with infinitesimal rotation of sidereal synodic relations in the rotating barycentric coordinate system.

To solve the single regular n-gon configuration orbiting about m_1 it is important to start with equation 3.1. These regular n-gons are central configurations where each particle is rotating with inertial angular velocity w within the infinitesimal interval at time zero. Basically, the n-gon can be considered to rotate as one unit. The angular velocity can be derived systematically as will be demonstrated starting with the three-body problem.

3.1.1 Lagrange Equilateral Triangular Three-Body Problem

It would be informative to review the analysis of the Lagrange equilateral three body problem prior to working the single n-gon problem. This will introduce the methodology for solving the general configuration type worked in the coming pages. Using equation 3.1 with type 1 geometry and assuming all three masses are in instantaneous circular planar orbits in the infinitesimal interval at time zero

$$-w_k^2 z_k = G\sum_{\substack{j=1 \\ j\neq k}}^{3} m_j z_{jk} \qquad \ddot{z_k} = \dot{z_k} = 0 \qquad \text{Equation 3.1.1.1}$$

Writing equation 3.1.1.1 in matrix form, the equations of motion with all masses at rest in the rotating reference frame at time zero becomes $A = 0$ where A is equal to

$$\begin{pmatrix} 1 - m_2\rho_{21} - m_3\rho_{31} & m_2\rho_{21} & m_3\rho_{31} \\ m_1\rho_{21} & 1 - m_1\rho_{21} - m_3\rho_{32} & m_3\rho_{32} \\ m_1\rho_{31} & m_2\rho_{32} & 1 - m_1\rho_{31} - m_2\rho_{32} \end{pmatrix} \begin{pmatrix} z_1 \\ z_2 \\ z_3 \end{pmatrix}$$

with $\rho_{ij} = \frac{G}{w^2 r_{ij}^3}$

Reformulating the above matrix using a symmetry argument based on conservation of energy

$$\begin{pmatrix} \rho_{32} & \rho_{21} & \rho_{31} \\ \rho_{21} & \rho_{31} & \rho_{32} \\ \rho_{31} & \rho_{32} & \rho_{21} \end{pmatrix} \begin{pmatrix} m_1 z_1 \\ m_2 z_2 \\ m_3 z_3 \end{pmatrix} = 0 \qquad \text{Equation 3.1.1.2}$$

results in $\rho_{21} = \rho_{31} = \rho_{32}$ and therefore $\rho_{21} + \rho_{31} + \rho_{32} = \frac{3}{M}$ where $M = m_1 + m_2 + m_3$. The resultant inertial angular velocity is $w^2 = \frac{GM}{r^3}$ with r= $r_{21} = r_{31} = r_{32}$ and all masses each different in magnitude are in circular instantaneous orbits at time zero in the infinitesimal interval with type 1 geometry. It would be expected prior to or after time zero masses exist in instantaneous non-circular orbits. Using the inertial angular velocity determined in the infinitesimal interval, state vectors can be calculated for the Lagrange equilateral three body problem. Numerically integrating the Lagrange triangular state vector determined from the above analysis will show that this equilateral configuration can not be maintained over a finite interval. It is not stable in the sense of Lagrange.

Validity for the symmetry argument formulating equation 3.1.1.2 can be made apparent using the conservation of energy equations. Showing 2T = U will verify this

$$U = \frac{G}{r}(m_1 m_2 + m_1 m_3 + m_2 m_3)$$

$$2T = \frac{GM}{r}(m_1 \frac{r_1^2}{r^2} + m_2 \frac{r_2^2}{r^2} + m_3 \frac{r_3^2}{r^2})$$

Computing the center of gravity will allow determination of the mass radii for the Lagrange triangular configuration ratios $\frac{r_i^2}{r^2}$, thus completing the verification.

3.1.2 Collinear Three-body Configuration

Although not a n-gon, the collinear three-body configuration could possibly be considered a central configuration. This is due to the monotonically increasing magnitude of the perturbation coefficients in a systematically growing single n-gon structure of masses. Where, the collinear three body problem is the initial configuration defining this n-gon structure of masses. Starting with the same initial equations of motion

(equation 3.1.1.1) as the Lagrange equilateral triangle we obtain the following relations

$$\left(\frac{1}{m\rho}-2\right)z_1+z_2+z_3=0 \qquad \text{Equation 3.1.2.1}$$

$$\frac{m_1}{m}z_1+\left(\frac{1}{m\rho}-\frac{m_1}{m}-\frac{1}{8}\right)z_2+\frac{1}{8}z_3=0$$

$$\frac{m_1}{m}z_1+\frac{1}{8}z_2+\left(\frac{1}{m\rho}-\frac{m_1}{m}-\frac{1}{8}\right)z_3=0$$

under conditions $m=m_2=m_3$, $\rho=\rho_{21}=\rho_{31}$, $r_{21}=r_{31}$ and m_1 at the barycenter. From these conditions it can be shown that $\rho_{32}=\frac{1}{8}\rho$. Defining $\alpha=\frac{1}{m\rho}-\frac{m_1}{m}-\frac{1}{8}$ from the second (or using the third) equation of motion and reformulating gives $\frac{m_1}{m}z_1+\alpha z_2+\frac{1}{8}z_3=0$. Using coordinates $z_1=0, z_2=1\ and\ z_3=-1$ from the collinear three-body configuration geometry in the complex plane results in $\alpha=\frac{1}{8}$. The resultant inertial angular velocity for this configuration is

$$w^2=G\frac{m_1\left(1+\frac{1}{4}\frac{m}{m_1}\right)}{r_{12}^3}$$

Formatting equation 3.1.2.1 as a matrix and solving the determinant is an alternate method to obtain the same solution for α.

$$\begin{pmatrix}\left(\frac{1}{m\rho}-2\right) & 1 & 1\\ \frac{m_1}{m} & \alpha & \frac{1}{8}\\ \frac{m_1}{m} & \frac{1}{8} & \alpha\end{pmatrix}\begin{pmatrix}z_1\\ z_2\\ z_3\end{pmatrix}=0 \qquad \text{Equation 3.1.2.2}$$

The collinear three-body angular velocity result can also be obtained by using the infinitesimal interval method derived in chapter two. Using resonance equation 2.1.18 for a 3$\underline{12}$ configuration

$$v_{12}^2=\frac{Gm_1}{r_{12}}\left(\beta-\left(\frac{1}{x^2}-\frac{1}{(1+x)^2}\right)s\right)$$

with $x=1,\quad \beta=1+Q,\quad Q=\frac{m_2}{m_1},\quad s=\frac{m_3}{m_1},\quad m=m_2=m_3$

$$v_{12}^2 = \frac{Gm_1}{r_{12}}\left(1 + \frac{m}{m_1} - \frac{m}{m_1} + \frac{1}{4}\frac{m}{m_1}\right) \qquad w^2 = G\frac{m_1\left(1+\phi\frac{m}{m_1}\right)}{r_{12}^3}$$

where the collinear three-body perturbation coefficient is $\phi = \frac{1}{4}$

All three methods give the same inertial angular velocity for this three-body configuration. Numerically integrating the collinear three-body state vector will show that this configuration will only maintain its initial configuration for a finite time interval as would be expected.

3.1.3 Four-Body Configuration

In the same methodology as the collinear three-body configuration the four-body configuration can be solved. As will be noted, with each additional mass the regular n-gon configuration takes on another equation of motion, as well as, an increased number of constraints. Of primary importance is the determination of the n-body perturbation coefficient ϕ, which results directly from the n-gon structural geometry. This geometrical perturbation is necessary to find the inertial angular velocity. Magnitude of perturbation term ϕ increases as the number of masses in the single n-gon increases.

let $\rho_{ij} = \frac{G}{w^2 r_{ij}^3}$

$$\left(\frac{1}{m\rho} - 3\right)z_1 + z_2 + z_3 + z_4 = 0$$

$$\frac{m_1}{m}z_1 + \left(\frac{1}{m\rho} - \frac{m_1}{m} - \frac{2}{\sqrt{3}^3}\right)z_2 + \frac{1}{\sqrt{3}^3}z_3 + \frac{1}{\sqrt{3}^3}z_4 = 0$$

$$\frac{m_1}{m}z_1 + \frac{1}{\sqrt{3}^3}z_2 + \left(\frac{1}{m\rho} - \frac{m_1}{m} - \frac{2}{\sqrt{3}^3}\right)z_3 + \frac{1}{\sqrt{3}^3}z_4 = 0$$

$$\frac{m_1}{m}z_1 + \frac{1}{\sqrt{3}^3}z_2 + \frac{1}{\sqrt{3}^3}z_3 + \left(\frac{1}{m\rho} - \frac{m_1}{m} - \frac{2}{\sqrt{3}^3}\right)z_4 = 0$$

under constraints

$$m = m_2 = m_3 = m_4$$

$$\rho = \rho_{21} = \rho_{31} = \rho_{41}$$

$$r_{32} = r_{42} = r_{43}$$

$$\rho_{32} = \rho_{42} = \rho_{43} = \frac{1}{\sqrt{3}}\rho.$$

Defining $\alpha = \frac{1}{m\rho} - \frac{m_1}{m} - \frac{2}{\sqrt{3}}$ from the second (or using the third or fourth) equation of motion and reformulating using complex coordinates $z_1 = 0, z_2 = 1, z_3 = -\frac{1}{2} + \frac{\sqrt{3}}{2}i \; and \; z_3 = -\frac{1}{2} - \frac{\sqrt{3}}{2}i$ there results $\alpha = \frac{1}{\sqrt{3}}$. Therefore, the inertial angular velocity for this configuration is

$$\frac{1}{\rho} = m_1 + \frac{3}{\sqrt{3}}m$$

$$w^2 = G\frac{m_1(1+\phi\frac{m}{m_1})}{r_{12}^3} \qquad \text{where} \quad \phi = \frac{\sqrt{3}}{3}$$

The single n-gon configuration structure for the four-body coupled equations of motion shows a logical evolution of a system of rotating masses. This is a result from dividing a circle into Increasingly smaller equal angular partitions where each of these partitions can be represented as an additional mass that will be formulated in the equations of motion.

3.1.4 Five-Body Configuration

Continuing in like manner to the three and four-body configurations, the five-body configuration will be derived under similar conditions and constraints. The recursive nature of the geometric equation structure is made manifest with increasing mass number. This can be seen from the five-body configuration equations listed below.

let $\rho_{ij} = \frac{G}{w^2 r_{ij}^3}$

$$\left(\frac{1}{m\rho} - 4\right)z_1 + z_2 + z_3 + z_4 + z_5 = 0 \qquad \text{Equation 3.1.4.1}$$

$$\frac{m_1}{m}z_1+\left(\frac{1}{m\rho}-\frac{m_1}{m}-\frac{2}{\sqrt{2}^3}-\frac{1}{8}\right)z_2+\frac{1}{\sqrt{2}^3}z_3+\frac{1}{\sqrt{2}^3}z_4+\frac{1}{8}z_5=0$$

$$\frac{m_1}{m}z_1+\frac{1}{\sqrt{2}^3}z_2+\left(\frac{1}{m\rho}-\frac{m_1}{m}-\frac{2}{\sqrt{2}^3}-\frac{1}{8}\right)z_3+\frac{1}{8}z_4+\frac{1}{\sqrt{2}^3}z_5=0$$

$$\frac{m_1}{m}z_1+\frac{1}{\sqrt{2}^3}z_2+\frac{1}{8}z_3+\left(\frac{1}{m\rho}-\frac{m_1}{m}-\frac{2}{\sqrt{3}^3}-\frac{1}{8}\right)z_4+\frac{1}{\sqrt{2}^3}z_5=0$$

$$\frac{m_1}{m}z_1+\frac{1}{8}z_2+\frac{1}{\sqrt{2}^3}z_3+\frac{1}{\sqrt{2}^3}z_4+\left(\frac{1}{m\rho}-\frac{m_1}{m}-\frac{2}{\sqrt{3}^3}-\frac{1}{8}\right)z_5=0$$

under constraints

$$m=m_2=m_3=m_4=m_5$$

$$\rho=\rho_{21}=\rho_{31}=\rho_{41}=\rho_{51}$$

$$\frac{1}{\sqrt{2}^3}\rho=\rho_{32}=\rho_{42}=\rho_{53}=\rho_{54}.$$

$$\frac{1}{8}\rho=\rho_{43}=\rho_{52}$$

$$r_{21}=r_{31}=r_{41}=r_{51}$$

$$r_{32}=r_{42}=r_{53}=r_{54}$$

Defining $\alpha=\frac{1}{m\rho}-\frac{m_1}{m}-\frac{2}{\sqrt{2}^3}-\frac{1}{8}$ from the second (or using the third, fourth or fifth) equation of motion and reformulating using complex coordinates $z_1=0, z_2=1, z_3=i, z_4=-i\ and\ z_5=-1$ there results $\alpha=\frac{1}{8}$. Therefore, the inertial angular velocity for this configuration is

$$\frac{1}{\rho}=m_1+(\frac{1}{4}+\frac{\sqrt{2}}{2})m \qquad \text{Equation 3.1.4.2}$$

$$w^2=G\frac{m_1(1+\phi\frac{m}{m_1})}{r_{12}^3} \qquad \text{were} \quad \phi=\frac{1}{4}+\frac{\sqrt{2}}{2}$$

The five-body configuration, as well as all other single n-gon configurations, are consistent with the conservation of energy equations in that 2T = U. Due to the logistics of working with large numbers of equations with growing mass number, alternate methods for solving these systems are provided next.

3.1.5 Alternate Conservation of Energy Method

The algebra becomes increasingly complex as the number of n-gon masses grows. Finding a method that does not use the equations of motion can possibly simplify the problem somewhat. Conservation of energy provides an alternate method to solve the n-gon configurations by using 2T=U. At time zero within the infinitesimal interval with type one geometry the kinetic energy can be written

$$2T = \sum_{i=1}^{n} m_i v_i^2 = m_1 v_1^2 + m_2 v_2^2 + \cdots + m_n v_n^2 \qquad \text{Equation 3.1.5.1}$$

where $v_1 = 0 \qquad v_2, v_3, \ldots, v_n = v$

$$V = wr \qquad w^2 = G\frac{(m_1 + \phi m)}{r^3}$$

therefore $2T = (n-1)mv^2 = R_n m v^2$ $\qquad R_n$ = n-gon mass number

The potential energy at time zero is

$$U = G\sum \frac{m_i m_j}{r_{ij}} = G\frac{m_1 m_2}{r_{12}} + \cdots + G\frac{m_{n-1} m_n}{r_{n-1,n}} \qquad \text{Equation 3.1.5.2}$$

where $m = m_2, m_3, \ldots, m_n$

Applying the conservation of energy method to the seven-body configuration (hexagon) orbiting m_1, we can solve for the angular velocity. Equating the kinetic (equation 3.1.5.1) and potential (equation 3.1.5.2) energies allows solving for the perturbation coefficient ϕ by adding individual terms on both sides of the 2T=U equation. This method avoids using the equations of motion directly as can be seen below.

$$2T = 6mv^2$$

Collecting and evaluating the twenty-one potential energy r_{ij} terms from the hexagon geometry yields

$$U = 6G\frac{m_1 m}{r} + 6G\frac{m^2}{\sqrt{3}r} + 6G\frac{m^2}{r} + 3G\frac{m^2}{2r}$$

$$6mv^2 = 6mG\frac{m_1 + m\phi}{r}$$

$$v^2 = G\frac{m_1 + m\phi}{r}$$

$$w^2 = G\frac{m_1+m\phi}{r^3} \qquad \text{where} \qquad \phi = {}^5/_4 + {}^{\sqrt{3}}/_3$$

The same above result can be obtained by writing out the equations of motion with their initial conditions and constraints. With larger n-gon mass number the conservation of energy method can also become somewhat tedious. As can be seen with the three, four and five body configurations, increasing n-gon mass number increases the perturbation coefficient magnitude ϕ.

3.1.6 Alternate Recursive Method

Another method to consider in working large n-gon configurations can be approached by taking advantage of recursive calculations. Essentially, with greater n-gon mass number a circle is subdivided into increasingly smaller angles. Utilizing this concept leads to simplifying the perturbation calculations. Circumventing the equations of motion and conservation of energy methods for perturbation coefficient calculation is to expand on the geometrical symmetry fundamental to the n-gon configurations. This can be accomplished by taking ϕ's from previous n-gon calculations and developing relations to solve for still greater n-gon configuration perturbation coefficients. Starting with an eleven-body configuration, calculations can be made for 10i + 1 mass configurations from the following formula to determine ϕ perturbations out to infinity.

$$\phi_{10i+1} = \frac{1}{4} + \frac{\sqrt{2}}{2}\sum_{\beta=0}^{5i-2}\left(1 - cos\frac{\beta+1}{5i}\pi\right)^{-\frac{1}{2}} \qquad \text{Equation 3.1.6.1}$$

where $\qquad i = 2^x \qquad x = 0, 1, 2, \ldots, \infty$

With some effort formulations can be derived to calculate systematically perturbations for selected single n-gon mass configurations. For example, in the next section a general method will be developed to calculate the perturbation coefficient ϕ for an infinite regular n-gon composed of even numbered masses. The table on the next page shows for selected single n-gon configurations how ϕ grows as a function of increasing mass number.

Replacing m with $\frac{m_T}{n-1}$ gives an inertial angular velocity of

$$w^2 = \frac{G}{r^3}\left(m_1 + \frac{\phi}{n-1}m_T\right)$$

where m_T is the total n-gon mass. Redefining $\frac{\phi}{n-1}$as C_n gives a ratio of ϕ to the total number of n-gon masses (sans m_1). This is also shown in the table. It appears that as the number of masses in the n-gon approaches infinity C_n may also approach infinity, however, due to the intra-singularities that exist between the masses it is difficult to determine to what value C_n actually approaches.

The analysis presented in this section gives a general idea of the perturbed inertial angular velocity relative to the single n-gon mass number. Starting with the concentric two n-gon configuration in the next section higher order n-gon configurations will be analyzed.

Table of Single N-Gon Perturbation Coefficients

N-Body	$C_n = \frac{\phi}{n-1}$	ϕ
3	.12500	$\frac{1}{4}$
4	.19245	$\frac{\sqrt{3}}{3}$
5	.23928	$\frac{1}{4}+\frac{\sqrt{2}}{2}$
6	.27528	$\frac{\sqrt{2}}{2}((1-cos\frac{2\pi}{5})^{-\frac{1}{2}}+(1-cos\frac{4\pi}{5})^{-\frac{1}{2}})$
7	.30456	$\frac{5}{4}+\frac{\sqrt{3}}{3}$
9	.35061	$\frac{1}{4}+\frac{\sqrt{2}}{2}+(2-\sqrt{2})^{-\frac{1}{2}}+(2+\sqrt{2})^{-\frac{1}{2}}$
11	.38625	$\frac{1}{4}+\frac{\sqrt{2}}{2}\sum_{n=0}^{3}(1-cos\frac{(n+1)}{5}\pi)^{-\frac{1}{2}}$
13	.41533	$\frac{\sqrt{3}}{3}+\frac{5}{4}+\frac{\sqrt{2}}{2}+(2-\sqrt{3})^{-\frac{1}{2}}+(2+\sqrt{3})^{-\frac{1}{2}}$
17	.46118	
21	.49673	$\frac{1}{4}+\frac{\sqrt{2}}{2}\sum_{n=0}^{8}(1-cos\frac{n+1}{10}\pi)^{-\frac{1}{2}}$
25	.52576	

41	.60708	$\frac{1}{4}+\frac{\sqrt{2}}{2}\sum_{n=0}^{18}(1-cos\frac{n+1}{20}\pi)^{-\frac{1}{2}}$
81	.71741	$\frac{1}{4}+\frac{\sqrt{2}}{2}\sum_{n=0}^{38}(1-cos\frac{n+1}{40}\pi)^{-\frac{1}{2}}$
161	.82773	$\frac{1}{4}+\frac{\sqrt{2}}{2}\sum_{n=0}^{78}(1-cos\frac{n+1}{80}\pi)^{-\frac{1}{2}}$
321	.93805	$\frac{1}{4}+\frac{\sqrt{2}}{2}\sum_{n=0}^{158}(1-cos\frac{n+1}{160}\pi)^{-\frac{1}{2}}$
641	1.04837	$\frac{1}{4}+\frac{\sqrt{2}}{2}\sum_{n=0}^{318}(1-cos\frac{n+1}{320}\pi)^{-\frac{1}{2}}$
1281	1.15869	$\frac{1}{4}+\frac{\sqrt{2}}{2}\sum_{n=0}^{638}(1-cos\frac{n+1}{640}\pi)^{-\frac{1}{2}}$
2561	1.26901	$\frac{1}{4}+\frac{\sqrt{2}}{2}\sum_{n=0}^{1278}(1-cos\frac{n+1}{1280}\pi)^{-\frac{1}{2}}$
5121	1.37932	$\frac{1}{4}+\frac{\sqrt{2}}{2}\sum_{n=0}^{2558}(1-cos\frac{n+1}{2560}\pi)^{-\frac{1}{2}}$

3.2 Multiple N-Gon Configurations

This section is a necessary preliminary to the infinite concentric n-gon problem. Starting with the single n-gon geometry previously worked and continuing with the multiple concentric n-gon allows one to evolve a methodology to determine the perturbations to calculate the ϕ's for the inertial angular velocities of the infinite n-gon configuration.

The multiple concentric n-gon problem is additionally made more complex due to the infinite ways each n-gon can be arranged contiguous to every other n-gon. This analysis will use a geometry specified as follows. A system of n mass particles can be arranged in many different configurations, where the motion of any given n-particle system satisfies Newton's second law. One such family of interest is the planar n-body n-gon configuration, with n-1 masses orbiting m_1 in an assembly consisting of R concentric n-gons and R_n particles per n-gon ($RR_n = n-1$). Relative to m_1, particles are placed at the vertices of equal sided regular n-gons inscribed in their respective circle of increasing radii such that the geometric center is coincident with the barycenter. Two fundamental n-body n-gon geometries are ray and rotated ray configurations. An example of these two geometries for a $R = 6, R_n = 6$ configuration can be seen in figures 3.2.1 and 3.2.2. Analysis in this chapter is restricted to the rotated ray

configuration defined in the infinitesimal interval at time zero using type 1 geometry with the sidereal synodic relations. There exist infinite solutions for n-gon configurations ($R \geq 2$) defined by the equations of motion (with sidereal synodic relations), and, if unique n-gon configurations are required, then additional constraints must be specified in the initial value problem. All n-gon configuration solutions are consistent with conservation of energy over the infinitesimal interval.

3.2.1 Two N-Gon Configuration

In the following sub-sections inertial angular velocities will be derived for two, three and four concentric n-gon configurations. These examples will be using six masses per n-gon ($R_n = 6$) to simplify the illustration of even and odd structural variations within the concentric n-gon configurations.

The rotated ray two n-gon configuration for $R = 2\ and\ R_n = 6$ masses is modelled using equation 3.1 and figure 3.2.2 as a reference

$$\ddot{z}_2 + 2wi\dot{z}_2 - w^2 z_2 = G\sum_{\substack{j=1 \\ j\neq k}}^{13} \frac{m_j}{r_{j2}^3} z_{j2} = G\frac{m_1}{r_{12}^3} z_{12} + G\sum_{\substack{j=3 \\ j\neq k}}^{13} \frac{m_j}{r_{j2}^3} z_{j2}$$

Equation 3.2.1.1

The inertial axis x and rotating axis x' have been chosen along a vector z_{81} at time zero. In the above equation vector z_{21} is infinitesimally rotating counterclockwise relative to vector z_{81}.

Sidereal synodic relations describing n-gon interactions in general exist under geometric conditions where all particle velocity vectors are perpendicular to all particle radii vectors in the configuration plane of motion relative to the barycenter at time zero. Within the infinitesimal interval for $R \geq 2$ synodic sidereal relations are

$$n_R P_R = (n_R + n_{R-1})P_{R-1} = \cdots = (n_R + n_{R-1} + \cdots + n_1)P_1$$

Equation 3.2.1.2

Where $n_R + n_{R-1} + \cdots + n_1$ are determinable coefficients of n-gon periods $P_R, P_{R-1}, \ldots P_1$ with innermost and outermost n-gon periods designated P_1 and P_R respectively. Sidereal synodic relations are defined in the rotating barycentric coordinate system, which is also known as the synodic coordinate system (Szebehely,1967, 13-16). Equation 3.2.1.2 sidereal

synodic relations are formulated equivalently (Bauer, 2001) to those derived for a family of type 1 (Roy, 1955, Roy, 1988, 119, Marchal, 2000, 286) collinear n-body problems (Lehman-Filhes, 1891, Moulton, 1900, 249), however, they can also be applied to planar n-gon configurations. Utilizing equations 3.2.1.1 and 3.2.1.2 yields

$$w_j^2 = (w_j^u)^2 + (w_j^p)^2 \qquad (w_j^u)^2 = \frac{Gm_1}{r_j^3} \qquad (w_j^p)^2 = \frac{Gm}{r_j^3}\phi_j$$

for j = 1, 2,3, ..,R.

Where w_j is sidereal j^{th} n-gon angular velocity, m $(m > 0)$ is mean mass $\frac{m_T}{n-1}$, m_T is total n-gon mass, $r_j (0 < r_j < \infty)$ is j^{th} n-gon radius $\alpha^{j-1} r_1$ $(\alpha \neq 1)$, and ϕ_j are intra/inter perturbations. The n-gon radii distribution r_j has been assumed to approximate a real particle distribution. In actuality r_j can have infinite formulations. Lower case p and u represent the perturbed and unperturbed angular velocities respectively.

Adapting the sidereal synodic relations from equation 3.2.1.2 for the two n-gon configuration gives $n_2 P_2 = (n_2 + n_1) P_1$. The second n-gon with period P_2 is rotating at an angular velocity of w relative to the inertial x axis. The first n-gon with period P_1 is rotating at an angular velocity relative to the second n-gon where $z_2 = r_1 e^{i\frac{n_1}{n_2}wt}$. Radius of the first n-gon is r_1 and the angular velocity relative to the second n-gon is $\frac{n_1}{n_2}w$. Equation 3.2.1.1 now becomes

$$-\frac{P_2^2}{P_1^2} w^2 z_2 = \frac{Gm_1}{r_{12}^3} z_{12} + Gm \sum_{\substack{i=3 \\ i\neq 2}}^{7} \frac{z_{i2}}{r_{i2}^3} + Gm \sum_{i=8}^{13} \frac{z_{i2}}{r_{i2}^3} \qquad \text{Equation 3.2.1.3}$$

Since each n-gon rotates as a rigid body over the infinitesimal interval, any particle rotating within that n-gon will be rotating at that n-gon angular velocity. The term on the left of the equal sign in equation 3.2.1.3 can be reformulated as $\frac{P_2}{P_1} w = w_{1nr}$ where w_{1nr} is the inertial angular velocity of the first n-gon relative to the x axis. From the reformulated equation and $z_{12} = z_1 - z_2 = -z_2$ equation 3.2.1.3 becomes

$$-w_{1nr}^2 z_2 = -\frac{Gm_1}{r_{12}^3} z_2 + Gm \sum_{\substack{i=3 \\ i\neq 2}}^{7} \frac{z_{i2}}{r_{i2}^3} + Gm \sum_{i=8}^{13} \frac{z_{i2}}{r_{i2}^3} \quad m_i = m_2 \ldots m_{13} = m$$

Equation 3.2.1.4

Taking equation 3.2.1.4 and writing it out in full for the inertial angular velocity of the first n-gon

$$-w_{1nr}^2 z_2 = -\frac{Gm_1}{r_{12}^3} z_2 + Gm\left(\frac{z_{32}}{r_{32}^3} + \frac{z_{42}}{r_{42}^3} + \frac{z_{52}}{r_{52}^3} + \frac{z_{62}}{r_{62}^3} + \frac{z_{72}}{r_{72}^3}\right)$$

$$+Gm\left(\frac{z_{82}}{r_{82}^3} + \frac{z_{92}}{r_{92}^3} + \frac{z_{10,2}}{r_{10,2}^3} + \frac{z_{11,2}}{r_{11,2}^3} + \frac{z_{12,2}}{r_{12,2}^3} + \frac{z_{13,2}}{r_{13,2}^3}\right) \quad \text{Equation 3.2.1.5}$$

Evaluating scaler terms in the denominator for masses three through seven for the first n-gon and masses eight through thirteen for the second n-gon yields

$$r_{32} = r_{72} = r_1 \qquad r_{82} = r_{92} = r_1(1 + \alpha^2 - \sqrt{3}\alpha)^{1/2}$$

$$r_{42} = r_{62} = \sqrt{3} r_1 \qquad r_{10,2} = r_{13,2} = r_1(1 + \alpha^2)^{1/2}$$

$$r_{52} = 2r_1 \qquad r_{11,2} = r_{12,2} = r_1(1 + \alpha^2 + \sqrt{3}\alpha)^{1/2}$$

Evaluating vector terms in the numerator for masses three through seven for the first n-gon and masses eight through thirteen for the second n-gon gives

$$z_{32} + z_{72} = -z_2 \qquad z_{82} + z_{92} = (\sqrt{3}\alpha - 2) z_2$$

$$z_{42} + z_{62} = -3z_2 \qquad z_{10,2} + z_{13,2} = -2z_2$$

$$z_{52} = -2z_2 \qquad z_{11,2} + z_{12,2} = -(\sqrt{3}\alpha + 2) z_2$$

After substituting scalar and vector terms into equation 3.2.1.5

$$\frac{w_{1nr}^2 r_1^2}{G} z_2 = m_1 z_2 + m\phi_{11} z_2 + m\phi_{21} z_2$$

the angular velocity and perturbation coefficients are

$$w_{1nr}^2 = G\frac{m_1 + m(\phi_{11} + \phi_{21})}{r_1^3} = G\frac{m_1 + m\phi_1}{r_1^3} \quad \text{Equation 3.2.1.6}$$

where $\phi_1 = \phi_{11} + \phi_{21}$

$$\phi_{11} = {}^5/_4 + {}^{\sqrt{3}}/_3$$

$$\phi_{21} = \frac{2 - \sqrt{3}\alpha}{(1 + \alpha^2 - \sqrt{3}\alpha)^{3/2}} + \frac{2}{(1 + \alpha^2)^{3/2}} + \frac{2 + \sqrt{3}\alpha}{(1 + \alpha^2 + \sqrt{3}\alpha)^{3/2}}$$

Coefficient ϕ_{11} is the intra perturbations of the first n-gon and coefficient ϕ_{21} Is the inter perturbations of the second n-gon relative to the first n-gon. It will be noticed that intra perturbation ϕ_{11} Is the same magnitude as for a seven body (rotating hexagon) single n-gon configuration.

Setting up for the second n-gon taking into account that z_8 is on the rotating x' axis

$$-w^2 z_8 = -\frac{Gm_1}{r_{18}^3} z_8 + Gm \sum_{i=2}^{7} \frac{z_{i8}}{r_{i8}^3} + Gm \sum_{\substack{i=9 \\ i\neq 8}}^{13} \frac{z_{i8}}{r_{i8}^3}$$

Following in the same manner as the first n-gon analysis, the angular velocity and perturbation coefficients will be

$$w_{2nr}^2 = G\frac{m_1 + m(\phi_{12} + \phi_{22})}{r_2^3} = G\frac{m_1 + m\phi_2}{r_2^3} \qquad \text{Equation 3.2.1.7}$$

where $\phi_2 = \phi_{12} + \phi_{22}$

$$\phi_{12} = \left(\frac{2\alpha - \sqrt{3}}{(1+\alpha^2 - \sqrt{3}\alpha)^{\frac{3}{2}}} + \frac{2\alpha}{(1+\alpha^2)^{\frac{3}{2}}} + \frac{2\alpha + \sqrt{3}}{(1+\alpha^2+\sqrt{3}\alpha)^{\frac{3}{2}}}\right)\alpha^2$$

$$\phi_{22} = {}^{5}/_{4} + {}^{\sqrt{3}}/_{3}$$

Coefficient ϕ_{12} is the inter perturbation of the first n-gon relative to the second n-gon. Perturbation coefficient ϕ_{22} is equal to ϕ_{11} due to the intra symmetry being proportionately the same for both n-gons. The perturbation coefficient geometry for the two n-gon problem can be summarized

$$\begin{matrix} \phi_{11} & \phi_{21} \\ \phi_{12} & \phi_{22} \end{matrix} = \begin{matrix} \phi_{11} & \phi_{21} \\ \phi_{12} & \phi_{11} \end{matrix}$$

3.2.2 Two N-Gon Sidereal Synodic Coefficients

The coefficients n_1 and n_2 from the sidereal synodic relation $n_2 P_2 = (n_2 + n_1)P_1$ used in solving the two n-gon problem can be determined analytically. Rewriting the sidereal synodic relation in an alternate form

$$\frac{n_1}{n_2} = \frac{P_2 - P_1}{P_1}$$

Taking the inertial angular velocities derived in equations 3.2.1.6 and 3.2.1.7 for n-gon one and two, the period ratio can be computed

$$\frac{P_2^2}{P_1^2} = \frac{1+\frac{m}{m_1}\phi_1}{1+\frac{m}{m_1}\phi_2}\alpha^3 = \frac{G_1^2}{G_2^2}\alpha^3 \quad \begin{pmatrix}\phi_1\\ \phi_2\end{pmatrix} = \begin{pmatrix}\phi_{11} & \phi_{21}\\ \phi_{12} & \phi_{11}\end{pmatrix}\begin{pmatrix}k_1\\ k_2\end{pmatrix} \quad \text{Equation 3.2.2.1}$$

where k_1 and k_2 are mass scaling parameters for the first and second n-gons respectively.

Rewriting the above two equations gives

$$n_2^2 P_2^2 = (n_2 + n_1)^2 P_1^2$$

$$G_2^2 P_2^2 = G_1^2 \alpha^3 P_1^2$$

For the 2π synodic case

$$n_1 = G_1\alpha^{3/2} - G_2 \qquad \text{Equation 3.2.2.2}$$

$$n_2 = G_2 \qquad G_i^2 = 1 + \frac{m}{m_1}\phi_i$$

Two n-gon configuration mass range, which is somewhat elusive, could be estimated to a rough degree by determining the period ratio of the two n-gons. From the period ratios in equation 3.2.2.1 and the sidereal synodic relations in equation 3.2.2.2, the terms $\frac{m}{m_1}\phi_1$ and $\frac{m}{m_1}\phi_2$ should be of near zero magnitude for the two n-gon configuration to continue in a semblance of their initial intra and inter geometry with respect to time zero. In terms of the configuration maintaining some given structure, it is expected that mass is neither of a magnitude that can be ignored relative to conservation laws, nor of a magnitude that can disrupt the configuration relative to some given finite epoch. It is assumed here when reference to a non-infinitesimal epoch is made that the mass, radii and angular distributions have determined a n-gon state vector to be numerically integrated relative to time zero. Mass range is dependent on system constraints such as two n-gon particle distribution evolution and period of interest. Terms ϕ_1 and ϕ_2 are a function of R_n with magnitudes in the approximate order of R_n, therefore as $R_n, \phi_1, \phi_2 \to \infty$ it is necessary that $\frac{m}{m_1} \to 0$. Using known values of ϕ_1 and ϕ_2 with an estimated magnitude of $\frac{m}{m_1}$. could allow an upper bound approximation for mean particle mass. Another possible mass range approximation method to consider for numerical integration can be found from $\frac{m}{m_1} < 2.3/R_n^3$. This relation is based on an analysis developed in Maxwell's work for a one n-gon configuration (Maxwell, 1859, Maxwell,

Brush and Everitt, 1983, 71, 144). Although this equation was derived for a single n-gon, it may prove useful for the two n-gon configuration.

3.2.3 Two N-Gon Optimization

The two n-gon solution as derived earlier results in non-unique mass and angular velocity distributions, thus requiring further analysis to find the unique solution. Constraining the solution by determining the potential energy extrema will result in unique concentric n-gon configurations. Mass scaling is a necessary condition needed to reformulate this problem for uniqueness. The two n-gon kinetic/potential energy is composed of perturbed and unperturbed components which can be separated. The general equation for the perturbed component to be optimized can be determined by expanding the kinetic/potential energy series as a function of concentric n-gon number using mass scaling k_j

$$2T = \sum_{j=1}^{R} m_j v_j^2 = R_n m G \sum_{j=1}^{R} \frac{m_1 + \phi_j m}{r_j} k_j$$

$$2T = R_n m G \sum_{j=1}^{R} \frac{m_1}{r_j} k_j + R_n m G \sum_{j=1}^{R} \frac{\phi_j m}{r_j} k_j = 2T^u + 2T^p$$

The first term to the right of the equal sign is the unperturbed kinetic energy, that is, there are no intra or inter perturbations in this term. Expanding the unperturbed kinetic energy using the radii distribution function $r_j = r_1 \alpha^{j-1}$ results in

$$2T^u = R_n m G \sum_{j=1}^{R} \frac{m_1}{r_j} k_j = \frac{G m_1}{r_1} \left(R_n m k_1 + \frac{1}{\alpha} R_n m k_2 + \frac{1}{\alpha^2} R_n m k_3 + \cdots + \frac{1}{\alpha^{R-1}} R_n m k_R \right)$$

$$2T^u = \frac{G m_1}{r_1} \sum_{j=1}^{R} \frac{m_{jNGON}^T}{\alpha^{j-1}}$$

where $R_n m k_R$ is the total n-gon mass for the R^{th} n-gon, represented as m_{jNGON}^T in the above summation. It is only necessary to incorporate the perturbed energy component of the concentric n-gons in the optimization process. The perturbed concentric n-gon kinetic energy term $2T^p$ can be expanded

$$2T^p = R_n m G \sum_{j=1}^{R} \frac{\phi_j m}{r_j} k_j = R_n \frac{G m^2}{r_1} \sum_{j=1}^{R} \frac{\phi_j}{\alpha^{j-1}} k_j$$

Therefore, the perturbed scaled form of the kinetic (potential) energy function to be optimized is

$$\Delta = \frac{2T - 2T^u}{R_N \frac{Gm^2}{r_1}} = \sum_{j=1}^{R} \frac{\phi_j k_j}{\alpha^{j-1}} \qquad \text{Equation 3.2.3.1}$$

where k_j represents mass scaling. Associated with each n-gon will be a unique k_j determined from the optimization process. Equation 3.2.3.1 is the general concentric n-gon formulation where substituting $R = 2$ gives the two n-gon case.

The n-gon extrema energy problem comprises a system of two constraints which can be quantified as $R = \sum_{j=1}^{R} k_j$ for the equality constraint and $k_j > 0$ for the inequality constraints. Initial case $R = 2$ is special in that no numerical optimization is required with the k_j solution. Taking the total derivative of $\sum_{j=1}^{R} \frac{\phi_j k_j}{\alpha^{j-1}}$ with respect to k_j and equating to zero locates the extrema. Resultant mass scaling parameters k_1 and k_2 are determined in the following manner

$$\Delta = \phi_1 k_1 + \frac{1}{\alpha}\phi_2 k_2 = k_1^2 \phi_{11} + \frac{1}{\alpha} k_2^2 \phi_{11} + (\phi_{21} + \frac{1}{\alpha}\phi_{12}) k_1 k_2$$

with $\phi_1 = k_1 \phi_{11} + k_2 \phi_{21}$

$$\phi_2 = k_1 \phi_{12} + k_2 \phi_{11}$$

results in the gradients

$$\frac{\partial \Delta}{\partial k_1} = 2k_1 \phi_{11} + k_2(\phi_{21} + \frac{1}{\alpha}\phi_{12})$$

$$\frac{\partial \Delta}{\partial k_2} = \frac{2}{\alpha} k_2 \phi_{11} + k_1(\phi_{21} + \frac{1}{\alpha}\phi_{12})$$

Taking the total derivative and equating to zero

$$d\Delta = \frac{\partial \Delta}{\partial k_1} dk_1 + \frac{\partial \Delta}{\partial k_2} dk_2 \qquad dk_1 = -dk_2 \qquad \text{Equation 3.2.3.2}$$

yields the k_1 and k_2 optimized solutions using $k_2 = 2 - k_1$ to find k_1 and $k_1 = 2 - k_2$ to find k_2. Substituting the above constraints into equation 3.2.3.2 gives for k_1

$$\left(\phi_{11}-\left(\phi_{21}+\frac{1}{\alpha}\phi_{12}\right)+\frac{1}{\alpha}\phi_{11}\right)k_1=\frac{2}{\alpha}\phi_{11}-\left(\phi_{21}+\frac{1}{\alpha}\phi_{12}\right)$$

$$k_1=\frac{\frac{2}{\alpha}\phi_{11}-\left(\phi_{21}+\frac{1}{\alpha}\phi_{12}\right)}{\left(1+\frac{1}{\alpha}\right)\phi_{11}-\left(\phi_{21}+\frac{1}{\alpha}\phi_{12}\right)}$$

and for k_2

$$\left(\phi_{11}-\left(\phi_{21}+\frac{1}{\alpha}\phi_{12}\right)+\frac{1}{\alpha}\phi_{11}\right)k_2=2\phi_{11}-\left(\phi_{21}+\frac{1}{\alpha}\phi_{12}\right)$$

$$k_2=\frac{2\phi_{11}-(\phi_{21}+\frac{1}{\alpha}\phi_{12})}{\left(1+\frac{1}{\alpha}\right)\phi_{11}-(\phi_{21}+\frac{1}{\alpha}\phi_{12})}$$

The k_1 and $k_2$solutions are consistent with the constraint equations $k_1 + k_2 = 2$ and $k_j > 0$. By observation it will be noted that trivial k_j solution for $R = 2$ is $k_j = 1$. Using a combination unperturbed and perturbed scaled kinetic energy optimizing function of $\Delta = \frac{2T}{R_N\frac{Gm^2}{r_1}}$ in place of equation 3.2.3.1 will give the same k_1 and k_2 mass scaling result as determined by the equality and inequality constraints. In the above analysis the potential energy equation could have been used in place of the kinetic energy equation, however, the resulting mass scaling optimizing function will have come out to be same as equation 3.2.3.1.

3.2.4 Two N-Gon Conservation of Energy Verification

Starting with the initial conservation of energy equations used for the determination of ϕ in the single n-gon analysis and extending this to the two n-gon configuration

$$2\mathrm{T} = \sum_{i=1}^{13} m_i v_i^2 = m_1 v_1^2 + m_2 v_2^2 + \cdots + m_{13} v_{13}^2 \qquad \text{Equation 3.2.4.1}$$

with $v_1 = 0$ $\qquad m_2, m_3, \ldots, m_{13} = m$

$v_2, v_3, \ldots, v_7 = v_{1nr}$ $\qquad v_8, v_9, \ldots, v_{13} = v_{2nr}$

gives $2T = 6mv_{1nr}^2 + 6mv_{2nr}^2$ $\qquad v_{1nr} = w_{1nr}r_1$ $\qquad v_{2nr} = w_{2nr}r_2$

$w_{1nr}^2 = G\frac{(m_1+\phi_1 m)}{r_1^3}$ $\qquad w_{2nr}^2 = G\frac{(m_1+\phi_2 m)}{r_2^3}$

$$2T = 6Gm\frac{m_1+\phi_1 m}{r_1} + 6Gm\frac{m_1+\phi_2 m}{r_2} \qquad \phi_1 = \phi_{11} + \phi_{21} \qquad \phi_2 = \phi_{12} + \phi_{22}$$

Looking at the potential energy for the first and second n-gons using the customary energy equations

$$U = G\sum\frac{m_i m_j}{r_{ij}} = G\frac{m_1 m_2}{r_{12}} + \cdots + G\frac{m_{12} m_{13}}{r_{12,13}} \qquad \text{Equation 3.2.4.2}$$

Symbolically representing the individual terms $m_i m_j$ in the potential sum as ij, the first n-gon becomes

12
13 23
14 24 34
15 25 35 45
16 26 36 46 56
17 27 37 47 57 67

Evaluating the 21 potential energy terms gives

$$6mG\frac{m_1 + m\phi_{11}}{r} \qquad \phi_{11} = {}^{5}/_{4} + {}^{\sqrt{3}}/_{3}$$

Looking at the potential energy for the second n-gon in the same manner as the first n-gon

18	28	.	.	.	.	78					
19	29	.			.	79	89				
1,10	2,10		.	.		7,10	8,10				
1,11	2,11		.	.		7,11	8,11	.			
1,12	2,12	.			.	7,12	8,12	.	.		
1,13	2,13	.	.	.	.	7,13	8,13	.	.	.	12,13

The terms outside of the block designated by 28….78 etc. result in the same analysis as for n-gon one. That is, $\phi_{22} = \phi_{11} = \frac{5}{4} + \frac{\sqrt{3}}{3}$. Blocked terms represent perturbations between n-gon one and n-gon two (ϕ_{21}, ϕ_{12}). When all potential energy terms are evaluated and combined conservation of energy will be maintained (2T=U).

$$U = 6Gm\frac{m_1 + \phi_{11} m}{r_1} + 6Gm\frac{\phi_{21} m}{r_1} + 6Gm\frac{\phi_{12} m}{r_2} + 6Gm\frac{m_1 + \phi_{22} m}{r_2} = 2T$$

3.2.5 Two N-Gon Configuration with Infinite Masses Per N-Gon

In the preceding sections, the two n-gon analysis was for the double hexagon configuration. This was a preliminary example in preparation for solving the problem of infinite masses in both n-gons, that is, for $R_n \to \infty$ (R_n even). Perturbation calculations for $\phi_{11}, \phi_{21}, \phi_{12}$, and , ϕ_{22} (where $\phi_{22} = \phi_{11}$) will proceed as follows. Consider, the two n-gon equations of motion with infinite masses for the first n-gon

$$-w_{1nr}^2 z_2 = -G\frac{m_1}{r_1^3} z_2 + G\sum_{\substack{j=3 \\ j\neq 2}}^{N} \frac{m_j}{r_{j2}^3} z_{j2} \qquad N = RR_n + 1$$

Looking at the second term right of the equal sign and separating out n-gon one and n-gon two respectively

$$G\sum_{\substack{j=3 \\ j\neq 2}}^{N} \frac{m_j}{r_{j2}^3} z_{j2} = Gm\sum_{\substack{j=3 \\ j\neq 2}}^{R_n+1} \frac{z_{j2}}{r_{j2}^3} + Gm\sum_{j=R_n+2}^{2R_n+1} \frac{z_{j2}}{r_{j2}^3} \qquad \text{Equation 3.2.5.1}$$

Reformulating in terms of ϕ_{11} and ϕ_{21} relative to the first n-gon

$$G\sum_{\substack{j=3 \\ j\neq 2}}^{N} \frac{m_j}{r_{j2}^3} z_{j2} = Gm\frac{z_2\phi_{11}}{r_1^3} + Gm\frac{z_2\phi_{21}}{r_1^3}$$

Solving for ϕ_{11} in the first n-gon

$$-\frac{z_2\phi_{11}}{r_1^3} = \left(\frac{z_{32}}{r_{32}^3} + \frac{z_{42}}{r_{42}^3} + \frac{z_{52}}{r_{52}^3} + \cdots + \frac{z_{R_n+1,2}}{r_{R_n+1,2}^3}\right)$$

$$-\frac{z_2\phi_{11}}{r_1^3} = \left(\frac{z_{32}+z_{R_n+1,2}}{r_{32}^3} + \frac{z_{42}+z_{R_n,2}}{r_{42}^3} + \frac{z_{52}+z_{R_n-1,2}}{r_{52}^3} + \cdots + \frac{z_{\frac{R_n}{2}+2,2}}{r_{\frac{R_n}{2}+2,2}^3}\right)$$

Evaluating the scaler and vector terms

$$r_{12} = r_{13} = r_{14} \ldots = r_{1,R_n+1} = r_1 \quad \text{(first n-gon radii)}$$

$$r_{23} = r_{34} = r_{45} \ldots = r_{R_n+1,2} = \sqrt{2}r_1\left(1 - cos\frac{2\pi}{R_n}\right)^{1/2}$$

$$r_{24} = r_{35} = r_{46} \ldots = r_{R_n+1,3} = \sqrt{2}r_1\left(1 - cos\frac{4\pi}{R_n}\right)^{1/2}$$

$$r_{25} = r_{36} = r_{47} \ldots = r_{R_n+1,4} = \sqrt{2}r_1\left(1 - cos\frac{6\pi}{R_n}\right)^{1/2}$$

$$r_{2,\frac{R_n}{2}+2} = r_{3,\frac{R_n}{2}+3} = r_{4,\frac{R_n}{2}+4} \ldots = r_{\frac{R_n}{2}+1,R_n+1} = 2r_1$$

$$z_{32} + z_{R_n+1,2} = z_3 - z_2 + z_{R_n+1} - z_2 = z_3 + z_{R_n+1} - 2z_2$$

$$z_{42} + z_{R_n,2} = z_4 - z_2 + z_{R_n} - z_2 = z_4 + z_{R_n} - 2z_2$$

$$z_{\frac{R_n}{2}+2,2} = -2z_2$$

yields

$$-\frac{z_2\phi_{11}}{r_1^3} = \frac{1}{\sqrt{2}^3 r_1^3}\left(\frac{z_{32}+z_{R_n+1,2}}{(1-cos\frac{2\pi}{R_n})^{\frac{3}{2}}} + \frac{z_{42}+z_{R_n,2}}{(1-cos\frac{4\pi}{R_n})^{\frac{3}{2}}} + \frac{z_{52}+z_{R_n-1,2}}{(1-cos\frac{6\pi}{R_n})^{\frac{3}{2}}} + \cdots\right) + \frac{z_{\frac{R_n}{2}+2,2}}{8}$$

Using rotated ray geometry to find that $z_3 + z_{R_n+1} = 2z_2 cos\frac{2\pi}{R_n}$ etc. gives

$$z_2\phi_{11} = \frac{2z_2}{\sqrt{2}^3}\left(\frac{1-cos\frac{2\pi}{R_n}}{(1-cos\frac{2\pi}{R_n})^{\frac{3}{2}}} + \frac{1-cos\frac{4\pi}{R_n}}{(1-cos\frac{4\pi}{R_n})^{\frac{3}{2}}} + \frac{1-cos\frac{6\pi}{R_n}}{(1-cos\frac{6\pi}{R_n})^{\frac{3}{2}}} + \cdots\right) + \frac{z_2}{4}$$

Therefore

$$\phi_{11} = \frac{1}{4} + \frac{\sqrt{2}}{2}\sum_{j=1}^{\frac{1}{2}(R_n-2)}(1 - cos\frac{2\pi j}{R_n})^{-1/2} \qquad \text{Equation 3.2.5.2}$$

Continuing with ϕ_{21} from equation 3.2.5.1 for the first n-gon

$$-\frac{z_2\phi_{21}}{r_1^3} = \left(\frac{z_{R_n+2,2}}{r_{R_n+2,2}^3} + \frac{z_{R_n+3,2}}{r_{R_n+3,2}^3} + \frac{z_{R_n+4,2}}{r_{R_n+4,2}^3} + \cdots + \frac{z_{2R_n+1,2}}{r_{2R_n+1,2}^3}\right)$$

Regrouping the masses and evaluating the scaler and vector terms for ϕ_{11} results in

$$\phi_{21} = 2\sum_{j=1}^{\frac{1}{2}R_n}\frac{1-\alpha cos\theta_2}{(\alpha^2+1-2\alpha cos\theta_2)^{3/2}} \qquad \text{Equation 3.2.5.3}$$

Formulating the equation of motion to solving for ϕ_{12} in the second n-gon

$$-w^2 z_{R_n+2} = -G\frac{m_1}{r_2^3}z_{R_n+2} + G\sum_{j=2}^{N}\frac{m_j}{r_{j,R_n+2}^3}z_{j,R_n+2}$$

Looking at the second term on the right of the equal sign

$$G\sum_{j=2}^{N}\frac{m_j}{r_{j,R_n+2}^3}z_{j,R_n+2} = Gm\sum_{j=2}^{R_n+1}\frac{z_{j,R_n+2}}{r_{j,R_n+2}^3} + Gm\sum_{\substack{j=R_n+3\\ j\neq R_n+2}}^{2R_n+1}\frac{z_{j,R_n+2}}{r_{j,R_n+2}^3}$$

Reformulating in terms of ϕ_{21} and ϕ_{22} relative to the second n-gon

$$G\sum_{j=2}^{N}\frac{m_j}{r_{j,R_n+2}^3}z_{j,R_n+2} = Gm\frac{z_{R_n+2}\phi_{12}}{r_2^3} + Gm\frac{z_{R_n+2}\phi_{22}}{r_2^3}$$

After some analysis yields

$$\phi_{12} = 2\alpha^2\sum_{j=1}^{\frac{1}{2}R_n}\frac{\alpha-cos\theta_2}{(\alpha^2+1-2\alpha cos\theta_2)^{3/2}} \qquad \alpha = \frac{r_2}{r_1} \qquad \text{Equation 3.2.5.4}$$

Where, from the rotated ray geometry

$$\theta_1 = \pi - 2\theta_2$$

$\theta_2 = (2j-1)\frac{\pi}{R_n}$The next step in the infinite n-gon problem analysis is to study the three n-gon configuration. This is a necessary step in developing formulas for even n-gon ϕ's such as $\phi_{21}, \phi_{41}, ...,\phi_{12}, \phi_{14}$ ...and for odd n-gon ϕ's like $\phi_{31}, \phi_{51}, ...,\phi_{13}, \phi_{15}$ ....

3.2.6 Three N-Gon Configuration

First N-Gon

Applying equation 3.1 and the sidereal synodic relation equation 3.2.1.2 to the three n-gon configuration will result in the same structural mathematical analysis as the two n-gon configuration. From these equations the three n-gon configuration follows basic systematic n-gon geometry to determine perturbation coefficients for each n-gon within the three n-gon configuration. Mass fourteen is the reference mass on the third n-gon that determines the orientation of the rotating x' axis relative to mass one. Mass two with period one (P_1) in the first n-gon rotates relative to mass fourteen with period (P_3) in the third n-gon. Therefore, with these initial conditions the equation of motion for the first n-gon can be written

$$-\frac{P_3^2}{P_1^2}w^2 z_2 = -\frac{Gm_1}{r_{12}^3}z_2 + Gm\sum_{\substack{i=3\\ i\neq 2}}^{7}\frac{z_{i2}}{r_{i2}^3} + Gm\sum_{i=8}^{13}\frac{z_{i2}}{r_{i2}^3} + Gm\sum_{i=14}^{19}\frac{z_{i2}}{r_{i2}^3}$$

Equation 3.2.6.1

$$-w_{1nr}^2 z_2 = -\frac{Gm_1}{r_1^3}z_2 + \frac{Gm}{r_1^3}\phi_{11} + \frac{Gm}{r_1^3}\phi_{21} + \frac{Gm}{r_1^3}\phi_{31}$$

$$\phi_{11} = r_1^3\sum_{\substack{i=3\\ i\neq 2}}^{7}\frac{z_{i2}}{r_{i2}^3} \quad \phi_{21} = r_1^3\sum_{i=8}^{13}\frac{z_{i2}}{r_{i2}^3} \quad \phi_{31} = r_1^3\sum_{i=14}^{19}\frac{z_{i2}}{r_{i2}^3}$$

For the three n-gon configuration the vector from mass one to mass fourteen is used as the rotating x' axis as well as the non-rotating x axis within the infinitesimal interval at time zero. Mass two is rotating relative to mass fourteen. Evaluating denominator (scalar) and numerator (vector) terms for particles two through nineteen for the above equation will be done in the same manner as for the two n-gon geometry. In this derivation the following n-gon radii distribution has been used

$$\frac{r_2}{r_1} = \alpha \qquad \frac{r_3}{r_2} = \alpha \qquad \frac{r_3}{r_1} = \alpha^2 \qquad \text{where } r_j = \alpha^{j-1}r_1$$

Generally, the n-gon radii distribution r_j can have infinite forms. Using $r_j = \alpha^{j-1}r_1$ simplifies an otherwise complex problem. To determine real r_j distributions would probably require numerical optimization/analysis of real planetary/stellar ring systems.

The resulting inertial angular velocity for the first n-gon of the three n-gon configuration is

$$w_{1nr}^2 = G\frac{(m_1 + m(\phi_{11}+\phi_{21}+\phi_{31}))}{r_1^3} = G\frac{(m_1+m\phi_1)}{r_1^3}$$

where $\phi_1 = \phi_{11} + \phi_{21} + \phi_{31}$

$$\phi_{11} = {}^5/_4 + {}^{\sqrt{3}}/_3$$

$$\phi_{21} = \frac{2-\sqrt{3}\alpha}{(1+\alpha^2-\sqrt{3}\alpha)^{3/2}} + \frac{2}{(1+\alpha^2)^{3/2}} + \frac{2+\sqrt{3}\alpha}{(1+\alpha^2+\sqrt{3}\alpha)^{3/2}}$$

$$\phi_{31} = \frac{2-\alpha^2}{(1+\alpha^4-\alpha^2)^{3/2}} + \frac{2+\alpha^2}{(1+\alpha^4+\alpha^2)^{3/2}} - \frac{1}{(\alpha^2-1)^2} + \frac{1}{(\alpha^2+1)^2}$$

As can be seen from the three n-gon configuration, perturbations ϕ_{11} and ϕ_{21} are the same as for the first n-gon of the two n-gon configuration. Perturbation ϕ_{31} is new and of different form.

Three N-Gon Configuration

Second N-Gon

Under the same conditions as described for the first n-gon, this process is continued for the second n-gon. Mass eight in the second n-gon with period two (P_2) rotates relative to mass fourteen in the third n-gon with period (P_3). The equation of motion for the second n-gon is structurally like that of equation 3.2.6.1 for the first n-gon. Solution for perturbation coefficients are stated without analysis.

$$-\frac{P_3^2}{P_2^2}w^2 z_8 = -\frac{Gm_1}{r_{18}^3}z_8 + Gm\sum_{i=2}^{7}\frac{z_{i8}}{r_{i8}^3} + Gm\sum_{\substack{i=9\\ i\neq 8}}^{13}\frac{z_{i8}}{r_{i8}^3} + Gm\sum_{i=14}^{19}\frac{z_{i8}}{r_{i8}^3}$$

$$w_{21nr}^2 z_8 = -\frac{Gm_1}{r_2^3}z_8 + \frac{Gm}{r_2^3}\phi_{12} + \frac{Gm}{r_2^3}\phi_{22} + \frac{Gm}{r_2^3}\phi_{32}$$

$$\phi_{12} = r_2^3\sum_{i=2}^{7}\frac{z_{i8}}{r_{i8}^3} \qquad \phi_{22} = r_2^3\sum_{\substack{i=9\\ i\neq 8}}^{13}\frac{z_{i8}}{r_{i8}^3} \qquad \phi_{32} = r_2^3\sum_{i=14}^{19}\frac{z_{i8}}{r_{i8}^3}$$

After evaluation of the scalar and vector quantities for mass particles two through nineteen, there results the second n-gon inertial angular velocity

$$w_{2nr}^2 = G\frac{(m_1+m(\phi_{12}+\phi_{22}+\phi_{32}))}{r_2^3} = G\frac{(m_1+m\phi_2)}{r_2^3}$$

where

$$\phi_2 = \phi_{12} + \phi_{22} + \phi_{32}$$

$$\phi_{12} = \left(\frac{2\alpha-\sqrt{3}}{(1+\alpha^2-\sqrt{3}\alpha)^{3/2}} + \frac{2\alpha}{(1+\alpha^2)^{3/2}} + \frac{2\alpha+\sqrt{3}}{(1+\alpha^2+\sqrt{3}\alpha)^{3/2}}\right)\alpha^2$$

$$\phi_{22} = {}^{5}/_{4} + {}^{\sqrt{3}}/_{3}$$

$$\phi_{32} = \frac{2-\sqrt{3}\alpha}{(1+\alpha^2-\sqrt{3}\alpha)^{3/2}} + \frac{2}{(1+\alpha^2)^{3/2}} + \frac{2+\sqrt{3}\alpha}{(1+\alpha^2+\sqrt{3}\alpha)^{3/2}}$$

Due to the rotated ray symmetry the ϕ_{11} and ϕ_{21} perturbation coefficients from the first n-gon analysis are the same as the perturbation coefficients ϕ_{22} and ϕ_{12} from the second n-gon analysis. Taking advantage

of this recursive geometry in the concentric n-gon configurations allows much simplification.

Three N-Gon Configuration

Third N-Gon

Angular velocity and perturbation coefficient results are listed below for the third n-gon using the same methods as for the first and second n-gons of the three n-gon configuration. Mass fourteen on the rotating x' axis is rotating relative to the inertial x axis with inertial angular velocity w. Since mass fourteen on the third n-gon is the reference point that determines the orientation of the rotating x' axis, the vector velocity $\dot{z}_{14}$ and the vector acceleration $\ddot{z}_{14}$ are both zero. The equation of motion for the third n-gon of the three n-gon configuration is as follows

$$-w^2 z_{14} = -\frac{Gm_1}{r_{1,14}^3} z_{14} + Gm\sum_{i=2}^{7}\frac{z_{i,14}}{r_{i,14}^3} + Gm\sum_{i=9}^{13}\frac{z_{i,14}}{r_{i,14}^3} + Gm\sum_{\substack{i=15\\ i\neq 14}}^{19}\frac{z_{i,14}}{r_{i,14}^3}$$

$$-w_{3nr}^2 z_{14} = -\frac{Gm_1}{r_3^3} z_{14} + \frac{Gm}{r_3^3}\phi_{13} + \frac{Gm}{r_3^3}\phi_{23} + \frac{Gm}{r_3^3}\phi_{33}$$

$$\phi_{13} = r_3^3\sum_{i=2}^{7}\frac{z_{i,14}}{r_{i,14}^3} \qquad \phi_{23} = r_3^3\sum_{i=8}^{13}\frac{z_{i,14}}{r_{i,14}^3} \qquad \phi_{33} = r_3^3\sum_{\substack{i=15\\ i\neq 14}}^{19}\frac{z_{i,14}}{r_{i,14}^3}$$

$$w_{3nr}^2 = G\frac{(m_1+m(\phi_{13}+\phi_{23}+\phi_{33}))}{r_3^3} = G\frac{(m_1+m\phi_3)}{r_3^3}$$

where

$$\phi_3 = \phi_{13} + \phi_{23} + \phi_{33}$$

$$\phi_{13} = \left(\frac{2\alpha^2-1}{(1+\alpha^4-\alpha^2)^{3/2}} + \frac{2\alpha^2+1}{(1+\alpha^4+\alpha^2)^{3/2}} + \frac{1}{(\alpha^2-1)^2} + \frac{1}{(\alpha^2+1)^2}\right)\alpha^4$$

$$\phi_{23} = \left(\frac{2\alpha-\sqrt{3}}{(1+\alpha^2-\sqrt{3}\alpha)^{\frac{3}{2}}} + \frac{2\alpha}{(1+\alpha^2)^{\frac{3}{2}}} + \frac{2\alpha+\sqrt{3}}{(1+\alpha^2+\sqrt{3}\alpha)^{\frac{3}{2}}}\right)\alpha^2$$

$$\phi_{33} = {}^{5}/_{4} + {}^{\sqrt{3}}/_{3}$$

The perturbation coefficients summarized for the three n-gon configuration can be seen below

$$\begin{matrix} \phi_{11} & \phi_{21} & \phi_{31} \\ \phi_{12} & \phi_{22} & \phi_{32} \\ \phi_{13} & \phi_{23} & \phi_{33} \end{matrix} = \begin{matrix} \phi_{11} & \phi_{21} & \phi_{31} \\ \phi_{12} & \phi_{11} & \phi_{21} \\ \phi_{13} & \phi_{12} & \phi_{11} \end{matrix}$$

As indicated earlier there is a well-defined n-gon symmetry using the rotated ray geometry. From the summarized perturbations listed above $\phi_{11} = \phi_{22} = \phi_{33}, \phi_{12} = \phi_{23}$ and, $\phi_{21} = \phi_{32}$. There are R^2 ϕ_{ij} terms to be evaluated for the three n-gon configuration, however, due to the α independent ϕ_{ii} intra symmetry and the ϕ_{ij} redundancies the total evaluations reduce to 2R-1. This is a direct result of the rotated ray geometry.

3.2.7 Four N-Gon Configuration

The four n-gon configuration is the last configuration in the multiple concentric n-gon section to be studied before moving on to the infinite n-gon problem. Only perturbation coefficients new to the four n-gon configuration are ϕ_{41} and ϕ_{14}, the remaining ϕ_{ij}'s have been previously determined from the two and three n-gon configuration analysis. Perturbation symmetry displayed in equations 3.2.7.1 from recursive geometry can be extended to the infinite n-gon configuration. The analytical basis formulating the problem of the two n-gon configuration with infinite masses has been presented in subsection 3.2.5. Using the two n-gon infinite mass procedure along with the three and four n-gon perturbation analysis will allow the infinite n-gon configuration solution to be worked out in section 3.3. See figure 3.2.2 as a reference for the four n-gon geometry. The four n-gon configuration will be summarized in equation 3.2.7.1 with minimal analytical analysis.

First N-Gon

$$w_{1nr}^2 = G\frac{m_1+m\phi_1}{r_1^3}$$ Equations 3.2.7.1

$$\phi_1 = \phi_{11} + \phi_{21} + \phi_{31} + \phi_{41}$$

$$\phi_{11} = {}^{5}/_{4} + {}^{\sqrt{3}}/_{3}$$

$$\phi_{21} = \frac{2-\sqrt{3}\alpha}{(1+\alpha^2-\sqrt{3}\alpha)^{3/2}} + \frac{2}{(1+\alpha^2)^{3/2}} + \frac{2+\sqrt{3}\alpha}{(1+\alpha^2+\sqrt{3}\alpha)^{3/2}}$$

$$\phi_{31} = \frac{2-\alpha^2}{(1+\alpha^4-\alpha^2)^{3/2}} + \frac{2+\alpha^2}{(1+\alpha^4+\alpha^2)^{3/2}} - \frac{1}{(\alpha^2-1)^2} + \frac{1}{(\alpha^2+1)^2}$$

$$\phi_{41} = \frac{2-\sqrt{3}\alpha^3}{(1+\alpha^6-\sqrt{3}\alpha^3)^{3/2}} + \frac{2}{(1+\alpha^6)^{3/2}} + \frac{2+\sqrt{3}\alpha^3}{(1+\alpha^6+\sqrt{3}\alpha^3)^{3/2}}$$

Second N-Gon

$$w_{2nr}^2 = G\frac{m_1+m\phi_2}{r_2^3}$$

$$\phi_2 = \phi_{12} + \phi_{22} + \phi_{32} + \phi_{42}$$

$$\phi_{12} = \left(\frac{2\alpha-\sqrt{3}}{(1+\alpha^2-\sqrt{3}\alpha)^{3/2}} + \frac{2\alpha}{(1+\alpha^2)^{3/2}} + \frac{2\alpha+\sqrt{3}}{(1+\alpha^2+\sqrt{3}\alpha)^{3/2}}\right)\alpha^2$$

$$\phi_{22} = {}^{5}/_{4} + {}^{\sqrt{3}}/_{3}$$

$$\phi_{32} = \frac{2-\sqrt{3}\alpha}{(1+\alpha^2-\sqrt{3}\alpha)^{3/2}} + \frac{2}{(1+\alpha^2)^{3/2}} + \frac{2+\sqrt{3}\alpha}{(1+\alpha^2+\sqrt{3}\alpha)^{3/2}}$$

$$\phi_{42} = \frac{2-\alpha^2}{(1+\alpha^4-\alpha^2)^{3/2}} + \frac{2+\alpha^2}{(1+\alpha^4+\alpha^2)^{3/2}} - \frac{1}{(\alpha^2-1)^2} + \frac{1}{(\alpha^2+1)^2}$$

Third N-Gon

$$w_{3nr}^2 = G\frac{m_1+m\phi_3}{r_3^3}$$

$$\phi_3 = \phi_{13} + \phi_{23} + \phi_{33} + \phi_{43}$$

$$\phi_{13} = \left(\frac{2\alpha^2-1}{(1+\alpha^4-\alpha^2)^{3/2}} + \frac{2\alpha^2+1}{(1+\alpha^4+\alpha^2)^{3/2}} + \frac{1}{(\alpha^2-1)^2} + \frac{1}{(\alpha^2+1)^2}\right)\alpha^4$$

$$\phi_{23} = \left(\frac{2\alpha-\sqrt{3}}{(1+\alpha^2-\sqrt{3}\alpha)^{\frac{3}{2}}} + \frac{2\alpha}{(1+\alpha^2)^{\frac{3}{2}}} + \frac{2\alpha+\sqrt{3}}{(1+\alpha^2+\sqrt{3}\alpha)^{\frac{3}{2}}}\right)\alpha^2$$

$$\phi_{33} = {}^5/_4 + {}^{\sqrt{3}}/_3$$

$$\phi_{43} = \frac{2-\sqrt{3}\alpha}{(1+\alpha^2-\sqrt{3}\alpha)^{3/2}} + \frac{2}{(1+\alpha^2)^{3/2}} + \frac{2+\sqrt{3}\alpha}{(1+\alpha^2+\sqrt{3}\alpha)^{3/2}}$$

Fourth N-Gon

$$w_{4nr}^2 = G\frac{m_1+m\phi_4}{r_4^3}$$

$$\phi_4 = \phi_{14} + \phi_{24} + \phi_{34} + \phi_{44}$$

$$\phi_{14} = \left(\frac{2\alpha^3-\sqrt{3}}{(1+\alpha^6-\sqrt{3}\alpha^3)^{\frac{3}{2}}} + \frac{2\alpha^3}{(1+\alpha^6)^{\frac{3}{2}}} + \frac{2\alpha^3+\sqrt{3}}{(1+\alpha^6+\sqrt{3}\alpha^3)^{\frac{3}{2}}}\right)\alpha^6$$

$$\phi_{24} = \left(\frac{2\alpha^2-1}{(1+\alpha^4-\alpha^2)^{3/2}} + \frac{2\alpha^2+1}{(1+\alpha^4+\alpha^2)^{3/2}} + \frac{1}{(\alpha^2-1)^2} + \frac{1}{(\alpha^2+1)^2}\right)\alpha^4$$

$$\phi_{34} = \left(\frac{2\alpha-\sqrt{3}}{(1+\alpha^2-\sqrt{3}\alpha)^{\frac{3}{2}}} + \frac{2\alpha}{(1+\alpha^2)^{\frac{3}{2}}} + \frac{2\alpha+\sqrt{3}}{(1+\alpha^2+\sqrt{3}\alpha)^{\frac{3}{2}}}\right)\alpha^2$$

$$\phi_{44} = {}^5/_4 + {}^{\sqrt{3}}/_3$$

The inter and intra perturbations listed above show that the four n-gon system maintains the same intrinsic symmetry as the three n-gon configuration. Unique inter and intra perturbations require only 2R-1 evaluations per n-gon configuration resulting from α and inter perturbation symmetry redundancies. Summarized perturbation coefficients for the four n-gon configuration are listed below

$$\begin{matrix}\phi_{11} & \phi_{21} & \phi_{31} & \phi_{41} \\ \phi_{12} & \phi_{22} & \phi_{32} & \phi_{42} \\ \phi_{13} & \phi_{23} & \phi_{33} & \phi_{43} \\ \phi_{14} & \phi_{24} & \phi_{34} & \phi_{44}\end{matrix} = \begin{matrix}\phi_{11} & \phi_{21} & \phi_{31} & \phi_{41} \\ \phi_{12} & \phi_{11} & \phi_{21} & \phi_{31} \\ \phi_{13} & \phi_{12} & \phi_{11} & \phi_{21} \\ \phi_{14} & \phi_{13} & \phi_{12} & \phi_{11}\end{matrix}$$

3.2.8 Four N-Gon Sidereal Synodic Coefficients

Solving the sidereal synodic coefficients for the four n-gon system can proceed along the same lines as that of the two n-gon configuration in subsection 3.2.2. Starting from the equation 3.2.1.2 definition with

$$n_4P_4 = (n_4 + n_3)P_3 = (n_4 + n_3 + n_2)P_2 = (n_4 + n_3 + n_2 + n_1)P_1$$

it can be found after some algebraic manipulation

$$\frac{n_3}{n_4} = \frac{P_4 - P_3}{P_3} \qquad \frac{n_2}{n_4} = \frac{P_4}{P_3}\frac{P_3 - P_2}{P_2} \qquad \frac{n_1}{n_4} = \frac{P_4}{P_2}\frac{P_2 - P_1}{P_1}$$

$$\frac{P_4^2}{P_3^2} = \frac{G_3^2}{G_4^2}\alpha^3 \qquad \frac{P_3^2}{P_2^2} = \frac{G_2^2}{G_3^2}\alpha^3 \qquad \frac{P_2^2}{P_1^2} = \frac{G_1^2}{G_2^2}\alpha^3$$

using the above equations to formulate n_3 and n_4

$$n_4^2P_4^2 = (n_4 + n_3)^2P_3^2$$

$$G_4^2P_4^2 = G_3^2\alpha^3P_3^2$$

and n_2

$$(n_4 + n_3)^2P_3^2 = (n_4 + n_3 + n_2)^2P_2^2$$

$$G_3^2\alpha^3P_3^2 = G_2^2\alpha^6P_2^2$$

and finally for n_1

$$(n_4 + n_3 + n_2)^2P_2^2 = (n_4 + n_3 + n_2 + n_1)^2P_1^2$$

$$G_2^2\alpha^6P_2^2 = G_1^2\alpha^9P_1^2$$

solving for n_1 through n_4 results in

$$n_1 = \alpha^3(G_1\alpha^{3/2} - G_2) \qquad n_2 = \alpha^{3/2}(G_2\alpha^{3/2} - G_3)$$

$$n_3 = G_3\alpha^{3/2} - G_4 \qquad n_4 = G_4$$

where $G_i^2 = 1 + \frac{m}{m_1}\phi_i$

Like the two n-gon configuration, the sidereal synodic coefficients could be used to estimate the four n-gon mass range to find potential finite stable systems. However, instead of one period ratio to deal with there are now six ratios for the four n-gon configuration to consider. This method could easily become overwhelming and better methods such as numerical optimization may prove more useful.

$$\frac{P_4}{P_1} \quad \frac{P_4}{P_2} \quad \frac{P_4}{P_3}$$

$$\frac{P_3}{P_1} \quad \frac{P_3}{P_2}$$

$$\frac{P_2}{P_1}$$

3.3 Infinite N-Gon Configuration

3.3.1 Infinite Concentric N-Gon Formulation

The n-gon perturbations derived from the n-body equations are $\phi_j = \sum_{i=1}^{R} k_j \phi_{ij}$ for j = 1, 2, , …,R, where ϕ_{jj}, ϕ_{ij} and $k_j \left(k_j > 0\right)$ represent intra/inter perturbations and mass scaling respectively. Intra perturbations are interactions between particles within the n-gon, whereas inter perturbations are particle interactions between n-gons. Scalar α reduces ϕ_{ij} inter perturbation evaluations resulting from redundancies $\phi_{i,i-1}, \phi_{i-1,i}, \phi_{i,i-2}, \phi_{i-2,i}, etc.$. Intra perturbations ϕ_{jj} evaluations are also reduced, for every concentric n-gon maintains the same geometric proportion, resulting in α independent $\phi_{11} = \phi_{22} = \cdots = \phi_{RR}$. There are R^2 ϕ_{ij} terms to be evaluated per n-gon configuration; however, due to ϕ_{ij} redundancies resulting from α and intra symmetry, ϕ_{ij} evaluations can be reduced to 2R – 1. Therefore, the only non-redundant terms are in the first row and first column of ϕ_{ij}. Perturbation series ϕ_{ij} can be rewritten

$$\phi_j = k_j \phi_{jj} + \sum_{\substack{i=1 \\ R-j \geq 1}}^{R-j} k_{i+j} \phi_{i+1,1} + \sum_{\substack{i=1 \\ j-1 \geq 1}}^{j-1} k_{j-i} \phi_{1,i+1} \quad \text{Equation 3.3.1.1}$$

where $j = 1, 2, 3, \ldots, R$

The equation for infinite masses within a given n-gon (ϕ_{jj}) orbiting mass one has already been developed for the two n-gon configuration. Intra perturbations for each regular n-gon within the infinite n-gon configuration are the same, that is, $\phi_{11} = \phi_{22,} = \cdots = \phi_{jj}$. Therefore, as described in subsection 3.2.5

$$\phi_{jj} = \frac{1}{4} + \frac{\sqrt{2}}{2}\sum_{i=1}^{\frac{1}{2}(R_n-2)}(1 - cos\frac{2\pi i}{R_n})^{-1/2} \quad R_n = 4,6,\ldots\infty \quad j_{max} = 2,4,\ldots R$$

As can be seen from the geometry of the rotated ray configuration the n-gon row and column perturbations are grouped in terms of even and odd coefficients outlined below

Row	Column
$\phi_{21}, \phi_{41}, \cdots, \phi_{2j,1}$	$\phi_{12}, \phi_{14}, \cdots, \phi_{1,2j}$
$\phi_{31}, \phi_{51}, \cdots, \phi_{2j+1,1}$	$\phi_{13}, \phi_{15}, \cdots, \phi_{1,2j+1}$

The three n-gon configuration displays a different perturbation structure as seen with terms ϕ_{31} and ϕ_{13} than found with terms ϕ_{21}, ϕ_{12} and ϕ_{41}, ϕ_{14}. This will be true for the even and odd perturbations for higher order n-gon configurations. Equations for all four perturbation groups can be derived from the following method by starting with the evaluation of $\phi_{21}, \phi_{31}, \ldots, \phi_{R1}$. Expanding $G\sum_{i=3}^{N}\frac{m_i}{r_{i2}^3}z_{i2}$ from the first n-gon for the even perturbations $(-z_2\phi_{21}, -z_2\phi_{41}, \ldots)$ yields

$$-z_2\phi_{21} = r_1^3\sum_{i=R_n+2}^{2R_n+1}\frac{z_{i2}}{r_{i2}^3} = r_1^3\left(\frac{z_{R_n+2,2}}{r_{R_n+2,2}^3} + \frac{z_{R_n+3,2}}{r_{R_n+3,2}^3} + \cdots + \frac{z_{2R_n+1,2}}{r_{2R_n+1,2}^3}\right)$$

$$-z_2\phi_{41} = r_1^3\sum_{i=3R_n+2}^{4R_n+1}\frac{z_{i2}}{r_{i2}^3} = r_1^3\left(\frac{z_{3R_n+2,2}}{r_{3R_n+2,2}^3} + \frac{z_{3R_n+3,2}}{r_{3R_n+3,2}^3} + \cdots + \frac{z_{4R_n+1,2}}{r_{4R_n+1,2}^3}\right)$$

$$-z_2\phi_{R1} = r_1^3\sum_{i=R_nR_n(R-1)+2}^{R_nR+1}\frac{z_{i2}}{r_{i2}^3} = r_1^3\left(\frac{z_{R_n(R-1)+2,2}}{r_{R_n(R-1)+2,2}^3} + \frac{z_{R_n(R-1)+3,2}}{r_{R_n(R-1)+3,2}^3} + \cdots + \frac{z_{R_nR+1,2}}{r_{R_nR+1,2}^3}\right)$$

The odd perturbation coefficients for the first n-gon $(-z_2\phi_{31}, -z_2\phi_{51}, \ldots)$ can be expressed in a similar format.

$$-z_2\phi_{31} = r_1^3 \sum_{i=2R_n+2}^{3R_n+1} \frac{z_{i2}}{r_{i2}^3} = r_1^3 \left(\frac{z_{2R_n+2,2}}{r_{2R_n+2,2}^3} + \frac{z_{2R_n+3,2}}{r_{2R_n+3,2}^3} + \cdots + \frac{z_{3R_n+1,2}}{r_{3R_n+1,2}^3}\right)$$

$$-z_2\phi_{51} = r_1^3 \sum_{i=4R_n+2}^{5R_n+1} \frac{z_{i2}}{r_{i2}^3} = r_1^3 \left(\frac{z_{4R_n+2,2}}{r_{4R_n+2,2}^3} + \frac{z_{4R_n+3,2}}{r_{4R_n+3,2}^3} + \cdots + \frac{z_{5R_n+1,2}}{r_{5R_n+1,2}^3}\right)$$

$$-z_2\phi_{(R-1),1} = r_1^3 \sum_{i=R_n(R-2)+2}^{R_n(R-1)+1} \frac{z_{i2}}{r_{i2}^3} = r_1^3 \left(\frac{z_{R_n(R-2)+2,2}}{r_{R_n(R-2)+2,2}^3} + \frac{z_{R_n(R-2)+3,2}}{r_{R_n(R-2)+3,2}^3} + \cdots + \frac{z_{R_nR-1,2}}{r_{R_nR-1,2}^3}\right)$$

Collecting even and odd coefficients from the first n-gon and resolving $G\sum_{i=3}^{N} \frac{m_i}{r_{i2}^3} z_{i2}$ into its individual terms gives the following result. Total number of concentric n-gon particles is $N = RR_n + 1$.

$$Gm\sum_{i=3}^{N} \frac{z_{i2}}{r_{i2}^3} = -\frac{Gm}{r_1^3} z_2\phi_{11} - \frac{Gm}{r_1^3} z_2\phi_{21} - \frac{Gm}{r_1^3} z_2\phi_{31} - \cdots - \frac{Gm}{r_1^3} z_2\phi_{R1}$$

where $$-w_{1NR}^2 z_2 = -\frac{Gm_1}{r_1^3} z_2 + Gm\sum_{i=3}^{N} \frac{z_{i2}}{r_{i2}^3}$$

$$w_{1NR}^2 z_2 = \frac{Gm_1}{r_1^3} z_2 + \frac{Gm}{r_1^3} z_2 \sum_{i=1}^{R} \phi_{i1}$$

and $$w_{1NR}^2 = G\frac{m_1 + \phi_1 m}{r_1^3} \qquad \phi_1 = \sum_{i=1}^{R} \phi_{i1} \qquad \text{Equation 3.3.1.2}$$

Continuing this procedure for the second n-gon

$$Gm\sum_{\substack{i=2 \\ i\neq R_n+2}}^{N} \frac{z_{i,R_n+2}}{r_{i,R_n+2}^3} = -\frac{Gm}{r_2^3} z_{R_n+2}\phi_{12} - \frac{Gm}{r_2^3} z_{R_n+2}\phi_{22} - \frac{Gm}{r_2^3} z_{R_n+2}\phi_{32} - \cdots - \frac{Gm}{r_2^3} z_{R_n+2}\phi_{R2}$$

where $$-w_{2NR}^2 z_2 = -\frac{Gm_1}{r_2^3} z_{R_n+2} + Gm\sum_{\substack{i=2 \\ i\neq R_n+2}}^{N} \frac{z_{i,R_n+2}}{r_{i,R_n+2}^3}$$

$$w_{2NR}^2 z_{R_n+2} = \frac{Gm_1}{r_2^3} z_{R_n+2} + \frac{Gm}{r_2^3} z_{R_n+2} \sum_{i=1}^{R} \phi_{i2}$$

and $$w_{2NR}^2 = G\frac{m_1 + \phi_2 m}{r_2^3} \qquad \phi_2 = \sum_{i=1}^{R} \phi_{i2} \qquad \text{Equation 3.3.1.3}$$

Formulating the infinite n-gon

$$Gm\sum_{\substack{i=2\\ i\neq N-R_n+1}}^{N}\frac{z_{i,N-R_n+1}}{r_{i,N-R_n+1}^3}=-\frac{Gm}{r_R^3}z_{N-R_n+1}\phi_{1R}-\frac{Gm}{r_R^3}z_{N-R_n+1}\phi_{2R}-\frac{Gm}{r_R^3}z_{N-R_n+1}\phi_{3R}-\ldots-\frac{Gm}{r_R^3}z_{N-R_n+1}\phi_{RR}$$

where $$-w_R^2z_2=-\frac{Gm_1}{r_R^3}z_{N-R_n+1}+Gm\sum_{\substack{i=2\\ i\neq N-R_n+1}}^{N}\frac{z_{i,N-R_n+1}}{r_{i,N-R_n+1}^3}$$

$$w_R^2z_{N-R_n+1}=\frac{Gm_1}{r_R^3}z_{N-R_n+1}+\frac{Gm}{r_R^3}z_{N-R_n+1}\sum_{i=1}^{R}\phi_{iR}$$

and $$w_R^2=G\frac{m_1+\phi_Rm}{r_R^3}\qquad \phi_R=\sum_{i=1}^{R}\phi_{iR}$$ Equation 3.3.1.4

Where the even row perturbation coefficients are $\phi_{21},\phi_{41},$ ...etc.

$$\phi_{2j,1}=2\sum_{i=1}^{\frac{1}{2}R_n}\frac{1-\alpha^{\beta}cos\theta_2}{(\alpha^{2\beta}+1-2\alpha^{\beta}cos\theta_2)^{3/2}}$$ Equation 3.3.1.5

for rotated ray θ_1 and θ_2 geometry conditions

$i=1,2,3,\ldots,\frac{1}{2}R_n$ β = 2j-1 $\theta_1=\pi-2\theta_2=(R_n-2(2i-1))\frac{\pi}{R_n}$

j= $1,2,3,\ldots,\frac{1}{2}R$ $\theta_2=(2i-1)\frac{\pi}{R_n}$ $R_n\geq 4$ $R\geq 2$

The odd row perturbation coefficients are $\phi_{31},\phi_{51},$ ...etc.

$$\phi_{2j+1,1}=-\frac{1}{(\alpha^{\gamma}-1)^2}+\frac{1}{(\alpha^{\gamma}+1)^2}+2\sum_{i=1}^{\frac{1}{2}(R_n-2)}\frac{1-\alpha^{\gamma}cos\theta_4}{(\alpha^{2\gamma}+1-2\alpha^{\gamma}cos\theta_4)^{3/2}}$$

Equation 3.3.1.6

for rotated ray θ_3 and θ_4 geometry conditions

$i=1,2,3,\ldots,\frac{1}{2}(R_n-2)$ γ = 2j $\theta_3=\pi-2\theta_4=(R_n-4i)\frac{\pi}{R_n}$

j = $1,2,3,\ldots,\frac{1}{2}(R\ \ -2)$ $\theta_4=2\frac{\pi i}{R_n}$ $R_n\geq 4$ $R\geq 2$

The even column perturbation coefficients are $\phi_{12},\phi_{14},$ ...etc.

$$\phi_{1,2j} = 2\alpha^{2\beta}\sum_{i=1}^{\frac{1}{2}R_n}\frac{\alpha^{\beta}-cos\theta_2}{(\alpha^{2\beta}+1-2\alpha^{\beta}cos\theta_2)^{3/2}} \qquad \text{Equation 3.3.1.7}$$

the rotated ray θ_1 and θ_2 geometry conditions for the even row $\phi_{2j,1}$ case also apply to the even column $\phi_{1,2j}$ case.

The odd column perturbations coefficients are ϕ_{13}, ϕ_{15}, ...etc.

$$\phi_{1,2j+1} = \frac{\alpha^{2\gamma}}{(\alpha^{\gamma}-1)^2} + \frac{\alpha^{2\gamma}}{(\alpha^{\gamma}+1)^2} + 2\alpha^{2\gamma}\sum_{i=1}^{\frac{1}{2}(R_n-2)}\frac{\alpha^{\gamma}-cos\theta_4}{(\alpha^{2\gamma}+1-2\alpha^{\gamma}cos\theta_4)^{3/2}}$$

Equation 3.3.1.8

the rotated ray θ_3 and θ_4 geometry conditions for the odd row $\phi_{2j+1,1}$ case also apply to the odd column $\phi_{1,2j+1}$ case.

Intra and inter perturbations for the infinite n-gon configurations are summarized in the following table

ϕ_j	ϕ_{ij}		
ϕ_1	ϕ_{11}	...	ϕ_{R1}
⋮	⋮	...	⋮
ϕ_R	ϕ_{1R}	...	ϕ_{11}

Mathematically this can be written as

$$\phi_j = \sum_{i=1}^{R}\phi_{ij}$$

where ϕ_j does not take into account mass scaling or ϕ_{ij} redundancies resulting from α and intra n-gon symmetry. Taking into account mass scaling without ϕ_{ij} redundancies gives

$$\phi_j = \sum_{i=1}^{R}k_j\phi_{ij}$$

Considering only ϕ_{ij} redundancies without mass scaling

$$\phi_j = \phi_{jj} + \sum_{i=1}^{R-j}\phi_{i+1,j} + \sum_{i=1}^{j-1}\phi_{1,i+1}$$

The full up equation with mass scaling and ϕ_{ij} redundancies results in equation 3.3.1.1

$$\phi_j = k_j\phi_{jj} + \sum_{\substack{i=1 \\ R-j\geq 1}}^{R-j} k_{i+j}\phi_{i+1,1} + \sum_{\substack{i=1 \\ j-1\geq 1}}^{j-1} k_{j-i}\phi_{1,i+1}$$

Equation 3.3.1.1 is the formulation that will be used in the next subsection for perturbation coefficient calculation to determine numerically optimized infinite concentric n-gon configuration mass. The inertial angular velocity for each n-gon as a function of ϕ_j in the infinite n-gon configuration is

$$w_j^2 = G\frac{(m_1+m\phi_j)}{r_j^3}$$

For simplicity the even and odd row coefficients can be written as one equation consistent with equations 3.3.1.5 and 3.3.1.6

$$\phi_{j+1,1} = -\frac{4\alpha^j}{(\alpha^{2j}-1)^2}\delta_j + 2\sum_{i=1}^{\frac{1}{2}(R_n-2\delta_j)} \frac{1-\alpha^j cos\theta}{(\alpha^{2j}+1-2\alpha^j cos\theta)^{3/2}} \qquad \text{Equation 3.3.1.9}$$

where $\delta_j = 0\ (j\ odd), = 1\ (j\ even) \qquad \theta = (2i-1+\delta_j)\frac{\pi}{R_n}$

$$R \geq 2\ (R\ even) \qquad R_n \geq 4$$

Even and odd column perturbation coefficients can be written as one equation consistent with equations 3.3.1.7 and 3.3.1.8

$$\phi_{1,j+1} = \frac{2\alpha^{2j}(\alpha^{2j}+1)}{(\alpha^{2j}-1)^2}\delta_j + 2\alpha^{2j}\sum_{i=1}^{\frac{1}{2}(R_n-2\delta_j)} \frac{\alpha^j-cos\theta}{(\alpha^{2j}+1-2\alpha^j cos\theta\ )^{3/2}}$$

Equation 3.3.1.10

where δ_j, θ, R and R_n are the same as for equation 3.3.1.9.

From rotated ray symmetry, the ϕ_{jj} intra perturbation equation can be rewritten using trigonometric identities. Although, this reformulation reduces the terms in the sum by half, the number of ϕ_{jj} that can be evaluated is also reduced by half

$$\phi_{jj} = \frac{1}{4} + \sum_{i=1}^{\frac{1}{4}(R_n-2)} \frac{cos\theta + sin\theta}{sin2\theta} = \frac{1}{4} + \frac{1}{2}\sum_{i=1}^{\frac{1}{4}(R_n-2)} \left(\frac{1}{sin\theta} + \frac{1}{cos\theta}\right)$$

$$R_n = 6, 10, 14, 18 \ldots \infty \qquad \theta = \frac{\pi i}{R_n}$$

Perturbation equations $\phi_{j+1,1}$ and $\phi_{1,j+1}$ can also be rewritten to reduce the sum of terms by one half using trigonometric identities. Although the number of terms to be evaluated has been reduced by half, the evaluation per term appears to have increased.

A state vector can be constructed from a given n-gon configuration by using the inertial angular velocities calculated and the n-gon particle coordinate locations. Numerically integrating this state vector will show the n-gon evolving over time. These state vectors are not unique for a given n-gon configuration as was found with the two n-gon configuration. Equation 3.3.1.1 with mass scaling parameter k makes it possible to perform numerical optimization to obtain a unique solution

Evaluating the inertial angular velocities from

$$w_j^2 = G\frac{(m_1 + m\phi_j)}{r_j^3}$$

and using equation 3.3.1.1 to determine the inter intra perturbation coefficients ϕ_{ij}, the n-gon optimization process can be started on the constraint surface with the equality and inequality constraints being $k_j = 1$ and $k_j > 0$. The unique n-gon is defined by determination of an absolute minimum potential energy configuration. This will be discussed in section 3.3.2.

3.3.2 Infinite N-Gon Numerical Optimization

For a given concentric n-gon configuration there will be a unique set of k_j's for input parameters m_1 and m_T. Applying Lagrange's 1788 absolute minimum energy principle, a configuration is in equilibrium if an absolute minimum potential energy configuration can be found. Lyapunov's direct method could show if this equilibrium configuration is stable or unstable by expanding the potential energy in the v function in a series to determine if it is positive definite (using the Sylvester criterion). First, however, it is necessary to find the minimum potential energy of a given concentric n-gon configuration.

To find the minimum potential energy for the n-gon configuration will require numerical optimization. This process establishes constraints necessary to initiate the optimization process and the determination of the particular n-gon function to be optimized. Total n-gon mass m_T is formulated as a series, where each n-gon consists of an equal number of identical mass particles multiplied by mass scaling k_j. This equates to $m_T = mR_n \sum_{j=1}^{R} k_j = mR_nR$ which defines equality constraint to $R = \sum_{j=1}^{R} k_j$. Considering mass positive defines inequality constraint $k_j > 0$. For $R \geq 2$, there are infinite k_j. and w_j distributions consistent with equality constraint $R = \sum_{j=1}^{R} k_j$. By observation, it will be noted that a trivial solution for any R is $k_j = 1$. For zero mass n-gon configurations ($m_T = 0, m = 0$) system constraints are violated and the infinite n-gon angular velocity distribution reduces to a unique central force angular velocity distribution, that is, there is an infinite two body velocity distribution. For non-zero mass n-gon configurations ($m_T > 0, m > 0, R \geq 2$) system constraints are preserved as specified by $R = \sum_{j=1}^{R} k_j$ and $k_j > 0$, however, resulting k_j and w_j distributions will not be unique. Unique distributions can be found from the following condition; that the potential energy of the conservative n-gon configuration is at an absolute minimum (Gantmacher, 1970, 169, Jeans, 1935, 348-352, Ramsey, 1929, 257). From this condition, the minimum potential energy k_j. and w_j distributions are unique for $m_T > 0, m > 0, R \geq 2$ with $r_j = \alpha^{j-1} r_1$ $(\alpha \neq 1)$ over region $0 < r_j < \infty$. The inertial angular velocity can be written in terms of the perturbed and unperturbed components respectively

$$w_j^2 = (w_j^p)^2 + (w_j^u)^2 \qquad (w_j^u)^2 = \frac{Gm_1}{r_j^3} \qquad (w_j^p)^2 = \frac{Gm}{r_j^3}\phi_j$$

The general equation for the perturbed scaled component to be optimized can be determined by expanding the kinetic potential energy series as a function of concentric n-gon number. For example,

$$2T = \sum_{j=1}^{R} m_j v_j^2 = R_n mG \sum_{j=1}^{R} \frac{m_1 + \phi_j m}{r_j} k_j \qquad \text{Equation 3.3.2.1}$$

$$2T = R_n mG \sum_{j=1}^{R} \frac{m_1}{r_j} k_j + R_n mG \sum_{j=1}^{R} \frac{\phi_j m}{r_j} k_j = 2T^u + 2T^p$$

where the angular velocity has been substituted into equation 3.3.2.1

The first term to the right of the equal sign is the unperturbed kinetic energy, that is, there are no intra or inter perturbations in this term. Expanding the unperturbed kinetic energy results in

$$2T^u = R_n mG \sum_{j=1}^{R} \frac{m_1}{r_j} k_j = \frac{Gm_1}{r_1} \sum_{j=1}^{R} \frac{m_{jNGON}^T}{\alpha^{j-1}}$$

where m_{jNGON}^T is the total n-gon mass per n^{th} n-gon. Radii distribution $r_j = r_1 \alpha^{j-1}$ determines the n-gon spacing for the perturbed and unperturbed kinetic energy equation. Perturbed kinetic energy $2T^p$ defines the optimization function used to calculate the scaled mass $k_j's$. Equation 3.3.2.1 perturbed kinetic energy $2T^p$ can be written as follows

$$2T^p = R_n mG \sum_{j=1}^{R} \frac{\phi_j m}{r_j} k_j = R_n \frac{Gm^2}{r_1} \sum_{j=1}^{R} \frac{\phi_j}{\alpha^{j-1}} k_j$$

Therefore, the perturbed scaled form of the kinetic (potential) energy function to be optimized is

$$\Delta = \frac{2T - 2T^u}{R_N \frac{Gm^2}{r_1}} = \sum_{j=1}^{R} \frac{\phi_j k_j}{\alpha^{j-1}} \qquad \text{Equation 3.2.3.2}$$

Equivalent analysis for the scaled potential energy will give

$$\frac{2U - 2U^u}{R_N \frac{Gm^2}{r_1}} = \sum_{j=1}^{R} \frac{\phi_j^U k_j}{\alpha^{j-1}}$$

Geometric perturbations with mass and radii scaling $\sum_{j=1}^{R} \frac{\phi_j k_j}{\alpha^{j-1}}$ have been isolated in equation 3.2.3.2 for the purpose of numerical optimization. Scaled kinetic energy is used for optimization in place of the scaled potential energy, however, either series is valid due to their equivalence. Theoretically, desired k_j and w_j particle distributions occur at the absolute minimum, however, with large n-gon particle configurations there does not exist complete knowledge of the absolute minimum. In practice it is expected that most likely minimums will be relative. Let the n-gon mass and angular velocity distributions for the minimization process be defined by optimization problem $F = \sum_{j=1}^{R} \frac{\phi_j k_j}{\alpha^{j-1}}$, subject to constraints $R = \sum_{j=1}^{R} k_j$ and $k_j > 0$ with input parameters $\phi_{ij}, m_1, m_T, \alpha, R, R_n, r_1 \; and \; r_R$. The gradient function necessary for optimization is determined by taking the partials of F relative to the k_j's.

$$F = \phi_1 k_1 + \frac{1}{\alpha}\phi_2 k_2 + \frac{1}{\alpha^2}\phi_3 k_3 + \cdots + \frac{1}{\alpha^{R-1}}\phi_R k_R$$

$$\frac{\partial F}{\partial k_1} = k_1\phi_{11} + \frac{1}{\alpha}k_2\phi_{12} + \frac{1}{\alpha^2}k_3\phi_{13} + \cdots + \frac{1}{\alpha^{R-1}}k_R\phi_{1R} + \phi_1$$

$$\frac{\partial F}{\partial k_2} = k_1\phi_{21} + \frac{1}{\alpha}k_2\phi_{11} + \frac{1}{\alpha^2}k_3\phi_{12} + \cdots + \frac{1}{\alpha^{R-1}}k_R\phi_{1,R-1} + \frac{1}{\alpha}\phi_2$$

$$\frac{\partial F}{\partial k_R} = k_1\phi_{R1} + \frac{1}{\alpha}k_2\phi_{R-1,1} + \frac{1}{\alpha^2}k_3\phi_{R-2,1} + \cdots + \frac{1}{\alpha^{R-1}}k_R\phi_{11} + \frac{1}{\alpha^{R-1}}\phi_R$$

The gradient equation can be summarized

$$\frac{\partial F}{\partial k_j} = \frac{1}{\alpha^{j-1}}\left(k_j\phi_{11} + \phi_j\right) + \sum_{\substack{i=1 \\ R-j\geq 1}}^{R-j} \frac{k_{i+j}\phi_{1,i+1}}{\alpha^{i+j-1}} + \sum_{\substack{i=1 \\ j\geq 2}}^{j-1} \frac{k_{j-i}\phi_{i+1,1}}{\alpha^{j-i-1}}$$

where $\phi_{1,i+1}$ and where $\phi_{i+1,1}$ are calculated prior to optimization.

The numerical minimization process can be simplified by starting on the constraint surface, that is, inputting k_j consistent with equality and inequality constraints. This may be accomplished when equality constraint trivial solution $k_j = 1$ is used. Small n-gon configurations need only one initial run to converge, however, large n-gon configurations may require the output from an initial run as input into the next successive optimization run until this process reaches convergence.

The end result of the infinite n-gon configuration analysis is a minimum energy state vector in a planar array of particles orbiting m_1 at time zero determined by numerically optimizing the scaled potential energy. These minimum energy states exist within infinitesimal interval Δt and represent particles in circular instantaneous orbits. Therefore, mass radii and angular velocity distributions determined from the minimization process define the minimum energy circular instantaneous state vector at time zero. The conservative system state vector is a point in particle position and velocity space, and over time in accordance with the equations of motion represents the past, present and future of some particular planar (phase) space trajectory. Consistent with classical deterministic mechanics this trajectory history theoretically can be found when the instantaneous state vector is completely known.

Knowledge of n-gon configuration past/future evolution requires numerical state vector integration starting at time zero with the necessary modelling of particle collision systems. System evolution will determine to

what extent particle migration redistributes n-gon mass with respect to time, thus, illustrating the degree to which a given configuration remains near its initial intra geometry. Particle redistribution evolution for large n-gon systems may also include periodic mass migration oscillating between relative minimum potential energy states at possible resonance locations. Large magnitude n-body interaction particle simulations could be accomplished with future generation special purpose research computers such as GRAPE-6 and GRAPE-DR (Aarseth, 2003, 247, Makino, Fukushige, Koga and Namura, 2003, 1163, Makino, 2008, 457-466).

Under the conditions where $R_n \to \infty$ and $\alpha \to 1$, intra/intra geometrical perturbations become infinite presenting difficulties in numerically optimizing the scaled potential energy or large densely populated systems. Therefore, it is important to investigate the nature of these singularities to determine whether they are removeable. To accomplish this, it would be instructive to have the n-gon configuration collapse into one n-gon, that is, α equals one. This single n-gon system is composed of $2R_n$ points where each point has ½ R particles occupying the same location. Geometrically, multiple points at the same location do not pose a problem since points are zero dimensional and can be packed in any manner. However, gravitationally this introduces an infinite valued scaled potential energy function in the $\alpha \to 1$ environment and cannot be optimized. Multiple particles at the same point are inter singularities that occur when the rotated ray structure approaches an alpha of one. Proper redistribution of the rotated ray configuration will align the mass particles in such an orientation that individual n-gons when collapsed into one n-gon will not result in over lapping particles, thus, removing the inter singularity problem. Remaining, however, are the intra singularities and although perturbation magnitude becomes infinite as $R_n \to \infty$, the mass particles never overlap. The intra n-gon population can always be increased no matter how many zero-dimensional particles occupy the n-gon. Under these conditions as specified, the intra singularities do not appear to be removeable. Remodeling discrete particles into continuous mass circles may resolve the intra singularity problem, however, this would require a complete restructuring of the n-gon formulation in the near one alpha regime.

3.3.3 Conservation of Energy Verification

It is important to show the infinite n-gon solution is consistent with conservation of energy for the rotated ray configuration. This is a required step verifying the infinite concentric n-gon analysis has determined the

correct solution in that twice the kinetic energy is equal to the potential energy. Reformulating kinetic and potential energy equations in terms of the concentric n-gons initiates this process.

Relationship between kinetic and potential energy at time zero is determined using perturbed angular velocity and the customary energy equations. Kinetic energy $2T = \sum_{i=1}^{N} m_i v_i^2$ series defined by n-gon becomes $2T = R_n mG \sum_{j=1}^{R} \frac{m_1 + \phi_j m}{r_j} k_j$ as previously demonstrated. The potential energy function $U = G \sum_{1 \le i < j \le N}^{N} \frac{m_i m_j}{r_{ij}}$ is somewhat more complex and will be worked by n-gon. Analyzing the first infinite n-gon in a similar manner as Section 3.2.4 results in

$$R_n m k_1 \frac{G(m_1 + \phi_1^U m)}{r_1} \qquad \phi_1^U = k_1 \phi_{11}$$

for the second n-gon

$$R_n m k_2 \frac{G(m_1 + \phi_2^U m)}{r_2} \qquad \phi_2^U = k_1 \phi_{12c} + k_2 \phi_{22}$$

for the third n-gon

$$R_n m k_3 \frac{G(m_1 + \phi_3^U m)}{r_3} \qquad \phi_3^U = k_1 \phi_{13c} + k_2 \phi_{23c} + k_3 \phi_{33}$$

for the R^{th} n-gon

$$R_n m k_R \frac{G(m_1 + \phi_R^U m)}{r_R} \; \phi_R^U = k_1 \phi_{1Rc} + k_2 \phi_{2Rc} + \cdots + k_{R-1} \phi_{R-1,Rc} + k_R \phi_{RR}$$

Summing these terms

$$U = R_n mG \sum_{j=1}^{R} \frac{m_1 + \phi_j^U m}{r_j} k_j \qquad \text{Equation 3.3.3.1}$$

$$\phi_j^U = k_j \phi_{11} + \sum_{\substack{i=1 \\ j-1 \ge 1}}^{j-1} k_{j-i} \phi_{1,(i+1)c}^U$$

The superscript U in equation 3.3.3.1 refers to the perturbation coefficient series derived from the potential energy function. Blocked terms such as $\phi_{R-1,Rc}$ for example represents a $R_n \mathrm{X} R_n$ array of perturbations between n-gon $R-1$ and n-gon R. This is similar to the blocked potential energy

perturbation terms illustrated for the two n-gon configuration shown in Section 3.2.4. There exist redundancies between these blocked terms as for example $\phi_{12c} = \phi_{23c} = \phi_{34c} = \cdots = \phi_{j,(j+1)c}$. Relations between the potential energy perturbation terms and the kinetic energy perturbation terms will be developed in the coming analysis.

Condition $2T = U$ can be demonstrated utilizing difference function Δ_j, defined as

$$\Delta_j = \phi^U_{j+1} - \phi_{j+1}.$$

where

$$\phi^U_j = k_j\phi_{11} + \sum_{\substack{i=1 \\ j-1\geq 1}}^{j-1} k_{j-i}\phi^U_{1,(i+1)c} \qquad \text{Equation 3.3.3.2}$$

$$\phi_j = k_j\phi_{11} + \sum_{\substack{i=1 \\ R-j\geq 1}}^{R-j} k_{i+j}\phi_{i+1,1} + \sum_{\substack{i=1 \\ j-1\geq 1}}^{j-1} k_{j-i}\phi_{1,i+1} \qquad \text{Equation 3.3.3.3}$$

Substituting, to find Δ_j by replacing j with $j+1$ in equations 3.3.3.2 and 3.3.3.3

$$\Delta_j = \sum_{i=1}^{j} k_{j+1-i}(\phi^U_{1,(i+1)c} - \phi_{1,i+1}) + \sum_{\substack{i=1 \\ R-j-1\geq 1}}^{R-1-j} k_{j+1+i}\phi_{i+1,1}$$

Where the difference $\phi^U_{1,(i+1)c} - \phi_{1,i+1}$ needs to be evaluated from the general even and odd n-gon cases. For the even case

$$\phi^U_{1,2jc} - \phi_{1,2j} = \alpha^{2j-1}\phi_{2j,1} \qquad \text{Equation 3.3.3.4}$$

For the odd case

$$\phi^U_{1,(2j+1)c} - \phi_{1,2j+1} = \alpha^{2j}\phi_{2j+1,1} \qquad \text{Equation 3.3.3.5}$$

Listing the even and odd terms from equations 3.3.3.4 and 3.3.3.5 in a monotonic sequence, that is, formatting these equations into one continuous n-gon equation results in

$$\phi^U_{1,(i+1)c} - \phi_{1,i+1} = \alpha^i\phi_{i+1,1}$$

Therefore

$$\Delta_j = \sum_{i=1}^{j} k_{j+1-i}\alpha^i\phi_{i+1,1}) + \sum_{\substack{i=1 \\ R-j-1\geq 1}}^{R-1-j} k_{j+1+i}\phi_{i+1,1} \quad \text{Equation 3.3.3.6}$$

Starting with potential energy equation 3.3.3.1 and Δ_j, yields

$$U = R_n mG\left(\frac{m_1+\left(\phi_1^U+k_1^{-1}\sum_{j=1}^{R-1}\frac{\Delta_j}{\alpha^j}k_{j+1}\right)m}{r_1}k_1 + \sum_{j=2}^{R}\frac{m_1+\phi_j m}{r_j}k_j\right)$$

Equation 3.3.3.7

Evaluating $\sum_{j=1}^{R-1}\frac{\Delta_j k_{j+1}}{\alpha^j}$ in the equation 3.3.3.7 is necessary to verify potential and kinetic energy equal for j = 1, with $\sum_{j=1}^{R}\frac{m_1+\phi_j\, m}{r_j}k_j$ matching kinetic energy for $j \geq 2$. Multiplying equation 3.3.3.6 by $\frac{k_{j+1}}{\alpha^j}$ and summing over j gives

$$\sum_{j=1}^{R-1}\frac{\Delta_j}{\alpha^j}k_{j+1} = \sum_{j=1}^{R-1}\frac{k_{j+1}}{\alpha^j}\left(\sum_{i=1}^{j}k_{j+1-i}\alpha^i\phi_{i+1,1} - \sum_{\substack{i=1 \\ R-j-1\geq 1}}^{R-1-j}k_{j+1+i}\phi_{i+1,1}\right)$$

Finally, we find $\sum_{j=1}^{R-1}\frac{\Delta_j}{\alpha^j}k_{j+1} = k_1\sum_{j=1}^{R-1}k_{j+1}\phi_{j+1,1}$ verifies first term of kinetic energy matches first term of potential energy, thus establishing condition 2T = U. Therefore, all rotated ray n-1 particles are in circular instantaneous orbits relative to m_1 at time zero. Prior to or after time zero, it would be expected that all n-1 particles exist in non-circular instantaneous orbits.

3.3.4 Infinite N-Gon Sidereal Synodic Coefficients

The general sidereal synodic equation where $n_R, n_{R-1}, \ldots n_1$ are the determinable coefficients for the infinite n-gon configurations is of the form

$$n_R = (n_R + n_{R-1})P_{R-1} = \cdots (n_R + n_{R-1} + \cdots + n_1)P_1$$

can be solved by the same method used for the two and four n-gon configurations. Expanding on that method results in the solution

$$n_1 = \alpha^{3/2(R-2)}(G_1\alpha^{3/2} - G_2)$$

$$n_2 = \alpha^{3/2(R-3)}(G_2\alpha^{3/2} - G_3)$$

...

$$n_i = \alpha^{3/2(R-(i+1))}(G_i\alpha^{3/2} - G_{i+1})$$

$$n_R = G_R$$

where $G_i = (1 + \frac{m}{m_1}\phi_i)^{\frac{1}{2}}$ I = 1,2,...,R-1 $R \geq 2$ (R even)

Mass estimation for large n-gon configurations would be analogous to mass estimation for the two and four n-gon configuration. The number of n-gon period ratios for increasing R will grow as $\frac{R!}{2!(R-2!)}$. This is illustrated below

$$\frac{P_R}{P_1} \ldots\ldots\ldots\ldots \frac{P_R}{P_{R-1}}$$

$$\frac{P_{R-1}}{P_1} \ldots\ldots \frac{P_{R-1}}{P_{R-2}}$$

.....

$$\frac{P_2}{P_1}$$

N-gon configuration period ratios along the diagonal $\frac{P_2}{P_1}, \frac{P_{R-1}}{P_{R-2}} \ldots\ldots \frac{P_R}{P_{R-1}}$ could roughly estimate an upper bound mean particle mass using the following equations

$$\frac{P_j^2}{P_{i-j}^2} = \frac{1+\frac{m}{m_1}\phi_{i-j}}{1+\frac{m}{m_1}\phi_i}\alpha^{3j} \quad i = R, R-1, \ldots 2 \quad j = 1, 2, \ldots \quad i - j \geq 1$$

$$\begin{pmatrix} \phi_1 \\ . \\ \phi_R \end{pmatrix} = \begin{pmatrix} \phi_{11} & . & \phi_{R1} \\ . & . & . \\ \phi_{1R} & . & \phi_{11} \end{pmatrix} \begin{pmatrix} k_1 \\ . \\ k_R \end{pmatrix}$$

This process involves estimating mass ratio magnitude from $\frac{m}{m_1}$ such that terms $\frac{m}{m_1}\phi_1 \ldots\ldots \frac{m}{m_R}\phi_R$ are of near zero magnitude to maintain intra and inter geometry for finite intervals. It is obvious that using the sidereal

synodic method to estimate mass for large n-gon configurations to find relatively stable systems will be difficult and tedious. As mentioned for the four n-gon stability analysis, numerical optimization is most likely the better choice for the infinite n-gon mass estimation.

3.3.5 Inter N-Gon Singularity Resolution

In process of optimizing concentric n-gon scaled potential energy, oscillations in the geometrical perturbations are found to exist when the n-gons are not properly rotated in their initial concentric orientation at time zero. These oscillations are a function of how mass is packed in the n-gons and are formed as a result of inter n-gon singularities. Inter n-gon singularities develop when n-gon density increases (in the limit) such that their contiguous alignment causes overlay of the individual masses in the rotated ray configuration. This inter n-gon singularity problem can be resolved by differentially rotating the n-gon concentric configurations in the infinite interval in such a way as to have them collapse into a single n-gon. With individual masses in the one n-gon that are equidistant to each other by regular n-gon definition, inter singularities will cease to exist. Thus, allowing an expansion of the single n-gon to produce n-gon populations that should converge efficiently in the minimum energy planar problem. Differential rotation is a necessary 'mathematical' constraint placed on the concentric n-gons to prevent inter n-gon singularities.

It is not known if further consideration is necessary for concentric n-gon positioning in the optimizing process when the n-gons are properly configured in the above manner. For the situation exists that the n-gons which are inter singularity free at time zero will not exhibit a unique configuration. There are infinite configurations as the concentric n-gon population becomes infinite that possess no inter n-gon singularities. It is not clear which if any configuration is preferred over any other configuration in this population. This is a problem that can only be solved under some specified 'physical' constraint assuming that one exists. A physical constraint of this nature may require initializing the n-gon masses to orient in some preferred geometric singularity free structure that reflects a real system of particles. This would be in conjunction with determining a 'stable' n-gon total mass relative to the primary. Real particle system knowledge could be the basis in defining the 'physical' constraint.

In constructing the inter singularity free n-gon configuration it appears that when all regular n-gons are used the symmetry necessary for solution cannot be maintained. That is, a combination of regular and non-regular n-

gons are now required, thus resulting in a more complicated analysis. Symmetry constrains the n-gon configuration to have at least one axis that allows paired vectors z_{ij} relative to either side of that axis to be added with a common denominator r_{ij}^3. Figure 3.3.1 illustrates a differentially rotated configuration with all regular n-gons that has no axis meeting this symmetry constraint. Examples of differentially rotated regular and non-regular n-gons consistent with the symmetric paired vector axis constraint can be found in figures 3.3.2 and 3.3.3.

3.3.6 Inverse Problem of Dynamics

The infinite concentric n-gon configuration can be solved by method of inverse process of dynamics (Galiullin, 1984, 25-28, Santilli, 1978, 219-223). This is an inductive method of solution as an alternate to the standard deductive process of solving the equations of motion directly. Here, the inverse process formulates that the system forces are determined by the given properties of the motion. Inductively solving the inverse problem requires position, velocity, acceleration and any other dynamical constraints relative to the particular problem. The resultant solution must be verified by being consistent with the equations of motion. Showing conservation of energy consistency will meet this requirement.

Basic conditions for the inverse dynamical problem such as geometry, coordinate systems, time frame and constraints have already been presented for the general concentric n-gon problem, however, it will be repeated here for clarity.

A planar gravitational system of masses defined as Newtonian, discrete, non-relativistic and classical is in an assembly consisting of R concentric regular n-gons and R_n particles per n-gon ($RR_n = N - 1$) orbiting a central mass m_1. The particles are placed at the vertices of the equal sided regular n-gons inscribed in their respective circle of increasing radii such that the geometric center is coincident with the barycenter. The n-gons rotate as rigid bodies about m_1 within the infinitesimal time interval. This configuration is restricted to be a rotated ray configuration defined in the infinitesimal interval at time zero using type 1 geometry with the sidereal synodic relations (Bauer, 2010). Type 1 geometry is defined where all particle position vectors are perpendicular to all particle velocity vectors relative to the barycenter in the configuration plane of motion in the infinitesimal interval at time zero. Concentric n-gon configurations rotate

relative to specified geometric conditions determined mathematically by the sidereal synodic relations. These relations are

$$n_R P_R = (n_R + n_{R-1})P_{R-1} = \cdots = (n_R + n_{R-1} + \cdots + n_1)P_1$$

All motion formulated for the inverse problem of dynamics is in the complex plane.

The initial phase of the inverse problem provides position constraints by defining the existence of particles arrayed within the regular n-gon. All masses in a n-gon are the same, however, any given n-gon may not have the same mass as any other n-gon. Hence, the n-gon masses are scaled. Each concentric n-gon rotates about m_1 with a determinable inertial angular velocity. This inertial angular velocity distribution requires knowledge of n-gon interactions and sidereal synodic relations to determine particle perturbations. Formulating the inverse process as a perturbed two body problem with the j^{th} n-gon under perturbation by each and every other n-gon, there exists

$$w_j^2 = \Delta_1 + \Delta_2 \qquad j = 1, 2, 3, \ldots, R \qquad \text{Equation 3.3.6.1}$$

where n-gon angular velocity Δ_2 represents perturbations to the unperturbed n-gon angular velocity Δ_1. These terms are

$$\Delta_1 = (w_j^u)^2 = \frac{Gm_1}{r_j^3}.$$

$$\Delta_2 = (w_j^p)^2 = \frac{Gm}{r_j^3}\phi_j$$

defining $\phi_j = \sum_{i=1}^{R} k_i \phi_{ij}$ geometric perturbations

m_1 = central mass k_j = mass scaling r_j = n-gon radii

m = mean mass J = n-gon number R = Total n-gon number

Having knowledge of conservation of energy principals allows derivation of the perturbation coefficients. Since the n-gon geometry has already been formulated, the ϕ_j perturbations can be derived by applying these principals. Kinetic energy $2T = \sum_{i=1}^{N} m_i v_i^2$ series defined by regular n-gon becomes $2T = R_n mG \sum_{j=1}^{R} \frac{m_1 + \phi_j m}{r_j} k_j$. Potential energy $U =$

$G\sum_{1\le i<j\le N}^{N}\frac{m_i m_j}{r_{ij}}$ series formulated by regular n-gon arrays becomes $U = R_n m G\sum_{j=1}^{R}\frac{m_1+\phi_j^U m}{r_j}k_j$ where $\phi_j^U = k_j\phi_{11} + \sum_{\substack{i=1\\ j-1\ge 1}}^{j-1} k_{j-i}\phi_{1,(i+1)c}^U$. Evaluating n-gon kinetic and potential energy functions has been detailed in Sections 3.2.4 and 3.3.3.

For every particle in the concentric n-gon configuration there exists a coupled differential equation of motion. All particles have the same angular velocity within a given n-gon in the infinitesimal time interval, therefore, only one equation of motion is necessary per n-gon. The other particle equations of motion for that n-gon are redundant, for a given n-gon rotates as a rigid body. First n-gon Inertial angular velocity can be written from equation 3.3.6.1 for $j = 1$

$$w_j^2 = \frac{Gm_1}{r_j^3} + \frac{Gm}{r_j^3}\phi_j \qquad \text{Equation 3.3.6.2}$$

where ϕ_j are the n-gon perturbations derived from the n-body problem representing intra/inter perturbations. Formulating equation 3.3.6.2 as a vector equation in the complex plane, with z_2 (a complex vector from m_1 to m_2 in the first n-gon) rotating relative to the inertial x-axis

$$w_{1NR}^2 z_2 = \frac{Gm_1}{r_1^3}z_2 + \frac{Gm}{r_1^3}z_2\sum_{i=1}^{R}k_i\phi_{i1} \qquad \text{where} \quad z_k = x_k' + iy_k'$$

where w_{1NR} is the inertial angular velocity of the first n-gon relative to the inertial x-axis and k_i are the mass scaling parameters per n-gon. This axis is defined by the direction from m_1 to some designated point on the R^{th} n-gon. Expanding the inter/intra perturbations on n-gon one from all other n-gons results in

$$\frac{Gm}{r_1^3}z_2\sum_{i=1}^{R}k_i\phi_{i1} = \frac{Gm}{r_1^3}k_1 z_2\phi_{11} + \frac{Gm}{r_1^3}k_2 z_2\phi_{21} + \frac{Gm}{r_1^3}k_3 z_2\phi_{31} + \cdots + \frac{Gm}{r_1^3}k_R z_2\phi_{R1} \qquad \text{Equation 3.3.6.3}$$

with mass scaling per n-gon being structured

$$m_2 = m_3 \ldots = m_{R_n+1} = k_1 m \quad \text{first n-gon}$$

$$m_{R_n+2} = \cdots = m_{2R_n+1} = k_2 m \quad \text{second n-gon}$$

$$m_{R_n(R_n-1)+2} = \cdots = m_{R_nR+1} = k_R m \quad \text{last } R^{th} \text{ n-gon}$$

Perturbation terms $\frac{z_2\phi_{ij}}{r_1^3}$ from equation 3.3.6.3 can be written (detailed in subsection 3.3.1)

$$\frac{z_2\phi_{11}}{r_1^3} = -\sum_{i=3}^{R_n+1}\frac{z_{i2}}{r_{i2}^3}\frac{z_2\phi_{21}}{r_1^3} = -\sum_{i=R_n+2}^{2R_n+1}\frac{z_{i2}}{r_{i2}^3}\frac{z_2\phi_{R1}}{r_1^3} = -\sum_{i=R_n(R-1)+1}^{RR_n+1}\frac{z_{i2}}{r_{i2}^3}$$

Equation 3.3.6.4

Combining equations 3.3.6.3 and 3.3.6.4 for the first n-gon gives

$$\frac{Gm}{r_1^3}z_2\sum_{i=1}^{R}k_i\phi_{i1} = -Gmk_1\sum_{\substack{i=3\\ i\neq 2}}^{R_n+1}\frac{z_{i2}}{r_{i2}^3} - \mathrm{G}mk_2\sum_{i=R_n+2}^{2R_n+1}\frac{z_{i2}}{r_{i2}^3} - \cdots - Gmk_R\sum_{i=R_n(R-1)+1}^{RR_n+1}\frac{z_{i2}}{r_{i2}^3} = -G\sum_{\substack{i=3\\ i\neq 2}}^{RR_n+1}\frac{m_i z_{i2}}{r_{i2}^3}$$

The first n-gon equation of motion becomes

$$w_{1NR}^2 z_2 = \frac{Gm_1}{r_1^3}z_2 - G\sum_{\substack{i=3\\ i\neq 2}}^{RR_n=1}\frac{m_i}{r_{i2}^3}z_{i2}$$

Since m_1 is the geometric center and center of gravity of the infinite concentric n-gon configuration

$$z_{12} = z_1 - z_2 = -z_2$$

The first n-gon equation of motion in the synodic coordinate system is

$$w_{1NR}^2 z_2 = -\frac{Gm_1}{r_1^3}z_{12} - G\sum_{\substack{i=3\\ i\neq 2}}^{RR_n+1}\frac{m_i}{r_{i2}^3}z_{i2}$$

$$w_{1NR}^2 z_2 = -G\sum_{\substack{i=1\\ i\neq 2}}^{N}\frac{m_i}{r_{i2}^3}z_{i2} \qquad \text{where } N = RR_n + 1$$

The inertial angular velocity w_{1NR} is the sum of the first n-gon angular velocity w_1 that rotates relative to the x'-axis and w which is the inertial angular velocity of the x'-axis relative to the inertial x-axis ($w_{1NR} = w_1 + w$). This gives the first n-gon formulation

$$-(w_1 + w_R)^2 z_2 = G\sum_{\substack{i=1\\ i\neq 2}}^{N}\frac{m_i}{r_{i2}^3}z_{i2}$$

Over the infinitesimal interval Δt the vector z_2 rotates in the synodic coordinate system such that

$$z_2 = r_2 e^{iw_1 t}$$

$$\dot{z}_2 = iw_1 z_2$$

$$\ddot{z}_2 = -w_1^2 z_2$$

Only time varies within the infinitesimal interval, therefore, the time derivative of angular velocity and radius is defined to be zero for the rotating n-gon . Squaring the sum of the relative and inertial angular velocities results in

$$-(w_1 + w)^2 z_2 = -(w_1^2 + 2w_1 w + w^2) z_2 = -w_1^2 z_2 - 2w_1 w z_2 - w^2 z_2$$

and

$$-w_1^2 z_2 - 2w_1 w z_2 - w^2 z_2 = \ddot{z}_2 + 2wi\dot{z}_2 - w^2 z_2$$

This becomes the equation of motion for the first n-gon for particle two as seen below

$$\ddot{z}_2 + 2wi\dot{z}_2 - w^2 z_2 = G \sum_{\substack{i=1 \\ i \neq 2}}^{N} \frac{m_i}{r_{i2}^3} z_{i2}$$

All particles within the first n-gon have the equivalent equation of motion and are therefore redundant. Each n-gon has an equation of motion determined from any particle within that n-gon. General equation for all R n-gons will be (equation 3.1)

$$\ddot{z}_2 + 2wi\dot{z}_2 - w^2 z_k = G \sum_{\substack{i=1 \\ i \neq k}}^{N} \frac{m_j}{r_{jk}^3} z_{jk} \qquad k = 1, 2, 3, \ldots, N$$

Knowledge of classical mechanics allows application of the inverse problem of dynamics to solve structured n-body problems without solving the equations of motion directly. Starting with the position constraints immediately results in determination of the state vector position coordinates at time zero within the infinitesimal interval. Velocity/ acceleration /time etc. constraints being the most difficult to determine can be simplified somewhat by taking advantage of configuration symmetry and formulating a geometrical structure that can be solved.

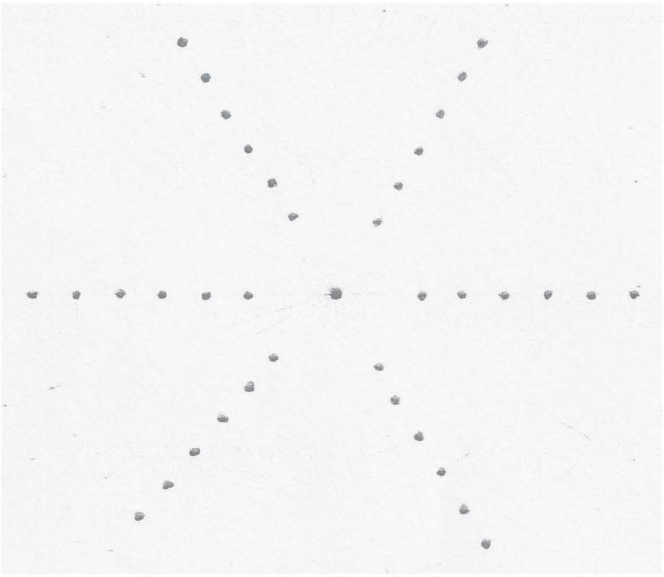

FIGURE 3.2.1. Regular N-Gon Ray Configuration ($R = 6, R_n = 6$)

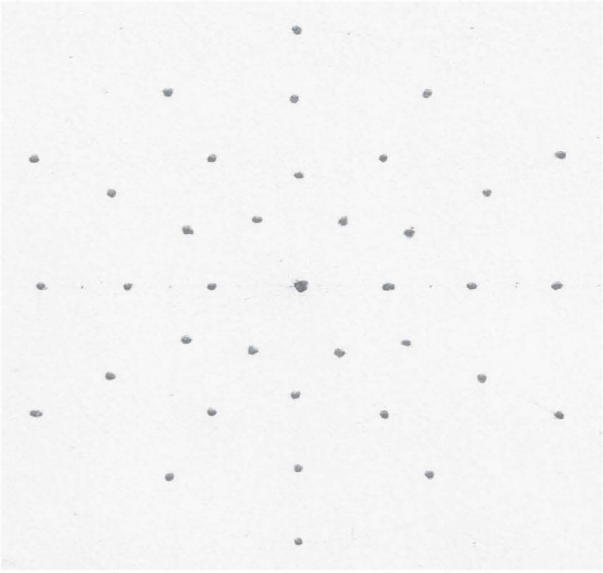

FIGURE 3.2.2. Regular N-Gon Rotated Ray Configuration ($R = 6, R_n = 6$)

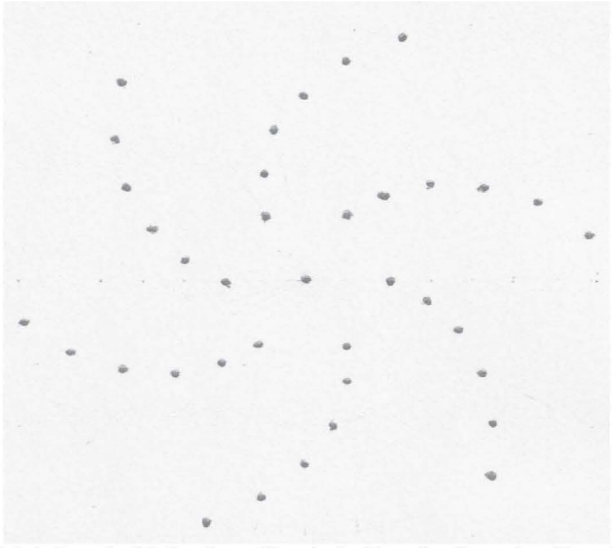

FIGURE 3.3.1. Regular N-Gon Inter-Singularity Free Configuration ($R = 6, R_n = 6$)

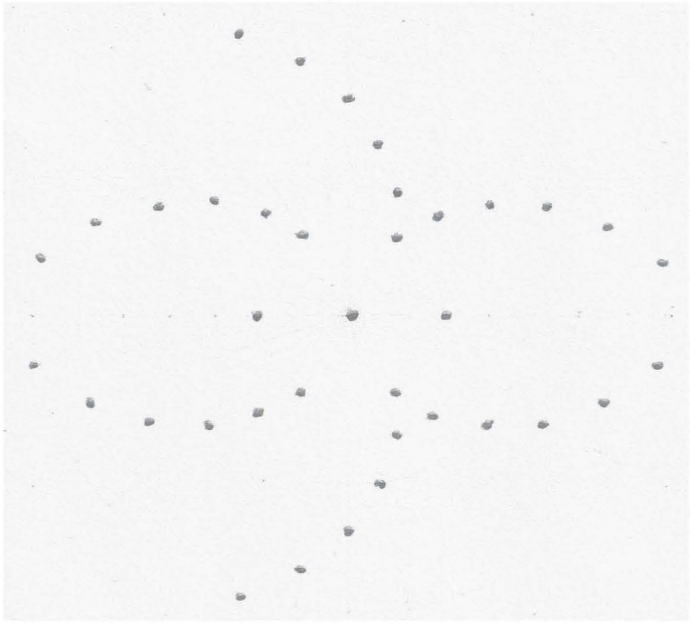

FIGURE 3.3.2. Regular and Non-Regular N-Gon Inter-Singularity Free Configuration ($R = 6, R_n = 6$)

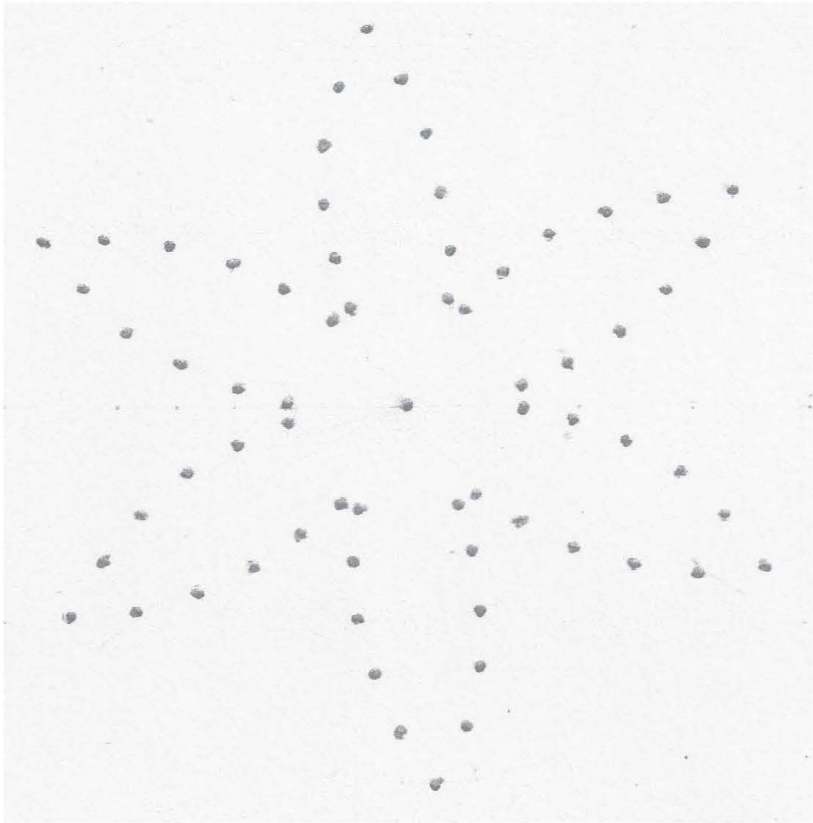

FIGURE 3.3.3. Regular and Non-Regular N-Gon Inter-Singularity Free Configuration ($R = 6$)

3.4 Problems

Section 3.1

1 Validity for the equation 3.1.1.2 symmetry argument depends on showing twice the kinetic energy is equal to the potential energy for the Lagrange equilateral triangular three body configuration. Verify the conservation of energy condition. Consider using the geometrical center of the triangle as a reference for the center of gravity calculation to determine $\frac{r_i}{r}$.

2 Solve the determinant in equation 3.1.2.2 to verify that the collinear three-body configuration angular velocity is the same as determined

from equation 3.1.2.1. Show that conservation of energy is conserved for the collinear three-body problem (2T = U).

3 Solve equation 3.1.4.1 for the regular five-body n-gon configuration inertial angular velocity using either the third, fourth or fifth equation of motion. The result should be the same as equation 3.1.4.2. Verify conservation of energy for the five n-gon configuration.

4 Derive the perturbation coefficient ϕ for the six-body configuration using the equations of motion method. Use the alternate conservation of energy method for the same problem. Both methods should give the same result.

5 Determine the perturbation coefficient ϕ for the seven-body configuration using the equations of motion method. Compare the solution to the conservation of energy method worked in the text.

6 Using equation 3.1.6.1 to determine perturbation coefficient ϕ_{10i+1} for N=1 (N=2^x, x=0), compute ϕ_{11} and C_N.

7 Derive perturbation coefficient ϕ_{10i+1} for the single n-gon configuration as listed in equation 3.1.6.1.

8 Compute perturbation coefficient ϕ for the 17-body configuration using any of the three methods discussed in the text.

Section 3.2

1. Perform the infinitesimal rotation analysis to determine the inertial angular velocity and perturbation coefficients ϕ_{12} and ϕ_{22} for the two n-gon configuration in equation 3.2.1.7.
2. Take the total derivative of the two n-gon optimizing function (equation 3.2.3.1) and verify the k_1 and k_2 solutions. Why won't this method work for R = 3 and higher values of R.
3. Evaluate potential energy for the two n-gon configuration using $R_n = 6$, $R = 6$ and show mathematical verification of conservation of energy in that equation 3.2.4.1 is equal to equation 3.2.4.2.
4. Derive perturbation coefficients ϕ_{11}, ϕ_{21} and ϕ_{12} in equations 3.2.5.2, 3.2.5.3 and 3.2.5.4 respectively for the two n-gon configuration when $R_N \to \infty$.
5. Derive perturbation coefficients ϕ_{11}, ϕ_{21} and ϕ_{31} for the first n-gon of the three n-gon configuration.
6. Derive perturbation coefficients ϕ_{41} *and* ϕ_{14} for the four n-gon configuration, also verify the angular velocities $w_{1NR}, w_{2NR}, w_{3NR}$ *and* w_{4NR}.

Section 3.3

1. By method of the infinite concentric n-gon formulation derive the inertial angular velocity w_{1NR} for the first n-gon (equation 3.3.1.2) within the infinite n-gon configuration, second n-gon angular velocity w_{2NR} (equation 3.3.1.3) and the R^{th} n-gon (equation3.3.1.4).
2. Infinite n-gon even and odd row perturbation coefficients are shown in equations 3.3.1.5 and 3.3.1.6. Verify these results for the concentric n-gons and show that equations 3.3.1.5 and 3.3.1.6 can be combined as one equation (equation 3.3.1.9).
3. Follow the same procedure sequence in the above problem for the even and odd column perturbation coefficients (see equations 3.3.1.7, 3.3.1.8 and 3.3.1.10).
4. The perturbation coefficient series ϕ_j^U (equation 3.3.3.1) has been derived from the potential energy series. To best see this, it is helpful to write the potential energy in n-gon blocks. Using this procedure show $\phi_3^U = k_1\phi_{13c} + k_2\phi_{23c} + k_3\phi_{33}$.
5. The differentially rotated regular n-gon configuration in figure 3.3.1 is inter singularity free. Due to this configuration having no workable symmetry axis, show that this configuration cannot be worked by the symmetry method used in this chapter.
6. Figure 3.3.2 represents a differentially rotated configuration containing both regular and non-regular n-gons that meets the symmetry constrains consistent with this chapter. Find the perturbation coefficient of the first n-gon for this configuration using $R = 6$ and $R_n = 6$.

3.5 References

Aarseth, S. J., 2003, *Gravitational N-Body Simulations*, Cambridge, Cambridge University Press.

Bauer, T. A. 2001. Resonance Induced Coupled Planar N-Body Collinear Point Solutions. *AAS/AIAA Space Flight Mechanics.*

Bauer, T. A. 2010. N-Gon Minimum Energy Solutions of the Planar N-body Problem. *AAS/AIAA Space Flight Mechanics.*

Chenciner, A. 2003. Perverse Solutions of the Planar N-Body Problem. *Asterisque.*

Galiullin, A. S., 1984, *Inverse Problems of Dynamics*, Moscow, MIR.

Gantmacher, F., 1970, *Lectures in Analytical Mechanics*, Moscow, MIR.

Hagihara, Y., 1970, *Celestial Mechanics*, Cambridge, Massachusetts, MIT Press.

Jeans, J. H., 1935, *Theoretical Mechanics*, Boston, Massachusetts, Ginn and Company.

Kurth, R., 1959, *Introduction to the Mechanics of the Solar System*, New York, Pergamon Press,.

Lass, H.,1957, *Elements of Pure and Applied Mathematics*, New York, McGraw-Hill.

Lehman-Filhes, R., 1891, *Astron. Nach.* CXXVII, 3033.

Makino, J. 2008. Current Status of the GRAPE Project, Dynamical Evolution of Dense Stellar Systems. *IAU Symposium Vol. 246*.

Makino, J., Fukushige, T., Koga, M., and Namura, K. 2003. GRAPE-6: Massively Parallel Special Purpose Computer for Astrophysical Simulations, *PASJ*, p. 1163.

Marchal, C. 2000. The Family P12 of the Three-body Problem – The simplest Family of Periodic Orbits, with Twelve Symmetries per Period, *CMDA 78*.

Maxwell, J. C., 1859, *On the Stability of the Motion of Saturn's Rings*, University of Cambridge, MacMillan.

Maxwell J., Brush, S., Everitt, C., 1983, *Maxwell on Saturn's Ring*, Cambridge, Massachusetts, MIT Press.

Moulton, F. R., 1900, Abstract, *Bull. Am. Soc.* VII, 249.

Pollard, H., 1966, *Mathematical Introduction to Celestial Mechanics*, Englewood Cliffs, NJ, Prentice Hall.

Ramsey, A. S., 1929, *Dynamics*, London, Cambridge University Press.

Roy, A. E., 1988, *Orbital Motion*, Bristol, Institute of Physics Publishing.

Roy, A. E., and Ovenden M. W. 1955. On the Occurrence of Commensurable Mean Motions in the Solar System II. The Mirror Theorem, *Mon., Not., Roy., Astr., Soc.*.

Roy, A. E., and Steves, B. A. 1998. Some Special Restricted Four-Body Problems-II. From Caledonia to Copenhagen, *Planet. Space Sci.*, p. 1475.

Santilli, R. M., 1978, *Foundations of Theoretical Mechanics I – The Inverse Problem in Newtonian Mechanics*, Berlin, Springer Verlag.

Szebehely, V., 1967, *Theory of Orbits*, New York, Academic Press.

Wintner, A., 1964, *The Analytical Foundations of Celestial Mechanics*, Princeton, NJ, PUP.

CHAPTER FOUR

ORTHOGONAL COLLINEAR CONFIGURATIONS

Constructing n-body structures along the inertial x and y axes leads to interesting problems to study and solve. One such group are the orthogonal collinear configurations. They possess symmetry where the geometric center and the barycenter are the same. Masses are balanced on the x-axis as well as balanced on the y-axis to insure this symmetry. These are even massed restricted configurations symmetric relative to the barycenter which can be subdivided in two basic groups. Those with a central mass and those without a central mass. Orthogonal collinear n-body structures analyzed in this chapter do not have a central mass which results in configurations possessing n-2 Jacoby coordinates instead of the usual n-1 Jacoby coordinates found in the standard equations of motion. There are infinite orthogonal mass configurations that can be formulated and solved using the methods found in this chapter. High ordered orthogonal configurations are structured by placing collinear mass systems symmetrically on the x and y axis.

The most fundamental of the orthogonal collinear structures is the restricted double binary four-body configuration. Solving the orthogonal double binary configuration is a straight forward process and results in a two-dimensional (or three dimensional) state vector at time zero using infinitesimal rotation in the complex plane with type 1 geometry. These solutions are consistent with conservation of energy ($2T = U$) where all the particles are in instantaneous circular orbits at time zero. Double binary equations of motion have been analyzed using a first order approximation to determine stability in the sense of Lagrange. Numerical integrated state vectors from the solution domain are used to compare the first order approximation from the eigen value problem to the double binary trajectories.

Section 4.1 provides the solution and stability analysis of the restricted double binary configuration. Six and eight-body orthogonal collinear configurations are worked in sections 4.2 and 4.3 respectively to provide insight into the evolution of these higher order configurations.

4.1 Double Binary

In many respects the fundamental conditions for the double binary orthogonal collinear configurations are the same as for the concentric n-gon configurations. For example, this is a conservative dynamical system defined at origin (0,0,0) fixed in two-dimensional Euclidean space with an inertial right-handed coordinate system x, y, z where z = 0 is the orthogonal collinear configuration plane of motion. Let x and y be the inertial planar coordinate system, with (0,0,0) located at the barycenter (also the geometrical center). The inertial y-axis is perpendicular to and counterclockwise from the x-axis. Let x' and y' define a coincident coordinate system in the same plane as x and y rotating at angular velocity w with respect to x and y and origin at the barycenter. The y'-axis is perpendicular to and counterclockwise from the x'-axis, with inertial and rotating coordinate system x and x'-axes coincident at time zero.

Starting with the n-body equations of motion formulated into the complex plane over the infinitesimal interval as derived in equation 3.1

$$\ddot{z}_k + 2wi\dot{z}_k - w^2 z_k = G\sum_{\substack{j=1 \\ j\neq k}}^{N} \frac{m_j}{r_{jk}^3} z_{jk} \qquad k = 1,2,3\ and\ 4$$

where $\quad i = \sqrt{-1}, \quad z_k = x'_k + iy'_k \quad$ and $\quad r_{jk} = |z_j - z_k|$

there will be the sidereal synodic relations that specify the general geometric conditions under which the double binary rotates

$$n_R P_R = (n_R + n_{R-1})P_{R-1} = \cdots = (n_R + n_{R-1} + \cdots + n_1)P_1$$

The four-body equations of motion have been transformed using Jacoby coordinates. Coupling mass one with mass two forms the r binary subsystem and coupling mass three with mass four forms the ρ binary subsystem. Mass one and mass two being individually equal to M are placed equidistant either side of the xy coordinate system origin along the x-axis. Mass three and mass four being individually equal to m are placed equidistant either side of the xy coordinate system origin along the y-axis such that the geometrical center of the double binary is the same as the barycenter. Using Jacoby coordinates has reduced the four-body system from four coupled non-linear differential equation to two coupled non-linear differential equations. This mass distribution subsequently defines the restricted double binary configuration geometry. See figure 4.1.1 restricted double binary geometry.

Writing the Jacoby r and ρ coupled equations of motion in the complex plane gives

$$-w^2 z = -\frac{G\mu}{r^3} z + \frac{Gm_3}{r_{32}^3} z_{32} - \frac{Gm_3}{r_{31}^3} z_{31} + \frac{Gm_4}{r_{42}^3} z_{42} - \frac{Gm_4}{r_{41}^3} z_{41} \qquad \text{Equation 4.1.1}$$

$$\ddot{z}_{43} + 2wi\dot{z}_{43} - w^2 z_{43} = -\frac{G\mu_{43}}{r_{43}^3} z_{43} + \frac{Gm_1}{r_{41}^3} z_{14} - \frac{Gm_1}{r_{31}^3} z_{13} + \frac{Gm_2}{r_{42}^3} z_{24} - \frac{Gm_2}{r_{32}^3} z_{23}$$

where $\vec{r} = \overrightarrow{r_2} - \overrightarrow{r_1}$ $\vec{\rho} = \overrightarrow{r_4} - \overrightarrow{r_3}$ $\mu = m_1 + m_2$ $\mu_{43} = m_3 + m_4$

First equation in equation 4.1.1 is the r binary subsystem and it is on the x'axis in the rotating $x'y'$ coordinate system with $\ddot{z} = \dot{z} = 0$. The second equation represents the ρ binary subsystem and it is rotating relative to the r binary subsystem. Letting let $\rho_{ij} = \frac{G}{w^2 r_{ij}^3}$ and using $n_r P_r = (n_r + n_\rho) P_\rho$ for the sidereal synodic relations, equation 4.1.1 with the rotating z_{43} coordinate can be reformulated as

$$z_{43} = r_{43} e^{i\frac{n_\rho}{n_r} wt} \qquad z_{43} = z_\rho \qquad \text{Equation 4.1.2}$$

$$(\rho_{21}\mu - 1)z = (\rho_{32} z_{32} - \rho_{31} z_{31}) m_3 + (\rho_{42} z_{42} - \rho_{41} z_{41}) m_4$$

$$\left(\rho_{43}\mu_{43} - \frac{P_{21}^2}{P_{43}^2}\right) z_{43} = (\rho_{41} z_{14} - \rho_{31} z_{13}) m_1 + (\rho_{42} z_{24} - \rho_{32} z_{23}) m_2$$

A special characteristic of the double binary geometry is $\rho_{31} = \rho_{32} = \rho_{41} = \rho_{42}$ from all sides of the double binary being equal. Evaluating equation 4.1.2 over the infinitesimal interval with type 1 geometry and the sidereal synodic relations at time zero for the r-binary velocity

$$\mu - \frac{w^2 r^3}{G} = -m\left(\frac{r^3}{r_{32}^3} + \frac{r^3}{r_{42}^3}\right)$$

$$V_r^2 = \frac{G}{r}(2M + \phi_r) \qquad \phi_r = 2m\frac{r^3}{r_{32}^3} \qquad \text{Equation 4.1.3}$$

and for the ρ binary velocity

$$\mu_{43} - \frac{w^2 r_{43}^3}{G} \frac{P_{21}^2}{P_{43}^2} = -M\left(\frac{r_{43}^3}{r_{41}^3} + \frac{r_{43}^3}{r_{42}^3}\right)$$

$$V_\rho^2 = \frac{G}{r_{43}}(2m + \phi_\rho) \qquad \phi_\rho = 2M\frac{r_{43}^3}{r_{32}^3} \qquad \text{Equation 4.1.4}$$

Perturbation coefficient ϕ_r is the effect of the ρ binary perturbing the r binary and ϕ_ρ is the effect of the r binary perturbing the ρ binary. Perturbed and unperturbed components in the r and the ρ binary velocity equations are easily discernable in equations 4.1.3 and 4.1.4. Restricted double binary state vectors can now be found since the position and velocity components have been determined.

$$\begin{aligned} x_1 &= -\frac{1}{2}r & \dot{x}_1 &= 0 \\ y_1 &= 0 & \dot{y}_1 &= -\frac{1}{2}V_r \end{aligned} \qquad \text{Equation 4.1.5}$$

$$\begin{aligned} x_2 &= \frac{1}{2}r & \dot{x}_2 &= 0 \\ y_2 &= 0 & \dot{y}_2 &= \frac{1}{2}V_r \end{aligned}$$

$$\begin{aligned} x_3 &= 0 & \dot{x}_3 &= -\frac{1}{2}V_\rho \\ y_3 &= \frac{1}{2}\rho & \dot{y}_3 &= 0 \end{aligned}$$

$$\begin{aligned} x_4 &= 0 & \dot{x}_4 &= \frac{1}{2}V_\rho \\ y_4 &= -\frac{1}{2}\rho & \dot{y}_4 &= 0 \end{aligned}$$

Restricted double binary configuration state vectors are in the inertial barycentric coordinate system.

4.1.1 Double Binary Conservation of Energy Verification

The restricted double binary configuration is consistent with conservation of energy and this can be verified by evaluating the kinetic and potential energies

$$2T = \sum_{i=1}^{4} m_i V_i^2 \qquad U = G\sum\frac{m_i m_j}{r_{ij}}$$

Vector velocities for the four masses are $\vec{V}_1 = -\frac{1}{2}\vec{V}_r$, $\vec{V}_2 = \frac{1}{2}\vec{V}_r$, $\vec{V}_3 = -\frac{1}{2}\vec{V}_\rho$ and $\vec{V}_4 = \frac{1}{2}\vec{V}_\rho$ as can be determined from figure 4.1.1. Substituting these velocities into the kinetic energy equation gives

$$2T = \frac{M}{2}V_r^2 + \frac{m}{2}V_\rho^2$$

where $\frac{M}{2}$ and $\frac{m}{2}$ are the reduced masses of the double binary system. The potential energy after evaluating all six terms in the sum becomes

$$U = G\sum\frac{m_i m_j}{r_{ij}} = \frac{GM^2}{r} + 4\frac{GMm}{d} + \frac{Gm^2}{\rho} \qquad \text{Equation 4.1.6}$$

Parameter d in equation 4.1.6 takes advantage of the double binary symmetry where

$$d = r_{31} = r_{32} = r_{41} = r_{42} \qquad d^2 = \frac{r^2}{4} + \frac{\rho^2}{4}$$

Substituting the r and ρ binary velocities determined in equations 4.1.3 and 4.1.4 into the kinetic energy equation will verify that 2T = U

$$\frac{M}{2}V_r^2 = \frac{GM^2}{r} + GMm\frac{r^2}{r_{32}^3} \qquad \text{Equation 4.1.7}$$

$$\frac{m}{2}V_\rho^2 = \frac{Gm^2}{\rho} + GMm\frac{\rho^2}{r_{32}^3}$$

Collecting and adding the kinetic energy terms in equation 4.1.7

$$2T = \frac{GM^2}{r} + \frac{Gm^2}{\rho} + \frac{GMm}{r_{32}^3}(r^2 + \rho^2)$$

since $d^2 = \frac{r^2}{4} + \frac{\rho^2}{4}$ then 2T = U. Therefore, in the infinitesimal interval with type 1 geometry at time zero the double binary configuration is consistent with conservation of energy. Each mass is in a circular instantaneous orbit at time zero where it is not expected that this circular orbit can be maintained outside the infinitesimal interval. Numerical integration of these double binary state vectors shows this conclusion to be valid. The r and ρ binary numerically integrated trajectories when plotted reveal that they are symmetric relative to each other.

4.1.2 Double Binary Configuration Space

With the derivation of the fundamental r and ρ binary quantities, there now exists a systematic approach in analyzing the restricted double binary configuration solution domain. This solution domain is structured in terms of binary period ratios, binary separation distance ratios, and binary mass

ratios. Configuration space is defined as binary mass ratio as a function of binary period ratio and binary separation distance ratio. These ratios can be constructed from the solution of the orthogonal double binary problem. Starting with the r and ρ instantaneous binary periods

$$P_r^2 = 4\pi^2\left(\frac{r^3}{G(2M+\phi_r)}\right)$$

$$P_\rho^2 = 4\pi^2\left(\frac{\rho^3}{G(2m+\phi_\rho)}\right)$$

derivation of the configuration space equation can be determined by scaling mass, distance and period

$$\frac{P_r^2}{P_\rho^2} = \frac{ck_2+k_1^3}{c+k_2}\frac{1}{k_1^3} \qquad \text{Equation 4.1.2.1}$$

where $k_1 = \frac{\rho}{r}$ $k_2 = \frac{m}{M}$ $c = \left(\frac{1+k_1^2}{4}\right)^{3/2}$

Scaling the variable parameters into the set k_1, k_2, and $\frac{P_r}{P_\rho}$ is an optimal strategy for regionalizing the r and ρ binary mass distance period inter-relationships. For example, the k_i's exist over range $0 < k_i < \infty$ for all non-zero mass. The ρ binary is mass dominate for k_2 in the region of $1< k_2 < \infty$ and the r binary is mass dominate for k_2 within the region $0< k_2 < 1$. All masses are equal along dividing curve $k_2 = 1$, and all points in the ρ binary dominant configuration space are inversely related to all points in the r binary dominate configuration space.

Configuration space (figure 4.1.2.1) is a useful mapping tool to visualize double binaries of interest to numerically integrate. Any point in configuration space can be mapped into phase space. That is, every point in figure 4.1.2.1 represents a state vector whose trajectory can be analyzed by transforming from configuration space to phase space using equations 4.1.3, 4.1.4 and 4.1.5 to study double binary finite stability.

The interval $1/\sqrt{3} < k_1 < \sqrt{3}$ in figure 4.1.2.1 is one such region of interest where the r binary period and the ρ binary period are equal. Region end points are Lagrange configurations where the ρ binary approaches total system mass with $k_1 \to 1/\sqrt{3}$ and $k_2 \to \infty$ ($M \to 0, m \to 1$) at the beginning of the interval and the r binary approaches total system mass with $k_1 \to \sqrt{3}$ and $k_2 \to 0$ ($M \to 1, m \to 0$) at the end of the interval. At the point $k_1 =$

$1, k_2 = 1, \frac{P_r}{P_\rho} = 1$ within this interval resides a central configuration. All points between the central configuration and the Lagrange configurations are inversely related.

Numerically integrating the central configuration $k_1 = 1$ for $\frac{P_r}{P_\rho} = 1$, the Lagrange configuration $k_1 \to \sqrt{3}$, and two configurations between ($k_1 = 1.3, k_1 = 1.5$) for a given mass and distance ratio resulted in near circular semi-stable trajectories being maintained for a finite period of time before becoming unstable. The Lagrange configuration appears to spiral away from its initial finite stable circular orbit as can be seen in figure 4.1.2.2. It is highly probable that all the trajectories within interval $1/\sqrt{3} < k_1 < \sqrt{3}$ for $\frac{P_r}{P_\rho} = 1$ are finite stable circular orbits for the proper mass distance ratios.

Numerical integration tends to indicate for the various state vectors integrated in figure 4.1.2.1 that the trajectories may be perturbed spirals. A special case where this can be seen is $k_1 = 1$ $k_2 \to 0$ ($k_1 = 1, k_2 \to \infty$). Integrated trajectory results for this configuration in figure 4.1.2.3 indicate possible exponential escape orbits for masses three and four and stable circular orbits for masses one and two.

Another region of numerical interest is when $k_1 \to 0$ ($\rho \to 0$) and $k_2 \to 0$ ($m \to 0$),where it is found that the ρ binary trajectory resides inside the rotating r binary for an extended period. Specifically, the ρ binary trajectory is moving relative to the Euler point in a possible finite stable orbit. This Euler point motion has yet to be studied in greater detail. Other interesting regions in the restricted double binary configuration space are expected to exist, however, a systematic search for these trajectories has not been initiated for further analysis.

4.1.3 Restricted Double Binary Configuration Stability

There are infinite families comprising the distribution of tiered n-body configurations where each family is populated by infinite member configurations and those infinite members in turn have infinite variations. Deterministic solutions can be obtained for every family, their members and member variations by formulating and solving the collinear geometry problem at time zero using Jacoby coordinates within an infinitesimal interval relative to the barycenter. This approach requires position, velocity and acceleration constraints (also known as the inverse problem of

dynamics) consistent with the dynamics of the infinitesimal interval collinear geometry. Additionally, the instantaneous subsystem orbital rotation motions within each configuration are modelled by a unique set of synodic and sidereal equations. Position and velocity constraints are a function of type 1 geometry where all the particle velocity vectors are perpendicular to all the particle position vectors within the infinitesimal interval relative to the barycenter at time zero relative to the given plane of motion. The collinear infinitesimal interval constraint has resulted in the solution domain existing at time zero, that is, this restriction to the general n-body problem has reduced the solution from all time to that of one time point only. Solution results are in the form of state vectors, velocity distributions and period ratios for every mass subsystem in the configuration. All the particles at time zero can be shown to be in instantaneous circular orbits by verifying the collinear solution is consistent with conservation of energy where twice the kinetic energy is equal to the potential energy. A particular characteristic of the instantaneous state vectors is they are optimized such that all the resultant particle trajectories within the configuration when numerically integrated result in the most circular/least elliptical of all possible orbits. There is a final phase in the infinitesimal interval problem and that is the analysis of system and subsystem stability.

Stability methods in the sense of Lagrange, Routh (Routh, 1877) and Lyapunov are used to analyze coupled sets of nonlinear differential equations of motion to determine the orbital evolution of a system of masses over an epoch for all time. In general, these stability results tend to indicate that n-body mass systems are unstable for all time. Numerically integrating n-body coupled sets of nonlinear differential equations for some given mass system known to be unstable for all time may show that system can be stable for a finite time. Therefore, the concern here is how long can a mass system in a given n-body configuration maintain a semblance of that given structure before that structure degenerates. Lagrange, Routh and Lyapunov stability does not give the answer to that question such as would be found with a deterministic solution. Since generally n-body deterministic solutions don't exist over finite epochs there is the question of how a method could be formulated to breach this gap.

This subsection looks into an alternate method to determine stability of a n-body system of masses without resorting to the linear approximation method to find stability in the sense of Lagrange, Routh and the more advanced linear/nonlinear methods of Lyapunov. Accomplishing this objective initially requires the n-body problem to be systematically

restructured into tiered configurations rather than considering the n-body problem as a group of random masses in motion. This n-body tiered structure is based on arraying configurations in terms of their Jacoby coordinates where each configuration may be composed of binary, trinary and higher order subsystems. Stability is then a process of analyzing any given individual n-body configuration by studying the subsystems that make up that configuration. Interest is directed not so much in the stability/instability of the complete configuration as it is in the resulting gravitational perturbations on the binary, trinary etc. subsystems within the configuration.

Applying an alternate stability method requires reformulation of the r and ρ binary periods

$$P_r = 2\pi\left(\frac{r^3}{2MG}\right)^{1/2}\left(\frac{1}{1+\frac{\phi_r}{2M}}\right)^{1/2} \qquad \phi_r = 2m\frac{r^3}{r_{32}^3}$$

$$P_\rho = 2\pi\left(\frac{\rho^3}{2mG}\right)^{1/2}\left(\frac{1}{1+\frac{\phi_\rho}{2m}}\right)^{1/2} \qquad \phi_\rho = 2M\frac{\rho^3}{r_{32}^3}$$

defining $\quad D_r = \left(\frac{1}{1+\frac{\phi_r}{2M}}\right)^{1/2} \qquad D_\rho = \left(\frac{1}{1+\frac{\phi_\rho}{2m}}\right)^{1/2}$

where D_r represents the ρ binary perturbing the r binary subsystem and D_ρ represents the r binary perturbing the ρ binary subsystem. Rewriting D_r and D_ρ in terms of k_1 and k_2 gives

$$D_r = \left(\frac{1}{1+\frac{8k_2}{(k_1^2+1)^{3/2}}}\right)^{1/2} \qquad D_\rho = \left(\frac{1}{1+\frac{8k_1^3}{k_2(k_1^2+1)^{3/2}}}\right)^{1/2}$$

with the perturbing coefficients ranging in the domain $0 < D_i < 1$ $(i = r, \rho)$.

Using D_r and D_ρ with figure 4.1.2.1 could possibly determine double binary subsystem stability over the infinitesimal interval. For example, when $k_2 \to 0$ for all k_1 then $D_r \to 1$ and the r binary trajectory will approach a circular orbit. Although, theoretically this is over the infinitesimal interval, the r binary near circular orbit will extend well beyond a small neighborhood of time zero. The perturbed ρ binary trajectories become unstable when the period $P_\rho \to 0$ as a direct result of $D_\rho \to 0$. Mass three and mass four will move beyond the initial instantaneous circular orbit outside the infinitesimal interval.

Consider the case where $k_1 \to 0$ and $k_2 \to 0$ Perturbation parameter $D_r \to 1$ and assuming that k_1^3 is approaching zero faster than k_2 is approaching zero, the ρ binary perturbation will be $D_\rho \to 1$. This double binary configuration geometry has the ρ binary orbiting within the r binary. The r binary will approach a circular orbit over an epoch extending outside the infinitesimal interval due to it having almost all of the configuration mass. The ρ binary which is in a close vicinity of the Euler point, will stay within the r binary for an extended time. This has been verified by numerical integration. However, the ρ binary is not expected to stay in the vicinity of the Euler point for all time. Restricted double binary stability for all time can only occur under the condition $D_r = D_\rho = 1$, which will only happen when ρ binary mass and separation distance are identically zero. Since this condition can never occur than the restricted double configuration will not be stable for all time.

It is assumed from numerical integration of a subset of double binary configurations, that every point within the special case for $P_r = P_\rho$ over mass range $0 < k_2 < \infty$ that finite stable near circular perturbed orbits exist in the infinitesimal interval $1/\sqrt{3} < k_1 < \sqrt{3}$. However, mathematically verifying this finite stability region exists has proved to be elusive. The above stability method can indicate that r and ρ binaries are unstable, but does not indicate where finite stability exists within the binary trajectory domain. This same problem haunts the other stability methods as well.

At endpoints $1/\sqrt{3} < k_1 < \sqrt{3}$, both Lagrange configurations are unstable for all time being consistent with previous work on the three-body problem (Pollard, 1966, 72-84, Szebehely, 1967, 232-249). In this interval is the n-gon where binary mass, radii and period ratio are all equal to one. The n-gon is a homographic (central) configuration system that maintains its same relative geometry as time varies (Boccaletti and Pucacco, 1996, 219-229, Diacu, 1992, 47-74, Wintner, 1964, 284-295).

4.1.4 Stability in the Sense of Lagrange

A traditional stability method such as that of Lagrange, is used in this subsection to analyze the restricted double binary configuration for comparison to the alternate stability method derived in the previous subsection. Initiating this stability analysis requires two transformations to properly format the discrete Newtonian coupled differential equations of motion into a workable system of coordinates. First transformation changes Cartesian coordinates to Jacoby coordinates essentially reformulating the

equations of motion from particle barycenter distance to that of binary separation distance. The second transformation expands the Jacoby coordinates about an initial double binary configuration point geometry, which then allows a set of second order differential equations to be derived as a function of binary separation growth with respect to time zero. A reformulation of the second transformation differential equations results in four first order differential equations that could then be solved by linear approximation (eigenvalue problem).

Mathematically starting the formulation of the above outlined method will involve describing the conservative dynamical system. Define at the origin (0,0,0) fixed in three-dimensional Euclidian space an inertial right-handed coordinate system xyz where the xy plane (z = 0) is the plane of motion. Let x and y be the inertial planar coordinate system where the inertial y-axis is perpendicular to and counterclockwise from the inertial x-axis. General four body equations of motion describing four particles in this inertial xy reference frame are written

$$\ddot{\vec{r}}_k = \sum_{j=1}^{4} \frac{Gm_j}{r_{jk}^3} \vec{r}_{jk} \qquad j \neq k \qquad k = 1,2,3,4 \qquad \text{Equation 4.1.4.1}$$

It is necessary to transform the four body equations of motion from four second order differential relative to the barycenter into four first order differential equations as a function of binary separation. The resulting four linear first order equations can then be solved using a linear approximation (eigenvalue problem) to study stability of the restricted double binary. There are two coordinate transformations required to accomplish this task. The first is to transform the four body equations of motion into Jacoby coordinates by coupling mass one with mass two forming the r binary subsystem and then coupling mass three with mass four forming the ρ binary subsystem. Mass one and mass two being individually equal to M are placed equidistant either side of the xy coordinate system origin along the x axis and mass three and four being individually equal to m are placed equidistant either side of the xy coordinate system origin along the y axis such that the geometric center is the same as the barycenter. This mass distribution subsequently defines the restricted double binary problem geometry. Mass distance relationships needed for the Jacoby transformation are then determined from the binary configuration geometry are as follows

$$\vec{r}_{31} = (\vec{r} - \vec{\rho})/2 \quad \vec{r}_{32} = -(\vec{r} + \vec{\rho})/2 \quad \vec{r}_{41} = (\vec{r} + \vec{\rho})/2 \quad \vec{r}_{42} = -(\vec{r} - \vec{\rho})/2$$

Using the mass and distance relationships with equation 4.1.4.1 gives the Jacoby accelerations for the r and ρ binaries respectively

$$\ddot{\vec{r}} = -2G(\frac{M}{r^3} + \frac{m}{d^3})\vec{r} \quad \ddot{\vec{\rho}} = -2G(\frac{m}{\rho^3} + \frac{M}{d^3})\vec{\rho} \quad \text{Equation 4.1.4.2}$$

where $\vec{r} = \overrightarrow{r_2} - \overrightarrow{r_1}$ $\vec{\rho} = \overrightarrow{r_4} - \overrightarrow{r_3}$ $d^2 = \frac{r^2}{4} + \frac{\rho^2}{4}$

Scaler form of equation 4.1.4.2 can be written as

$$\ddot{r} = \frac{2GM}{r^2} + \frac{2Gm}{r^2}\frac{r^3}{d^3} \qquad \ddot{\rho} = \frac{2Gm}{\rho^2} + \frac{2GM}{\rho^2}\frac{\rho^3}{d^3}$$

These binary acceleration equations are only valid in a small neighborhood of time zero. Notice the binary symmetry where r and ρ can be interchanged as well as M and m. Equation 4.1.4.2 acceleration vectors $\ddot{\vec{r}}$ and $\ddot{\vec{\rho}}$ are opposite in direction to their respective position vectors and are along a straight line passing through the barycenter at time zero.

The second transformation involves expanding equation 4.1.4.2 about the point (r_0, ρ_0) utilizing the Euler-Lagrange method (Besant and Ramsey, 1914, 140-144, Ramsey, 1929, 253-254) or the Taylor series expansion. Zero subscripts refer to the initial start at time zero. To continue with this analysis, the Euler-Lagrange method can be started by formulating r and ρ for the linear approximation

$$r = r_0 + \epsilon_r = r_0(1 + {}^{\epsilon_r}/_{r_0}) \qquad r_0 > \epsilon_r$$

$$\rho = \rho_0 + \epsilon_\rho = \rho_0(1 + {}^{\epsilon_\rho}/_{\rho_0}) \qquad \rho_0 > \epsilon_\rho$$

and then substituting these equations into the scalar form of equation 4.1.4.2 with ϵ_r and ϵ_ρ representing the infinitesimal change in the respective binary distances after time zero. This results in a coupled set of second order linear homogeneous differential equations with constant coefficients in ϵ_r and ϵ_ρ coordinates where only linear ϵ_r and ϵ_ρ terms are considered in the transformation. As a result of the two coordinate transformations, equation 4.1.4.1 has been reduced to a workable form to determine stability for the restricted double binary configuration

$$\ddot{\epsilon}_r = a_{11}\epsilon_r + a_{12}\epsilon_\rho \qquad \text{Equation 4.1.4.3}$$

$$\ddot{\epsilon}_\rho = a_{21}\epsilon_r + a_{22}\epsilon_\rho$$

with initial conditions $\epsilon_r(0) = \epsilon_\rho(0) = 0$ and constant coefficients

$$a_{11} = \rho_0^2 mQ \qquad a_{12} = -\rho_0 r_0 mQ$$

$$a_{21} = -\rho_0 r_0 MQ \qquad a_{22} = r_0^2 MQ$$

and $$Q = {}^{3G}/_{2d_0^5}$$

Essentially, the above differential equations represent transformations from barycentric distance coordinates that are difficult to work with to a hybrid system of binary separation coordinates that easily allow a linear approximation. However, these coordinates are initialized to the origin of ϵ_r ϵ_ρ (0, 0) at time zero, thus resulting in zero initial conditions which in turn result in general non-unique solutions to the homogeneous differential equations. Therefore, the available options are either a unique solution in the particle barycentric coordinate system that may not be solvable in closed form or the linear approximation solution that can only be solved in general form. The linear approximation can be further extended to look at non-linear terms of equation 4.1.4.3 for an improved solution, but the end result is still a general non-unique solution.

Equation 4.1.4.3 can also be derived by Taylor series expansion for a function of two variables about an initial point (r_0, ρ_0) using the first order approximation below

$$f(r,\rho) = f(r_0,\rho_0) + \left(\frac{\partial f}{\partial r}\epsilon_r + \frac{\partial f}{\partial \rho}\epsilon_\rho\right)|_{r_0,\rho_0}$$

where the function $f(r,\rho)$ is the scaler form of the acceleration presented in equation 4.1.4.2 and Jacoby coordinates (r,ρ) are as defined by the Euler-Lagrange method. The diagonal terms will be in a different form as equation 4.1.4.3, however, they are equal by identity.

To proceed with the stability analysis equation 4.1.4.3 will be written in terms of four first order differential equations so that the eigenvalue problem can be formulated

$$\begin{pmatrix} \dot{x}_1 \\ \dot{x}_2 \\ \dot{x}_3 \\ \dot{x}_4 \end{pmatrix} = \begin{pmatrix} 0 & 0 & 1 & 0 \\ 0 & 0 & 0 & 1 \\ a_{11} & a_{12} & 0 & 0 \\ a_{21} & a_{22} & 0 & 0 \end{pmatrix} \begin{pmatrix} x_1 \\ x_2 \\ x_3 \\ x_4 \end{pmatrix} \qquad \text{Equation 4.1.4.4}$$

where the new variables are $x_1 = \epsilon_r$, $x_2 = \epsilon_\rho$, $x_3 = \dot{\epsilon}_r$ and $x_4 = \dot{\epsilon}_\rho$.

Assuming the solution for equation 4.1.4.4 can be represented in terms of exponentials $x(t) = Ae^{\lambda t}$, then the eigenvalue problem can be formulated as $(A - \lambda)X = 0$ with the resulting determinant

$$\begin{vmatrix} \lambda' & 0 & 1 & 0 \\ 0 & \lambda' & 0 & 1 \\ a_{11} & a_{12} & \lambda' & 0 \\ a_{21} & a_{22} & 0 & \lambda' \end{vmatrix} = 0 \quad \lambda' = -\lambda \qquad \text{Equation 4.1.4.5}$$

evaluated to give a quartic polynomial

$$\lambda^4 - (a_{11} + a_{22})\lambda^2 + C_{ij} = 0 \qquad \text{Equation 4.1.4.6}$$

From equation 4.1.4.3 and equation 4.1.4.5

$$C_{ij} = \begin{vmatrix} a_{11} & a_{12} \\ a_{21} & a_{22} \end{vmatrix} = 0$$

therefore $\lambda^2(\lambda^2 - (a_{11} + a_{22})) = 0$

and $\lambda_1 = (a_{11} + a_{22})^{1/2} \quad \lambda_2 = -(a_{11} + a_{22})^{1/2} \quad \lambda_3 = 0 \quad \lambda_4 = 0$

Equation 4.1.4.6 double zero eigenvalues denote degenerate λ solutions. Constructing the solution of equation 4.1.4.3 from the eigenvalues and the initial conditions leads to

$$\epsilon_r = A_{11}\left(e^{\lambda_1 t} - 1\right) + A_{12}(e^{-\lambda_1 t} - 1) \qquad \text{Equation 4.1.4.7}$$

$$\epsilon_\rho = A_{21}\left(e^{\lambda_1 t} - 1\right) + A_{22}(e^{-\lambda_1 t} - 1)$$

If $A_{N1} = -A_{N2}$ for N = 1,2 than equation 4.1.4.7 will take the form

$$\epsilon_r = A_{11} sinh\lambda_1 t \quad \epsilon_\rho = A_{21} sinh\lambda_1 t$$

This result can be found by substituting $\epsilon_r = K\epsilon_\rho$ (K is a constant) in equation 4.1.4.3 and then solving the quadratic equation for K where the

two solutions are $1/k_1$ and $-k_1k_2$. Using this result the solution of equation 4.1.4.3 becomes

$$\epsilon_r = B_{11}\left(e^{\lambda_1 t} - 1\right) + B_{12}(e^{-\lambda_1 t} - 1) \qquad \text{Equation 4.1.4.8}$$

$$\epsilon_\rho = B_{21}\left(e^{\lambda_1 t} - 1\right) + B_{22}(e^{-\lambda_1 t} - 1)$$

The $K = -k_1k_2$ quadratic solution validates $\lambda_1 = (a_{11} + a_{22})^{1/2}$ and $\lambda_2 = -(a_{11} + a_{22})^{1/2}$ from equation 4.1.4.6 and the $K = 1/k_1$ quadratic solution validates $\lambda_3 = \lambda_4 = 0$.

Both equations 4.1.4.7 and 4.1.4.8 have the same form, therefore the assumption for the first order linear approximation appears to be valid. The A coefficients (constants) are not determinable from the linear approximation so insight into the binary behavior will have to be discerned by other means. Understanding the double binary state at time zero provides some insight and this insight necessitates the formulation of the infinitesimal interval problem (discussed in section 4.1) which, when solved, gives the double binary periods and inertial velocities relative to an initial point at time zero. Knowledge of the double binary velocities, in addition to providing the means for finding the deterministic state vector, allows the lambda exponents in equation 4.1.4.7 to be written as a function of angular velocity, thus giving the capability to get some insight into the angular variation of the binary trajectories with time. This lambda relationship to angular velocity is

$$\lambda_1 = aw_r = bw_\rho$$

Coefficients a and b are constants determined from the infinitesimal interval problem velocities and the eigenvalue lambda solutions; being a function of binary mass ratios and radii ratios at time zero

$$a^2 = \frac{24(1+k_1^2k_2)}{(1+k_1^2)^{\frac{5}{2}}+8k_2(1+k_1^2)} \qquad \text{Equation 4.1.4.9}$$

$$b^2 = \frac{24k_1^3(1+k_1^2k_2)}{k_2(1+k_1^2)^{\frac{5}{2}}+8k_1^3(1+k_1^2)}$$

Substituting lambda into the solution exponentials in equation 4.1.4.7

$$e^{\lambda_1 t} = e^{aw_r t} = e^{a\theta_r} \qquad e^{\lambda_1 t} = e^{bw_\rho t} = e^{b\theta_\rho}$$

Certain numerically integrated double binary configurations are observed to spiral outward as they separate over time. It therefore seems likely that from the linear approximation the double binary system growth could be described as a composition of perturbed spirals. A mathematical candidate for this observed motion is the logarithmic equiangular spiral which can be written in the form S= $e^{n\theta}$ where S is the radii, n is a constant and theta is the angular variation. Exponentials in the double binary solution are in the same form as logarithmic spirals, where, it appears the binary motion may essentially be composed of a summation of dilating and contracting spirals for the linear approximation. These dilating and contracting spirals occur from the positive and negative exponents in equation 4.1.4.7.

Numerical integration of various double binaries in configuration space (figure 4.1.2.1) has shown that most trajectories appear to be much more complicated than the linear approximation can model over the initial phase of their orbits. There are some special configurations that do exhibit behavior similar to pure spirals and are found where the subsystem binary mass ratio is near zero ($k_1 = 1, k_2 \to 0, \infty$). The region where both binaries have the same initial period (includes the Lagrange configurations) is special in that the binaries will maintain stable near circular orbits for a finite period after time zero. In general, a non-linear analysis would be needed to more accurately understand to what extent perturbed spirals represent dilating and contracting orbital motion as seen in the numerically integrated trajectories of the double binary configurations.

Solutions to homogeneous differential equations with zero initial conditions are not unique thereby resulting in general solutions seen in equation 4.1.4.7. As equation 4.1.4.7 indicates, binary subsystem separation distance grows exponentially with time. Although, this linear approximation can only show the simplest particle motion it does show the binary system is unstable in the sense of Lagrange. Stability in the sense of Lagrange refers to setting up the first order homogenous linear differential equations with constant coefficients and then solving the eigenvalue problem assuming exponential solutions where positive exponents indicate unstable systems and negative exponents indicate stable systems. As is known in Lyapunov stability theory the linear approximation is usually not sufficient to determine stability, whereas, a system that is unstable in the sense of Lagrange is also unstable in the sense of Lyapunov. A stable system in the sense of Lagrange is only a candidate for stability in the sense of Lyapunov for it is necessary to further analyze the non-linear terms in the differential equations as found in the first method of Lyapunov (Lehnigh, 1966, 25-71, Merkin, 1996, 103-111).

Solving a non-linear version of equation 4.1.4.3 may provide insight into a possible form of the trajectory structure which approximates what is found in the numerically integrated trajectories over some given time period. Expanding equation 4.1.4.2 to include quadratic and cubic terms in addition to the linear terms found in equation 4.1.4.3 will require using the Taylor series expansion. Letting $x = \epsilon_r$ and $y = \epsilon_\rho$ the scalar form of equation 4.1.4.2 can be rewritten

$$\ddot{x} = a_{11}x + a_{12}y + a_{13}x^2 + a_{14}xy + a_{15}y^2 + a_{16}x^3 + a_{17}x^2y + a_{18}xy^2 + a_{19}y^3$$

$$\ddot{y} = a_{21}x + a_{22}y + a_{23}x^2 + a_{24}xy + a_{25}y^2 + a_{26}x^3 + a_{27}x^2y + a_{28}xy^2 + a_{29}y^3$$

where coefficients are

$$a_{11} = \rho_0^2 mQ \qquad a_{21} = -\rho_0 r_0 MQ \quad \text{Equation 4.1.4.10}$$

$$a_{12} = -\rho_0 r_0 mQ \qquad a_{22} = r_0^2 MQ$$

$$a_{13} = -(\frac{\rho_0^2}{r_0} + \frac{5}{8}\frac{r_0\rho_0^2}{d_0^2})mQ \qquad a_{23} = (-\frac{\rho_0}{2} + \frac{5}{8}\frac{r_0^2\rho_0}{d_0^2})MQ$$

$$a_{14} = (-\rho_0 + \frac{5}{4}\frac{r_0^2\rho_0}{d_0^2})mQ \qquad a_{24} = (-r_0 + \frac{5}{4}\frac{r_0\rho_0^2}{d_0^2})MQ$$

$$a_{15} = (-\frac{r_0}{2} + \frac{5}{8}\frac{r_0\rho_0^2}{d_0^2})mQ \qquad a_{25} = -(\frac{r_0^2}{\rho_0} + \frac{5}{8}\frac{r_0^2\rho_0}{d_0^2})MQ$$

$$a_{16} = (\frac{4}{3}\frac{\rho_0^2}{r_0^2} + \frac{5}{24}\frac{\rho_0^2}{d_0^2} + \frac{35}{96}\frac{r_0^2\rho_0^2}{d_0^4})mQ \qquad a_{26} = (\frac{5}{8}\frac{r_0\rho_0}{d_0^2} - \frac{35}{96}\frac{r_0^3\rho_0}{d_0^4})MQ$$

$$a_{17} = (\frac{15}{8}\frac{r_0\rho_0}{d_0^2} - \frac{35}{32}\frac{r_0^3\rho_0}{d_0^4})mQ \qquad a_{27} = (2 - \frac{35}{32}\frac{r_0^2\rho_0^2}{d_0^4})MQ$$

$$a_{18} = (2 - \frac{35}{32}\frac{r_0^2\rho_0^2}{d_0^4})mQ \qquad a_{28} = (\frac{15}{8}\frac{r_0\rho_0}{d_0^2} - \frac{35}{32}\frac{r_0\rho_0^3}{d_0^4})MQ$$

$$a_{19} = (\frac{5}{8}\frac{r_0\rho_0}{d_0^2} - \frac{35}{96}\frac{r_0\rho_0^3}{d_0^4})mQ \qquad a_{29} = (\frac{4}{3}\frac{r_0^2}{\rho_0^2} + \frac{5}{24}\frac{r_0^2}{d_0^2} + \frac{35}{96}\frac{r_0^2\rho_0^2}{d_0^4})MQ$$

and $\quad Q = {}^{3G}/_{2d_0^5}$

A Solution to this non-linear coupled set of differential equations for the restricted double binary configuration would require some effort. These differential equations are only valid in a small neighborhood of time zero, and assuming a viable solution does exist their practical use may be of limited application. Using a set of differential equations that are valid for all time would resolve this situation, however, solving such a set of equations is not expected to be doable. For example, from conservation of energy a candidate set of differential equations in Jacoby coordinates can be derived that are valid for all time

$$\ddot{r} = 2\frac{GM}{r^2} + Gmr\left(\frac{1}{r_{14}^3} + \frac{1}{r_{13}^3}\right) + Gm\rho\left(\frac{1}{r_{14}^3} - \frac{1}{r_{13}^3}\right)cos\theta - \frac{Gm}{2}r\rho\left(\frac{1}{r_{14}^3} - \frac{1}{r_{13}^3}\right)sin\theta\frac{d\theta}{dr} \qquad \text{Equation 4.1.4.11}$$

$$\ddot{\rho} = 2\frac{Gm}{\rho^2} + GM\rho\left(\frac{1}{r_{14}^3} + \frac{1}{r_{13}^3}\right) + GMr\left(\frac{1}{r_{14}^3} - \frac{1}{r_{13}^3}\right)cos\theta - \frac{GM}{2}r\rho\left(\frac{1}{r_{14}^3} - \frac{1}{r_{13}^3}\right)sin\theta\frac{d\theta}{d\rho}$$

where $r_{13}^2 = r_{24}^2 = \frac{r^2}{4} + \frac{\rho^2}{4} - \frac{r\rho}{2}cos\theta \qquad r_{14}^2 = r_{23}^2 = \frac{r^2}{4} + \frac{\rho^2}{4} + \frac{r\rho}{2}cos\theta$

As can be seen in the above equations a third variable theta has been introduced and is defined to be the angle between r and ρ. This makes the double binary problem more difficult in that there is not a corresponding second order equation in theta to help obtain a solution. A consistency check will show that when $r_{14} = r_{13}$ and $\theta = \frac{\pi}{2}$ these equations default to the scalar form of equations 4.1.4.2 valid over the infinitesimal interval at time zero.

The restricted double binary analyzed in this chapter is a specialized Jacoby double binary configuration rather than the classical Jacoby double binary configuration. General n-body equations of motion can be transformed into n-1 coupled equations in n-1 Jacoby coordinates. Consistent with this requires the general double binary configuration to have three coupled equations in three coordinates, where the first two Jacoby coordinates are defined as the distance between the two binaries respectively and the third Jacoby coordinate is the vector between the center of gravities of the two binary subsystems. The double binary formulated in this chapter does not require a third Jacoby coordinate for this configuration need only be defined by n-2 Jacoby coordinates. The general double binary

second order linear homogeneous differential equations for the linear approximation analogous to equation 4.1.4.3 have the form

$$\begin{pmatrix} \ddot{\epsilon}_{r1} \\ \ddot{\epsilon}_{r2} \\ \ddot{\epsilon}_{\rho} \end{pmatrix} = \begin{pmatrix} a_{11} & a_{12} & a_{13} \\ a_{21} & a_{22} & a_{23} \\ a_{31} & a_{32} & a_{33} \end{pmatrix} \begin{pmatrix} \epsilon_{r1} \\ \epsilon_{r2} \\ \epsilon_{\rho} \end{pmatrix}$$

where subscripts r1 and r2 reference the first and second binaries respectively and ρ is the distance between gravity centers of the binary subsystems. The general three Jacoby coordinate double binary will be considered a non-degenerate double binary configuration whereas the two Jacoby coordinate double binary will be assumed (without proof) to be a degenerate double binary configuration. The degenerate double binary is a special case of the non-degenerate double binary.

4.1.5 Inverse Problem of Dynamics

There are two ways in which the infinitesimal interval restricted double binary problem can be analyzed. The first was the deductive method presented in the preceding subsections of this chapter. A second method is to apply the inverse problem of dynamics (Galiullin, 1984, 25-28), that is, forces are determined by the given properties of their motion. This method gives the same deterministic state vector found from the deductive method while also verifying the n-body equations of motion as a final result.

Constraints necessary to achieve this solution of state are placed on the particle mass, position, velocity and acceleration geometry (Santilli, 1978, 219-223). Velocity properties for the double binary configuration are defined such that all particle velocity vectors are perpendicular to all particle position vectors at time zero relative to the barycenter within the configuration plane of motion. This constraint placed on the binary velocity is type one geometry (Roy and Ovenden, 1955, Lass, 1957, 314-319, Marchal, 2000, 286). Type one geometry also constrains acceleration vectors to be opposite in direction relative to their respective position vectors and are directed along a straight line passing through the barycenter at time zero. The deterministic state vector within the infinitesimal interval using the inverse problem of dynamics with the necessary constraints is consistent with conservation of energy where twice the kinetic energy is equal to the potential energy. All particles will be in instantaneous circular orbits at time zero, otherwise non-circular orbits before or after time zero.

Applying the aforementioned constraints, instantaneous double binary velocities can be determined by formulating a binary velocity equation that is a function of unperturbed and perturbed velocity components. Starting with a perturbed Kepler two-body velocity equation to formulate the r and ρ binaries

$$V_r^2 = 2\frac{GM}{r} + \phi_r' \qquad V_\rho^2 = 2\frac{Gm}{\rho} + \phi_\rho' \qquad \text{Equation 4.1.5.1}$$

with mass and position constraints

$$m_1 = m_2 = M \; m_3 = m_4 = m \; d = r_{31} = r_{32} = r_{41} = r_{42} \; r = r_{21} \; \rho = r_{43}$$

where terms $2\frac{GM}{r}$ and $2\frac{Gm}{\rho}$ are the unperturbed binary two body velocities with ϕ_r' and ϕ_ρ' the unknown binary perturbations.

It is known from the binary velocity vector geometry that $2T = \frac{M}{2}V_r^2 + \frac{m}{2}V_\rho^2$ is the kinetic energy and from the binary position geometry that potential energy is $U = \frac{GM^2}{r} + 4\frac{GMm}{d} + \frac{Gm^2}{\rho}$ (see figure 4.1). Equating 2T = U gives

$$\frac{M}{2}\phi_r' + \frac{m}{2}\phi_\rho' = 4\frac{GMm}{d} \qquad \text{Equation 4.1.5.2}$$

where $\frac{M}{2}$ and $\frac{m}{2}$ are the reduced masses for the r and ρ binaries respectively.

Reformulating $d^2 = \frac{r^2}{4} + \frac{\rho^2}{4}$ into $\frac{r^2}{4d^3} + \frac{\rho^2}{4d^3} = \frac{1}{d}$ and using equation 4.1.5.2 the unknown binary perturbations can be determined

$$\phi_r' = 2Gm\frac{r^2}{d^3} \qquad \phi_\rho' = 2GM\frac{\rho^2}{d^3}$$

Substituting these perturbations into equation 4.1.5.1

$$V_r^2 = 2\frac{GM}{r} + 2Gm\frac{r^2}{d^3} = \frac{G}{r}(2M + 2m\frac{r^3}{d^3}) \qquad \text{Equation 4.1.5.3}$$

$$V_\rho^2 = 2\frac{Gm}{\rho} + 2GM\frac{\rho^2}{d^3} = \frac{G}{\rho}(2m + 2M\frac{\rho^3}{d^3})$$

These are the same velocity results found using the deductive method in equations 4.1.3 and 4.1.4. With knowledge of the binary positions and velocities the state vector at time zero is also known (see equation 4.1.5).

Deriving r and ρ binary accelerations using Infinitesimal rotations and type one geometry within the infinitesimal interval gives

$$a_r = \frac{V_r^2}{r} = w^2 r = \frac{2GM}{r^2} + \frac{2Gm}{r^2}\frac{r^3}{d^3} \qquad \text{Equation 4.1.5.4}$$

$$a_\rho = \frac{V_\rho^2}{\rho} = w^2 \rho = \frac{2Gm}{\rho^2} + \frac{2GM}{\rho^2}\frac{\rho^3}{d^3}$$

In a small neighborhood around time zero in a domain just outside of the infinitesimal interval, equation 4.1.5.4 would be replaced by

$$\ddot{r} = \frac{2GM}{r^2} + \frac{2Gm}{r^2}\frac{r^3}{d^3} \qquad \text{Equation 4.1.5.5}$$

$$\ddot{\rho} = \frac{2Gm}{\rho^2} + \frac{2GM}{\rho^2}\frac{\rho^3}{d^3}$$

Equation 4.1.5.5 is the scalar form of equation 4.1.4.2.

4.2 Triple Binary

The double binary orthogonal configuration worked in the previous subsection is the simplest of all collinear configurations in the orthogonal family. Next in the orthogonal family sequence to be analyzed is the triple binary (six-body) configuration which can be viewed in figure 4.2.1. Inertial coordinate system definition is the same as the double binary configuration as well as formulating the triple-binary problem in the complex plane.

Triple binary equations of motion formulated in the infinitesimal interval as derived in equation 3.1

$$\ddot{z}_k + 2wi\dot{z}_k - w^2 z_k = G\sum_{\substack{j=1 \\ j\neq k}}^{N} \frac{m_j}{r_{jk}^3} z_{jk} \qquad k = 1, 2, \ldots, 6$$

sidereal synodic relations that specify the general geometric conditions under which the six-body configuration rotates

$$n_R P_R = (n_R + n_{R-1})P_{R-1} = \cdots = (n_R + n_{R-1} + \cdots + n_1)P_1$$

The six-body equations of motion have been transformed using Jacoby coordinates. Coupling mass one with mass two forms the r binary subsystem, coupling mass three with mass four forms the r_{43} binary subsystem and coupling mass five with mass six forms the r_{65} binary subsystem. There is a forth binary subsystem ρ defined by the distance between the center of gravity of the r_{43} and r_{65} binary subsystems. Mass one and mass two being individually equal to M are placed equidistant either side of the xy coordinate system origin along the x-axis. Mass three and mass four being individually equal to m are placed at a distance ρ/2 (relative to the r_{43} center of gravity) along the positive y-axis from the barycenter. Mass five and mass six has the same geometry except that the r_{65} binary is along the negative y-axis. The geometrical center of the six-body configuration is the same as the barycenter. Using Jacoby coordinates has reduced the six-body system from six coupled non-linear differential equation to four coupled non-linear differential equations. This mass distribution subsequently defines the restricted six-body configuration geometry.

Complex plane coupled equations of motion for the z_{21}, z_{43} and z_{65} binaries respectively

$$-w^2 z_{21} = \frac{G\mu}{r^3} z_{21} + \frac{Gm_3}{r_{32}^3} z_{32} - \frac{Gm_3}{r_{31}^3} z_{31} + \frac{Gm_4}{r_{42}^3} z_{42} - \frac{Gm_4}{r_{41}^3} z_{41} + \frac{Gm_5}{r_{52}^3} z_{52} - \frac{Gm_5}{r_{51}^3} z_{51} + \frac{Gm_6}{r_{62}^3} z_{62} - \frac{Gm_6}{r_{61}^3} z_{61}$$

$$\ddot{z}_{43} + 2wi\acute{z}_{43} - w^2 z_{43} = \frac{G\mu_{43}}{r_{43}^3} z_{43} + \frac{Gm_1}{r_{14}^3} z_{14} - \frac{Gm_1}{r_{13}^3} z_{13} + \frac{Gm_2}{r_{24}^3} z_{24} - \frac{Gm_2}{r_{23}^3} z_{23} + \frac{Gm_5}{r_{54}^3} z_{54} - \frac{Gm_5}{r_{53}^3} z_{53} + \frac{Gm_6}{r_{64}^3} z_{64} - \frac{Gm_6}{r_{63}^3} z_{63}$$

$$\ddot{z}_{65} + 2wi\acute{z}_{65} - w^2 z_{65} = \frac{G\mu_{65}}{r_{65}^3} z_{65} + \frac{Gm_1}{r_{16}^3} z_{16} - \frac{Gm_1}{r_{15}^3} z_{15} + \frac{Gm_2}{r_{26}^3} z_{26} - \frac{Gm_2}{r_{25}^3} z_{25} + \frac{Gm_3}{r_{36}^3} z_{36} - \frac{Gm_3}{r_{35}^3} z_{35} + \frac{Gm_4}{r_{46}^3} z_{46} - \frac{Gm_4}{r_{45}^3} z_{45}$$

The z_{21} binary is on the rotating x'-axis and therefore $\ddot{z}_{21} = \dot{z}_{21} = 0$. Mass binary coupling terms are defined as $\mu_{43} = m_3 + m_4$ and $\mu_{65} = m_5 + m_5$. Combining the above equations and setting $\rho_{ij} = \frac{G}{w^2 r_{ij}^3}$ to simplify the analysis leads to the following

$$(\rho_{21}\mu - 1)z_{21} = (\rho_{32}z_{32} - \rho_{31}z_{31})m_3 + (\rho_{42}z_{42} - \rho_{41}z_{41})m_4 + (\rho_{52}z_{52} - \rho_{51}z_{51})m_5 + (\rho_{62}z_{62} - \rho_{61}z_{61})m_6$$

$$\left(\rho_{43}\mu_{43} - \frac{P_{21}^2}{P_{43}^2}\right)z_{43} = (\rho_{14}z_{14} - \rho_{13}z_{13})m_1 + (\rho_{24}z_{24} - \rho_{23}z_{23})m_2 + (\rho_{54}z_{54} - \rho_{53}z_{53})m_5 + (\rho_{64}z_{64} - \rho_{63}z_{63})m_6$$

$$\left(\rho_{65}\mu_{65} - \frac{P_{21}^2}{P_{65}^2}\right)z_{65} = (\rho_{16}z_{16} - \rho_{15}z_{15})m_1 + (\rho_{26}z_{26} - \rho_{25}z_{25})m_2 + (\rho_{36}z_{36} - \rho_{35}z_{35})m_3 + (\rho_{46}z_{46} - \rho_{45}z_{45})m_4$$

where $\rho_{ij} = \rho_{ji}$

Mass and position constraints needed for evaluating the above z_{21}, z_{43} and z_{65} binary equations can be determined from figure 4.2.1

$$\rho_{31} = \rho_{32} = \rho_{61} = \rho_{62}$$

$$\rho_{41} = \rho_{42} = \rho_{51} = \rho_{52}$$

$$m_3 = m_4 = m_5 = m_6 = m \qquad m_1 = m_2 = M$$

Inertial velocity determination for the z_{21} binary

$$(\rho_{21}\mu - 1)z_{21} = -2\rho_{32}m - 2\rho_{42}m$$

$$\mu - \frac{w^2r^3}{G} = -2m\left(\frac{r^3}{r_{32}^3} + \frac{r^3}{r_{42}^3}\right)$$

$$V_r^2 = \frac{G}{r}(2M + \phi_r) \qquad \phi_r = 2m\left(\frac{r^3}{r_{32}^3} + \frac{r^3}{r_{42}^3}\right)$$

Inertial velocity determination for the z_{43} binary

$$\left(\rho_{43}2m - \frac{P_{21}^2}{P_{43}^2}\right)z_{43} = \rho_{42}Ml_1z_{43} - \rho_{32}Ml_2z_{43} + \rho_{45}ml_1z_{43} - \rho_{36}ml_2z_{43}$$

$$V_{r_{43}}^2 = \frac{G}{r_{43}}(2m - \phi_{43}) \qquad \phi_{43} = \frac{r_{43}^3}{r_{42}^3}Ml_1 - \frac{r_{43}^3}{r_{32}^3}Ml_2 + \frac{r_{43}^3}{r_{45}^3}ml_1 - \frac{r_{43}^3}{r_{36}^3}ml_2$$

The $l_1$and l_2 scaling terms for the z_{43} and z_{65} binary subsystems (see figure 4.2.1) are derived as follows

$$r_{54} = l_1 r_{43} \qquad r_{36} = l_2 r_{43}$$

$$\rho = l_1 r_{43} + r_{43} \qquad \rho = l_2 r_{43} - r_{43}$$

$$l_1 = \frac{\rho - r_{43}}{r_{43}} \qquad l_2 = \frac{\rho + r_{43}}{r_{43}}$$

Inertial velocity determination for the z_{65} binary

$$\left(\rho_{65} 2m - \frac{P_{21}^2}{P_{65}^2}\right) z_{65} = \rho_{52} M l_1 z_{65} - \rho_{62} M l_2 z_{65} + \rho_{54} m l_1 z_{65} - \rho_{63} m l_2 z_{65}$$

$$V_{r_{65}}^2 = \frac{G}{r_{65}}(2m - \phi_{65}) \qquad \phi_{65} = \frac{r_{65}^3}{r_{52}^3} M l_1 - \frac{r_{65}^3}{r_{62}^3} M l_2 + \frac{r_{65}^3}{r_{54}^3} m l_1 - \frac{r_{65}^3}{r_{63}^3} m l_2$$

The inertial velocity determination for the fourth binary z_ρ is more complex than the z_{21}, z_{43} and z_{65} binary velocities. This occurs due to z_ρ being embedded within the ρ double binary subsystem, that is, the z_{43} z_{65} center of gravity separation distance requires additional equations of motion to analyze. Procedurally this can be worked using either center of gravity of the z_{43} binary subsystem or the center of gravity of the z_{65} binary subsystem.

$$z_{43c} = \frac{m_3 z_3 + m_4 z_4}{\mu_{43}} \qquad z_{65c} = \frac{m_5 z_5 + m_6 z_6}{\mu_{65}} \qquad \text{Equation 4.2.1}$$

In this analysis the center of gravity of the z_{43} binary subsystem will be used for derivation after taking a double time derivative. Multiplying the left side of the m_3 equation of motion by $\frac{m_3}{\mu_{43}}$ and the left side of the m_4 equation of motion by $\frac{m_4}{\mu_{43}}$ then adding both left side equations results in

$$\ddot{z}_{43c} + 2wi\dot{z}_{43c} - w^2 z_{43c} = \cdots$$

The z_ρ equation taking into account the infinitesimal rotations within the infinitesimal interval and adding the right side of the m_3 and m_4 equations of motion

$$\frac{1}{2}\frac{P_{21}^2}{P_\rho^2} z_\rho = (\rho_{13} m_3 z_{13} + \rho_{14} m_4 z_{14})\frac{m_1}{\mu_{43}} + (\rho_{23} m_3 z_{23} + \rho_{24} m_4 z_{24})\frac{m_2}{\mu_{43}} + (\rho_{53} m_3 z_{53} + \rho_{54} m_4 z_{54})\frac{m_5}{\mu_{43}} + (\rho_{63} m_3 z_{63} + \rho_{64} m_4 z_{64})\frac{m_6}{\mu_{43}}$$

Collecting terms and taking advantage of the figure 4.2.1 geometry

$$\left(\frac{p_{21}^2}{p_\rho^2} - 2m\rho_{53}\right) z_\rho = (\rho_{13}z_{63} + \rho_{14}z_{54})M + (\rho_{54}z_{54} + \rho_{63}z_{63})m$$

Equation 4.2.2

$$V_\rho^2 = \frac{G}{\rho}(2m + \phi_\rho) \qquad \phi_\rho = \frac{\rho^3}{r_{13}^3}Ml_3 + \frac{\rho^3}{r_{14}^3}Ml_4 + \frac{\rho^3}{r_{54}^3}ml_4 + \frac{\rho^3}{r_{63}^3}ml_3$$

The $l_3$and l_4 scaling terms for the z_ρ double binary subsystem (see figure 4.2.1) are derived as follows

$$r_{54} = l_4\rho \qquad r_{63} = l_3\rho$$

$$\rho = l_4\rho + r_{43} \qquad \rho = l_3\rho - r_{43}$$

$$l_4 = \frac{\rho - r_{43}}{\rho} \qquad l_3 = \frac{\rho + r_{43}}{\rho}$$

With the derivation of the binary velocities a three-dimensional orthogonal collinear state vector for the six-body configuration can be constructed (the vector $\vec{\rho}$ rotates inplane).

First binary state vector

$$x_1 = -\frac{1}{2}r \qquad \dot{x}_1 = 0 \qquad \text{Equation 4.2.3}$$
$$y_1 = 0 \qquad \dot{y}_1 = -\frac{1}{2}V_r$$
$$z_1 = 0 \qquad \dot{z}_1 = 0$$
$$x_2 = \frac{1}{2}r \qquad \dot{x}_2 = 0$$
$$y_2 = 0 \qquad \dot{y}_2 = \frac{1}{2}V_r$$
$$z_2 = 0 \qquad \dot{z}_1 = 0$$

Second binary state vector

$$x_3 = 0 \qquad \dot{x}_3 = -\frac{1}{2}(V_\rho + V_{r_{43}}cosi_{r_{43}})$$
$$y_3 = \frac{1}{2}(\rho + r_{43}) \qquad \dot{y}_3 = 0$$
$$z_3 = 0 \qquad \dot{z}_3 = -\frac{1}{2}V_{r_{43}}sini_{r_{43}}$$
$$x_4 = 0 \qquad \dot{x}_4 = \frac{1}{2}(V_\rho - V_{r_{43}}cosi_{r_{43}})$$
$$y_4 = \frac{1}{2}(\rho - r_{43}) \qquad \dot{y}_4 = 0$$
$$z_4 = 0 \qquad \dot{z}_4 = \frac{1}{2}V_{r_{43}}sini_{r_{43}}$$

Third binary state vector

$$x_5 = 0 \qquad \dot{x}_5 = -\frac{1}{2}(V_\rho - V_{r_{65}} cosi_{r_{65}})$$
$$y_5 = -\frac{1}{2}(\rho - r_{65}) \qquad \dot{y}_5 = 0$$
$$z_5 = 0 \qquad \dot{z}_5 = -\frac{1}{2} V_{r_{65}} sini_{r_{65}}$$
$$x_6 = 0 \qquad \dot{x}_6 = \frac{1}{2}(V_\rho + V_{r_{65}} cosi_{r_{65}})$$
$$y_6 = -\frac{1}{2}(\rho + r_{65}) \qquad \dot{y}_6 = 0$$
$$z_6 = 0 \qquad \dot{z}_6 = \frac{1}{2} V_{r_{65}} sini_{r_{65}}$$

Note that binary inclination $i_{r_{43}} = i_{r_{65}}$ and binary velocity $V_{r_{43}} = V_{r_{65}}$. For the two-dimensional version of the above three-dimensional state vector set

$$sini_{r_{43}} = sini_{r_{65}} = 0$$

$$\text{cos}i_{r_{43}} = cosi_{r_{65}} = 1$$

Input orbit parameters to the two-dimensional or three-dimensional state vector are considered to be instantaneous values, however, mean orbit parameters could be used instead of instantaneous values if necessary. Barycentric inertial is the coordinate system for numerical integration.

4.2.1 Triple Binary Conservation of Energy Verification

Starting with the kinetic energy equation and converting to Jacoby coordinates in addition to utilizing the triple binary vector geometry in figure 4.2.1

$$2T = \sum_{i=1}^{6} m_i V_i^2 = \left(m_1\left(\frac{m_1 - m_2 - \theta}{2\theta}\right)^2 + m_2\left(\frac{m_1 - m_2 + \theta}{2\theta}\right)^2\right) V_r^2 + \frac{m_3 m_4}{\mu_{43}} V_{r_{43}}^2 + \frac{m_5 m_6}{\mu_{65}} V_{r_{65}}^2 + \frac{\theta - \mu}{4} V_\rho^2$$

where mass is defined

$$\mu = \sum_1^2 m_i = 2M \qquad \theta = \sum_1^6 m_i = 2M + 4m$$

After combining masses, the kinetic energy equation becomes

$$2T = \frac{M}{2} V_r^2 + \frac{m}{2} V_{r_{43}}^2 + \frac{m}{2} V_{r_{65}}^2 + m V_\rho^2 \qquad \text{Equation 4.2.1.1}$$

The binary velocities in Jacoby coordinates determined from the previous subsection are

$$V_r^2 = \frac{G}{r}(2M + \phi_r) \quad \phi_r = 2m(\frac{r^3}{r_{32}^3} + \frac{r^3}{r_{42}^3}) \qquad \text{Equation 4.2.1.2}$$

$$V_{r_{43}}^2 = \frac{G}{r_{43}}(2m - \phi_{43}) \qquad \phi_{43} = \frac{r_{43}^3}{r_{42}^3}Ml_1 - \frac{r_{43}^3}{r_{32}^3}Ml_2 + \frac{r_{43}^3}{r_{45}^3}ml_1 - \frac{r_{43}^3}{r_{36}^3}ml_2$$

$$V_{r_{65}}^2 = \frac{G}{r_{65}}(2m - \phi_{65}) \qquad \phi_{65} = \frac{r_{65}^3}{r_{52}^3}Ml_1 - \frac{r_{65}^3}{r_{62}^3}Ml_2 + \frac{r_{65}^3}{r_{54}^3}ml_1 - \frac{r_{65}^3}{r_{63}^3}ml_2$$

$$V_\rho^2 = \frac{G}{\rho}(2m + \phi_\rho) \qquad \phi_\rho = \frac{\rho^3}{r_{13}^3}Ml_3 + \frac{\rho^3}{r_{14}^3}Ml_4 + \frac{\rho^3}{r_{54}^3}ml_4 + \frac{\rho^3}{r_{63}^3}ml_3$$

$$l_1 = \frac{\rho - r_{43}}{r_{43}} \qquad l_2 = \frac{\rho + r_{43}}{r_{43}} \qquad l_3 = \frac{\rho + r_{43}}{\rho} \qquad l_4 = \frac{\rho - r_{43}}{\rho}$$

Substituting equation 4.2.1.2 into equation 4.2.1.1 identifies all the kinetic energy terms that will be combined and regrouped to match the potential energy equation. Potential energy after transforming into Jacoby coordinates

$$U = G\sum\frac{m_i m_j}{r_{ij}} = \frac{GM^2}{r} + 2\frac{Gm^2}{r_{43}} + 4\frac{GMm}{r_{31}} + 4\frac{GMm}{r_{41}} + 2\frac{Gm^2}{\rho} + \frac{Gm^2}{r_{54}} + \frac{Gm^2}{r_{63}}$$

Equation 4.2.1.3

Collecting $r_{31}, r_{41}, r_{54}, r_{63}$ terms by denominator in groups for evaluation will simplify kinetic potential energy matching. Going through this exercise is somewhat extensive, however, it is worth the effort to see in the final analysis that conservation of energy is verified to be 2T = U.

4.2.2 Triple Binary Configuration Space

Most fundamental of all orthogonal collinear configurations is the double binary with only one existing period ratio to determine configuration space and only one phase space transformation. The triple binary configuration space is determined by four binary periods with four binary ratios. This situation is more involved to map the binary geometry for interesting candidates to numerically integrate. For this study, only special cases will be considered. Indication of this configuration complexity is seen with binary ratios below

$$P_r^2 = 4\pi^2\left(\frac{r^3}{G(2M+\phi_r)}\right) \qquad P_\rho^2 = 4\pi^2\left(\frac{\rho^3}{G(2m+\phi_\rho)}\right)$$

$$P_{43}^2 = 4\pi^2\left(\frac{r_{43}^3}{G(2m+\phi_{43})}\right) \qquad P_{65}^2 = 4\pi^2\left(\frac{r_{65}^3}{G(2m+\phi_{65})}\right)$$

Combining the above periods

$$\frac{P_r^2}{P_\rho^2} = \frac{2m+\phi_\rho}{2M+\phi_r}\frac{r^3}{\rho^3} \qquad \frac{P_{43}^2}{P_{65}^2} = 1 \qquad \text{Equation 4.2.2.1}$$

$$\frac{P_r^2}{P_{43}^2} = \frac{2m+\phi_{43}}{2M+\phi_r}\frac{r^3}{r_{43}^3} \qquad \frac{P_\rho^2}{P_{43}^2} = \frac{2m+\phi_{43}}{2m+\phi_\rho}\frac{\rho^3}{r_{43}^3}$$

Rewriting equation 4.2.2.1 in a scaled format with $k_1 = \rho/r$, $k_2 = m/M$, $k_3 = r_{43}/r$ and $k_4 = r_{43}/\rho$

$$\frac{P_r^2}{P_\rho^2} = \frac{1}{k_1^3}\frac{2k_2+\frac{8k_1^3C_1}{C_3}+\frac{8k_1^3C_2}{C_4}+\frac{k_2}{C_1^2}+\frac{k_2}{C_2^2}}{2+16k_2\left(\frac{1}{C_3}+\frac{1}{C_4}\right)} \qquad \text{Equation 4.2.2.2}$$

$$\frac{P_r^2}{P_{43}^2} = \frac{1}{k_3^3}\frac{2k_2+\frac{8k_3^3C_1}{k_4C_3}-\frac{8k_3^3C_2}{k_4C_4}+\frac{k_4^2k_2}{C_1^2}-\frac{k_4^2k_2}{C_2^2}}{2+16k_2\left(\frac{1}{C_3}+\frac{1}{C_4}\right)}$$

$$\frac{P_\rho^2}{P_{43}^2} = \frac{1}{k_4^3}\frac{2k_2+\frac{8k_3^3C_1}{k_4C_3}-\frac{8k_3^3C_2}{k_4C_4}+\frac{k_4^2k_2}{C_1^2}-\frac{k_4^2k_2}{C_2^2}}{2k_2+\frac{8k_1^3C_1}{C_3}+\frac{8k_1^3C_2}{C_4}+\frac{k_2}{C_1^2}+\frac{k_2}{C_2^2}}$$

where $C_1 = 1+k_4$, $C_2 = 1-k_4$, $C_3 = (1+k_1^2C_1^2)^{3/2}$ and $C_4 = (1-k_1^2C_2^2)^{3/2}$.

With the addition of two masses, it can be seen from equation 4.2.2.2 that triple-binary configuration space is considerably more complex than the double binary configuration space. Computing state vectors is not a problem it is just that finding interesting configurations for numerical integration becomes difficult. It will take more time and effort to plot out all the possible regions of configuration space. However, some simplifications can be made, for example, when $m \to 0$ and $r_{63} \to r_{54}$ the six-body configuration space will approach the double binary configuration space. The difference being that the mass three and four binary subsystem as well as the mass five and six binary subsystem will be in their respective close binary orbits instead of being single masses. As r_{63} and r_{54} separate with $m \to 0$ the six-body

configuration space will difference itself from the double binary configuration space. Also looking into the region where $\rho = \sqrt{3}$ and increasing the separation distance of the r_{43} and r_{65} binaries could result in some interesting orbits.

4.3 Quadruple Binary

Next in logical sequence relative to figure 4.1 is the collinear eight-body configuration. There are two members in this family with multiple variations. The one analyzed in this subsection is the quadruple binary configuration. This configuration consists of four binary subsystems in orbit about the barycenter. Orbital geometry for this configuration is actually a double binary subsystem along the x-axis rotating about a double binary subsystem along the y-axis. The separation distance of each of the masses within the two binaries along the x-axis are the same with the barycenter equally divided between the two binary subsystems. The same is true for the two binary subsystems along the y-axis. All masses along the x-axis are of mass M and all masses along the y-axis are of mass m. Geometry of the quadruple binary can be viewed in figure 4.3. Approach to solving this configuration is the same as the double binary and six-body (triple binary) structures worked earlier in this chapter. Results are more apt to be summarized than derived due the same methodology used for the double and triple binary collinear configurations.

Jacoby coordinates has reduced this quadruple binary configuration to six coupled non-linear differential equations. After performing the infinitesimal rotations within the infinitesimal interval using sidereal synodic relations and collecting terms the binary subsystems are for the z_{21} binary

$$\left(\rho_{21}\mu - \frac{p_{\rho_1}^2}{p_{21}^2}\right) z_{21} = (\rho_{32}M + \rho_{52}m + \rho_{62}m)z_{32} - (\rho_{41}M + \rho_{51}m + \rho_{61}m)z_{41}$$

for the z_{43} binary

$$\left(\rho_{43}\mu_{43} - \frac{p_{\rho_1}^2}{p_{43}^2}\right) z_{43} = (\rho_{32}M + \rho_{35}m + \rho_{36}m)z_{32} - (\rho_{41}M + \rho_{45}m + \rho_{46}m)z_{41}$$

for the z_{65} binary

$$\left(\rho_{65}\mu_{65} - \frac{P_{\rho 2}^2}{P_{65}^2}\right) z_{65} = (\rho_{67}m + \rho_{61}M + \rho_{62}M)z_{76} - (\rho_{58}m + \rho_{51}M + \rho_{52}M)z_{85}$$

and for the z_{87} binary

$$\left(\rho_{87}\mu_{87} - \frac{P_{\rho 2}^2}{P_{87}^2}\right) z_{87} = (\rho_{67}m + \rho_{71}M + \rho_{72}M)z_{76} - (\rho_{58}m + \rho_{81}M + \rho_{82}M)z_{85}$$

where $\rho_{ij} = \rho_{ji}$

Constraints needed for evaluating the above z_{21}, z_{43} ,z_{65} and z_{87} binary equations can be determined from figure 4.3

$$\rho_{51} = \rho_{54} = \rho_{81} = \rho_{84} \qquad \mu = m_1 + m_2$$

$$\rho_{61} = \rho_{64} = \rho_{71} = \rho_{74} \qquad \mu_{43} = m_3 + m_4$$

$$\rho_{52} = \rho_{53} = \rho_{82} = \rho_{83} \qquad \mu_{65} = m_6 + m_5$$

$$\rho_{62} = \rho_{63} = \rho_{72} = \rho_{73} \qquad \mu_{87} = m_8 + m_7$$

$$m_1 = m_2 = m_3 = m_4 = M$$

$$m_5 = m_6 = m_7 = m_8 = m$$

Inertial velocity determination for the z_{21} binary

$$V_r^2 = \frac{G}{r}(\mu + \phi_1) = \frac{G}{r}(2M + \phi_1)$$

Inertial velocity determination for the z_{43} binary

$$V_{r_{43}}^2 = \frac{G}{r_{43}}(\mu_{43} + \phi_2) = \frac{G}{r}(2M + \phi_1) \qquad r = r_{43},\ \phi_1 = \phi_2,\ V_r = V_{r_{43}}$$

Inertial velocity determination for the z_{65} binary

$$V_{r_{65}}^2 = \frac{G}{r_{65}}(\mu_{65} + \phi_3) = \frac{G}{r_{65}}(2m + \phi_3)$$

Inertial velocity determination for the z_{87} binary

$$V_{r_{87}}^2 = \frac{G}{r_{87}}(\mu_{87} + \phi_4) = \frac{G}{r_{65}}(2m + \phi_3) \quad r_{87} = r_{65}, \phi_4 = \phi_3, V_{r_{87}} = V_{r_{65}}$$

and perturbation coefficients ϕ_i are

$$\phi_1 = (\frac{r^3}{r_{41}^3}M + \frac{r^3}{r_{51}^3}m + \frac{r^3}{r_{61}^3}m)l_2 - (\frac{r^3}{r_{32}^3}M + \frac{r^3}{r_{52}^3}m + \frac{r^3}{r_{62}^3}m)l_1$$

$$\phi_2 = (\frac{r_{43}^3}{r_{41}^3}M + \frac{r_{43}^3}{r_{45}^3}m + \frac{r_{43}^3}{r_{46}^3}m)l_2 - (\frac{r_{43}^3}{r_{32}^3}M + \frac{r_{43}^3}{r_{35}^3}m + \frac{r_{43}^3}{r_{36}^3}m)l_1$$

$$\phi_3 = (\frac{r_{65}^3}{r_{58}^3}m + \frac{r_{65}^3}{r_{51}^3}M + \frac{r_{65}^3}{r_{52}^3}M)l_4 - (\frac{r_{65}^3}{r_{67}^3}m + \frac{r_{65}^3}{r_{61}^3}M + \frac{r_{65}^3}{r_{62}^3}M)l_3$$

$$\phi_4 = (\frac{r_{87}^3}{r_{58}^3}m + \frac{r_{87}^3}{r_{81}^3}M + \frac{r_{87}^3}{r_{82}^3}M)l_4 - (\frac{r_{87}^3}{r_{67}^3}m + \frac{r_{87}^3}{r_{71}^3}M + \frac{r_{87}^3}{r_{72}^3}M)l_3$$

where $r_{32} = l_1 r = \rho_1 - r$ $\quad r_{41} = l_2 r = \rho_1 + r$

$r_{76} = l_3 r_{65} = \rho_2 - r_{65}$ $\quad r_{85} = l_4 r_{65} = \rho_2 + r_{65}$

$l_1 = \frac{\rho_1 - r}{r}$ $\quad l_2 = \frac{\rho_1 + r}{r}$ $\quad l_3 = \frac{\rho_2 - r_{65}}{r_{65}}$ $\quad l_4 = \frac{\rho_2 + r_{65}}{r_{65}}$

There are two more inertial velocity derivations and they are for the z_{ρ_1} and z_{ρ_2} binary subsystems. This is similar to the six-body configuration (triple binary) except that there are two double binaries to consider instead of one. Using the center of gravity of the z_{43} binary subsystem to find the z_{ρ_1} binary equation of motion

$$z_{43c} = \frac{m_3 z_3 + m_4 z_4}{\mu_{43}} \qquad \text{Equation 4.3.1}$$

there results after collecting and regrouping terms

$$1 - 2M\rho_{13} = (\rho_{23}l_5 + \rho_{14}l_6)M + (\rho_{53}l_5 + \rho_{54}l_6 + \rho_{63}l_5 + \rho_{64}l_6)m$$

$$V_{\rho_1}^2 = \frac{G}{\rho_1}(2M + \phi_{\rho_1})$$

where $\phi_{\rho_1} = \frac{\rho_1^3}{r_{23}^3}Ml_5 + \frac{\rho_1^3}{r_{14}^3}Ml_6 + \frac{\rho_1^3}{r_{53}^3}ml_5 + \frac{\rho_1^3}{r_{54}^3}ml_6 + \frac{\rho_1^3}{r_{63}^3}ml_5 + \frac{\rho_1^3}{r_{64}^3}ml_6$

Using the center of gravity of the z_{65} binary subsystem to find the z_{ρ_2} binary equation of motion

$$z_{65c} = \frac{m_5 z_5 + m_6 z_6}{\mu_{65}} \qquad \text{Equation 4.3.2}$$

there results after collecting and regrouping terms

$$\frac{P_{\rho_1}^2}{P_{\rho_2}^2} - 2m\rho_{75} = (\rho_{15} l_8 + \rho_{16} l_7 + \rho_{25} l_8 + \rho_{26} l_7)M + (\rho_{76} l_7 + \rho_{85} l_8)m$$

$$V_{\rho_2}^2 = \frac{G}{\rho_2}(2m + \phi_{\rho_2})$$

where $\phi_{\rho_2} = \frac{\rho_2^3}{r_{15}^3} M l_8 + \frac{\rho_2^3}{r_{16}^3} M l_7 + \frac{\rho_2^3}{r_{25}^3} M l_8 + \frac{\rho_2^3}{r_{26}^3} M l_7 + \frac{\rho_2^3}{r_{85}^3} m l_8 + \frac{\rho_2^3}{r_{76}^3} m l_7$

Scaling factors for the z_{ρ_1} and z_{ρ_2} binary velocities are listed below

$$r_{32} = l_5 \rho_1 = \rho_1 - r \qquad r_{41} = l_6 \rho_1 = \rho_1 + r$$

$$r_{76} = l_7 \rho_2 = \rho_2 - r_{65} \qquad r_{85} = l_8 \rho_2 = \rho_2 + r_{65}$$

$$l_5 = \frac{\rho_1 - r}{\rho_1} \quad l_6 = \frac{\rho_1 + r}{\rho_1} \qquad l_7 = \frac{\rho_2 - r_{65}}{\rho_2} \quad l_8 = \frac{\rho_2 + r_{65}}{\rho_2}$$

With knowledge of the quadruple double binary positions and inertial velocities the orthogonal collinear configuration state vector can be determined. This state vector is two dimensional and is in the barycentric inertial coordinate system.

First double binary state vector along the x-axis

$$x_1 = -\frac{1}{2}(\rho_1 + r) \qquad \dot{x}_1 = 0 \qquad \text{Equation 4.3.3}$$
$$y_1 = 0 \qquad \dot{y}_1 = -\frac{1}{2}(V_{\rho_1} + V_r)$$

$$x_2 = -\frac{1}{2}(\rho_1 - r) \qquad \dot{x}_2 = 0$$
$$y_2 = 0 \qquad \dot{y}_2 = \frac{1}{2}(V_{\rho_1} - V_r)$$

$$x_3 = \frac{1}{2}(\rho_1 - r) \qquad \dot{x}_3 = 0$$
$$y_3 = 0 \qquad \dot{y}_3 = -\frac{1}{2}(V_{\rho_1} - V_r)$$

$$x_4 = \frac{1}{2}(\rho_1 + r) \qquad \dot{x}_4 = 0$$
$$y_4 = 0 \qquad \dot{y}_4 = \frac{1}{2}(V_{\rho_1} + V_r)$$

Second double binary state vector along the y-axis

$$x_5 = 0 \qquad \dot{x}_5 = -\frac{1}{2}\left(V_{\rho_2} + V_{r_{65}}\right)$$
$$y_5 = \frac{1}{2}(\rho_2 + r_{65}) \qquad \dot{y}_5 = 0$$

$$x_6 = 0 \qquad \dot{x}_6 = \frac{1}{2}(V_{\rho_2} - V_{r_{65}})$$
$$y_6 = \frac{1}{2}(\rho_2 - r_{65}) \qquad \dot{y}_6 = 0$$

$$x_7 = 0 \qquad \dot{x}_7 = -\frac{1}{2}(V_{\rho_2} - V_{r_{65}})$$
$$y_7 = -\frac{1}{2}(\rho_2 - r_{65}) \qquad \dot{y}_7 = 0$$

$$x_8 = 0 \qquad \dot{x}_8 = \frac{1}{2}(V_{\rho_2} + V_{r_{65}})$$
$$y_8 = -\frac{1}{2}(\rho_2 + r_{65}) \qquad \dot{y}_8 = 0$$

The quadruple binary or the two double binary configuration is a specialized Jacoby system in that there are only six Jacoby coordinates rather than the collinear Jacoby double binary configuration which has seven Jacoby coordinates. Since, in general n-body equations of motion can be transformed into n-1 coupled equations in n-1 Jacoby coordinates, then, this orthogonal collinear configuration is missing one coupled equation of motion and one Jacoby coordinate. The missing Jacoby coordinate is the vector from the center of gravity of the first double binary configuration to the center of gravity of the second double binary configuration. The general seven Jacoby coordinate quadruple binary is a non-degenerate quadruple binary configuration where the six Jacoby coordinate binary is assumed (without proof) to be a degenerate quadruple binary configuration. The degenerate quadruple binary is a special case of the non-degenerate quadruple double binary.

4.3.1 Quadruple Binary Conservation of Energy Verification

Small increases in n-body mass number require great amounts of additional effort. The double and triple binary orthogonal configurations worked so far are indicative of the solution methods in general for the different aspects of the orthogonal collinear configurations. Therefore, only an outline of the kinetic potential energy verification will be given. Using the quadruple binary vector relations

$$\vec{V}_1 = -\frac{1}{2}(\vec{V}_r + \vec{V}_{\rho_1}) \qquad \vec{V}_5 = -\frac{1}{2}(\vec{V}_{r_{65}} + \vec{V}_{\rho_2})$$

$$\vec{V}_2 = \frac{1}{2}(\vec{V}_r - \vec{V}_{\rho_1}) \qquad \vec{V}_6 = \frac{1}{2}(\vec{V}_{r_{65}} - \vec{V}_{\rho_2})$$

$$\vec{V}_3 = -\frac{1}{2}(\vec{V}_{r_{43}} - \vec{V}_{\rho_1})) \qquad \vec{V}_7 = -\frac{1}{2}(\vec{V}_{r_{87}} - \vec{V}_{\rho_2})$$

$$\vec{V}_4 = \frac{1}{2}(\vec{V}_{r_{43}} + \vec{V}_{\rho_1}) \qquad \vec{V}_8 = \frac{1}{2}(\vec{V}_{r_{87}} + \vec{V}_{\rho_2})$$

and the velocity identities $V_r^2 = V_{r_{43}}^2 = V_1^2$ and $V_{r_{65}}^2 = V_{r_{87}}^2 = V_2^2$ give

$$2T = \sum_{i=1}^{8} m_i V_i^2 = \frac{M}{2}V_r^2 + \frac{M}{2}V_{r_{43}}^2 + \frac{m}{2}V_{r_{65}}^2 + \frac{m}{2}V_{r_{87}}^2 + MV_{\rho_1}^2 + mV_{\rho_2}^2$$

After combining masses, the kinetic energy equation becomes due to symmetry

$$2T = MV_1^2 + mV_2^2 + MV_{\rho_1}^2 + mV_{\rho_2}^2 \qquad \text{Equation 4.3.1.1}$$

The binary velocities in Jacoby coordinates determined from section 4.3 are

$$V_r^2 = \frac{G}{r}(2M + \phi_1)$$

$$\phi_1 = (\frac{r^3}{r_{41}^3}M + \frac{r^3}{r_{51}^3}m + \frac{r^3}{r_{61}^3}m)l_2 - (\frac{r^3}{r_{32}^3}M + \frac{r^3}{r_{52}^3}m + \frac{r^3}{r_{62}^3}m)l_1$$

$$V_{r_{43}}^2 = \frac{G}{r}(2M + \phi_1)$$

$$\phi_2 = (\frac{r_{43}^3}{r_{41}^3}M + \frac{r_{43}^3}{r_{45}^3}m + \frac{r_{43}^3}{r_{46}^3}m)l_2 - (\frac{r_{43}^3}{r_{32}^3}M + \frac{r_{43}^3}{r_{35}^3}m + \frac{r_{43}^3}{r_{36}^3}m)l_1$$

$$V_{r_{65}}^2 = \frac{G}{r_{65}}(2m + \phi_3)$$

$$\phi_3 = (\frac{r_{65}^3}{r_{58}^3}m + \frac{r_{65}^3}{r_{51}^3}M + \frac{r_{65}^3}{r_{52}^3}M)l_4 - (\frac{r_{65}^3}{r_{67}^3}m + \frac{r_{65}^3}{r_{61}^3}M + \frac{r_{65}^3}{r_{62}^3}M)l_3$$

$$V_{r_{87}}^2 = \frac{G}{r_{87}}(2m + \phi_3)$$

$$\phi_4 = (\frac{r_{87}^3}{r_{58}^3}m + \frac{r_{87}^3}{r_{81}^3}M + \frac{r_{87}^3}{r_{82}^3}M)l_4 - (\frac{r_{87}^3}{r_{67}^3}m + \frac{r_{87}^3}{r_{71}^3}M + \frac{r_{87}^3}{r_{72}^3}M)l_3$$

$$V_{\rho_1}^2 = \frac{G}{\rho_1}(2M + \phi_{\rho_1})$$

$$\phi_{\rho_1} = \frac{\rho_1^3}{r_{23}^3}Ml_5 + \frac{\rho_1^3}{r_{14}^3}Ml_6 + \frac{\rho_1^3}{r_{53}^3}ml_5 + \frac{\rho_1^3}{r_{54}^3}ml_6 + \frac{\rho_1^3}{r_{63}^3}ml_5 + \frac{\rho_1^3}{r_{64}^3}ml_6$$

$$V_{\rho_2}^2 = \frac{G}{\rho_2}(2m + \phi_{\rho_2})$$

$$\phi_{\rho_2} = \frac{\rho_2^3}{r_{15}^3}Ml_8 + \frac{\rho_2^3}{r_{16}^3}Ml_7 + \frac{\rho_2^3}{r_{25}^3}Ml_8 + \frac{\rho_2^3}{r_{26}^3}Ml_7 + \frac{\rho_2^3}{r_{85}^3}ml_8 + \frac{\rho_2^3}{r_{76}^3}ml_7$$

Substituting the above equations into equation 4.3.1.1 identifies all the kinetic energy terms that will be combined and regrouped to match the potential energy. Transforming U into Jacoby coordinates

$$U = G\sum\frac{m_i m_j}{r_{ij}} = 2\frac{GM^2}{r} + 2\frac{Gm^2}{r_{65}} + 4\frac{GMm}{r_{51}} + 4\frac{GMm}{r_{61}} + 4\frac{GMm}{r_{52}} + 4\frac{GMm}{r_{62}} + 2\frac{Gm^2}{\rho_2} + \frac{Gm^2}{r_{76}} + \frac{Gm^2}{r_{85}} + 2\frac{GM^2}{\rho_1} + \frac{GM^2}{r_{32}} + \frac{GM^2}{r_{41}}$$

(where $\rho_1 = r_{31} = r_{42}$ and $\rho_2 = r_{75} = r_{86}$), verifies that twice the kinetic energy is equal to the potential energy.

4.3.2 Quadruple Binary Configuration Space

The quadruple binary configuration space is determined by six binary periods with eight binary ratios. This is simplified by two period ratios being unity. As is obvious from the fast-growing number of period ratios the configuration space geometry becomes increasing more complex to map. Period ratios without scaling are shown below

$$P_{21}^2 = 4\pi^2\left(\frac{r^3}{G(2M+\phi_1)}\right) \qquad P_{87}^2 = 4\pi^2\left(\frac{r_{87}^3}{G(2m+\phi_4)}\right)$$

$$P_{43}^2 = 4\pi^2\left(\frac{r_{43}^3}{G(2M+\phi_2)}\right) \qquad P_{\rho_1}^2 = 4\pi^2\left(\frac{\rho_1^3}{G(2M+\phi_{\rho_1})}\right)$$

$$P_{65}^2 = 4\pi^2\left(\frac{r_{65}^3}{G(2m+\phi_3)}\right) \qquad P_{\rho_2}^2 = 4\pi^2\left(\frac{\rho_2^3}{G(2m+\phi_{\rho_2})}\right)$$

Combining the above periods gives

$$\frac{P_{\rho_1}^2}{P_{\rho_2}^2} = \frac{2m+\phi_{\rho_2}}{2M+\phi_{\rho_1}}\frac{\rho_1^3}{\rho_2^3} \qquad \frac{P_{21}^2}{P_{43}^2} = 1 \qquad \text{Equation 4.3.2.1}$$

$$\frac{P_{\rho_1}^2}{P_{21}^2} = \frac{2M+\phi_1}{2M+\phi_{\rho_1}}\frac{\rho_1^3}{r_{21}^3} \qquad \frac{P_{\rho_2}^2}{P_{65}^2} = \frac{2m+\phi_3}{2m+\phi_{\rho_2}}\frac{\rho_2^3}{r_{65}^3}$$

$$\frac{P_{\rho_1}^2}{P_{65}^2} = \frac{2m+\phi_3}{2M+\phi_{\rho_1}}\frac{\rho_1^3}{r_{65}^3} \qquad \frac{P_{65}^2}{P_{87}^2} = 1$$

$$\frac{P_{\rho_2}^2}{P_{21}^2} = \frac{2M+\phi_1}{2m+\phi_{\rho_2}}\frac{\rho_2^3}{r_{21}^3} \qquad \frac{P_{21}^2}{P_{65}^2} = \frac{2m+\phi_3}{2M+\phi_1}\frac{r_{21}^3}{r_{65}^3}$$

Note that $P_{21} = P_{43}$, $P_{65} = P_{87}$,. $\phi_1 = \phi_2$ and $\phi_3 = \phi_4$

The challenge of the quadruple binary configuration is to find finite stability regions existing in the configuration space geometry. One such region would be to have ρ_1 and ρ_2 very large relative to r_{21}, r_{43}, r_{65} and r_{87} binary separation distances, thus assuring that the perturbations between the quadruple binaries are minimal as they orbit the barycenter. This configuration is actually the collinear double binary when the quadruple binary separation distances approach zero. Another region would have the first double binary well inside the second double binary. Configuration space mapping would aid in selection of these regions to provide state vectors for numerical integration to verify finite stability

Orthogonal collinear configurations beyond the quadruple binary become increasingly more complex and would need a systematic approach to solve a given family. Without a systematic approach the procedures for solving individual cases would become quite laborious. Applications for these configurations appear to be nebulous with the main interest being theoretical.

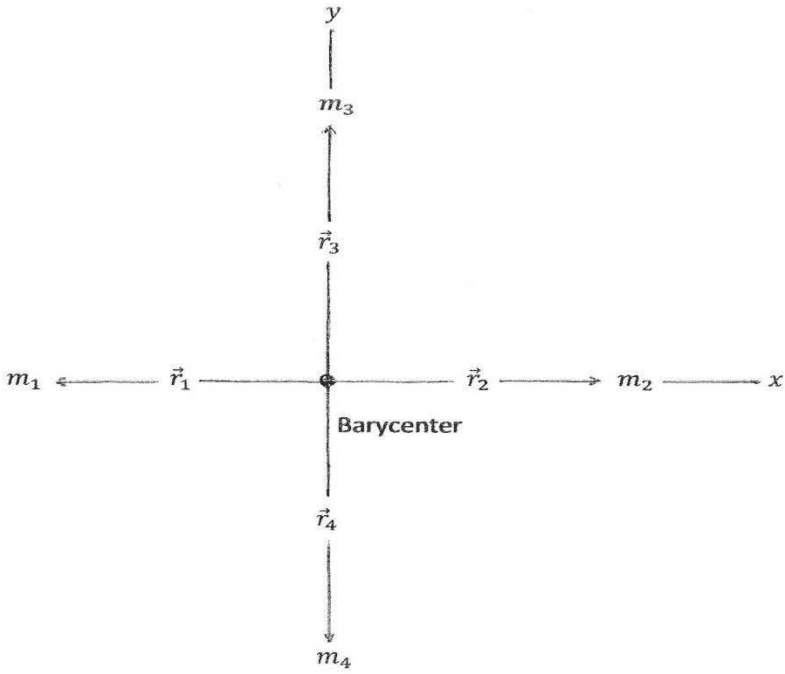

FIGURE 4.1.1. Orthogonal Double Binary Configuration Geometry

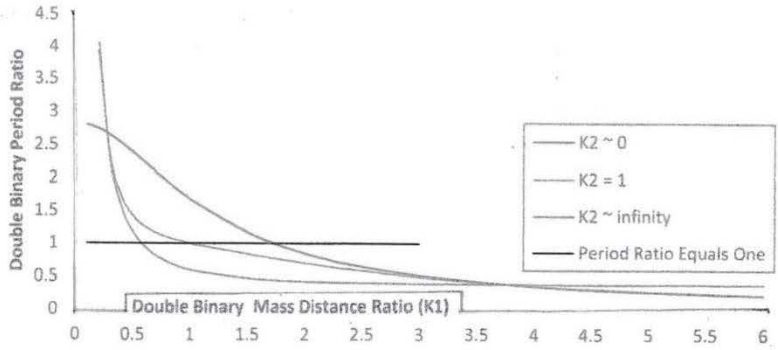

FIGURE 4.1.2.1. Orthogonal Double Binary Configuration Space

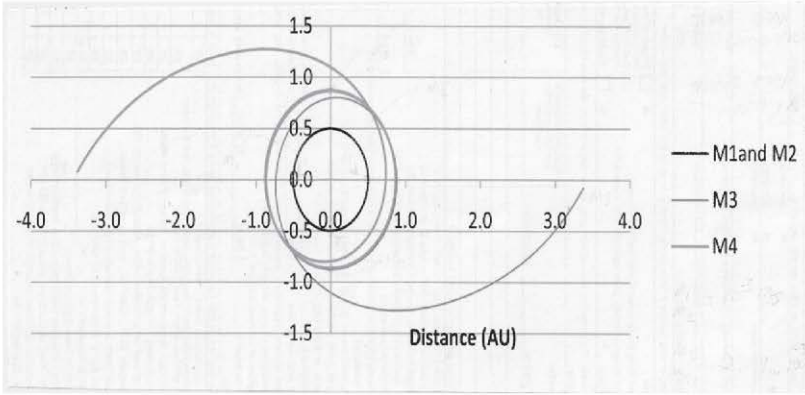

FIGURE 4.1.2.2. Orthogonal Double Binary Lagrange Configuration

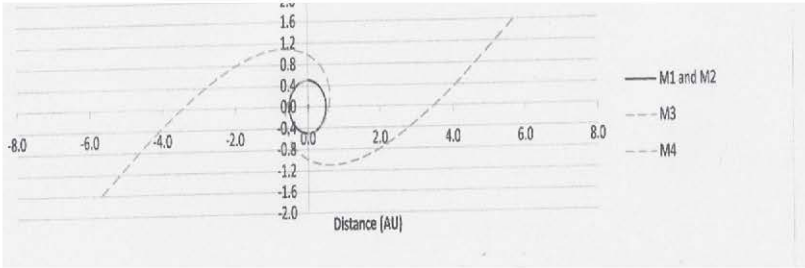

Figure 4.1.2.3. Orthogonal Double Binary Configuration ($k_1 = 1, m_3 = m_4 \to 0$)

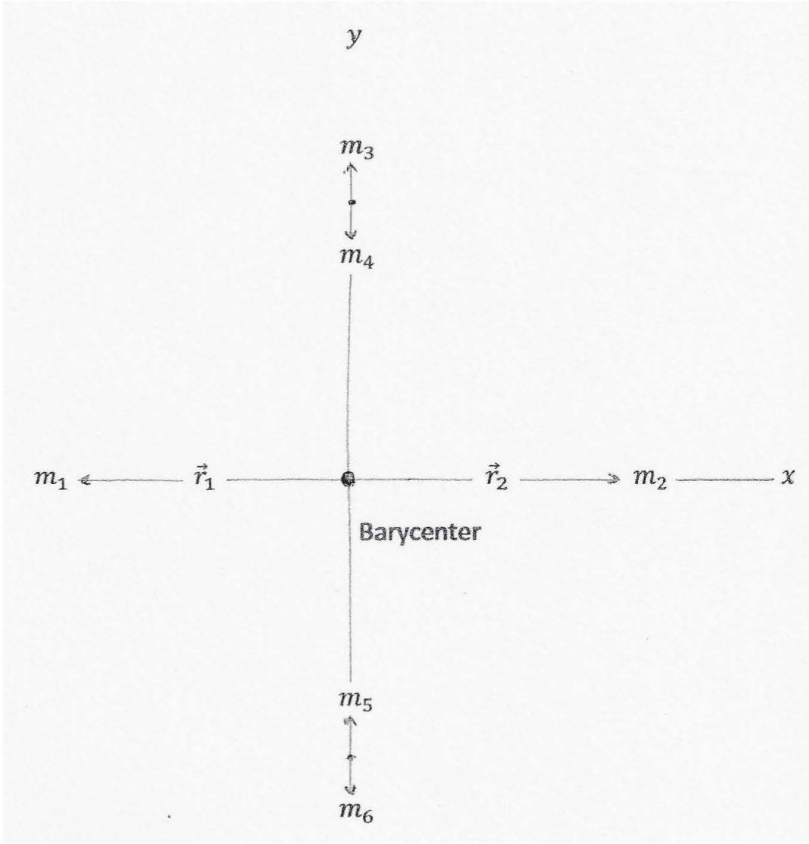

FIGURE 4.2.1. Orthogonal Triple Binary Configuration Geometry

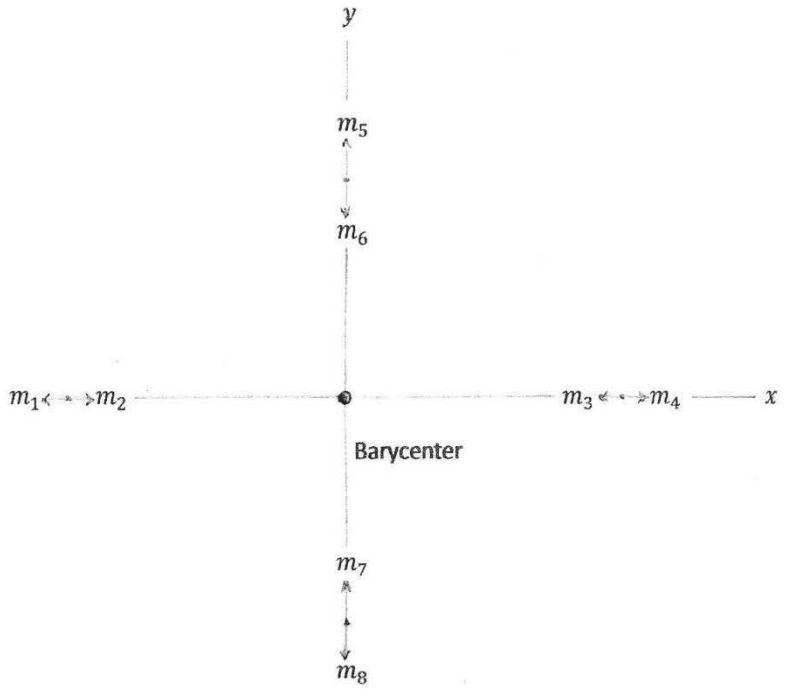

FIGURE 4.3. Orthogonal Quadruple Binary Configuration Geometry

4.4 Problems

Section 4.1

1. Starting from equation 4.1.1, derive the instantaneous restricted double binary velocities V_r and V_ρ shown in equations 4.1.3 and 4.1 4. Also verify the double binary state vector in equation 4.1.5.
2. Substituting equations 4.1.3 and 4.1.4 into the kinetic energy equation verify that the double binary configuration is consistent with conservation of energy where twice the kinetic energy is equal to the potential energy at time zero.
3. Map from double binary configuration space the central configuration $(k_1 = k_2 = \frac{P_r}{P_\rho} = 1)$ into phase space, that is, compute the central configuration state vector.
4. Construct a finite stability plot of D_r (y-axis) versus D_ρ (x-axis) where the range of parameter D_r is $0 < D_r < 1$ and the range of parameter D_ρ

is $0 < D_\rho < 1$. Include the period ratio $\frac{P_r}{P_\rho} = 1$ in this plot. Will help to plot lines of constant k_2. Can any conclusions be drawn from plotting finite stability.

5. Expand the scalar form of the Jacoby accelerations listed in equation 4.1.4.2 in a Taylor series to verify equation 4.1.4.3 for the linear approximation. Resulting Taylor series expansion coefficients a_{ij} may not be in the same form as in equation 4.1.4.3.
6. Further expand equation 4.1.4.2 in a Taylor series to compute the quadratic and cubic terms of the restricted double binary to verify equation 4.1.4.10.
7. Since a second order differential equation can be written as two first order differential equations solve the eigenvalue problem setup in equation 4.1.4.4 to verify the first order approximation solution shown in equation 4.1.4.7.
8. Double binary periods and inertial velocities derived from the infinitesimal interval problem allow the lambda exponents in equation 4.1.4.7 to be written as a function of angular velocity where $\lambda_1 = aw_r = bw_\rho$. Find a and b as shown in 4.1.4.9.
9. Integrate the r and ρ restricted double binary acceleration equations valid for all time in equation 4.1.4.11 and show that they are consistent with conservation of energy where twice the kinetic energy is equal to the potential energy. Note that $\frac{d\theta}{dr} = \frac{\dot{\theta}}{\dot{r}}$ and $\frac{d\theta}{d\rho} = \frac{\dot{\theta}}{\dot{\rho}}$.
10. Using conservation of energy show that equation 4.1.5.5 is the end result when applying the inverse problem of dynamics.

Section 4.2

1. Determine the inertial velocity V_ρ by using the z_{65c} center of gravity relation in equation 4.2.1 instead of the z_{43c} center of gravity relation. Verify the velocity result is the same as found in equation 4.2.2.
2. The triple binary state vector in equation 4.2.3 is formulated to have the vector $\vec{\rho}$ rotating inplane. Rewrite equation 4.2.3 for the case where $\vec{\rho}$ rotates out of plane.
3. The triple-binary velocities in equation 4.2.1.2 when substituted into the kinetic energy equation 4.2.1.1 will be equal to the potential energy. Mathematically verify that this is true. See equation 4.2.1.3.
4. Triple binary configuration space can be determined by scaling period ratios found in equation 4.2.2.1. Using $k_1, k_2, \ldots, k_4$ rewrite equation

4.2.2.1 to verify equation 4.2.2.2. Consider the case where k_1 is large and k_3, $k_4 \to 0$. Could this configuration be finite stable.

5. What is the period ratio result when $k_4 \to 0$ for $\frac{P_\tau^2}{P_\rho^2}$ in equation 4.2.2.2? How does it compare to the double binary configuration period ratio in equation 4.1.2.1?
6. Plot $\frac{P_\tau}{P_\rho}$ versus k_1 using lines of constant k_4. How does this plot compare to the double binary graph of $\frac{P_\tau}{P_\rho}$ versus k_1 with lines of constant k_2?

Section 4.3

1. Derive V_{ρ_1} using the center of gravity z_{43c} equation. That is, supply the missing equations that lead to the inertial velocity V_{ρ_1} of the first double binary subsystem in equation 4.3.1.
2. Reformulate the two-dimensional quadruple binary state vector in equation 4.3.3 to represent a three-dimensional orbital configuration.
3. Mathematically verify that the solution of the quadruple binary is consistent with conservation of energy. Show that equation 4.3.1.1 is equal to the potential energy.
4. Using equation 4.3.2.1 determine the configuration space period ratios for the quadruple binary in terms of scaled parameters k_1, k_2,…,k_n in similar format as that of equation 4.2.2.2.

4.5 References

Besant, W. H., Ramsey, A. S., 1914, *A Treatise on Dynamics*, London, Bell and Sons.

Boccaletti, D., Pucacco, G., 1996, Theory of Orbits, Berlin, Springer Verlag.

Diacu, F. N., 1992, *Singularities of the N-Body Problem-An Introduction to Celestial Mechanics,* Montreal, Les Publications CRM.

Galiullin, A. S., 1984., *Inverse Problem of Dynamics*, Moscow, MIR Publishers.

Lass, H., 1957, *Elements of Pure and Applied Mathematics*, New York, McGraw-Hill.

Lehnigh, S. H., 1966., *Stability Theorems for Linear Motions with an Introductions to Liapunov's Direct Method,* Englewood Cliffs, NJ, Prentice Hall.

Marchal, C. 2000. The Family P12 of the Three-body Problem- The Simplest Family of Periodic Orbits, with Twelve Symmetries per Period. *CMDA* 78.

Merkin, D. R., 1996, *Introduction to the Theory of Stability*, New York, Springer Verlag.

Pollard, H., 1966, *Mathematical Introduction to Celestial Mechanics*, Englewood Cliffs, NJ, Prentice Hall.

Ramsey, A. S., 1929, *Dynamics*, London, Cambridge at the University Press.

Routh, E. J. 1877, *A Treatise on the Stability of a Given State of Motion*, UK, MacMillan and Company.

Roy, A. E. Ovenden, M. W. 1955. On the Occurrence of Commensurable Mean Motions in the Solar System II–The Mirror Theorem. *Mon., Not., Roy., Astr., Soc.*

Santilli, R. M., 1978., *Foundations of Theoretical Mechanics I-The inverse Problem in Newtonian Mechanics*, New York, Springer-Verlag,

Szebehely, V. G., 1967, *Theory of Orbits*, New York, Academic Press.

Wintner, A., 1964, *The Analytical Foundations of Celestial Mechanics*, Princeton NJ, Princeton University Press.

APPENDIX A

COLLINEAR CONFIGURATIONS ORBITING L4 AND L5 LAGRANGE LOCATIONS

Analyzing the problem of placing binary collinear structures into orbit about the L4 and L5 points individually, where the L4 and L5 position is treated as a pseudo mass location. Purpose is to derive state vectors to determine if finite stable orbits exist for these configurations, thus verifying collinear configurations at time zero can reside at the L4 and L5 points. Techniques developed in chapters one and two with basic classical mechanics will be used in structuring and solving this type of problem. The L4 and L5 binary configurations are aligned along the vector starting from the barycenter to the respective L4 and L5 Lagrange equilibrium point. The barycenter exists anywhere along the line from mass one to the halfway point between mass one and mass two depending on the mass two to mass one ratio. Due to assumptions made in this analysis, such as not solving for the inertial velocities directly from the equations of motion within the infinitesimal interval, conservation of energy will not be maintained. Structural analysis is worked in two parts, where the state vector is derived directly from the rotating binary mass configuration in the first part and then the binary velocities are corrected using the equations of motion in the second part.

A.1 Single Binary in Orbit about the L4 and L5 Location

The first case worked is a single binary at the L4 and L5 location composing a six-mass configuration. Geometry for this configuration is illustrated in figure A1. Binary mass position vector equations relative to the barycenter are in terms of Jacoby coordinates $\vec{r}$, $\vec{r}_{43}$ and $\vec{r}_{65}$ with $\vec{r} = \overrightarrow{r_2} - \overrightarrow{r_1}$, $\vec{r}_{43} = \overrightarrow{r_4} - \overrightarrow{r_3}$ and $\vec{r}_{65} = \overrightarrow{r_6} - \overrightarrow{r_5}$. The barycenter location is defined by position vectors $\overrightarrow{r_1}$ and $\overrightarrow{r_2}$ and their respective masses. Expanding the geometry in figure A1 by diagraming the rotating binary structure in terms of position and velocity vectors to compute the components of the L4 and L5 binary configuration, will need to consider working the inverse problem of dynamics. That is, the forces are determined by the given properties of

their motion using position, velocity, acceleration and other constraints to solve the problem. The L4 and L5 single binary structured planar state vector at time zero has been derived under these stated conditions and is found below. Coordinate system for this state vector is barycentric inertial. All binaries are rotating counterclockwise.

First Binary

$$x_1 = -\frac{m_2+\mu_{43}}{\mu+2\mu_{43}}r \qquad \dot{x}_1 = 0 \qquad \text{Equation A1.1}$$

$$y_1 = 0 \qquad \dot{y}_1 = -\frac{m_2+\mu_{43}}{\mu+2\mu_{43}}V_r$$

$$x_2 = \frac{m_1+\mu_{43}}{\mu+2\mu_{43}}r \qquad \dot{x}_2 = 0$$

$$y_2 = 0 \qquad \dot{y}_2 = \frac{m_1+\mu_{43}}{\mu+2\mu_{43}}V_r$$

Second Binary

$$x_3 = \frac{\alpha}{2}r + \alpha\beta\frac{m_4}{\mu_{43}}r_{43} \qquad \dot{x}_3 = -\frac{\sqrt{3}}{2}V_r - \sqrt{3}\beta\frac{m_4}{\mu_{43}}V_{r_{43}}$$

$$y_3 = \frac{\sqrt{3}}{2}r + \sqrt{3}\beta\frac{m_4}{\mu_{43}}r_{43} \qquad \dot{y}_3 = \frac{\alpha}{2}V_r + \alpha\beta\frac{m_4}{\mu_{43}}V_{r_{43}}$$

$$x_4 = \frac{\alpha}{2}r - \alpha\beta\frac{m_3}{\mu_{43}}r_{43} \qquad \dot{x}_4 = -\frac{\sqrt{3}}{2}V_r + \sqrt{3}\beta\frac{m_3}{\mu_{43}}V_{r_{43}}$$

$$y_4 = \frac{\sqrt{3}}{2}r - \sqrt{3}\beta\frac{m_3}{\mu_{43}}r_{43} \qquad \dot{y}_4 = \frac{\alpha}{2}V_r - \alpha\beta\frac{m_3}{\mu_{43}}V_{r_{43}}$$

Third Binary

$$x_5 = \frac{\alpha}{2}r - \alpha\beta\frac{m_6}{\mu_{65}}r_{65} \qquad \dot{x}_5 = \frac{\sqrt{3}}{2}V_r - \sqrt{3}\beta\frac{m_6}{\mu_{65}}V_{r_{65}}$$

$$y_5 = -\frac{\sqrt{3}}{2}r + \sqrt{3}\beta\frac{m_6}{\mu_{65}}r_{65} \qquad \dot{y}_5 = \frac{\alpha}{2}V_r - \alpha\beta\frac{m_6}{\mu_{65}}V_{r_{65}}$$

$$x_6 = \frac{\alpha}{2}r + \alpha\beta\frac{m_5}{\mu_{65}}r_{65} \qquad \dot{x}_6 = \frac{\sqrt{3}}{2}V_r + \sqrt{3}\beta\frac{m_5}{\mu_{65}}V_{r_{65}}$$

$$y_6 = -\frac{\sqrt{3}}{2}r - \sqrt{3}\beta\frac{m_5}{\mu_{65}}r_{65} \qquad \dot{y}_6 = \frac{\alpha}{2}V_r + \alpha\beta\frac{m_5}{\mu_{65}}V_{r_{65}}$$

where $\alpha = \frac{m_1 - m_2}{\theta}$, $\theta = \sum_i^6 m_i$ and $\beta = (3 + \alpha^2)^{-1/2}$.

Velocities V_r, $V_{r_{43}}$ and $V_{r_{65}}$ in the above L4 and L5 binary state vector are not known in terms of their interactive mass perturbations. From the collinear equations of motion velocity magnitude is estimated in the infinitesimal interval with type one geometry and the sidereal synodic relations at time zero. Equations of motion for this six-mass configuration in the complex plane with the sidereal synodic relations are

$$n_{21}P_{21} = (n_{21} + n_\rho)P_\rho = (n_{21} + n_\rho + n_{43})P_{43} = (n_{21} + n_\rho + n_{65})P_{65}$$

Equation A1.2

$$-w^2 Z = -\frac{G\mu}{r^3}Z + \frac{G m_3}{r_{32}^3}Z_{32} - \frac{G m_3}{r_{31}^3}Z_{31} + \frac{G m_4}{r_{42}^3}Z_{42} - \frac{G m_4}{r_{41}^3}Z_{41} + \frac{G m_5}{r_{52}^3}Z_{52} - \frac{G m_5}{r_{51}^3}Z_{51} + \frac{G m_6}{r_{62}^3}Z_{62} - \frac{G m_6}{r_{61}^3}Z_{61}$$

$$\ddot{z}_{43} + 2wi\dot{z}_{43} - w^2 Z_{43} = -\frac{G\mu_{43}}{r_{43}^3}Z_{43} + \frac{G m_1}{r_{41}^3}Z_{14} - \frac{G m_1}{r_{31}^3}Z_{13} + \frac{G m_2}{r_{42}^3}Z_{24} - \frac{G m_2}{r_{32}^3}Z_{23} + \frac{G m_5}{r_{54}^3}Z_{54} - \frac{G m_5}{r_{53}^3}Z_{53} + \frac{G m_6}{r_{64}^3}Z_{64} - \frac{G m_6}{r_{63}^3}Z_{63}$$

$$\ddot{z}_{65} + 2wi\dot{z}_{65} - w^2 Z_{65} = -\frac{G\mu_{65}}{r_{65}^3}Z_{65} + \frac{G m_1}{r_{61}^3}Z_{16} - \frac{G m_1}{r_{51}^3}Z_{15} + \frac{G m_2}{r_{62}^3}Z_{26} - \frac{G m_2}{r_{52}^3}Z_{25} + \frac{G m_3}{r_{63}^3}Z_{36} - \frac{G m_3}{r_{53}^3}Z_{35} + \frac{G m_4}{r_{64}^3}Z_{46} - \frac{G m_4}{r_{54}^3}Z_{45}$$

where $\mu = m_1 + m_2$ $\mu_{43} = m_3 + m_4$ $\mu_{65} = m_5 + m_6$

The first binary composed of mass one and mass two is on the rotating x' axis and therefore $\ddot{z} = \dot{z} = 0$. Simplifying the equation format in A1.3 to compute perturbation coefficients and binary velocities gives the result

$$(\rho_{21}\mu - 1)z = (\rho_{32}z_{32} - \rho_{31}z_{31})m_3 + (\rho_{42}z_{42} - \rho_{41}z_{41})m_4 + (\rho_{52}z_{52} - \rho_{51}z_{51})m_5 + (\rho_{62}z_{62} - \rho_{61}z_{61})m_6$$

$$\left(\rho_{43}\mu_{43} - \frac{P_{21}^2}{P_{43}^2}\right)z_{43} = (\rho_{41}z_{14} - \rho_{31}z_{13})m_1 + (\rho_{42}z_{24} - \rho_{32}z_{23})m_2 + (\rho_{45}z_{54} - \rho_{35}z_{53})m_5 + (\rho_{46}z_{64} - \rho_{36}z_{63})m_6$$

$$\left(\rho_{65}\mu_{65} - \frac{P_{21}^2}{P_{65}^2}\right) z_{65} = (\rho_{61}z_{16} - \rho_{51}z_{15})m_1 + (\rho_{62}z_{26} - \rho_{52}z_{25})m_2$$

$$+(\rho_{63}z_{36} - \rho_{53}z_{35})m_3 + (\rho_{64}z_{46} - \rho_{54}z_{45})m_4$$

where $\rho_{ij} = \frac{G}{w^2 r_{ij}^3}$ Equation A1.3

Equations A1.2 and A1.3 have treated the binaries at the L4 and L5 locations as a n-body collinear configuration, where z, z_{43} and z_{65} will divide out of their respective equation of motion allowing a calculation of the perturbation coefficients and velocities. This will not happen for this problem in general due to $\vec{r}_{43}$ and $\vec{r}_{65}$ not being aligned with the vector between the L4 and L5 points. The only way these vectors will align is when mass one is equal to mass two. Therefore, approximations must be made to remedy this situation. Assuming the following conditions where each binary distance approaches zero and z_{43} aligns with z_{65}, the perturbation coefficient and binary velocity problem will be resolved. Restrictions made on binary mass and distance are listed below

$$m_3 = m_6 \quad m_4 = m_5 \quad \mu_{43} = \mu_{65} \quad x_1 = x_2 \qquad \text{Equation A1.4}$$

$$\frac{r_{43}}{r} = \frac{r_{65}}{r} \to 0 \qquad \rho_{31} = \rho_{41} = \rho_{51} = \rho_{61}$$

$$\rho_{32} = \rho_{42} = \rho_{52} = \rho_{62} \qquad \rho_{53} = \rho_{54} = \rho_{63} = \rho_{64}$$

Mass position vectors and mass position difference vectors are also needed to derive the binary velocities in equation A1.3. The mass position vector equations relative to the barycenter from the geometry illustrated in figure A1 can be found listed below

$$\vec{r}_1 = \frac{m_1 - m_2 - \theta}{2\theta}\vec{r} \qquad \vec{r}_2 = \frac{m_1 - m_2 + \theta}{2\theta}\vec{r} \qquad \text{Equation A1.5}$$

$$\vec{r}_3 = \frac{m_1 - m_2}{2\theta}\vec{r} - \frac{m_4}{\mu_{43}}\vec{r}_{43} - \frac{1}{2}\vec{\rho}$$

$$\vec{r}_4 = \frac{m_1 - m_2}{2\theta}\vec{r} + \frac{m_3}{\mu_{43}}\vec{r}_{43} - \frac{1}{2}\vec{\rho}$$

$$\vec{r}_5 = \frac{m_1 - m_2}{2\theta}\vec{r} - \frac{m_6}{\mu_{65}}\vec{r}_{65} + \frac{1}{2}\vec{\rho}$$

$$\vec{r}_6 = \frac{m_1 - m_2}{2\theta}\vec{r} + \frac{m_5}{\mu_{65}}\vec{r}_{65} + \frac{1}{2}\vec{\rho}$$

where $\theta = \sum_i^6 m_i$. Mass one is the dominant mass with mass one greater or equal to mass two. Using the mass position vectors from equation A1.5, the binary mass position difference equations in terms of the Jacoby coordinates $\vec{r}$, $\vec{r}_{43}$, $\vec{r}_{65}$ and $\vec{\rho}$ are determined by Equation A1.6 below

$$\vec{r}_{31} = \frac{1}{2}\vec{r} - \frac{m_4}{\mu_{43}}\vec{r}_{43} - \frac{1}{2}\vec{\rho} \qquad \vec{r}_{41} = \frac{1}{2}\vec{r} + \frac{m_3}{\mu_{43}}\vec{r}_{43} - \frac{1}{2}\vec{\rho}$$

$$\vec{r}_{32} = -\frac{1}{2}\vec{r} - \frac{m_4}{\mu_{43}}\vec{r}_{43} - \frac{1}{2}\vec{\rho} \qquad \vec{r}_{42} = -\frac{1}{2}\vec{r} + \frac{m_3}{\mu_{43}}\vec{r}_{43} - \frac{1}{2}\vec{\rho}$$

$$\vec{r}_{51} = \frac{1}{2}\vec{r} - \frac{m_6}{\mu_{65}}\vec{r}_{65} + \frac{1}{2}\vec{\rho} \qquad \vec{r}_{53} = \frac{m_4}{\mu_{43}}\vec{r}_{43} - \frac{m_6}{\mu_{65}}\vec{r}_{65} + \vec{\rho}$$

$$\vec{r}_{52} = -\frac{1}{2}\vec{r} - \frac{m_6}{\mu_{65}}\vec{r}_{65} + \frac{1}{2}\vec{\rho} \qquad \vec{r}_{54} = -\frac{m_3}{\mu_{43}}\vec{r}_{43} - \frac{m_6}{\mu_{65}}\vec{r}_{65} + \vec{\rho}$$

$$\vec{r}_{61} = \frac{1}{2}\vec{r} + \frac{m_5}{\mu_{65}}\vec{r}_{65} + \frac{1}{2}\vec{\rho} \qquad \vec{r}_{63} = \frac{m_4}{\mu_{43}}\vec{r}_{43} + \frac{m_5}{\mu_{65}}\vec{r}_{65} + \vec{\rho}$$

$$\vec{r}_{62} = -\frac{1}{2}\vec{r} + \frac{m_5}{\mu_{65}}\vec{r}_{65} + \frac{1}{2}\vec{\rho} \qquad \vec{r}_{64} = -\frac{m_3}{\mu_{43}}\vec{r}_{43} + \frac{m_5}{\mu_{65}}\vec{r}_{65} + \vec{\rho}$$

Substituting equations A1.4 and A1.6 into equation A1.3 yields an approximate velocity and perturbation coefficient result

$$(\rho_{21}\mu - 1)z = -\rho_{32}m_3 z - \rho_{31}m_3 z - \rho_{42}m_4 z - \rho_{41}m_4 z \quad \text{Equation A1.7}$$

$$V_r^2 = \frac{G(\mu - \phi_1)}{r} \qquad \phi_1 = \frac{r^3}{r_{31}^3}m_3 + \frac{r^3}{r_{32}^3}m_3 + \frac{r^3}{r_{41}^3}m_4 + \frac{r^3}{r_{42}^3}m_4$$

$$\left(\rho_{43}\mu_{43} - \frac{P_{21}^2}{P_{43}^2}\right)z_{43} = -\rho_{41}m_1 z_{43} - \rho_{42}m_2 z_{43} - \rho_{54}m_5 z_{43} - \rho_{64}m_6 z_{43}$$

$$V_{r_{43}}^2 = \frac{G(\mu_{43} - x_1^3\phi_2)}{r_{43}} \qquad r_{43} = x_1 r \qquad \phi_2 = \frac{r^3}{r_{41}^3}m_1 + \frac{r^3}{r_{42}^3}m_2 + \frac{r^3}{r_{54}^3}m_5 + \frac{r^3}{r_{64}^3}m_6$$

$$\left(\rho_{65}\mu_{65} - \frac{P_{21}^2}{P_{65}^2}\right)z_{65} = -\rho_{61}m_1 z_{65} - \rho_{62}m_2 z_{65} - \rho_{63}m_3 z_{65} - \rho_{64}m_4 z_{65}$$

$$V_{r_{65}}^2 = \frac{G(\mu_{65} - x_2^3\phi_3)}{r_{65}} \qquad r_{65} = x_2 r \qquad \phi_3 = \frac{r^3}{r_{61}^3}m_1 + \frac{r^3}{r_{62}^3}m_2 + \frac{r^3}{r_{63}^3}m_3 + \frac{r^3}{r_{64}^3}m_4$$

velocities V_{43} and V_{65} are equal.

From the state vector equation A1.1 and the mass position difference definition r_{ij}, the ratio $\frac{r_{ij}}{r}$ can be evaluated to determine the perturbation coefficients and velocities derived in equation A1.7

$$r_{31} = ((x_3 - x_1)^2 + (y_3 - y_1)^2)^{1/2}$$

$$r_{32} = ((x_3 - x_2)^2 + (y_3 - y_2)^2)^{1/2}$$

. . .

$$r_{64} = ((x_6 - x_4)^2 + (y_6 - y_4)^2)^{1/2}$$

the above equations yield

$$\frac{r_{31}}{r} = (1 + (3 + \alpha)\beta\frac{m_4}{\mu_{43}}x_1 + (\frac{m_4}{\mu_{43}}x_1)^2)^{1/2} \quad \text{Equation A1.8}$$

$$\frac{r_{32}}{r} = (1 + (3 - \alpha)\beta\frac{m_4}{\mu_{43}}x_1 + (\frac{m_4}{\mu_{43}}x_1)^2)^{1/2}$$

$$\frac{r_{41}}{r} = (1 - (3 + \alpha)\beta\frac{m_3}{\mu_{43}}x_1 + (\frac{m_3}{\mu_{43}}x_1)^2)^{1/2}$$

$$\frac{r_{42}}{r} = (1 - (3 - \alpha)\beta\frac{m_3}{\mu_{43}}x_1 + (\frac{m_3}{\mu_{43}}x_1)^2)^{1/2}$$

$$\frac{r_{51}}{r} = (1 - (3 + \alpha)\beta\frac{m_6}{\mu_{65}}x_2 + (\frac{m_6}{\mu_{65}}x_2)^2)^{1/2}$$

$$\frac{r_{52}}{r} = (1 - (3 - \alpha)\beta\frac{m_6}{\mu_{65}}x_2 + (\frac{m_6}{\mu_{65}}x_2)^2)^{1/2}$$

$$\frac{r_{53}}{r} = ((\sqrt{3} - \frac{\sqrt{3}}{\mu_{65}}\beta x_2(m_6 - m_5))^2 + \alpha^2\beta^2x_2^2)^{1/2}$$

$$\frac{r_{54}}{r} = \sqrt{3} - 2\sqrt{3}\beta\frac{m_6}{\mu_{65}}x_2$$

$$\frac{r_{61}}{r} = (1 + (3 + \alpha)\beta\frac{m_5}{\mu_{65}}x_2 + (\frac{m_5}{\mu_{65}}x_2)^2)^{1/2}$$

$$\frac{r_{62}}{r} = (1 + (3 - \alpha)\beta\frac{m_5}{\mu_{65}}x_2 + (\frac{m_5}{\mu_{65}}x_2)^2)^{1/2}$$

$$\frac{r_{63}}{r} = \sqrt{3} + 2\sqrt{3}\beta\frac{m_5}{\mu_{65}}x_2$$

$$\frac{r_{64}}{r} = ((\sqrt{3} - \frac{\sqrt{3}}{\mu_{65}}\beta x_2(m_6 - m_5))^2 + \alpha^2\beta^2 x_2^2)^{1/2}$$

Equation A1.7 velocities V_r, $V_{r_{43}}$ and $V_{r_{65}}$ computed using the distance ratios in equation A1.8 give the final quantities needed to do numerically integration of the L4 and L5 binary state vector in equation A1.1.

The distance between the center of gravity of the mass three four binary and the center of gravity of the mass five six binary has been approximated to be $\rho = \sqrt{3}r$ for the problem analyzed above. This is the value that was determined from the restricted three-body problem for zero mass at the equilibrium positions. However, It appears that for non-zero mass binaries at the L4 and L5 locations, the equilibrium regions may migrate away from $\rho = \sqrt{3}r$. This situation was noted to have occurred in chapter four 4.2.2.

It appears from this analysis that any geometry in the mathematical logical system may be incorporated at the L4 and L5 equilibrium points to produce a state vector to numerically integrate for studying particle motion. To give credibility to this conclusion a double binary configuration has been embedded at the L4 and L5 points and a state vector for this system has been successfully derived and numerically integrated. This problem will be presented in the next part of the appendix.

A.2 Double Binary in Orbit about the L4 and L5 Location

The L4 and L5 double binary problem is solved in the same manner as the single binary configuration, that is, using the inverse problem of dynamics with type one geometry and the sidereal synodic relations in the collinear infinitesimal interval at time zero. Configuration geometry can be found in figure A2. As seen in figure A2 the vector geometry is more complex with the addition of the extra binary at each equilibrium location. For example, there are other rotating vectors ($\vec{\rho}_1$ and, $\vec{\rho}_2$) in the double binary configuration to consider in formulating the double binary motion. These vectors extend between the binary centers of gravity for each double binary configuration at the L4 and L5 locations. This situation was encountered in chapter one where the collinear double binary problem was solved. The difference here is that this double binary problem is an approximate solution and not a deterministic solution. Double binary mass equations of motion are in terms of Jacoby coordinates $\vec{r}$, $\vec{r}_{43}$, $\vec{r}_{65}$, $\vec{r}_{87}$, $\vec{r}_{10,9}$, $\vec{\rho}_1$ and, $\vec{\rho}_2$ relative to the barycenter in the infinitesimal interval at time zero. Ten-body state vector is derived in the first part analysis for the double

binary L4 and L5 configuration and is given by individual binary below. State vector coordinate system is barycentric inertial. All binaries in the double binary configurations at the L4 and L5 locations are rotating counterclockwise.

First Binary

$$x_1 = -\frac{m_2+\mu_{43}+\mu_{65}}{\mu+2\mu_{43}+2\mu_{65}}r \qquad \dot{x}_1 = 0 \qquad \text{Equation A2.1}$$

$$y_1 = 0 \qquad \dot{y}_1 = -\frac{m_2+\mu_{43}+\mu_{65}}{\mu+2\mu_{43}+2\mu_{65}}V_r$$

$$x_2 = \frac{m_1+\mu_{43}+\mu_{65}}{\mu+2\mu_{43}+2\mu_{65}}r \qquad \dot{x}_2 = 0$$

$$y_2 = 0 \qquad \dot{y}_2 = \frac{m_1+\mu_{43}+\mu_{65}}{\mu+2\mu_{43}+2\mu_{65}}V_r$$

Second Binary

$$x_3 = \frac{\alpha}{2}r + \alpha\beta\frac{m_4}{\mu_{43}}r_{43} + \alpha\beta\frac{\mu_{65}}{\mu_{\rho_1}}\rho_1 \qquad \dot{x}_3 = -\frac{\sqrt{3}}{2}V_r - \sqrt{3}\beta\frac{m_4}{\mu_{43}}V_{r_{43}} - \sqrt{3}\beta\frac{\mu_{65}}{\mu_{\rho_1}}V_{\rho 1}$$

$$y_3 = \frac{\sqrt{3}}{2}r + \sqrt{3}\beta\frac{m_4}{\mu_{43}}r_{43} + \sqrt{3}\beta\frac{\mu_{65}}{\mu_{\rho_1}}\rho_1 \qquad \dot{y}_3 = \frac{\alpha}{2}V_r + \alpha\beta\frac{m_4}{\mu_{43}}V_{43} + \alpha\beta\frac{\mu_{65}}{\mu_{\rho_1}}V_{\rho 1}$$

$$x_4 = \frac{\alpha}{2}r - \alpha\beta\frac{m_3}{\mu_{43}}r_{43} + \alpha\beta\frac{\mu_{65}}{\mu_{\rho_1}}\rho_1 \qquad \dot{x}_4 = -\frac{\sqrt{3}}{2}V_r + \sqrt{3}\beta\frac{m_3}{\mu_{43}}V_{r_{43}} - \sqrt{3}\beta\frac{\mu_{65}}{\mu_{\rho_1}}V_{\rho 1}$$

$$y_4 = \frac{\sqrt{3}}{2}r - \sqrt{3}\beta\frac{m_3}{\mu_{43}}r_{43} + \sqrt{3}\beta\frac{\mu_{65}}{\mu_{\rho_1}}\rho_1 \qquad \dot{y}_4 = \frac{\alpha}{2}V_r - \alpha\beta\frac{m_3}{\mu_{43}}V_{43} + \alpha\beta\frac{\mu_{65}}{\mu_{\rho_1}}V_{\rho 1}$$

Third Binary

$$x_5 = \frac{\alpha}{2}r + \alpha\beta\frac{m_6}{\mu_{65}}r_{65} - \alpha\beta\frac{\mu_{43}}{\mu_{\rho_1}}\rho_1 \qquad \dot{x}_5 = -\frac{\sqrt{3}}{2}V_r - \sqrt{3}\beta\frac{m_6}{\mu_{65}}V_{r_{65}} + \sqrt{3}\beta\frac{\mu_{43}}{\mu_{\rho_1}}V_{\rho 1}$$

$$y_5 = \frac{\sqrt{3}}{2}r + \sqrt{3}\beta\frac{m_6}{\mu_{65}}r_{65} - \sqrt{3}\beta\frac{\mu_{43}}{\mu_{\rho_1}}\rho_1 \qquad \dot{y}_5 = \frac{\alpha}{2}V_r + \alpha\beta\frac{m_6}{\mu_{65}}V_{r_{65}} - \alpha\beta\frac{\mu_{43}}{\mu_{\rho_1}}V_{\rho 1}$$

$$x_6 = \frac{\alpha}{2}r - \alpha\beta\frac{m_5}{\mu_{65}}r_{65} - \alpha\beta\frac{\mu_{43}}{\mu_{\rho_1}}\rho_1 \qquad \dot{x}_6 = -\frac{\sqrt{3}}{2}V_r + \sqrt{3}\beta\frac{m_5}{\mu_{65}}V_{r_{65}} + \sqrt{3}\beta\frac{\mu_{43}}{\mu_{\rho_1}}V_{\rho 1}$$

$$y_6 = \frac{\sqrt{3}}{2}r - \sqrt{3}\beta\frac{m_5}{\mu_{65}}r_{65} - \sqrt{3}\beta\frac{\mu_{43}}{\mu_{\rho_1}}\rho_1 \qquad \dot{y}_6 = \frac{\alpha}{2}V_r - \alpha\beta\frac{m_5}{\mu_{65}}V_{r_{65}} - \alpha\beta\frac{\mu_{43}}{\mu_{\rho_1}}V_{\rho 1}$$

Fourth Binary

$$x_7 = \frac{\alpha}{2}r - \alpha\beta\frac{m_8}{\mu_{87}}r_{87} - \alpha\beta\frac{\mu_{10,9}}{\mu_{\rho_1}}\rho_1 \qquad \dot{x}_7 = \frac{\sqrt{3}}{2}V_r - \sqrt{3}\beta\frac{m_8}{\mu_{87}}V_{r_{87}} - \sqrt{3}\beta\frac{\mu_{10,9}}{\mu_{\rho_1}}V_{\rho 1}$$

$$y_7 = -\frac{\sqrt{3}}{2}r + \sqrt{3}\beta\frac{m_8}{\mu_{87}}r_{87} + \sqrt{3}\beta\frac{\mu_{10,9}}{\mu_{\rho_1}}\rho_1 \qquad \dot{y}_7 = \frac{\alpha}{2}V_r - \alpha\beta\frac{m_8}{\mu_{87}}V_{r_{87}} - \alpha\beta\frac{\mu_{10,9}}{\mu_{\rho_1}}V_{\rho 1}$$

$$x_8 = \frac{\alpha}{2}r + \alpha\beta\frac{m_7}{\mu_{87}}r_{87} - \alpha\beta\frac{\mu_{10,9}}{\mu_{\rho_1}}\rho_1 \qquad \dot{x}_8 = \frac{\sqrt{3}}{2}V_r + \sqrt{3}\beta\frac{m_7}{\mu_{87}}V_{r_{87}} - \sqrt{3}\beta\frac{\mu_{10,9}}{\mu_{\rho_1}}V_{\rho 1}$$

$$y_8 = -\frac{\sqrt{3}}{2}r - \sqrt{3}\beta\frac{m_7}{\mu_{87}}r_{87} + \sqrt{3}\beta\frac{\mu_{10,9}}{\mu_{\rho_1}}\rho_1 \qquad \dot{y}_8 = \frac{\alpha}{2}V_r + \alpha\beta\frac{m_7}{\mu_{87}}V_{r_{87}} - \alpha\beta\frac{\mu_{10,9}}{\mu_{\rho_1}}V_{\rho 1}$$

Fifth Binary

$$x_9 = \frac{\alpha}{2}r - \alpha\beta\frac{m_{10}}{\mu_{10,9}}r_{10,9} + \alpha\beta\frac{\mu_{87}}{\mu_{\rho_1}}\rho_1 \qquad \dot{x}_9 = \frac{\sqrt{3}}{2}V_r - \sqrt{3}\beta\frac{m_{10}}{\mu_{10,9}}V_{r_{10,9}} + \sqrt{3}\beta\frac{\mu_{87}}{\mu_{\rho_1}}V_{\rho 1}$$

$$y_9 = -\frac{\sqrt{3}}{2}r + \sqrt{3}\beta\frac{m_{10}}{\mu_{10,9}}r_{10,9} - \sqrt{3}\beta\frac{\mu_{87}}{\mu_{\rho_1}}\rho_1 \qquad \dot{y}_9 = \frac{\alpha}{2}V_r - \alpha\beta\frac{m_{10}}{\mu_{10,9}}V_{r_{10,9}} + \alpha\beta\frac{\mu_{87}}{\mu_{\rho_1}}V_{\rho 1}$$

$$x_{10} = \frac{\alpha}{2}r + \alpha\beta\frac{m_9}{\mu_{10,9}}r_{10,9} + \alpha\beta\frac{\mu_{87}}{\mu_{\rho_1}}\rho_1 \qquad \dot{x}_{10} = \frac{\sqrt{3}}{2}V_r + \sqrt{3}\beta\frac{m_9}{\mu_{10,9}}V_{r_{10,9}} + \sqrt{3}\beta\frac{\mu_{87}}{\mu_{\rho_1}}V_{\rho 1}$$

$$y_{10} = -\frac{\sqrt{3}}{2}r - \sqrt{3}\beta\frac{m_9}{\mu_{10,9}}r_{10,9} - \sqrt{3}\beta\frac{\mu_{87}}{\mu_{\rho_1}}\rho_1 \qquad \dot{y}_{10} = \frac{\alpha}{2}V_r + \alpha\beta\frac{m_9}{\mu_{10,9}}V_{r_{10,9}} + \alpha\beta\frac{\mu_{87}}{\mu_{\rho_1}}V_{\rho 1}$$

where $\alpha = \frac{m_1 - m_2}{\mu + 2\mu_{43} + 2\mu_{65}}$ and $\beta = (3 + \alpha^2)^{-1/2}$

Velocities V_r, $V_{r_{43}}$, $V_{r_{65}}$, $V_{r_{87}}$, $V_{r_{10,9}}$ and $V_{\rho 1}$ in the ten body L4 and L5 binary state vector are derived from the equations of motion in the second part of this analysis and will need to use the infinitesimal interval method with type one geometry and the sidereal synodic relations at time zero to estimate their magnitude. The infinitesimal interval calculation allows determination of the perturbation coefficients which ensures that gravitational interaction between the masses has been accounted for in the approximation. Equations of motion for this ten-mass configuration in the complex plane with the sidereal synodic relations are

$$\begin{aligned} n_{21}P_{21} &= (n_{21} + n_{\rho 1})P_{\rho 1} = (n_{21} + n_{\rho 1} + n_{43})P_{43} \\ &= (n_{21} + n_{\rho 1} + n_{65})P_{65} \end{aligned}$$

$$\begin{aligned} n_{21}P_{21} &= (n_{21} + n_{\rho 2})P_{\rho 2} = (n_{21} + n_{\rho 2} + n_{87})P_{87} \\ &= (n_{21} + n_{\rho 2} + n_{10,9})P_{10,9} \end{aligned}$$

Due the double binary configuration symmetry the following constraints apply

$$P_{\rho 1} = P_{\rho 2} \quad P_{65} = P_{87} \quad P_{43} = P_{10,9}$$

$$n_{\rho 1} = n_{\rho 2} \quad n_{43} = n_{10,9} \quad n_{65} = n_{87}$$

$$\rho 1 = \rho 2 \quad r_{43} = r_{10,9} \quad r_{65} = r_{87}$$

The mass one and mass two first binary is on the rotating x' axis and therefore $\ddot{z} = \dot{z} = 0$. Double binary equations of motion are

$$(\rho_{21}\mu - 1)z = (\rho_{32}z_{32} - \rho_{31}z_{31})m_3 + (\rho_{42}z_{42} - \rho_{41}z_{41})m_4$$
$$+(\rho_{52}z_{52} - \rho_{51}z_{51})m_5 + (\rho_{62}z_{62} - \rho_{61}z_{61})m_6$$
$$+(\rho_{72}z_{72} - \rho_{71}z_{71})m_7 + (\rho_{82}z_{82} - \rho_{81}z_{81})m_8$$
$$+(\rho_{92}z_{92} - \rho_{91}z_{91})m_9 + \left(\rho_{10,2}z_{10,2} - \rho_{10,1}z_{10,1}\right)m_{10}$$

$$V_r^2 = \frac{G(\mu+\phi_1)}{r} \qquad \text{Equation A2.2}$$

$$\phi_1 = \frac{r^3}{r_{31}^3}m_3 + \frac{r^3}{r_{41}^3}m_4 + \frac{r^3}{r_{51}^3}m_5 + \frac{r^3}{r_{61}^3}m_6 + \frac{r^3}{r_{71}^3}m_7 + \frac{r^3}{r_{81}^3}m_8 +$$
$$\frac{r^3}{r_{91}^3}m_9 + \frac{r^3}{r_{10,1}^3}m_{10}$$

$$\left(\rho_{43}\mu_{43} - \frac{P_{21}^2}{P_{43}^2}\right)z_{43} = (\rho_{41}z_{14} - \rho_{31}z_{13})m_1 + (\rho_{42}z_{24} - \rho_{32}z_{23})m_2$$
$$+(\rho_{45}z_{54} - \rho_{35}z_{53})m_5 + (\rho_{46}z_{64} - \rho_{36}z_{63})m_6$$
$$+(\rho_{47}z_{74} - \rho_{37}z_{73})m_7 + (\rho_{48}z_{84} - \rho_{38}z_{83})m_8$$
$$+(\rho_{49}z_{94} - \rho_{39}z_{93})m_9 + \left(\rho_{4,10}z_{10,4} - \rho_{3,10}z_{10,3}\right)m_{10}$$

$$V_{r_{43}}^2 = \frac{G(\mu_{43}+x_1^3\phi_2)}{r_{43}} \qquad r_{43} = x_1 r$$

$$\phi_2 = \frac{r^3}{r_{41}^3}m_1 + \frac{r^3}{r_{42}^3}m_2 + \frac{r^3}{r_{45}^3}m_5 + \frac{r^3}{r_{46}^3}m_6 + \frac{r^3}{r_{47}^3}m_7 +$$
$$\frac{r^3}{r_{48}^3}m_8 + \frac{r^3}{r_{49}^3}m_9 + \frac{r^3}{r_{4,10}^3}m_{10}$$

$$\left(\rho_{65}\mu_{65}-\frac{P_{21}^2}{P_{65}^2}\right)z_{65}=(\rho_{61}z_{16}-\rho_{51}z_{15})m_1+(\rho_{62}z_{26}-\rho_{52}z_{25})m_2$$
$$+(\rho_{63}z_{36}-\rho_{53}z_{35})m_3+(\rho_{64}z_{46}-\rho_{54}z_{45})m_4$$
$$+(\rho_{67}z_{76}-\rho_{57}z_{75})m_7+(\rho_{68}z_{86}-\rho_{58}z_{85})m_8$$
$$+(\rho_{69}z_{96}-\rho_{59}z_{95})m_9+\left(\rho_{6,10}z_{10,6}-\rho_{5,10}z_{10,5}\right)m_{10}$$

$$V_{r_{65}}^2=\frac{G(\mu_{65}+x_2^3\phi_3)}{r_{65}}\qquad r_{65}=x_2r$$

$$\phi_3=\frac{r^3}{r_{61}^3}m_1+\frac{r^3}{r_{62}^3}m_2+\frac{r^3}{r_{63}^3}m_3+\frac{r^3}{r_{64}^3}m_4+\frac{r^3}{r_{67}^3}m_7+$$
$$\frac{r^3}{r_{68}^3}m_8+\frac{r^3}{r_{69}^3}m_9+\frac{r^3}{r_{6,10}^3}m_{10}$$

$$\left(\rho_{87}\mu_{87}-\frac{P_{21}^2}{P_{87}^2}\right)z_{87}=(\rho_{81}z_{18}-\rho_{71}z_{17})m_1+(\rho_{82}z_{28}-\rho_{72}z_{27})m_2$$
$$+(\rho_{83}z_{38}-\rho_{73}z_{37})m_3+(\rho_{84}z_{48}-\rho_{74}z_{47})m_4$$
$$+(\rho_{85}z_{58}-\rho_{75}z_{57})m_5+(\rho_{86}z_{68}-\rho_{76}z_{67})m_6$$
$$+(\rho_{89}z_{98}-\rho_{79}z_{97})m_9+\left(\rho_{8,10}z_{10,8}-\rho_{7,10}z_{10,7}\right)m_{10}$$

$$V_{r_{87}}^2=\frac{G(\mu_{87}+x_3^3\phi_4)}{r_{87}}\qquad r_{87}=x_3r$$

$$\phi_4=\frac{r^3}{r_{81}^3}m_1+\frac{r^3}{r_{82}^3}m_2+\frac{r^3}{r_{83}^3}m_3+\frac{r^3}{r_{84}^3}m_4+\frac{r^3}{r_{85}^3}m_5+$$
$$\frac{r^3}{r_{86}^3}m_6+\frac{r^3}{r_{89}^3}m_9+\frac{r^3}{r_{8,10}^3}m_{10}$$

$$\left(\rho_{10,9}\mu_{10,9}-\frac{P_{21}^2}{P_{10,9}^2}\right)z_{10,9}$$
$$=\left(\rho_{10,1}z_{1,10}-\rho_{91}z_{19}\right)m_1+\left(\rho_{10,2}z_{2,10}-\rho_{92}z_{29}\right)m_2$$
$$+\left(\rho_{10,3}z_{3,10}-\rho_{93}z_{39}\right)m_3+\left(\rho_{10,4}z_{4,10}-\rho_{94}z_{49}\right)m_4$$
$$+\left(\rho_{10,5}z_{5,10}-\rho_{95}z_{59}\right)m_5+\left(\rho_{10,6}z_{6,10}-\rho_{96}z_{69}\right)m_6$$
$$+\left(\rho_{10,7}z_{7,10}-\rho_{97}z_{79}\right)m_7+\left(\rho_{10,8}z_{8,10}-\rho_{98}z_{89}\right)m_8$$

$$V_{r_{10,9}}^2 = \frac{G(\mu_{10,9}+x_4^3\phi_5)}{r_{10,9}} \qquad r_{10,9} = x_4 r$$

$$\phi_5 = \frac{r^3}{r_{10,1}^3}m_1 + \frac{r^3}{r_{10,2}^3}m_2 + \frac{r^3}{r_{10,3}^3}m_3 + \frac{r^3}{r_{10,4}^3}m_4 + \frac{r^3}{r_{10,5}^3}m_5 + \frac{r^3}{r_{10,6}^3}m_6 + \frac{r^3}{r_{10,7}^3}m_7 + \frac{r^3}{r_{10,8}^3}m_8$$

where $\rho_{ij} = \frac{G}{w^2 r_{ij}^3}$

Equation A2.2 has treated the double binaries at the L4 and L5 locations as a n-body collinear problem, where the collinear double binary configuration at the L4 point aligns with the collinear double binary at the L5 point and both of these double binaries align with the vector from L4 to L5. This results in a simplification of the equations of motion. Other than this approximation, the only way these vectors will align is when mass one is equal to mass two. It is also assumed that the distance between mass three and mass six at the L4 location is small relative to the distance between the L4 and L5 locations. The same is true for the double binary at the L5 location. Therefore, the distances between the binaries will approach zero and the problem in determining the perturbation coefficients and binary velocities is resolved. There are some additional restrictions made on double binary mass and distance as seen below

$$m_3 = m_{10} \quad m_4 = m_9 \quad m_5 = m_8 \quad m_6 = m_7 \quad \mu_{43} = \mu_{10,9}\,\mu_{65} = \mu_{87}$$

$$\rho_{31} = \rho_{10,1} \quad \rho_{41} = \rho_{91} \quad \rho_{51} = \rho_{81} \quad \rho_{61} = \rho_{71} \quad x_2 = x_3$$

$$x_1 = x_4 \qquad \phi_2 = \phi_5 \qquad \phi_3 = \phi_4 \qquad \text{Equation A2.3}$$

Velocity computation for $V_{\rho 1}$ and $V_{\rho 2}$ is a function of the perturbation coefficients that are derived from the $\rho 1$ and $\rho 2$ equations of motion. Jacoby coordinates $\rho 1$ and $\rho 2$ are the distances between the binary subsystem centers of gravity for the mass three through mass six and mass seven through mass ten respectively. The equation of motion for the Jacoby coordinate $\rho 1$ between the mass three and mass four binary and the mass five and mass six binary can be derived by using $z_{43c} = \frac{m_3 z_3 + m_4 z_4}{\mu_{43}}$. Equation 1.3.5 can be used to start this derivation.

$$\ddot{z}_{43c} + 2wi\acute{z}_{43c} - w^2 z_{43c} = \frac{Gm_1}{\mu_{43}}\left(\frac{m_3}{r_{13}^3} z_{13} + \frac{m_4}{r_{14}^3} z_{14}\right) + \frac{Gm_2}{\mu_{43}}\left(\frac{m_3}{r_{23}^3} z_{23} + \frac{m_4}{r_{24}^3} z_{24}\right) + \cdots + \frac{Gm_{10}}{\mu_{43}}\left(\frac{m_3}{r_{10,3}^3} z_{10,3} + \frac{m_4}{r_{10,4}^3} z_{10,4}\right)$$

Result of this analysis for $V_{\rho 1}$ ($V_{\rho 1} = V_{\rho 2}$) and perturbation coefficient ϕ_6 are shown below

$$V_{\rho 1}^2 = \frac{l}{2}\frac{\mu_{\rho 1}}{\mu_{65}}\beta^{-1} V_r^2 - \frac{G\mu_{\rho 1}}{\rho 1}\frac{l^2}{\mu_{65}}\phi_6$$

$$\phi_6 = \frac{r^2}{r_{13}^2} m_1 - \frac{r^3}{r_{23}^2}\left(\frac{m_1 + \mu_{\rho 1}}{\mu + 2\mu_{\rho 1}} - \frac{1}{2}\beta^{-1}\right) - \frac{r^2}{r_{53}^2} m_5 - \frac{r^2}{r_{63}^2} m_6$$

It can be shown that due to symmetry $V_{\rho 1} = V_{\rho 2}$.

The ratio $\frac{r_{ij}}{r}$ can be evaluated from equation A2.1 to determine the perturbation coefficients and velocities derived in equation A2.2. Starting with the double binary distance ratios in L4

$$\frac{r_{31}}{r} = \left(\left(\frac{1}{2} + \alpha\beta\frac{m_{65}}{\mu_{\rho 1}} x_3 + \alpha\beta\frac{m_4}{\mu_{43}} x_1\right)^2 + \left(\frac{\sqrt{3}}{2} + \sqrt{3}\beta\frac{m_{65}}{\mu_{\rho 1}} x_3 + \sqrt{3}\beta\frac{m_4}{\mu_{43}} x_1\right)^2\right)^{1/2} \qquad \text{Equation A2.4}$$

$$= \left((x_3 - x_1)^2 + y_3^2\right)^{1/2} r^{-1}$$

$$\frac{r_{41}}{r} = \left(\left(\frac{1}{2} + \alpha\beta\frac{m_{65}}{\mu_{\rho 1}} x_3 - \alpha\beta\frac{m_3}{\mu_{43}} x_1\right)^2 + \left(\frac{\sqrt{3}}{2} + \sqrt{3}\beta\frac{m_{65}}{\mu_{\rho 1}} x_3 - \sqrt{3}\beta\frac{m_3}{\mu_{43}} x_1\right)^2\right)^{1/2}$$

$$= \left((x_4 - x_1)^2 + y_4^2\right)^{1/2} r^{-1}$$

$$\frac{r_{42}}{r} = \left((r - (x_4 - x_1))^2 + y_4^2\right)^{1/2} r^{-1}$$

$$\frac{r_{51}}{r} = \left(\left(\frac{1}{2} - \alpha\beta\frac{m_{43}}{\mu_{\rho 1}} x_3 + \alpha\beta\frac{m_6}{\mu_{65}} x_2\right)^2 + \left(\frac{\sqrt{3}}{2} - \sqrt{3}\beta\frac{m_{43}}{\mu_{\rho 1}} x_3 + \sqrt{3}\beta\frac{m_6}{\mu_{65}} x_2\right)^2\right)^{1/2}$$

$$= \left((x_5 - x_1)^2 + y_5^2\right)^{1/2} r^{-1}$$

$$\frac{r_{61}}{r} = ((\frac{1}{2} - \alpha\beta\frac{m_{43}}{\mu_{\rho 1}}x_3 - \alpha\beta\frac{m_5}{\mu_{65}}x_2)^2 + (\frac{\sqrt{3}}{2} - \sqrt{3}\beta\frac{m_{43}}{\mu_{\rho 1}}x_3 - \sqrt{3}\beta\frac{m_5}{\mu_{65}}x_2)^2)^{1/2}$$

$$= ((x_6 - x_1)^2 + y_6^2)^{1/2}r^{-1}$$

$$\frac{r_{62}}{r} = ((r - (x_6 - x_1))^2 + y_6^2)^{1/2}r^{-1}$$

$$\frac{r_{53}}{r} = x_3 - \frac{m_6}{\mu_{65}}x_2 + \frac{m_4}{\mu_{43}}x_1 \qquad \frac{r_{54}}{r} = x_3 - \frac{m_6}{\mu_{65}}x_2 - \frac{m_3}{\mu_{43}}x_1$$

$$\frac{r_{63}}{r} = x_3 + \frac{m_5}{\mu_{65}}x_2 + \frac{m_4}{\mu_{43}}x_1 \qquad \frac{r_{64}}{r} = x_3 + \frac{m_5}{\mu_{65}}x_2 - \frac{m_3}{\mu_{43}}x_1$$

The double binary geometry in L5 is symmetric to the double binary geometry in L4 and therefore the same equations in equation A2.4 can be used for L5. For example, $\frac{r_{31}}{r} = \frac{r_{10,1}}{r}$ etc.

Double binary ten-body state vector in equation A2.1 was numerically integrated for a period of five hundred years for the following masses and mass distances with results shown in figures A3 and A4.

$m_1 = 1\ SM \qquad m_2 = 9.553x10^{-4}\ SM$ (Jovan Mass)

$m_3\ through\ m_{10} = .05m_2 \qquad r_{21} = 2.5\ AU$

$r_{43}\ through\ r_{10,9} = x_1r_{21} \qquad \rho 1 = \rho 2 = x_3r_{21}$

$x_1 = x_2 = .2x10^{-2} \qquad x_3 = 1x10^{-2}$

Ten body configuration state vector trajectories in the numerically integrated ephemeris were analyzed by studying the double binary behavior in the L4 and L5 equilibrium locations. These binaries for the given mass and mass distance input are finite stable over the five-hundred year epoch in which they were run. The somewhat noisy binary separation distance variation seen in figures A3 and A4 may be caused by the approximation used to generate the double binary state vector. Also, the L4 and L5 separation distance of $\rho = \sqrt{3}r$ in the derivation, which may be an approximation, could possibly be contributing to this noise. It is not known how long this ten-body configuration will remain finite stable, however, by varying the binary mass and mass distance the finite stability span can be extended and controlled.

It is expected that more complex collinear configurations can successfully be derived and numerically integrated to show large numbers of particles can exist in finite stable orbits at the L4 and L5 equilibrium regions. This would be consistent with observation where many asteroids are known to exist at the Lagrange regions in our solar system.

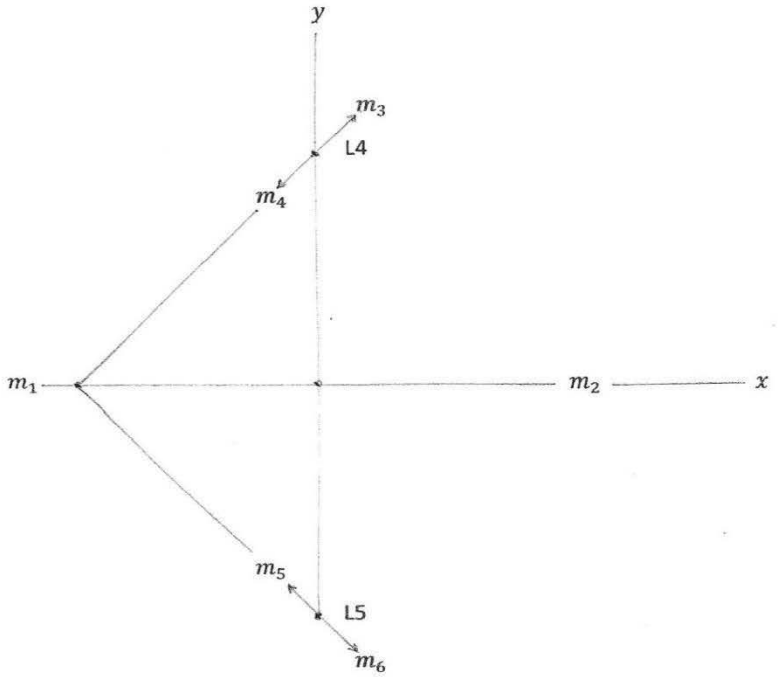

FIGURE A1. Single Binary Orbiting L4 and L5 Location

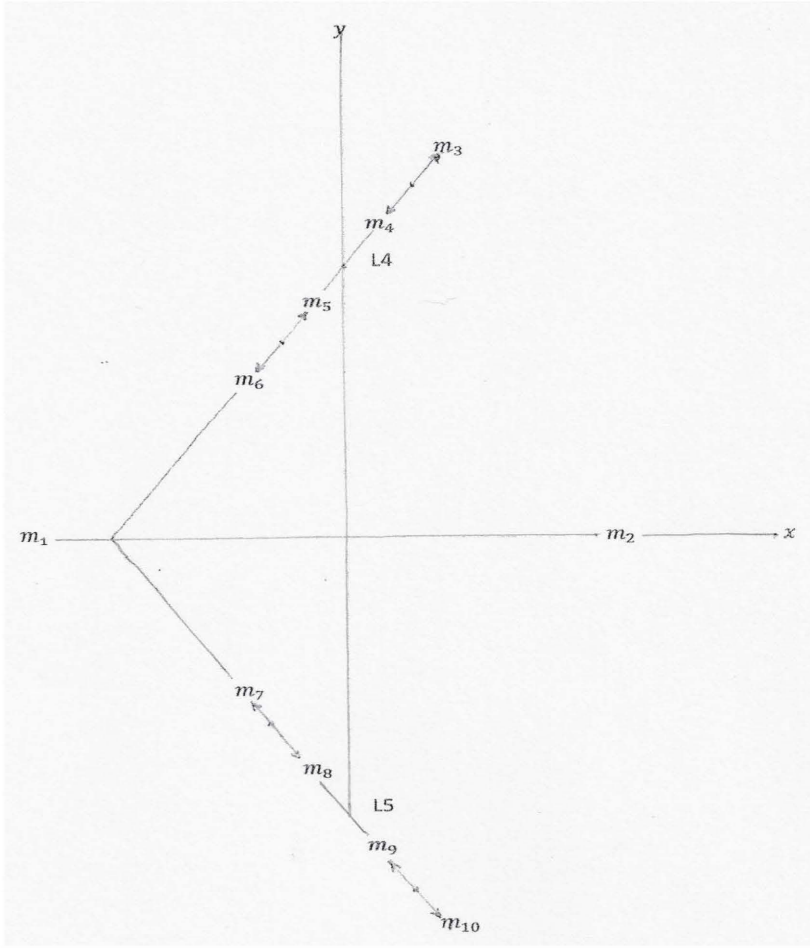

FIGURE A2. Double Binary Orbiting L4 and L5 Location

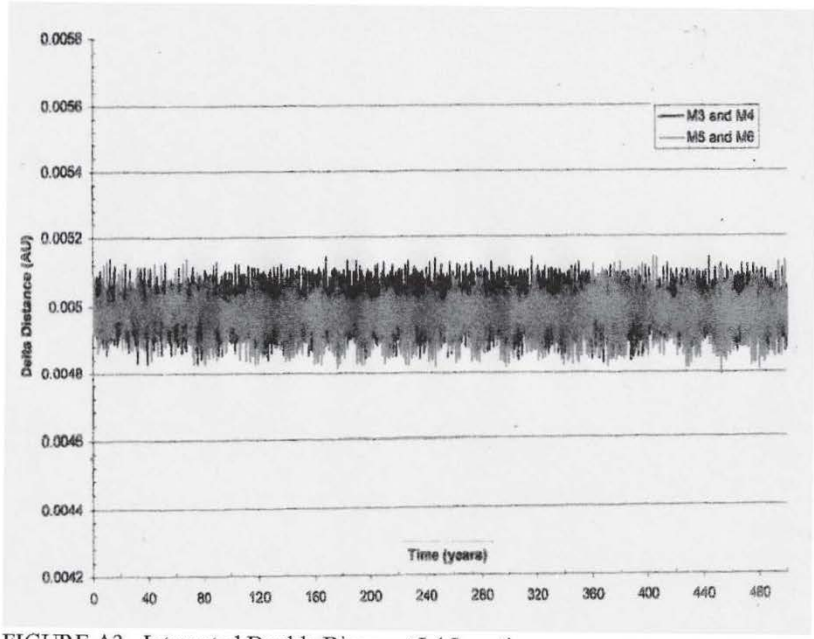

FIGURE A3. Integrated Double Binary at L4 Location

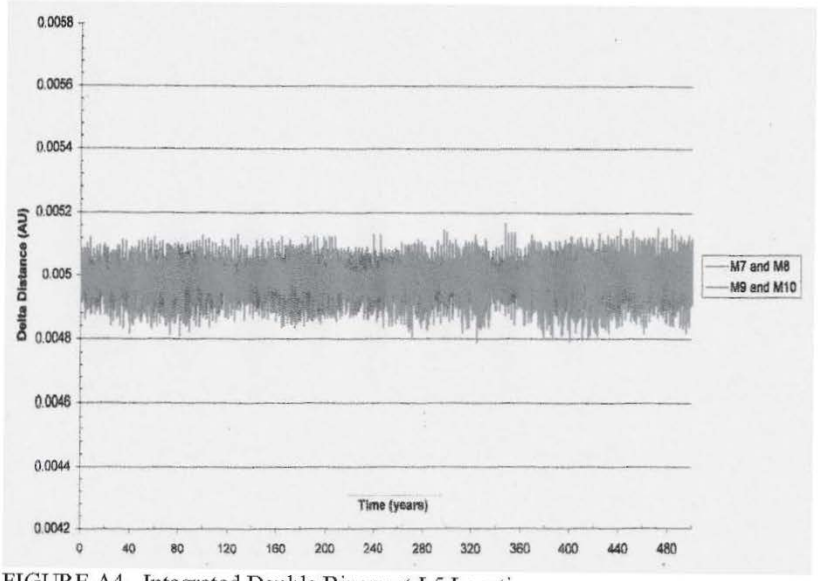

FIGURE A4. Integrated Double Binary at L5 Location

BIBLIOGRAPHY

Aarseth, S. J., 2003, *Gravitational N-Body Simulations – Tools and Algorithms*, Cambridge, Cambridge University Press.

Abraham, R., Marsden,J. E., 1967, *Foundations of Mechanics*, Arizona, W. A. Benjamin Inc..

Aizerman, M. A., Gantmacher, F. R., 1964, *Absolute Stability of Regulator Systems*, San Francisco, Holden Day.

Arnold, V. I., 1973, *Ordinary Differential Equations*, Massachusetts, MIT Press.

Arnold, V. I., 1978, Mathematical Methods of Classical Mechanics, Berlin, Springer Verlag.

Baker, R. M. L., Makemson, M. W., 1962, *An Introduction to Astrodynamics*, New York, Academic Press.

Baker, R. M. L., 1967, *Astrodynamics: Applications and Advanced Topics*, New York, Academic Press.

Ball, K. F., Osborne, G. F., 1967, *Space Vehicle Dynamics*, Oxford, Claredon Press.

Barbashin, E. A., 1970, *Introduction to the Theory of Stability*, Netherlands, Wolters Noordhoff.

Bate, R. R., Mueller, D. D., White, J. E., 1971, *Fundamentals of Astrodynamics*, New York, Dover.

Battin, R. H., 1987, An Introduction to the Mathematics of Astrodynamics, USA, AIAA.

Bellman, R., 1953, *Stability Theory of Differential Equations*, New York, McGraw Hill Company.

Berman, A. L., 1963, *The Physical Principles of Astrodynamics – Fundamentals of Dynamical Astronomy and Space Flight*, New Jersey, John Wiley and Sons.

Besant, W. H., Ramsey, A. S., 1914, *A Treatise on Dynamics*, London, Bell and Sons.

Beutler, G., 2005, *Methods of Celestial Mechanics-Physical, Mathematical and Numerical Principles, Volume I*, Berlin, Springer Verlag.

Beutler, G., 2005, *Methods of Celestial Mechanics – Application to Planetary System, Geodynamics and Satellite Geodesy, Volume II*, Berlin, Springer Verlag.

Bhatia, N. P., Szego, G. P., 1967, *Dynamical Systems: Stability Theory and Applications*, Berlin, Springer Verlag.

Birkhoff, G. D., 1927, *Dynamical Systems*, USA, American Mathematical Society.

Blanco, V. M., Mc Cusky, S. W., 1961, *Basic Physics of the Solar System*, Boston Addison Wesley.

Blitzer, L., 1960, *The Orbit of a Satellite in the Gravitational Field of the Earth*, Pasadena, JPL Handout.

Boccaletti, D., Pucacco, G., 1999, *Theory of Orbits 1. Integrable Systems and Non-Perturbative Methods*, Berlin, Springer Verlag.

Boccaletti, D., Pucacco, G., 2004, *Theory of Orbits 2. Perturbative and Geometrical Methods*, Berlin, Springer Verlag.

Bond, V. R., Allman, M. C., 1996, *Modern Astrodynamics*, Princeton, Princeton University Press.

Brouwer, D., Clemence, G. M., 1961, *Methods of Celestial Mechanics*, New York, Academic Press.

Brown, E., 1896, *An Introductory Treatise on the Lunar Theory*, Cambridge, Cambridge University Press.

Brown, E., 1928, *Resonance in the Solar System*, USA, American Mathematical Society.

Brown, E., Shook, C., 1933, *Planetary Theory*, Cambridge, Cambridge University Press.

Cheboterav, G. A., 1967, *Analytical and Numerical Methods of Celestial Mechanics*, New York, American Elsevier.

Chenciner, A. 2003. Perverse Solutions of the Planar N-Body Problem. *Asterisque*.

Chetayev, N. G., 1961, *The Stability of Motion*, Oxford, Pergamon Press.

Cheyne, C. H. H., 1883, *An Elementary Treatise on the Planetary Theory*, Macmillan.

Collins, G. W., 1989, *The Foundations of Celestial Mechanics*, Tucson, AZ, Pachart Publishing House.

Danby, J. M. A., 1962, *Fundamentals of Celestial Mechanics*, UK, Macmillan.

Darwin, G. H., 1880, *On the Secular Changes in the Elements of the Orbit of a Satellite Revolving About a Tidally Distorted Planet*, England, The Royal Society.

Darwin, G. H., 1898, *The Tides*, Boston, Houghton Mifflin Company.

Deutsch, R., 1963, *Orbital Dynamics of Space Vehicles*, Englewood Cliffs, NJ, Prentice Hall.

Diacu, F. N., 1992, *Singularities of the N-Body Problem-An Introduction to Celestial Mechanics*, Montreal, Les Publications CRM.

Dubyago, A. D., 1961, *The Determination of Orbits*, New York, Macmillan.

Dziobek, O., 1892, *Mathematical Theories of Planetary Motions*, IL, Inland Press.
Eckhause, W., 1965, Studies in Nonlinear Stability Theory, Berlin, Springer Verlag.
Ehricke, K. A., 1960, *Space Flight Environment and Celestial Mechanics Volume* I, New York, Van Nostrand.
Ehricke, K. A., 1962, *Space Flight Space Dynamics Volume II*, New York, Van Nostrand.
El'sgol'ts, L. E., 1961, *Differential Equations*, India, Hindustan Publishing Company.
Escobal, P. R., 1965, *Methods of Orbit Determination*, John Wiley.
Escobal, P. R., 1968, *Methods of Astrodynamics*, New Jersey, John Wiley.
Finlay-Freundlich, E., 1958, Celestial Mechanics, Oxford, Pergamon Press.
Fitzpatrick, P. M., 1970, *Principles of Celestial Mechanics*, New York, Academics Press.
Galiullin, A. S., 1984, Inverse Problem of Dynamics, Moscow, MIR Publishers.
Galiullin, A. S., 2000, *An Introduction to the Theory of Stability of Motion*, Kathmandu, Kathmandu University.
Gantmacher, F., 1970, *Lectures in Analytical Mechanics*, Moscow, MIR Publishers.
Geyling, F. T., Westerman, H. R., 1971, *Introduction to Orbital Mechanics*, Boston, Addison-Wesley.
Giacaglia, G> E. O., 1970, *Periodic Orbits, Stability and Resonances*, D. Reidel Publishing Company.
Goldstein, H., 1965, *Classical Mechanics*, Boston, Addison Wesley.
Grossman, N., 1996, *The Sheer Joy of Celestial Mechanics*, Birkhauser.
Hagihara, Y. 1927. Preliminary Study of the Stability of Certain Satellite Systems., Japan, *Japanese Journal of Astronomy and Geophysics, Volume V No. I.*
Hagihara, Y., 1957, *Stability in Celestial Mechanics*, Tokyo Minato-Ku, Kasai Publishing.
Hagihara, Y., 1970, *Celestial Mechanics-Dynamical Principles and Transformation Theory, Volume I*, Cambridge, Massachusetts, MIT Press.
Hagihara, Y., 1971, *Celestial Mechanic-Perturbation Theory, Volume II Parts 1 and 2*, Cambridge, Massachusetts, MIT Press.
Hagihara, Y., 1974, *Celestial Mechanics-Differential Equations in Celestial Mechanics Volume III Parts 1 and 2*, Japan, Japan Society for the Promotion of Science.

Hagihara, Y., 1975, *Celestial Mechanics-Periodic and Quasi-Periodic Solutions Volume IV Parts 1 and 2*, Japan, Japan Society for the Promotion of Science.

Hagihara, Y., 1976, *Celestial Mechanics-Topology of the Three-Body Problem Volume V Parts 1 and 2*, Japan, Japan Society for the Promotion of Science.

Hahn, W., 1967, *Stability of Motion*, Berlin, Springer Verlag.

Herrick, S., 1972, *Astrodynamics: Orbit Determination, Space Navigation, Celestial Mechanics*, Van Nostrand Reinhold.

Herrick, S., 1971, *Astrodynamics: Orbit Correction, Perturbation Theory, Integration*, Van Nostrand.

Hohmann, W., (1925) 1960, *The Attainability of Heavenly Bodies*, NASA Technical Translation F-44.

Jeans, J. H., 1935, *Theoretical Mechanics*, Ginn and Company, Boston, Massachusetts.

Khilmi, G. F., 1961, *Qualitative Methods in the Many Body Problem*, Gorden and Breach.

Kovalevsky, J.,1967, *Introduction to Celestial Mechanics*, D. Reidal Publishing Company.

Krasovskii, N. N., 1963, *Stability of Motion*, California, Stanford University Press.

Kurth, R., 1957, *Introduction to the Mechanics of Stellar Systems*, Oxford, Pergamon Press.

Kurth, R., 1959, *Introduction to the Mechanics of the Solar System*, New York, Pergamon Press.

Laplace, 1966, (Translated by N. Bowditch), *Celestial Mechanics Volumes I through IV*, Chelsea Edition.

LaSalle, J., Lefschetz, S., 1961, Stability by Liapunov's Direct Method with Applications.

Lass, H., 1957, Elements of Pure and Applied Mathematics, New York, McGraw-Hill.

Lehnigh, S. H., 1966, *Stability Theorems for Linear Motions with an Introductions to Liapunov's Direct Method*, Englewood Cliffs, NJ, Prentice Hall.

Leimanis, E., Minorsky, N., 1958, *Dynamics and Non-Linear Mechanics*, New Jersey, John Wiley and Sons

Leipholz, H., 1970, *Stability Theory An Introduction to the Stability of Dynamic Systems and Rigid Bodies*, New York, Academic Press.

Liapunov, A. M., 1966, *Stability of Motion*, New York Academic Press.

Lyapunov, A. M., 1992, *The General Problem of the Stability of Motion*, UK, Taylor and Francis.

Macmillan W. D., 1909, *Periodic Orbits About an Oblate Spheroid*, Chicago, University of Chicago.

Macmillan W. D., 1927, *Statics and dynamics of a Particle*, New York, McGraw-Hill Book Company.

Madonna, R. G., 1997, *Orbital Mechanics*, Malabar, FL, Krieger Publishing Company.

Malkin, I. G., 1950, Certain Questions on the Theory of the Stability of Motion in the Sense of Liapounoff, USA, American Mathematical Society.

Malkin, I. G., 1958, Theory of Stability of Motion, USA, U. S. Atomic Energy Commission.

Maxwell, J. C., 1859, *On the Stability of the Motion of Saturn's Rings*: *An Essay, Which Obtained the Adams Prize for the Year 1856, In the University of Cambridge*, Cambridge, MacMillan and Company.

Maxwell J. C., Brush, S. G., Everitt, C. W. F., Garber, E., 1983, *Maxwell on Saturn's Rings*, Massachusetts, The MIT Press Cambridge.

McCuskey, S. W., 1963, *Introduction to Celestial Mechanics*, Boston, Addison Wesley.

Merkin, D. R., 1996, *Introduction to the Theory of Stability*, New York, Springer Verlag.

Meyer, K. R., 1999, *Periodic Solutions of the N-Body Problem*, New York, Springer Verlag.

Mittleman, D., 1980, *Motion About the Stable Libration Points in the Linearized Restricted Three-body Problem*, USA, NASA Reference Publication 1065.

Moulton, F. R., 1902, *An Introduction to Celestial Mechanics*, New York, Macmillan.

Moulton, F. R., 1903, *On Certain Rigorous Methods of Treating Problems in Celestial Mechanics*, Chicago, University of Chicago Press.

Moulton, F. R., Buchanan, D., Buck, T., Griffin, F. L., Longley, W. R., Macmillan, W. D., 1920, *Periodic Orbits*, Washington, Carnegie Institute of Washington.

Murray, C. D., Dermott, S. F., 1996, *Solar System Dynamics*, London, Cambridge.

Nelson, W. C., 1962, *Space Mechanics*, New Jersey, Prentice Hall.

Newcomb, S., 1874, *On the General Integrals of Planetary Motion*, Washington, Smithsonian Contributions to Knowledge.

Nieto, M. M., 1972, *The Titius-Bode Law of Planetary Distances–Its History and Theory*, Oxford, Pergamon Press.

Parks, P. C., 1993, Hahn, V., *Stability Theory*, Englewood Cliffs, NJ, Prentice Hall.

Pars, L. A., 1979, *A Treatise on Analytical Dynamics*, Woodbridge, CT, Ox Bow Press.

Peirce, B. O., 1902, *Elements of the Theory of the Newtonian Potential Function*, Oxford, Ginn.

Peirce, B. O.,1855, *Physical and Celestial Mechanics-A System of Analytical Mechanics*, Boston, Little Brown and Company.

Plummer, H. C., 1960, *An Introductory Treatise on Dynamical Astronomy*, New York, Dover.

Pogorelov, D. A., 1964, *Fundamentals of Orbital Mechanics*, San Francisco Holden Day.

Poincare, N.,1993, *Volume I-New Methods of Celestial Mechanics-Periodic and Asymptotic Solutions*, Edited by D. L. Goroff, New York, Springer-Verlag.

Poincare, N., 1993, *Volume II-New Methods of Celestial Mechanics-Approximations by Series*, Edited by D. L. Goroff, New York, Springer-Verlag.

Poincare, N., 1993, *Volume III-New Methods of Celestial Mechanics-Integral Invariants and Asymptotic Properties of Certain Solutions*, Edited by D. L. Goroff, New York, Springer-Verlag.

Pollard, H., 1966, *Mathematical Introduction to Celestial Mechanics*, New Jersey, Prentice Hall.

Porter, B. 1968, *Stability Criteria for Linear Dynamical Systems*, New York, Academic Press.

Ramsey, A. S.,1929, *Dynamics*, London, Cambridge at the University Press.

Ramsey, A. S., 1937, *Dynamics II*, London, Cambridge at the University Press.

Rimrott, F. P. J., 1989, *Introductory Orbit Dynamics*, Germany, Vieweg and Sohn.

Rouche, N., Habets, R., Laloy, M., 1977, *Stability Theory by Liapunov's Direct Method*, Berlin, Springer Verlag.

Rouche, N., Mawhin, J., 1980, *Ordinary Differential Equations – Stability and Periodic Solutions.* Denmark, Pitman.

Routh, E. J., 1877, A *Treatise on the Stability of a Given State of Motion*, UK, MacMillan and Company.

Roy, A. E., 1965, *Fundamentals of Astrodynamics*, UK, Macmillan.

Roy, A. E., 1988, *Orbital Motion*, Bristol, Institute of Physics Publishing.

Saaty, T. L., Bram, J., 1964, *Nonlinear Mathematics*, New York, Mc Graw Hill.

Santilli, R. M., 1978, *Foundations of Theoretical Mechanics I-The inverse Problem in Newtonian Mechanics*, New York, Springer-Verlag.

Seifert, H. S., Seifert, M. H., 1964, *Orbital Space Flight-The Physics of Satellite Motion*, New York, Holt, Rinehart, Winston.

Shtokalo, I. Z., 1961, *Linear Differential Equations with Variable Coefficients*, India, Hindustan Publishing.
Siegel, C. L., 1954, *Topics in Celestial Mechanics*, Maryland, Johns Hopkins University.
Skowronski, J. M., 1984, *Applied Liapunov Dynamics*, Brisbane, S.C.E.C.
Skowronski, J. M., 1990, *Nonlinear Liapunov Dynamics*, New Jersey, World Scientific.
Smart, W. M., 1938, *Stellar Dynamics*, Cambridge, Cambridge University Press.
Smart, W. M., 1949, *Text Book on Spherical Astronomy*, Cambridge, Cambridge University Press.
Smart, W. M., 1953, *Celestial Mechanics*, London, Longmans, Green and Company.
Sterne, T. E., 1960, *An Introduction to Celestial Mechanics*, New Jersey, Interscience.
Stiefel, E. L., Scheifele, G., 1971, *Linear and Regular Celestial Mechanics*, Berlin, Springer Verlag.
Szebehely, V. G., 1967, *Theory of Orbits*, New York, Academic Press.
Szebehely, V. G., 1989, *Adventures in Celestial Mechanics*, Texas, University of Texas Press.
Tan, A., 2008, *Theory of Orbital Motion*, New Jersey, World Scientific.
Thomson, W. T., 1961, *Introduction to Space Dynamics*, New Jersey John Wiley.
Tsiolkovsky, K. E., (1954) 1965, *Reactive Flying Machines*, (Moscow), NASA TT F-237, USSR, Academy of Sciences Publishing House.
Vallado, D. A., 2001, *Fundamentals of Astrodynamics and Applications*, Portland Oregon, Microcosom Press.
Varadi, F., Ghil, M., Newman, W. I., Kaula, W. M., Grazier, K., Goldstein, D. and Lessnick M., 1996, *NBI-A Set of Numerical Integrators for the Gravitational N-Body Problem*, Los Angeles, California, UCLA.
Wiesel, W. E., 1989, *Spaceflight Dynamics*, New York McGraw Hill.
Willems, J. L., 1970, *Stability Theory of Dynamical Systems*, New Jersey John Wiley and Sons.
Wintner, A., 1964, *The Analytical Foundations of Celestial Mechanics*, Princeton, NJ, Princeton University Press.
Yoshizawa, T., 1966, *Stability Theory by Liapunov's Second Method*, Japan, Mathematical Society of Japan.
Yoshizawa, T., 1975, *Stability Theory and the Existence of Periodic and Almost Periodic Solutions*, Berlin, Springer Verlag.
Zubov, V. I., 1964, *Methods of A. M. Lyapunov and their Application*, Netherlands, Noordhoff LTD.

INDEX